



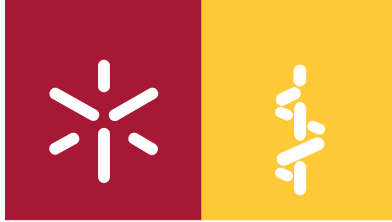
**Universidade do Minho**  
Escola de Ciências da Saúde

Anabela Silva Fernandes

**Development and characterization of transgenic mouse models for Machado-Joseph disease**

**Desenvolvimento e caracterização de modelos transgénicos em ratinho para a doença de Machado-Joseph**

Novembro de 2010



**Universidade do Minho**

Escola de Ciências da Saúde

Anabela Silva Fernandes

**Development and characterization of  
transgenic mouse models for  
Machado-Joseph disease**

**Desenvolvimento e caracterização de  
modelos transgênicos em ratinho  
para a doença de Machado-Joseph**

Tese de Doutoramento  
Ciências da Saúde – Ciências da Saúde

Trabalho efectuado sob a orientação do  
**Professora Doutora Patrícia Espinheira  
de Sá Maciel**

Professora Auxiliar da Escola de Ciências da Saúde,  
Universidade do Minho, Braga - Portugal.

Novembro de 2010

## DECLARAÇÃO

Nome: Anabela Silva Fernandes

Endereço Electrónico: [anabelasf@ecsau.de.uminho.pt](mailto:anabelasf@ecsau.de.uminho.pt)

Telefone: 967 775 628

N.º do Bilhete de Identidade: 12281244

Título dissertação:

Development and characterization of transgenic mouse models for Machado-Joseph disease

Desenvolvimento e caracterização de modelos transgénicos em ratinho para a doença de Machado-Joseph

Orientador:

Professora Doutora Patrícia Espinheira de Sá Maciel

Ano de conclusão: 2010

Ramo de Conhecimento do Doutoramento:

Ciências da Saúde – Ciências da Saúde

É AUTORIZADA A REPRODUÇÃO INTEGRAL DESTA TESE/TRABALHO APENAS PARA EFEITOS DE INVESTIGAÇÃO, MEDIANTE DECLARAÇÃO ESCRITA DO INTERESSADO, QUE A TAL SE COMPROMETE.

Universidade do Minho, 5 de Novembro de 2010

Assinatura: \_\_\_\_\_

“Não me desencorajo, porque cada tentativa errada descartada é outro passo à frente”

(Thomas Edison)

This work was supported by Fundação para a Ciência e a Tecnologia (FCT) through a Bolsa de Doutoramento (SFRH/BD/15910/2005) and the projects POCI/SAU-MMO/60412/2004 and PTDC/SAU-GMG/64076/2006; by the Ataxia MJD, USA.

## **AGRADECIMENTOS**

Gostaria de expressar o meu agradecimento a todos aqueles que contribuíram, de alguma forma, para realização deste trabalho. Em especial,

À Patrícia por todo o apoio e confiança que depositou em mim para levar a cabo este projecto. Pelas conversas científicas que me mostravam o caminho a seguir. Pela energia e disponibilidade. Sinceramente obrigada!

À Professora Cecília Leão por todo o apoio para que a realização deste doutoramento fosse possível.

À Sara Silva, por ter sido companheira de trabalho e também uma amiga, sempre presente e disponível.

Ao Professor Pedro Oliveira por tornar a estatística fácil de entender.

Ao Armando Almeida, Joana Palha, e Nuno Sousa.

Aos meus colegas de laboratório em especial: à Andreia Carvalho, à Ana João, à Mónica, à Carmo, e à Anabela Ferro.

À Andreia de Castro e à Fernanda por todas as aventuras que passámos e por todo o apoio que sempre me deram.

Aos restantes colegas das Neurociências pelas discussões científicas que todas as terças-feiras partilhámos.

A todas as pessoas que contribuem, diariamente, para o bom funcionamento do ICVS pelo apoio e disponibilidade.

À Fundação para a Ciência e Tecnologia pelo financiamento.

À minha Mãe, ao meu Pai, ao Luis, à Luz, Ricardo e aos meus amigos que são o meu suporte e o que tenho de mais valioso na vida.

Bem hajam!



## ABSTRACT

---

### **“Development and characterization of transgenic mouse models for Machado-Joseph disease”**

Since the early 90's a new class of inherited neurodegenerative diseases has been characterized, the polyglutamine (polyQ) expansion diseases. As the name indicates, the mutation underlying each of these disorders is an expansion of a CAG trinucleotide repeat that encodes a polyQ tract in the respective disease proteins. Although polyQ diseases present different clinical features and neuronal degeneration pattern, increasing evidences pointed out to important common features in the pathogenesis, in particular the abnormal protein conformation(s) promoted by polyQ expansion with the consequent accumulation in neuronal inclusions (NIs). Although the polyQ diseases are rare disorders individually, this group is composed by nine progressive and finally fatal disorders, which in general begin in adulthood and progress over 10 to 30 years, normally implicating the full time dedication to patient care by a member of the family. The economic and social impact of these neurodegenerative diseases has led several researchers worldwide to investigate the pathogenesis mechanism and therapeutic strategies for polyQ diseases. Animal models have proved to be an essential tool in this field due to their importance in the development of therapeutic trials but also for the performance of longitudinal studies of disease progression.

In the present study, we generated several novel transgenic mouse models of a polyQ disease, Machado-Joseph disease (MJD), in order to study its pathogenic mechanism and perform therapeutic trials. We have obtained three MJD transgenic lines carrying the cDNA variant MJD1-1 with three different expanded CAG repeats tracts; 83, 94 and 135 CAGs, respectively. The transgenic mice with the lower CAG repeat tract (CMVMJD83) did not manifest the disease even at advanced ages, while the CMVMJD94 transgenic mice developed a mild motor phenotype even in hemizygous animals (in accordance with the autosomal dominant feature of MJD) and brain pathology in the CNS in the absence of NIs. Interestingly, the motor phenotype manifestation in CMVMJD94 mice was correlated with the length of the CAG repeat tract. With the increase of the polyQ tract to 135 glutamines in the human ataxin-3 protein (ATXN3) expressed by transgenic animals (CMVMJD135), we have successfully established a mouse model displaying several of the neurological symptoms of MJD that appear gradually in time, allowing the study of the disease progression. In addition, to further validate the therapeutic value of autophagy activation in MJD we



have performed a pilot therapeutic trial, using lithium and the combination of lithium and temsirolimus; however, we could not find an amelioration of the MJD symptoms in our model CMVMJD135 at the doses of drugs used in this work.

## RESUMO

---

### **“Desenvolvimento e caracterização de modelos transgênicos em ratinho para a doença de Machado-Joseph”**

Desde o início dos anos noventa foi caracterizada uma nova classe de doenças neurodegenerativas hereditárias, as doenças de expansão de poliglutaminas (poliQ). Como o próprio nome indica, a mutação causadora da doença é a expansão de uma repetição de um trinucleótido de CAG que codifica um segmento de poliQ na proteína causadora da doença. Embora as doenças de poliQ apresentem diferenças clínicas e no padrão de neurodegenerescência, várias evidências apontam para a existência de características comuns na patogênese destas doenças, em particular a conformação anormal da proteína causada pela expansão de poliQ, que leva à sua acumulação em inclusões neuronais. Apesar das doenças de poliQ serem doenças raras no contexto individual, este grupo é constituído por nove doenças progressivas e fatais, com início na idade adulta e progredindo durante 10 a 30 anos, o que leva na maioria dos casos à necessidade de um membro da família prestar cuidados ao doente a tempo inteiro. O impacto sócio-económico destas doenças neurodegenerativas tem levado vários grupos de investigação pelo mundo inteiro a investigar o mecanismo patogénico assim como estratégias terapêuticas para as doenças de poliQ. Os modelos animais para as doenças de poliQ são uma ferramenta essencial no estudo destas doenças devido à sua enorme importância para o desenvolvimento de ensaios terapêuticos mas também para a realização de estudos longitudinais durante a progressão da doença.

No presente estudo, foram gerados modelos transgênicos para uma doença de poliQ, a doença de Machado-Joseph (DMJ) de modo a serem estabelecidos como modelos da doença, para o estudo do seu mecanismo patogénico e para a realização de ensaios terapêuticos. Foi possível estabelecer três modelos da DMJ em ratinho contendo a variante MJD1-1 de cDNA com três diferentes segmentos expandidos de CAGs, com 83, 94 e 135 unidades, respectivamente. A linha transgênica com o menor tamanho de CAG (CMVMJD83) não manifestou a doença mesmo em idades avançadas, enquanto os ratinhos transgênicos CMVMJD94 apresentaram um fenótipo motor ligeiro, presente tanto nos ratinhos hemizigóticos como nos homozigóticos (em concordância com a transmissão autossómica dominante da doença), assim como patologia no sistema nervoso central, apesar da ausência de inclusões neuronais. De salientar que a manifestação do fenótipo motor na linha CMVMJD94 apresentava uma correlação com o tamanho do segmento de CAGs. Com o

aumento do tracto de poliQ para 135 glutaminas na ataxina-3 humana (ATXN3) expressa nos ratinhos transgênicos (CMVMJD135) foi possível obter e estabelecer um modelo animal para a doença com mais sintomas neurológicos da DMJ que surgem de uma forma gradual ao longo da vida do animal, modelando a progressão da doença. De modo a validar a possível importância terapêutica da activação da autofagia na DMJ efectuámos um ensaio terapêutico piloto utilizando lítio e a combinação de lítio e temsirolimus; contudo, não observámos um melhoramento dos sintomas da DMJ no nosso modelo CMVMJD135 com as dosagens utilizadas neste trabalho.

## TABLE OF CONTENTS

---

|   |      |
|---|------|
| Agradecimientos.....  | v    |
| Abstract.....   | vii  |
| Resumo.....   | ix   |
| Abbreviations.....  | xiii |
| <b>Thesis Planning</b> .....  | xv   |
| <b>Chapter 1. Introduction</b> .....  | 1    |
| 1. Neurodegenerative diseases.....  | 3    |
| 1.1 Trinucleotide repeat disorders.....   | 5    |
| 1.2 Polyglutamine (polyQ) diseases: what is similar and what is different?..... | 9    |
| 1.2.1 Protein context in polyQ diseases.....                                    | 10   |
| 1.2.2 Genetic anticipation and repeat instability.....                          | 11   |
| 1.3 Pathogenic mechanism of polyQ diseases.....                                 | 14   |
| 1.3.1 Misfolding and aggregation of mutant polyQ proteins.....                  | 16   |
| 1.3.2 Post-translational modifications of mutant polyQ proteins.....            | 18   |
| 1.3.3 Role of nuclear localization of mutant polyQ proteins.....                | 20   |
| 1.3.4 Neuronal cell death versus neuronal dysfunctions.....                     | 20   |
| 1.3.5 Transcriptional deregulation in polyQ diseases.....                       | 21   |
| 1.4 Therapeutic approaches for polyQ diseases.....                              | 23   |
| 1.5 Machado-Joseph disease (MJD).....   | 26   |
| 1.5.1 Clinical symptoms and progression of MJD.....                             | 27   |
| 1.5.2 MJD neuropathology.....   | 27   |
| 1.5.3 The <i>MJD/ATXN3</i> gene.....  | 30   |
| 1.5.4 The ATXN3 protein(s).....   | 31   |
| 1.6 Animal models for MJD.....  | 33   |
| 1.6.1 MJD knockout model in <i>C.elegans</i> and <i>M. musculus</i> .....       | 33   |

|  |     |
|--|-----|
| 1.6.2 <i>Drosophila melanogaster</i> MJD model .....   | 34  |
| 1.6.3 MJD transgenic mice .....  | 35  |
| 1.7 Aims of the study.....   | 38  |
| 1.8 References .....   | 39  |
| <b>Chapter 2.</b> Motor uncoordination and neuropathology in a transgenic mouse model of Machado-Joseph disease lacking intranuclear inclusions and ataxin-3 cleavage products ..... | 57  |
| <b>Chapter 3.</b> Behavioral and pathological analysis of a novel transgenic mouse model of Machado-Joseph disease expressing full-length ataxin-3 with 135 CAGs.....                | 79  |
| <b>Chapter 4.</b> Autophagy activation as a therapeutic target strategy for MJD: assessment in the CMVMJD135 mouse model .....   | 115 |
| <b>Chapter 5.</b> General Discussion and future perspectives.....  | 137 |
| <b>References</b> .....  | 147 |

## ABBREVIATIONS

---

|  |   |
|--|---|
| µm: Micrometer   | Hsp70: Heat shock protein 70                        |
| ABC: Avidin-Biotin Complex                                 | Htt: Huntingtin Protein                             |
| AD: Alzheimer's Disease                                    | Iba-1: Ionized calcium-binding adapter molecule 1   |
| ALS: Amyotrophic Lateral Sclerosis                         | IHC: Immunohistochemistry                           |
| AR: Androgen Receptor protein                              | JD: Josephin domain                                 |
| ATN1: Atrophia 1   | Kb: kilobase  |
| ATP: Adenosine Triphosphate                                | kDa: kiloDalton                                     |
| ATXN1: Human Ataxin-1 protein                              | KO: Knockout  |
| ATXN3: Human Ataxin-3 protein                              | LCM: Laser-Captured Microdissection                 |
| <i>ATXN3</i> : Human Ataxin-3 gene                         | LRt: Lateral reticular nucleus                      |
| Atxn3: Murine ataxin-3 protein                             | M: molar  |
| BDNF: Brain-derived neurotrophic factor                    | mg: milligram                                       |
| bp: Base pairs   | MI: Moisaicism index                                |
| CAG: Trinucleotide codon encoding glutamine                | Min: minute   |
| CBP: CREB binding protein                                  | MJD: Machado-Joseph Disease                         |
| CCI-779: Cell Cycle inhibitor-779                          | mM: Milimolar                                       |
| CDK5: cyclin dependent kinase 5                            | <i>M. musculus</i> : <i>Mus musculus</i> , mouse    |
| cDNA: complementary DNA                                    | moPrP: mouse prion promoter                         |
| <i>C. elegans</i> : <i>Caenorhabditis elegans</i>          | MPT: mitochondrial membrane permeability transition |
| CMV: cytomegalovirus promoter                              | mRNA: Messenger RNA                                 |
| cm: centimeter   | mTOR: Mammalian target of rapamycin                 |
| CNS: Central nervous system                                | n: Number of animals in the study                   |
| CREB: cyclic AMP-response element binding protein          | NES: Nuclear export signal                          |
| CRM1: Exportin 1   | NI(s): Neuronal inclusion(s)                        |
| DAB: 3,3'-Diaminobenzidine                                 | NII(s): Neuronal intranuclear inclusion(s)          |
| DM: Myotonic Dystrophy                                     | NLS: Nuclear localization signal                    |
| DM1: Myotonic Dystrophy type 1                             | NMDA: N-methyl D-aspartate                          |
| DM2: Myotonic Dystrophy type 2                             | ORF's: Open reading frames                          |
| DNA: Deoxyribonucleic acid                                 | PBS: phosphate-buffered saline                      |
| DRPLA: Dentatorubral-pallidolusian Atrophy                 | pCAF: p300/CBP associated factor                    |
| DUB: Deubiquitylating                                      | PCR: Polymerase Chain Reaction                      |
| EDTA: ethylenediaminetetraacetic acid                      | PD: Parkinson's Disease                             |
| FRAXA: Fragile X syndrome                                  | PEG: polyethylene glycol                            |
| FRDA: Friedreich ataxia                                    | PFA: paraformaldehyde                               |
| GAPDH: Glyceraldehyde 3-phosphate dehydrogenase            | PMSF: phenylmethylsulfonyl fluoride                 |
| GFAP: Glial fibrillary acidic protein                      | PNO: Pontine Nuclei (oral)                          |
| HD: Huntington's Disease                                   | PNV: Pontine Nuclei (ventral)                       |
| <i>Hprt</i> : Hypoxanthine Phosphoribosyl Transferase gene | polyQ: Polyglutamine                                |
| HRP: Horseradish peroxidase                                | Q: Glutamine  |
| HSPs: Heat shock proteins                                  | QB1: PolyQ Binding Peptide 1                        |

|   |  |
|---|--|
| qRT-PCR: quantitative reverse-transcriptase PCR                       | SNP: single-nucleotide polymorphism                                |
| RB: Resuspension buffer   | SP1: Specificity Protein 1   |
| RNA: Ribonucleic acid   | TAFII130: TBP-associated factor                                    |
| RNAi: RNA interference  | TBS: Tris Buffered Saline  |
| rpm: Rotations per minute   | TH: tyrosine hydroxylase   |
| s: seconds  | TRs: Trinucleotide repeats   |
| SAHA: suberoylanilide hydroxamic acid                                 | TSEs: Transmissible Spongiform Encephalopathies                    |
| SB: sodium butyrate   | TUNEL: Terminal deoxynucleotide transferase dUTP Nick End Labeling |
| SBMA: Spinal and bulbar muscular Atrophy                              | Tween 20: polyoxyethylen-sorbitan-monolaurate                      |
| SCA: Spinocerebellar Ataxia   | Ub: ubiquitin  |
| SCA1: Spinocerebellar Ataxia Type 1                                   | UCHs: ubiquitin C-terminal hydrolases                              |
| SCA2: Spinocerebellar Ataxia Type 2                                   | UIMs: ubiquitin interacting motifs                                 |
| SCA3: Spinocerebellar Ataxia Type 3                                   | UPS: Ubiquitin-proteasome pathway                                  |
| SCA6: Spinocerebellar Ataxia Type 6                                   | USP: Ubiquitin-specific cysteine protease                          |
| SCA7: Spinocerebellar Ataxia Type 7                                   | UTRs: Untranslated regions   |
| SCA8: Spinocerebellar Ataxia Type 8                                   | Ve: Vestibular nuclei  |
| SCA10: Spinocerebellar Ataxia Type 10                                 | wt: Wild-type  |
| SCA17: Spinocerebellar Ataxia Type 17                                 | YAC: Yeast Artificial Chromosome                                   |
| SDS-PAGE: Sodium dodecyl sulphate- Polyacrilamide Gel Electrophoresis |  |
| SEM: Standard Error of the Mean                                       |  |
| SN: Substantia Nigra  |  |

## THESIS PLANNING

---

The present dissertation is organized in five different Chapters. Chapter 1 is the General Introduction, the experimental work is presented in Chapter 2 to 4 in the shape of scientific articles (published and in preparation) and Chapter 5 is the general discussion of the work.

In Chapter 1, a general introduction to the theme of this dissertation is presented. An overview about polyQ disease is given, concerning their major similarities and differences as well as their pathological mechanisms. Then, a review of the therapeutic approaches for polyQ diseases is provided, followed by a more extensive presentation about MJD and ataxin-3 with a description of the available animal models.

In Chapter 2, the article *“Motor uncoordination and neuropathology in a transgenic mouse model of Machado-Joseph disease lacking intranuclear inclusions and ataxin-3 cleavage products”*. In this study we have performed the characterization of two transgenic mouse models of MJD (CMVMJD83 and CMVMJD94) including the study of the somatic and intergenerational instability of the CAG repeat, phenotypic and pathological evaluation and the study of the neuroinflammatory profile of the cerebellum of CMVMJD94 mice. CMVMJD94 mice developed mild symptoms and for that reason this model could be useful in the study of the early events in the pathogenesis of MJD.

In Chapter 3, the work *“Behavioral and pathological analysis of a novel transgenic mouse model of Machado-Joseph disease expressing full-length ataxin-3 with 135 CAGs”* shows the behavioral evaluation of transgenic mice carrying 135 CAGs, as well as their pathological evaluation and study of genetic instability. This model displays a more severe phenotype, resembling MJD patients, as well as neuronal inclusions, and for that reason this model could be a powerful tool in the therapeutic field.

Chapter 4, *“Autophagy activation as a therapeutic target strategy for MJD: assessment in the CMVMJD135 mouse model”*, focuses on the treatment of MJD mice with drugs that activate the autophagy pathway, as a therapeutic strategy for MJD.

The General Discussion of the present dissertation, as well as the Future Perspectives, are presented in Chapter 5.





# Chapter 1

---

Introduction



**1. Neurogenerative diseases**

Since the past decades, the population life expectancy has been raised to more advanced ages leading to an increase of the prevalence of neurodegenerative diseases worldwide. For Alzheimer's Disease (AD), the most prevalent of all neurodegenerative disorders, currently affecting 15 million people worldwide, it is expected that the number of affected individuals will be 13.2 million in the United States and 16.2 million in Europe by 2050 (Hebert et al., 2003; Wancata et al., 2003; Forman et al., 2004). This aging-related brain disorders affect abstract thinking, skilled movements, emotional feelings, cognition, memory and other abilities (Martin, 1999). Therefore, the development of effective treatments or preventive interventions for these diseases is crucial, to prevent that their financial, social and emotional implications became astounding. This diverse group of diseases includes AD, Parkinson's disease (PD), Huntington's disease (HD) (and related polyQ disorders including several forms of spinocerebellar ataxia or SCA), transmissible spongiform encephalopathies (TSEs, which includes several human and animal diseases) and Amyotrophic Lateral Sclerosis (ALS) (Soto, 2003) (Table 1). The major hallmark of the mutations in the disease-causing genes is the altered processing and accumulation of misfolded protein in inclusions and/or plaques, although their role in the pathogenesis mechanism is not clear (Figure 1). Another important feature of these disorders is the neuronal population specific vulnerability, which differs in each disease and determines the characteristic clinical symptoms associated with each disorder. For instance, HD patients show neurodegeneration in the striatum leading to uncontrolled movements; whereas in SCA cell loss occurs mainly in the cerebellum, inducing ataxia. In AD patients, cerebral damage occurs mainly in the hippocampus, entorhinal cortex and neocortex causing dementia. In PD patients, cells of the substantia nigra degenerate, resulting in rigidity and tremor. Finally, in ALS, the progressive paralysis observed in the patients comes from the cellular damage in the spinal cord, brainstem and areas of the motor cortex. As expected, this association between affected cellular populations and clinical symptoms is more evident in early stages of the disease, when damage is less extensive.

Despite the effort of many towards the understanding of the pathogenic mechanism that lead to neuronal degeneration, it is still unclear what are the molecular pathways that ultimately lead to neuronal cell death in these disorders. For this reason, several animal models have been established in order to further characterize genes and pathways that are involved in the process of neurodegeneration. This thesis will focus on a polyQ disease, MJD or SCA3 (Spinocerebellar Ataxia

## Chapter 1. Introduction

type 3), namely on the establishment of a new transgenic mouse model and the study of the molecular pathogenesis of MJD.

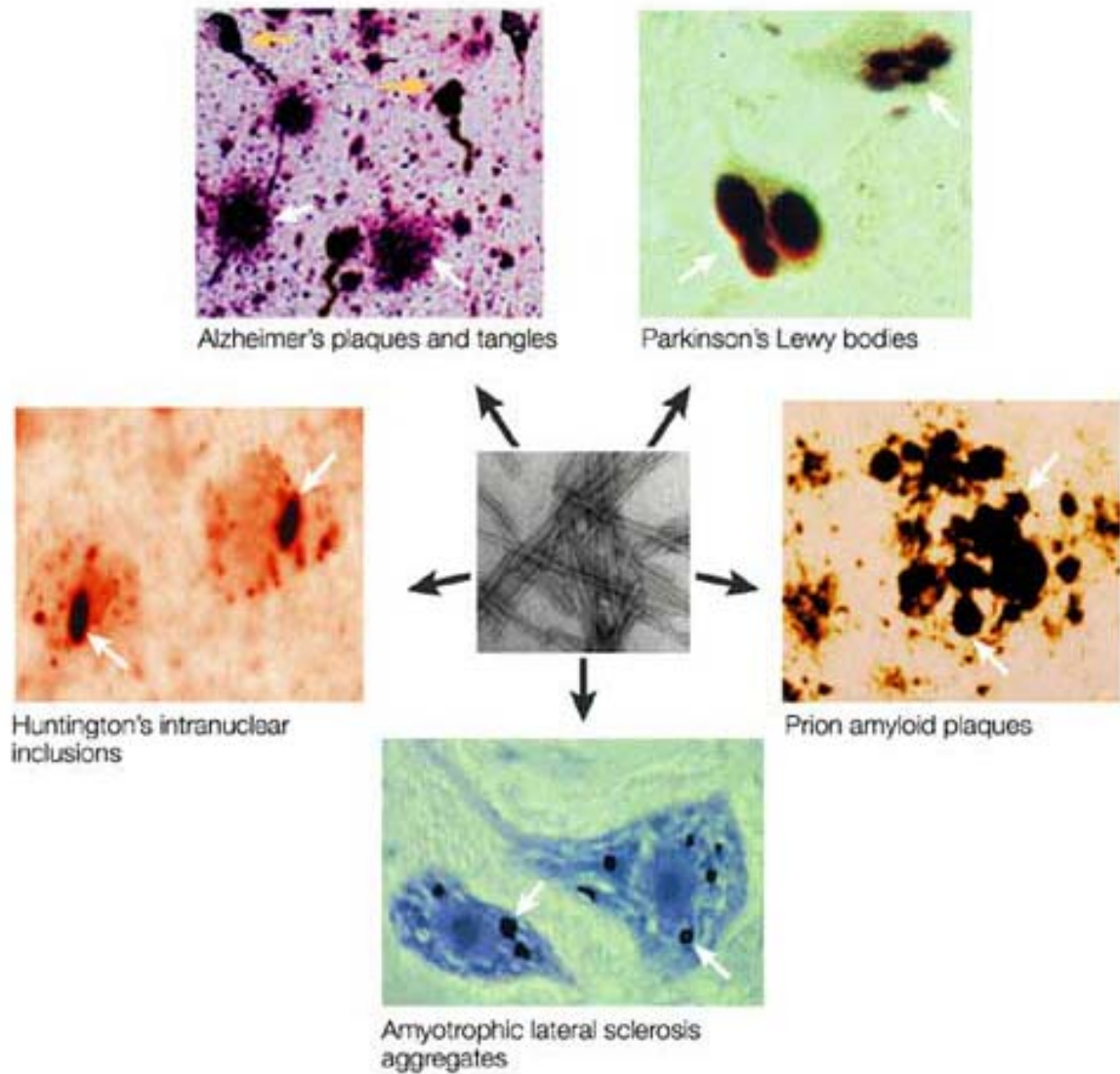


**Figure 1.** Cerebral aggregates in neurodegenerative diseases. Examples of protein aggregates present in a variety of neurodegenerative diseases are demonstrated. Extra cellular amyloid plaques (white arrows) and intra-cytoplasmic neurofibrillary tangles (yellow arrows) are characteristic of AD, while in PD and ALS patients usually present intra-cytoplasmic aggregates. Intranuclear inclusions of huntingtin are observed in HD patients and extracellular prion amyloid plaques that are located in different brain regions are present in some cases of transmissible spongiform encephalopathy. In spite of the different protein compositions, the ultrastructure of these deposits seems to be similar and composed mainly of a network of fibrillar polymers (centre). (Soto, 2003)

**Table 1.** Neurodegenerative diseases characterized by accumulation of aggregated proteins

| Toxic protein                  | Protein deposit                     | Familial disease                             | Gene mutated   | Sporadic disease                            | Risk factor                                       |
|--------------------------------|-------------------------------------|--|--|---|---|
| B-amyloid                      | Senile plaques                      | FAD  | <i>APP</i><br><i>PS1</i><br><i>PS2</i>                       | Alzheimer disease                           | <i>ApoE4</i>                                      |
| Tau                            | Neuronal and glial inclusions       | FTDP-17 inclusions                           | <i>MAPT</i>  | AD and tauopathies <sup>a</sup>             | <i>MAPT</i> haplotype                             |
| α-synuclein                    | Lewy bodies<br>Lewy neurites        | Familial Parkinson Disease (PD) <sup>b</sup> | SNCA (α-synuclein)   | Lewy body disease <sup>c</sup>              | <i>SNCA</i> polymorphism<br><i>MAPT</i> haplotype |
|                                | Glial cytoplasmic inclusions        | Not identified                               | Not applicable   | Multiple system atrophy                     | Not identified                                    |
| Polyglutamine repeat expansion | Nuclear and cytoplasmic inclusions  | Huntington disease                           | <i>HD</i> (Huntintin)  | Not applicable                              | Not identified                                    |
|                                |                                     | Kennedy disease                              | <i>AR</i> (androgen receptor)                                |   |   |
|                                |                                     | DRPLA  | <i>DRPLA</i> (atrophin-1)                                    |   |   |
|                                |                                     | SCA1   | <i>ATXN1</i> (ataxin-1)                                      |   |   |
|                                |                                     | SCA2   | <i>ATXN2</i> (ataxin-2)                                      |   |   |
|                                |                                     | SCA3   | <i>ATXN3</i> (ataxin-3)                                      |   |   |
|                                |                                     | SCA6   | <i>CACNA1</i> <sup>d</sup>                                   |   |   |
|                                |                                     | SCA7<br>SCA17                                | <i>ATXN7</i> (ataxin-7)<br><i>TBP</i> (TATA binding protein) |   |   |
| PrP <sup>SC</sup>              | Protease-resistant PrP <sup>E</sup> | Familial prion protein disease <sup>f</sup>  | <i>PRNP</i>  | Sporadic prion protein disease <sup>g</sup> | PRNP polymorphism                                 |
| SOD                            | Hyaline inclusions                  | Autosomal dominant familial ALS              | SOD1 (Cu/Zn SOD)   | Sporadic ALS                                | Not identified                                    |
| ABri/ADan                      | Amyloid plaques and angiopathy      | Familial British/Danish dementia             | BRI  | Not identified                              | Not identified                                    |
| Neuroserpin                    | Collins bodies                      | FENIB <sup>h</sup>                           | SERPINI 1 (neuroserpin)                                      | Not identified                              | Not identified                                    |

<sup>a</sup> Tauopathies: Pick Disease (PiD), corticobasal degeneration and progressive supranuclear palsy. <sup>b</sup> Four additional genes are implicated in familial PD including *PARK2*, *UCHL1*, *DJI* and *PINK1*. However, it is unclear if these genes are associated with Lewy Body (LB) pathology. <sup>c</sup> Lewy body diseases: PD and Dementia with Lewy Bodies (DLB). <sup>d</sup> CACNA1A encodes the α(1A) subunit of voltage-gated calcium channel, type P/Q. <sup>e</sup> Detected by immunohistochemistry or biochemically after digestion with proteinase K. <sup>f</sup> Familial prion protein disease: familial Creutzfeldt-Jakob Disease (CJD), Gerstmann-Scheinker disease and fatal familial insomnia. <sup>g</sup> Sporadic prion protein disease: CJD, variant CJD, iatrogenic CJD and kuru. <sup>h</sup> Familial encephalopathy with neuroserpin inclusion bodies (Forman et al., 2004).

### 1.1. Trinucleotide repeat disorders

Since the first descriptions (Fu et al., 1991; La Spada et al., 1991), 17 neurological disorders have been characterized based upon the presence of an unstable and abnormal expansions of trinucleotide repeats (TRs), that in the majority of these group is a CNG motif (N=G, A or T) with the exception of Friedreich ataxia, that is related with a (GAA)<sub>n</sub> repeat and polyalanine disorders that are associated with a (GCG)<sub>n</sub> motif (Table 2). In normal (wild-type) alleles, these TRs are also polymorphic, with repeat tracts that range from a few to nearly 40 repeat units. The presence of an expanded allele, with a size that exceeds the normal range, leads to expression of the disease phenotype. The variability in repeat size underlies the broad spectrum of phenotypes observed in each of these disorders (Orr and Zoghbi, 2007).

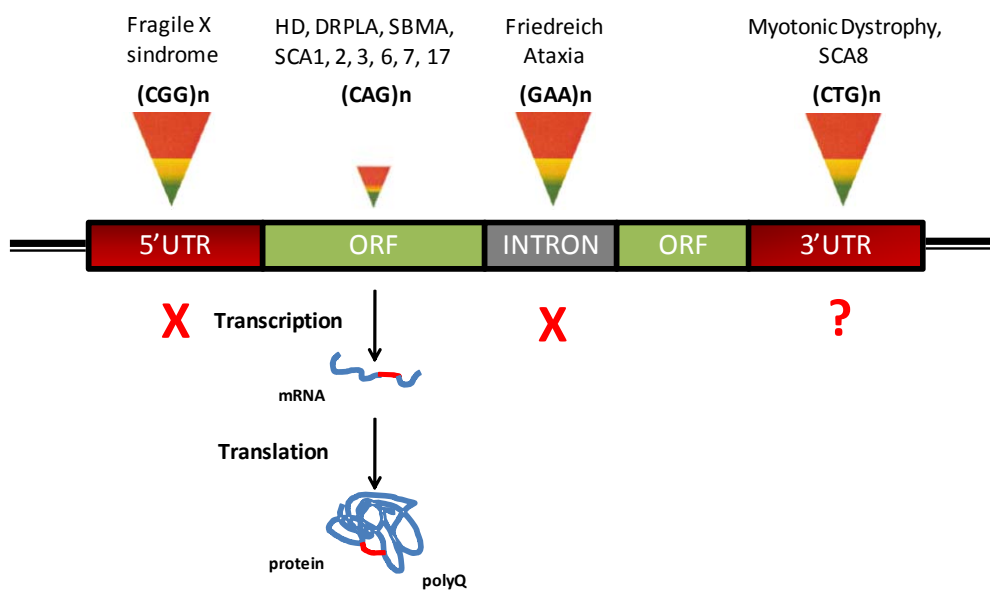


**Figure 2.** Schematic representation of repeat expansion disorders showing the gene location of the disease-causing mutations. The green area of each triangle represents the number of repeats in normal individuals, the yellow area the repeat number in individuals at risk for transmission of the disorder (carriers of ‘premutation’ alleles), and the red area the number of repeats in clinically affected patients. The repeat unit associated with each disorder is shown above the triangles. HD, Huntington’s disease; SCA, spinocerebellar ataxia; DRPLA, dentatorubral pallidoluysian atrophy; SBMA, spinal and bulbar muscular atrophy. The effect of the expansion on transcription and translation, where known, is shown schematically at the bottom of the figure. The red crosses indicate the step affected by the expansion. The expansions in the ORF’s (Open Reading Frames) are transcribed and translated into proteins containing expanded polyQ protein tracts. Adapted from (Usdin and Grabczyk, 2000).

Triplet repeats could be located at different regions of the gene (Figure 2), leading to the classification in two categories:

- disorders with non-coding repeat sequences**- these disorders result from expansion of a repeat sequence in untranslated regions namely the 3’, 5’-UTRs and intronic regions. This class of disorders displays several common features, specifically the multisystem involvement and the degeneration of many different tissues, resulting in the manifestation of multiple phenotypes for the same disorder. Moreover, the length and variation of the triplet repeat (CAG, CTG, CGG, CGG or GAA) are larger when compared with disorders with coding repeats (up to several thousand repeats).

- **disorders with coding repeat sequences (exonic)**- these disorders result from expansion of an exonic CAG trinucleotide repeat which is transcribed and translated into a polyQ tract within a protein (Di Prospero and Fischbeck, 2005). Although these disorders are clinically heterogeneous and caused by proteins with no homologies except for the polyQ tract, the similarities among these disorders suggests a common pathogenic mechanism triggering neurodegeneration (Gusella and MacDonald, 2000).

In addition, TRs disorders have been divided according to their pathogenic mechanism that can be loss of function of the protein, gain of function of the RNA or protein, or not determined so far (Table 2). Although expanded trinucleotide repeats are the most common repeats causing neurological disease, other repeats expansions such as tetra- and pentanucleotides are responsible for type 2 myotonic dystrophy (DM2) and Spinocerebellar Ataxia Type 10 (SCA10), respectively.



## Chapter 1. Introduction

**Table 2.** Molecular and clinical features of trinucleotide repeat expansion disorders

| Disease (acronym)  | MIM    | Gene product   | Putative protein function            | Repeat unit/location  | Repeat range |                       | Main clinical features  |
|--|--------|--|--------------------------------------|---|--------------|-----------------------|---|
|  |        |  |                                      |   | Normal       | Pathogenic            |   |
| <i>Disease caused by a gain-of-function mechanism</i>          |        |  |                                      |   |              |                       |   |
| Spinocerebellar ataxia type 1 (SCA1)                           | 164400 | Ataxin-1 (ATXN1)   | Transcription                        | (CAG) <sub>n</sub> /exon 8  | 6-38         | 39-82                 | Ataxia, slurred speech, spasticity, cognitive impairments   |
| Spinocerebellar ataxia type 2 (SCA2)                           | 183090 | Ataxin-2 (ATXN2)   | RNA metabolism                       | (CAG) <sub>n</sub> /exon 1  | 15-24        | 35-200                | Ataxia, slow saccades, decreases reflexes, polyneuropathy, motor neuropathy, infantile variant  |
| Machado-Joseph disease or Spinocerebellar ataxia type 3 (SCA3) | 109150 | Ataxin-3 (ATXN3)   | De-ubiquitylating activity           | (CAG) <sub>n</sub> /exon 10   | 12-44        | 52-86                 | Ataxia, ophthalmoplegia, severe spasticity  |
| Spinocerebellar ataxia type 6 (SCA6)                           | 183086 | α1A subunit of the neuronal P/Q-type voltage-gated calcium channel (CACNA1A) | Calcium channel subunit              | (CAG) <sub>n</sub> /exon 47   | 4-18         | 19-33                 | Ataxia, dysarthria, nystagmus, tremor   |
| Spinocerebellar ataxia type 7 (SCA7)                           | 164500 | Ataxin-7 (ATXN7)   | Transcription                        | (CAG) <sub>n</sub> /exon 3  | 4-27         | 37->200               | Ataxia, retinal degeneration, cardiac involvement in infantile variant  |
| Spinocerebellar ataxia type 17 (SCA17)                         | 607136 | TATA-binding protein (TBP)   | Transcription                        | CAG/CAA repeat/exon 3   | 25-42        | 45-63                 | Ataxia, behavioral changes or psychosis, intellectual deterioration, seizures   |
| Dentatorubropallydollysian atrophy (DRPLA)                     | 125370 | Atrophin-1 (ATN1)  | Transcription regulator              | (CAG) <sub>n</sub> /exon 5  | 6-34         | 49-88                 | Ataxia, epilepsy, choreoathetosis, dementia   |
| Spinal and bulbar muscular atrophy (SBMA; Kennedy disease)     | 313200 | Androgen receptor (AR)   | Steroid-hormone receptor             | (CAG) <sub>n</sub> /exon 1  | 9-36         | 38-62                 | Motor weakness, swallowing difficulty, gynecomastia, hypogonadism   |
| Huntington disease (HD)  | 143100 | Huntingtin (Htt)   | Signalling, transport, transcription | (CAG) <sub>n</sub> /exon 1  | 6-34         | 36-121                | Severe movement abnormalities, chorea, dystonia, cognitive decline, psychiatric features  |
| <i>Disease caused by a loss-of-function mechanism</i>          |        |  |                                      |   |              |                       |   |
| Friedreich ataxia (FRDA)                                       | 229300 | Frataxina  | Mitochondrial iron metabolism        | (GAA) <sub>n</sub> /intron 1  | 6-32         | 200-1700              | Sensory ataxia, cardiomyopathy, diabetes  |
| Fragile X syndrome (FRAXA)                                     | 309550 | FMRP   | Translational regulation             | (CGG) <sub>n</sub> /5'UTR   | 6-60         | >200 (full mutation)  | Mental retardation, macroorchidism, connective tissue dysplasia, attentional and behavioral abnormalities   |
| Fragile XE syndrome (FRAXE)                                    | 309548 | FMR2   | Transcription?                       | (CCG) <sub>n</sub> /5'UTR   | 4-39         | 200-900               | Mild mental retardation or learning impairment  |
| <i>Disease caused by a RNA-mediated mechanism</i>              |        |  |                                      |   |              |                       |   |
| Myotonic dystrophy type 1 (DM1)                                | 160900 | DMPK (serine/threonine kinase)   | RNA-mediated                         | (CTG) <sub>n</sub> /3'UTR   | 5-37         | 50-10,000             | Myotonia, weakness, wasting, cardiac conduction abnormalities, testicular atrophy, insulin resistance, cataracts, congenital form, potentially severe CNS involvement with mental retardation |
| Fragile X-associated tremor ataxia syndrome (FXTAS)            | 309550 | FMR1 RNA   | RNA-mediated                         | (CGG) <sub>n</sub> /5'UTR   | 6-60         | 60-200 (pre-mutation) | Tremor/ataxia, parkinsonism, cognitive defects  |
| <i>Disease caused by a mechanism not well understood</i>       |        |  |                                      |   |              |                       |   |
| Spinocerebellar ataxia type 8 (SCA8)                           | 608768 | SCA8 RNA, polyQ peptide?   | Unknown                              | (CTG) <sub>n</sub> /3-prime terminal exon                                 | 16-34        | >74                   | Ataxia, slurred speech, nystagmus   |
| Spinocerebellar ataxia type 8 (SCA12)                          | 603516 | PPP2R2B (regulatory subunit of phosphatase PP2A)                             | Phosphatase regulation               | (CAG) <sub>n</sub> /5'UTR   | 7-45         | 55-78                 | Ataxia and seizures   |
| Hungtinton disease-like 2 (HDLA2)                              | 606438 | Junctophilin   | PM/ER junction protein               | (CTG) <sub>n</sub> /splice acceptor site of na alternatively spliced exon | 7-28         | 66-78                 | Similar to HD   |

Note: In SCA1 alleles  $\geq 21$  CAG repeats are interrupted with 1-2 CAT units, while disease-causing alleles are pure (CAG)<sub>n</sub>. Adapted from (Orr and Zoghbi, 2007)

## 1.2. PolyQ diseases: what is similar and what is different?

Expansion of CAG trinucleotide repeat within the coding region of several genes results in the production of proteins with expanded polyQ stretch. The first disease connected with the expansion of a CAG repeat and causing progressive motor neuron degeneration was spinal bulbar muscular atrophy (SBMA) (La Spada et al., 1991). Eight other disorders including HD, dentatorubropallidoluysian atrophy (DRPLA), and six types of spinocerebellar ataxia (SCA1, 2, 3, 6, 7, and 17) (Orr and Zoghbi, 2007) have since been identified as associated with polyQ expansions (Table 2).

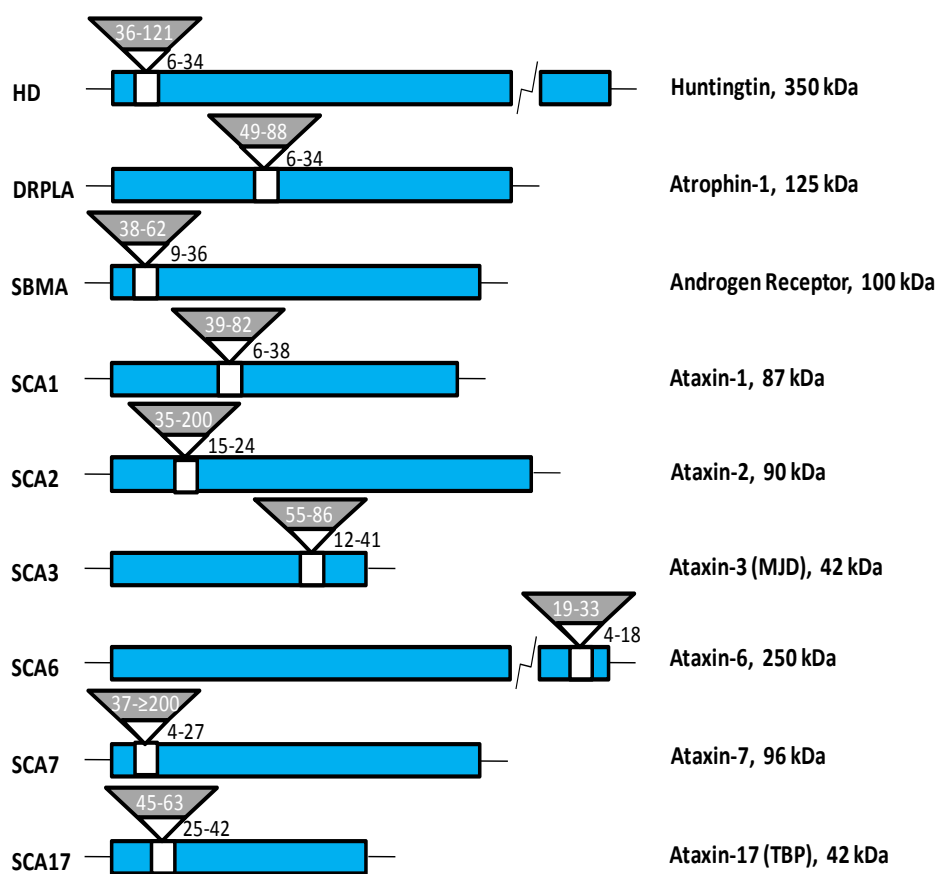


**Figure 3.** Schematic representation of the different polyQ disease genes with the normal and expanded CAG repeat number. Adapted from (Marsh et al., 2009).

The most common polyQ diseases worldwide are HD and SCA3 (Schols et al., 2004), but the incidence of these disorders differs between regions. All of these are dominantly inherited in an autosomal manner with the exception of SBMA, which is X-linked. In all cases, the disease only occurs when the glutamine expansions exceed a certain threshold (Ross, 1997). Although the disease-causing proteins are ubiquitously expressed in the Central Nervous System (CNS) and in the

## Chapter 1. Introduction

peripheral tissues, each polyQ disease is characterized by the specific loss of neuronal populations resulting in characteristic patterns of neurodegeneration and clinical manifestations. This suggests that probably certain specific cellular conditions exist in vulnerable neurons that may cause the selective cytotoxicity by their gene products. All are progressive, ultimately fatal disorders that typically begin in adulthood and progress over 10 to 30 years. Although polyQ disorders are rare diseases they are particularly delicate because normally the disease is manifested later in life, after having children.

### 1.2.1. Protein context in polyQ diseases

To date, the normal function of many of the genes causing polyQ disorders remains unclear and apart from the polyQ tract, these proteins share no homologies, are unrelated to each other, vary in size and contain the glutamine segment at distinct locations within the protein sequence (Figure 3). Although each of these CAG repeat disorders has characteristic clinical symptoms and neuropathology, some similarities could be observed suggesting a common molecular mechanism underlies these disorders (Cha and Dure, 1994): (1) for each of these progressive late-onset neurological disorders, the CAG repeat codes for a polyQ stretch; (2) the disease phenotypes are usually observed when the number of glutamines exceeds  $\sim 35-45$ . However, in the case of SCA6, the pathological threshold is  $\sim 20$  repeats, and in SCA3 it is closer to 55-60 repeats (Shao and Diamond, 2007); (3) the CAG repeat size correlates well with the age-at-onset in each disease: patients with a longer CAG repeat tend to demonstrate an earlier onset of symptoms (Gusella and MacDonald, 2000); (4) neuronal intranuclear inclusions (NIIs) that contain the polyQ portion of the disease protein are found in patient material and transgenic models of the disorders (Davies et al., 1998).

The creation of a transgenic mouse expressing an expanded CAG tract into a novel genetic context (HPRT locus) displaying several common features of the polyQ disorders of humans (late-onset progressive neurological symptoms and NIIs) has demonstrated that CAG-polyQ repeats do not need to reside in one of the classic repeat disorder genes to have neurotoxic effect (Ordway et al., 1997). The expression of a simple polyQ tract, in the absence of any additional protein context is also toxic, as shown in cell culture, *Mus musculus*, *Drosophila melanogaster* and *C. elegans* (Ikeda et al., 1996; Marsh et al., 2000; Morley et al., 2002; Brignull et al., 2006). However, some studies pointed to the importance of post-transcriptional modifications outside the polyQ expansion in determining the clinical and pathological effects of polyQ tracts and gives to the protein context an

important role in pathogenesis (Chen et al., 2003; Emamian et al., 2003; Steffan et al., 2004), (Zoghbi, 1996; Orr and Zoghbi, 2001; Humbert and Saudou, 2002; Gatchel and Zoghbi, 2005). Despite the existence of common mechanism among polyQ diseases, that raise the possibility of conserved pathogenic mechanisms, the striking differences in clinical and pathological features also suggest disease specific pathogenesis.

### **1.2.2. Genetic anticipation and repeat instability**

Unlike classic mutations, which are stably transmitted to the offspring and retained in somatic tissues, repeat mutations are dynamic, where products continue to mutate within the tissues and along generations (Pearson et al., 2005; Mirkin, 2007). It has been demonstrated that, at least in the case of diseases caused by expansions of (CAG)<sub>n</sub> repeats, there is an inverse correlation between the size of the expanded alleles and the age-at-onset (Gusella and MacDonald, 2000). The expanded CAG repeats may expand or contract, but more often their instability manifests through expansion of the polyQ tract (Duyao et al., 1993). This causes earlier age-at-onset and increased severity of the symptoms in successive generations, a phenomenon that was called anticipation. This phenomenon was first described in 1918 by Fleischer in myotonic dystrophy (DM) patients (Fleischer, 1918). Moreover, an earlier onset and more severe disease phenotype has been described in homozygous MJD patients, suggesting that gene dosage is an important determinant of age-at-onset and clinical symptoms (Lang et al., 1994; Lerer et al., 1996; Sobue et al., 1996). DNA repeats are particularly prone to this type of instability due to their unusual structural features that tend to disrupt cellular replication, repair and recombination machineries (Mirkin, 2007). Although normal alleles are relatively stable during germline transmission, mutant expanded alleles change in size in the majority of parent-descendent transmission, known as repeat instability. While a paternal expansion bias has been described for most polyQ disorders, in Fragile X syndrome (FRAXA) and Myotonic dystrophy type 1 (DM1) a bias towards expansion is observed in maternal transmissions. Furthermore, a paternal contraction bias also has been found for expanded repeats in patients with SCA8, FRDA and FRAXA (Pearson et al., 2005). Repeat instability appears to be more frequent and stronger when transmission occurs through a male than through a female, and expansions, rather than contractions, tend to occur frequently. The simplest explanation to what properties of the repeats contribute to the propensity to expand is that the repetitive nature of these expandable elements leads to an occasional strand slippage during DNA replication (Mirkin, 2006). However this theory does not explain many of the features observed, including why not every repeat expands. It is,

therefore, more likely that the mechanisms leading to repeat instability include not only DNA replication, but also DNA recombination, DNA repair or other (Pearson et al., 2005).

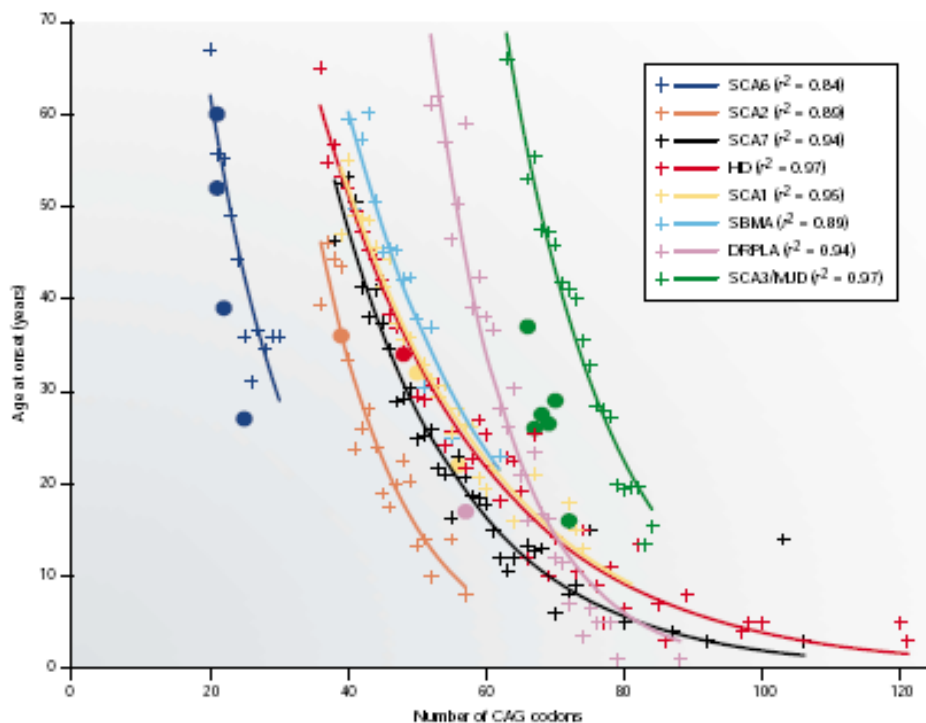


**Figure 4.** Correlation curves between age-at-onset and number of CAG repeats number for the different polyQ disease. (Gusella and MacDonald, 2000).

Besides the meiotic instability, tissue-specific somatic mosaicism has been observed in many polyQ diseases resulting in populations of cells, within or between tissues, carrying different repeat lengths. The analysis of repeat instability in the CNS for various disease loci has revealed crucial insights into the roles of *cis*-elements, *trans*factors and genome-maintenance repair. Although DNA replication contribution in CNS repeat instability is possible, it is unlikely to be the most important causative mechanism. Indeed, non-replication processes must be involved because repeat length varies in brains of numerous CAG transgenic mice (Lia et al., 1998; Sato et al., 1999; Fortune et al., 2000; van den Broek et al., 2002; Watase et al., 2003; Wheeler et al., 2003) and repeat instability was seen in one GAA mouse after the postnatal ‘brain growth spurt’ (Al-Mahdawi et al., 2004). Interestingly, several mouse models of polyQ diseases have demonstrated age-dependent somatic instability in brain (Sato et al., 1999; Kennedy et al., 2003), further supporting a role for genome-maintenance repair in repeat instability during aging.

Studies in humans and in mouse models have revealed that most of the polyQ disease genes display some similarities in their instability pattern across brain subregions (for example, the longest tracts are in the striatum or cerebrum, the shortest are in the cerebellum), which possibly reflects the developmental history of each subdivision (Chong et al., 1995; Lopes-Cendes et al., 1996; Hashida et al., 1997). However, not all CAG/CTG disease loci share tissue-specific patterns of instability. For example, distinct brain region instability patterns occur between DRPLA and other polyQ diseases (Hashida et al., 1997). In contrast with the neuronal instability observed in most polyQ disorders, SBMA polyQ tract length is stable in the CNS. Similarly, the high degree of instability in the muscle of patients who have SBMA, contrasts with the lowest instability in muscle seen in HD and DRPLA (Takano et al., 1996; Ansved et al., 1998; Tanaka et al., 1999).

Although inter-region length variations are common, there is only limited CAG-length heterogeneity within a single brain region. Analysis of individual cell types in the brains of DRPLA patients using laser-capture microdissection (LCM) has revealed different degrees of length heterogeneity between neuronal subtypes, with tracts that are shorter and longer than those in the blood (Watanabe et al., 2000; Hashida et al., 2001). Cerebellar granular cells had shorter CAG tracts and the lengths were less variable than in Purkinje cells or cerebral neuronal cells. Glial cells showed more CAG instability than neurons, which indicates that proliferation, at least in glia, might contribute to instability. Together, these variations in the pattern of repeat instability indicate that, in addition to tissue-specific or cell-specific trans-factors, gene-specific cis-elements also modulate the degree and pattern of repeat instability in the CNS.

In contrast to DM1, in which higher differences of repeat number was observed between the affected tissue (muscle) and blood with a marked increase with age, there is no clear understanding of the contribution of the somatic instability to the neurodegenerative polyQ diseases. So far, the majority of the studies performed to correlate repeat instability in the CNS with the pathological involvement of vulnerable brain regions (Lopes-Cendes et al., 1996; Maciel et al., 1997; Cancel et al., 1998; Watase et al., 2003) have shown slight repeat length variations (1-23 repeats), with only rare examples of individual cells having incurred large expansions (1000 repeats) (Kennedy et al., 2003). These results indicate that somatic instability probably does not have an important role in the cell-specific vulnerability observed in these disorders. However, in most of these studies CAG analyses were performed in post-mortem tissues or at advanced ages, increasing the possibility that cells carrying the largest expansions were no longer available for CAG-length analysis (Kennedy et al.,

2003). Animal models provide a good opportunity to study the phenomenon of somatic mosaicism in a longitudinal manner, starting before disease onset and in parallel with disease progression.

### 1.3. Pathogenic mechanism of polyQ diseases

PolyQ diseases are characterized clinically by the constant progression of the symptoms and molecularly, by the accumulation of mutant proteins inside neurons causing their dysfunction and eventually death. However, the mechanism that leads to neuronal degeneration and cell demise is still unknown. The most supported and well-accepted idea is that polyQ disorders are caused by “gain of toxic function” mechanisms induced by the expanded polyQ tract itself. Evidence supporting this notion comes from different observations: (1) Mice models that lack the disease protein, for example, ataxin-3 (ATXN3) or Huntingtin (Htt) (in the case of MJD and HD, respectively), are viable and fertile but do not display the characteristic MJD and HD clinical or neuropathological phenotypes (Duyao et al., 1995; Schmitt et al., 2007). On the contrary, the overexpression of the human protein with the CAG expansion leads to cell loss and characteristic neurodegenerative phenotypes even in the presence of the two copies of the mouse gene (Burrigh et al., 1995; Mangiarini et al., 1996; Cemal et al., 2002; Marsh et al., 2009); (2) The levels of wild-type and mutant protein are equivalent in human patients for several polyQ disorders (Sisodia, 1998), i.e. the mutation does not affect the expression levels of the protein; (3) The expression of the polyQ tract alone or in the context of an unrelated gene in animals models leads to the manifestation of neurological symptoms (Ikeda et al., 1996; Ordway et al., 1997; Marsh et al., 2000). Nevertheless, the dominance is not pure as homozygous individuals present a more severe clinical phenotype than individuals that carry only one mutated allele (Wexler et al., 1987; Lerer et al., 1996; Sobue et al., 1996). More recently, it has been proposed that although an important component of the pathology comes from a gain of function of the disease-causing protein, in some cases the loss of function of the normal gene contribute to disease (Orr and Zoghbi, 2007).

Many of the polyQ genes are ubiquitously expressed within and outside the CNS, including cells that do not degenerate. It is possible that some of the clinical symptoms arise from aberrant function(s) of the mutant polyQ proteins in tissues that do not degenerate. In fact, the ubiquitin–proteasome pathway appears to be perturbed before and after the onset of neurodegeneration in the skin and the brain of patients with HD (Seo et al., 2004). Moreover, non-neural HD cells (fibroblast cultures established from the R6/2 HD mouse model) have a progressive pathology, including

dysmorphic cells with aberrant nuclear morphology, multiple micronuclei, large vacuoles, numerous centrosomes, reduced mitotic index and increased aneuploidy (Sathasivam et al., 2001). Considering the prolonged disease course of many of the illnesses, it is likely that the neurons experience long periods of neuronal dysfunction before cell death. PolyQ expansions can selectively induce transcriptome alterations that can lead to neural dysfunction before degeneration (Lin et al., 2000). In fact, some patients with HD and transgenic mice with expanded polyQ show neurological symptoms in the absence of neurodegeneration (Xuereb et al., 1996; Mizuno et al., 2000; Adachi et al., 2001; Caramins et al., 2003).

There are several evidences supporting the role of protein context in polyQ toxicity. From the correlation curves of different polyQ diseases, is possible to observe that the same number of expanded glutamines placed in different protein context induce different age-at-onset which means that the protein context have a role in the protein toxicity (Figure 4). The creation of animal and cellular models with the full-length and truncated forms of the expanded protein has also demonstrated that the protein context, and not solely the polyQ tract, could modulate the disease progression and mediate the selective vulnerability associated with each different polyQ disease (Reddy et al., 1998). In the case of HD, although the transgenic mouse expressing a truncated fragment of Htt with the polyQ tract could recapitulate some elements of the disease phenotype (Mangiarini et al., 1996; Mangiarini et al., 1997) the (perhaps) most critical biological feature, neuronal degeneration, could only be observed when a full-length mutant Htt was expressed (Reddy et al., 1998). In addition, post-transcriptional modifications outside of the polyQ tract have been shown to be critical in determining the clinical and pathological effects of the corresponding proteins (Zoghbi, 1996; Orr, 2001; Humbert et al., 2002; Humbert and Saudou, 2002; Chen et al., 2003; Emamian et al., 2003; Steffan et al., 2004; de Chiara et al., 2005; Gatchel and Zoghbi, 2005; Riley et al., 2005; Tsuda et al., 2005). Identification of the key modifications in this context is of great relevance for the design of therapeutic strategies.

There are disease mechanisms that are likely to be common to all polyQ diseases (Figure 5). For example, protein misfolding and impairment in protein turnover have been implicated in all of these disorders (Sisodia, 1998; Orr, 2001; Humbert and Saudou, 2002; Soto, 2003; Everett and Wood, 2004; Ghosh and Feany, 2004; Riley and Orr, 2006). Accumulation of mutant polyQ protein in insoluble inclusions has been proposed to lead to the recruitment of components of the ubiquitin–proteasome system (UPS) and other protein quality-control pathways, although the implications of this recruitment for pathogenesis of polyQ diseases are unclear. Other mechanisms, such as altered



## Chapter 1. Introduction

gene expression, RNA processing, synaptic transmission, calcium homeostasis, axonal transport defects, cytoskeletal abnormalities and dysfunction or endoplasmic reticulum impairment have been implicated in the pathogenesis of one or more of these disorders (Everett and Wood, 2004; Hoshino et al., 2004). One important aspect is that several of the full-length polyQ proteins can also be cleaved by proteases to form fragments (Goldberg et al., 1996; Kobayashi et al., 1998; Wellington et al., 1998; Berke et al., 2004; Goti et al., 2004), which some authors propose are mediating pathogenic effects. However, the relevance of each of these events to pathogenesis in each disease has not been clarified yet.

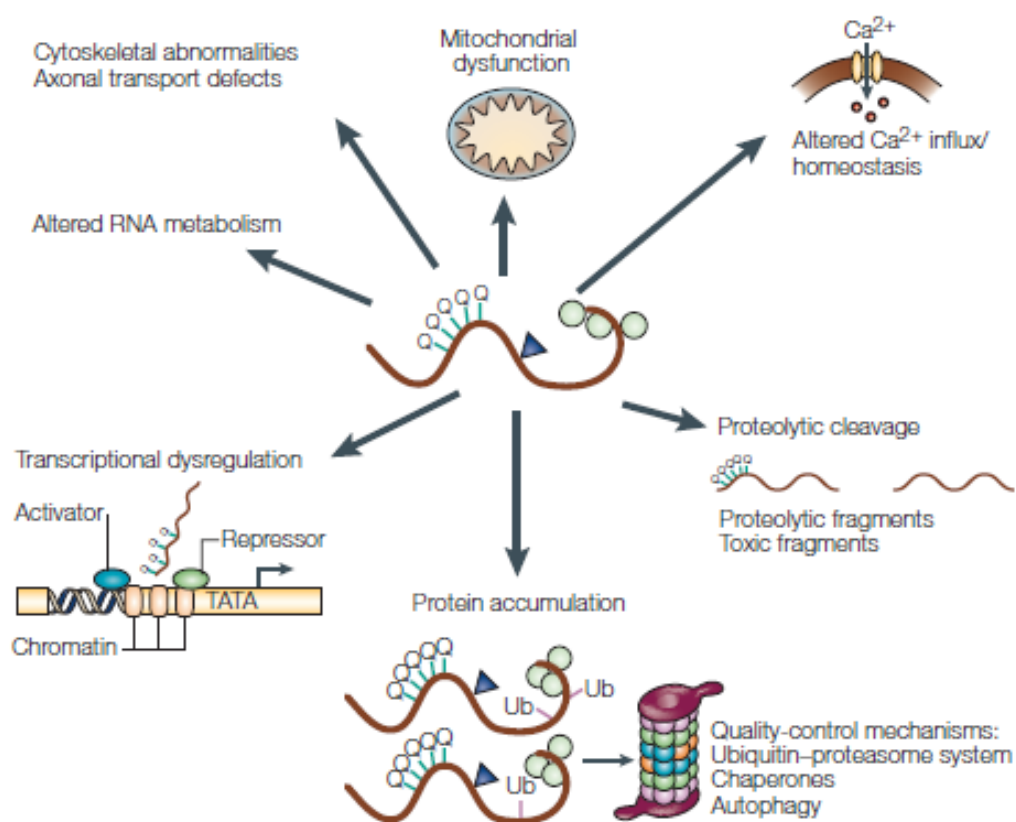


**Figure 5.** Possible mechanisms of pathogenesis in polyQ diseases. Expanded polyQ proteins might induce toxicity through a variety of mechanisms that range from altered transcription and RNA metabolism, mitochondrial dysfunction, proteolytic cleavage and protein accumulation in the cells. HDACs, histone deacetylases; Q, glutamine; Ub, ubiquitin. (Gatchel and Zoghbi, 2005).

### 1.3.1. Misfolding and aggregation of mutant polyQ proteins

An important pathological feature in most of these diseases is the misfolding of the expanded protein, leading to the accumulation of aggregated polyQ proteins in neurons, usually

termed NIs (Davies et al., 1997; DiFiglia et al., 1997). Besides the mutant polyQ protein these inclusions contain other proteins such as ubiquitin (Ub), chaperones and proteasome subunits (Zoghbi and Botas, 2002) as well as transcription activators or co-activators (Steffan et al., 2000; Nucifora et al., 2001; Dunah et al., 2002). The location of mutant protein aggregates can be mainly nuclear, as in the NIs which are present in SCA1, SCA7 and SCA17, or it can also be cytoplasmic, such as in SCA6, or present in both cytoplasm and nucleus as in HD, DRPLA, SBMA, SCA2 and SCA3 (Gatchel and Zoghbi, 2005; Al-Ramahi et al., 2007; Heng et al., 2010; Seidel et al., 2010). Although NIs are observed both in patients and in mouse models of these diseases their role in the pathogenesis mechanism is controversial, because it is not clear if the toxicity of the expanded polyQ proteins comes from the presence of visible inclusions or from smaller intermediate species produced during the aggregation process.

Since the detection of the NIs in the brains of patients the major idea was that NIs are pathogenic as they may sequester proteasome subunits, Ub, chaperones and even the wild-type proteins interfering with their normal function (Paulson et al., 1997b; Stenoien et al., 1999; Chai et al., 2001). In the case of SBMA, inclusions have been clearly associated with neuronal death, being specifically located in affected motor neurons in the spinal cord and brainstem (Apostolinas et al., 1999). On the other hand, studies have been demonstrated a discrepancy between the presence of these structures and the areas where severe loss is observed. In fact, for several polyQ diseases such as HD, SCA7 and SCA17, inclusions were detected in spared regions (Becher et al., 1998; Holmberg et al., 1998; Rolfs et al., 2003), whereas in human necropsied cases of SCA1, SCA2, SCA17 and DRPLA, NIs were absent in cerebellar Purkinje cells, which are targets of neurodegeneration in these polyQ diseases (Koyano et al., 2002; Rolfs et al., 2003). Studies in some cellular and animal models of polyQ diseases have been demonstrated the presence of cell death when few or no inclusions were present (Lunkes and Mandel, 1998; Saudou et al., 1998; Lunkes et al., 1999). In addition, a transgenic mouse for HD has been reported presenting minimal cell death with significant behavioral deficits and extensive NIs in the striatum (Mangiarini et al., 1996), while a SCA1 mouse model expressing an ataxin-1 (ATXN1) protein without the self-association region, essential for the formation of ataxin-1 aggregates, showed signs of the disease without formation of NIs (Klement et al., 1998). More recently, a MJD transgenic mouse model has been reported showing a motor phenotype after about 1 year of age, whereas the few and small intranuclear aggregates observed appeared later in life (Boy et al., 2010). Another evidence supporting this idea lays in the natural formation of the Marinesco bodies in the substantia nigra,

## **Chapter 1.** Introduction

which seems to be a strategy adopted by normal-aging neurons, throughout time (Fujigasaki et al., 2000). It is also possible, although scarcely supported, that NIs are neutral species to the toxicity. Supporting this idea there are some studies revealing that modulation of polyQ toxicity is possible without affecting protein aggregation (Klement et al., 1998; Kazemi-Esfarjani and Benzer, 2000; Cummings et al., 2001). More recently, it has been postulated that oligomeric species, namely protofibrils and microaggregates are the cause of polyQ toxicity whereas large protein inclusions are “cytoprotective” merely representing end products of the upstream toxic event (Arrasate et al., 2004). Oligomer species have been demonstrated to be implicated in the disease progression in a SBMA mouse model (Li et al., 2007). Moreover, oligomers have been detected in HD and mouse models before any measurable behavioural phenotype and the size of the aggregates correlated with disease progression (Weiss et al., 2008).

Another important and well-established pathological hallmark in polyQ diseases is the ubiquitylation of expanded polyQ proteins and once in the nucleus they recruit proteasome subunits into the NIs (Paulson et al., 1997b; Becher and Ross, 1998; Cummings et al., 1998). Moreover, HSPs have been observed to co-localize with nuclear aggregates in human patients and mouse models of several polyQ diseases (Cummings et al., 1998; Jana et al., 2000; Yvert et al., 2000; Zander et al., 2001; Schmidt et al., 2002). This finding suggests the involvement of the ubiquitin-proteasome degradation pathway in these pathologies, and also the activation of the heat shock response machinery in order to either refold or degrade the mutant polyQ proteins. Heat shock proteins (HSPs) play an important role in the cell stress response induced by the presence of proteins with a polyQ expansion. HSPs expression levels have shown to display a biphasic response beginning with an initial phase of up-regulation of the expression levels followed by a progressive decrease of HSPs levels during later stages in the disease progression (Hay et al., 2004; Huen and Chan, 2005). In addition, the overexpression of HSPs in cellular and animal models of polyQ diseases have been demonstrated to modulate the polyQ toxicity and/or disease manifestation (Cummings et al., 2001; Mitsui et al., 2002; Ishihara et al., 2003), however their putative involvement in aggregate formation has to be clarified.

### **1.3.2. Post-translational modifications of mutant polyQ proteins**

For some polyQ diseases including HD, SBMA and SCA3 it has been suggested that the mechanism of pathogenesis might involve the proteolysis of the mutant protein resulting in production of polyQ-containing fragments (Paulson, 1999; Paulson et al., 2000; Lunkes et al., 2002;

Goti et al., 2004; Gardian et al., 2005). Caspase-mediated cleavage sites were identified or predicted in Htt, atrophin-1 (ATN1), ATXN3, and androgen receptor (AR) proteins (Goldberg et al., 1996; Kobayashi et al., 1998; Wellington et al., 1998; Berke et al., 2004). As a consequence of the cleavage, the resulting fragment could have an enhanced toxic effect (Ellerby et al., 1999; Goti et al., 2004), could more easily enter the nucleus (Igarashi et al., 1998; Hackam et al., 1999) and/or more rapidly aggregate (Cooper et al., 1998; Igarashi et al., 1998). Indeed, it has been shown that truncated proteins with polyQ expansions are more prone to form inclusions or cause cell death by apoptosis than the respective full-length protein (Paulson et al., 1997b; Martindale et al., 1998; Merry et al., 1998; Goti et al., 2004). A more recent study has shown that inclusions from HD brains contain N-terminal fragments of mutant Htt rather than the full length protein (Hoffner et al., 2005). Although these fragments may result from unspecific proteolytic activities, it has been demonstrated that specific cleavage of the mutant protein is an early event in HD pathogenesis, supporting the idea that the smaller products of specific cleavage may seed the formation of inclusions followed by the recruitment of larger non-specific fragments (Wellington et al., 2002). Interestingly, nuclear translocation of expanded Htt was delayed in mice expressing mutant Htt resistant to caspase-6 cleavage (Graham et al., 2006).

Besides proteolytic cleavage, other post-translational modifications of mutant polyQ proteins such as phosphorylation have been shown to play a role in the pathogenesis mechanism of polyQ diseases. In fact phosphorylation of the mutant protein Htt has an impact in the proteolytic cleavage, the initial conversion of the protein to pathogenic conformations and in nuclear transport, which is a key step for the disease manifestation (Warby et al., 2009). It has been demonstrated in a cell- and rat-based model, that the toxicity of mutant Htt could be inhibited by the AKT-dependent phosphorylation of Htt at S421 (Humbert et al., 2002) or by cyclin dependent kinase 5 (CDK5)-mediated phosphorylation at S434 of Htt (Luo et al., 2005). Phosphorylation of Htt at S536 has also a decreasing effect in toxicity of the mutant protein by inhibiting its cleavage by calpain in this site (Gafni et al., 2004; Schilling et al., 2006). These results suggest a neuroprotective role of phosphorylation in HD (Pardo et al., 2006). A similar effect has been observed in MJD, in which ataxin-3 phosphorylation at S256 by glycogen synthase kinase 3 $\beta$  reduced mutant ATXN3 aggregation *in vitro* (Fei et al., 2007). CK2-dependent phosphorylation of ATXN3 at S236 and S340/S352 decreased the appearance of NIs and controlled the nuclear translocation of ATXN3 providing a reasonable therapeutic approach for SCA3 (Mueller et al., 2009). In contrary, phosphorylation of mutant ATXN1 at S776 is associated with the formation of aggregates and

## **Chapter 1.** Introduction

neurodegeneration (Chen et al., 2003). Together, these observations suggest that post-translational modification play an important role in the manifestation and/or progression of the disease, reinforcing the idea that the protein context in which the polyQ is located influences the pathology.

### **1.3.3. Role of nuclear localization of mutant polyQ proteins**

Accumulation of expanded polyQ proteins into the nucleus of cells has been shown to play an important role in the pathogenesis of these disorders (Klement et al., 1998; Saudou et al., 1998; Peters et al., 1999; Ross et al., 1999; Orr, 2001), whether by affecting gene expression (Zoghbi and Orr, 2000) or by disrupting nuclear organization and function (Sun et al., 2007). In fact, Yang and collaborators showed that polyQ aggregates were toxic only when localized in the nucleus but not in the cytoplasm (Yang et al., 2002). Nuclear accumulation of mutant proteins and inclusions have been identified as predominant in HD, SCA1, SCA3, SCA7, SCA17, DRPLA, and SBMA patients (Schols et al., 2004); however, cytoplasmic inclusions have also been found in affected brain regions of HD, SCA2, DRPLA, SBMA and MJD patients (Huynh et al., 2000; DiFiglia, 2002; Gatchel and Zoghbi, 2005; Heng et al., 2010).

In the case of MJD, Bichelmeier and co-workers (2007), showed the first *in vivo* evidence that nuclear localization of ATXN3 is required for the manifestation of symptoms, whereas the export of ATXN3 out of the nucleus prevents the manifestation of the phenotype (Bichelmeier et al., 2007). More recently, the functionality of the putative ATXN3 nuclear localization signal (NLS) has been confirmed in yeast and mammalian cells, and it has been shown that the nuclear export of ATXN3 is mediated by CRM1 (exportin 1)-dependent and -independent pathways (Macedo-Ribeiro et al., 2009).

### **1.3.4. Neuronal cell death versus neuronal dysfunctions**

The remarkable degree of brain atrophy observed in polyQ diseases indicates that neuronal cell loss is a major feature of the pathogenic process. The mechanism of cell death in polyQ diseases remains unknown and may be very complex, as many processes triggered by the presence of expanded polyQ proteins can lead to the cell death, such as direct activation of cell death pathways, mitochondrial abnormalities, transcriptional dysregulation, proteasome impairment, defects in axonal transport, or unfolded protein response. Indeed, several studies in cell models for polyQ diseases have confirmed that the presence of expanded polyQ disease proteins leads to caspase activation and apoptosis (Sanchez et al., 1999; Wellington and Hayden, 2000; Gervais et

al., 2002; Kouroku et al., 2002; Gafni et al., 2004; Chou et al., 2006). In addition, some transgenic mouse models for HD, SCA1, MJD and SCA7 showed evidence of neuronal degeneration and neuronal loss with an apparent astrogliosis (Burrigh et al., 1995; Ikeda et al., 1996; Mangiarini et al., 1996; Reddy et al., 1998; Hodgson et al., 1999; Schilling et al., 1999; Shelbourne et al., 1999; Yvert et al., 2000). However, other transgenic mouse models for polyQ diseases have been shown to develop motor symptoms in the absence of neuronal cell death (Mangiarini et al., 1996; Bates et al., 1998; Shelbourne et al., 1999; Turmaine et al., 2000; Adachi et al., 2001; Bichelmeier et al., 2007; Silva-Fernandes et al., 2010). In fact, in agreement with the slow progression of polyQ disorders, it is unlikely that neuronal cell death could be the responsible for symptoms early in the course of disease; instead, it could be a final stage after a long period of neuronal dysfunction. Neuronal cell death - whether apoptotic or nonapoptotic - probably occurs when neurons can no longer tolerate irreversible and widespread dysfunction of multiple cellular pathways. In HD patients at early stages of disease a functional deficit at the synaptic level has been observed, in particular a decrease in mRNA levels of D1 and D2 dopamine receptors (Leegwater-Kim and Cha, 2004). Several studies performed in HD mouse models demonstrated that neuronal dysfunction caused by transcriptional dysregulation, activation of cellular stress response, mitochondrial function deficit, reduction in levels of synaptic proteins and alterations of synaptic proteins that affect endocytosis and exocytosis in neurons, can lead to symptoms of HD without the occurrence of cell death (Mangiarini et al., 1996; Luthi-Carter et al., 2000; Tabrizi et al., 2000; Bogdanov et al., 2001; Smith et al., 2005; Desplats et al., 2006). Neuronal transmission is compromised in HD mice (Li et al., 2003; Smith et al., 2005), as is neuronal activity (Rebec et al., 2006) supporting the idea that major pathophysiological changes occur well before cell death. In the same manner, neuronal dysfunction likely underlies early features of disease in other polyQ disorders such as SCA1, SBMA and SCA6 (Matsuyama et al., 1999; Lin et al., 2000; Toru et al., 2000; Adachi et al., 2001; Serra et al., 2004).

### **1.3.5. Transcriptional deregulation in polyQ diseases**

As mentioned above, the translocation of polyQ proteins to the nucleus has been set as a prerequisite of their toxicity. Several evidences have supported the notion that major alterations in gene expression occur in the cell in polyQ-associated disorders (Okazawa, 2003). So far, three different mechanisms have been postulated to cause the polyQ-dependent transcription regulation/modulation: the recruitment of transcription activators or co-activators in the inclusions,

## Chapter 1. Introduction

the direct inhibition of acetyltransferase activity of transcription modulators and/or the direct repression of the transcriptional machinery.

The sequestration hypothesis suggests that polyQ proteins may “trap” rate-limiting transcriptional activators or co-activators, causing a unbalance that may have profound effects on gene expression, with potentially toxic effects. Mutant polyQ proteins have been shown to interact with proteins involved in the transcription machinery, namely the CREB-binding protein (CBP), p300/CBP associated factor (PCAF), TBP-associated factor (TAFII130), and Specificity Protein 1 (SP1) (Li et al., 2002b; Okazawa, 2003). Overexpression of these transcription regulators was shown to overcome polyQ toxicity, both *in vitro* in cellular models for MJD, SBMA, and HD (McC Campbell et al., 2000; Dunah et al., 2002), as well as *in vivo* in a polyQ model in *Drosophila* (Taylor et al., 2003).

A common transcriptional activator, cyclic AMP-response element binding protein (CREB), along with its co-activator CBP, has been strongly implicated in expanded polyQ-induced gene repression (Steffan et al., 2000). CBP is an important mediator of survival signals in neurons. It has histone acetyltransferase activity, which is important for allowing transcription factors access to DNA. In the presence of mutant Htt or ATN1, CBP is sequestered into the aggregates (Nucifora et al., 2001). CBP recruitment to intranuclear inclusions or the interaction with mutant polyQ proteins also occurs in SBMA, SCA3, and SCA7 (McC Campbell et al., 2000; Li et al., 2002a; Strom et al., 2005). In SCA1, CBP was not irreversibly trapped into nuclear aggregates but was rapidly exchanged. Although CBP has a short residence time within the inclusions, this may be sufficient to disrupt its normal function in maintaining cellular homeostasis (Stenoien et al., 2002). It appears that the disruption of CREB/CBP-mediated gene expression may be a common mechanism of neurodegeneration in polyQ repeat diseases. On the contrary, it was reported that in the R6/2 HD mouse model, CREB-mediated transcription was increased (Obrietan and Hoyt, 2004) and CBP was not depleted in the brain of a knock-in HD mouse (Yu et al., 2002).

Alternatively, polyQ proteins may exert their toxic effect through direct inhibition of the acetyltransferase activity of transcription modulators, leading to diminished histone acetylation and, subsequently, gene transcription activation. CBP and pCAF are transcription factors that regulate gene expression through their intrinsic acetylase activity (Ogryzko et al., 1996). A mutant truncated fragment of Htt has been shown to inhibit transcription, by repressing the histone acetylase activity of the CBP/p300/pCAF transcriptional co-activator (Steffan et al., 2001). ATXN3 has been reported to be a dual co-repressor of transcription by the interaction through its C-terminal with CBP, p300

and pCAF, inhibiting CREB-dependent gene transcription; and through its N-terminal interaction with histones, masking their acetylation sites (Li et al., 2002a).

Besides the analysis of the indirect consequences of the polyQ expression in cell or animal models, the involvement of mutant polyQ proteins in the direct repression of the transcriptional machinery as cause of neurodegeneration remains to be determined.

#### **1.4. Therapeutic approaches for polyQ diseases**

So far, MJD and all other polyQs are not curable although some symptoms can be controlled with specific treatments. Potential therapeutic strategies for polyQ disorders could be divided into those that target the pathological cascades of the disease, including the therapies decreasing the levels and inhibiting the (relevant) aggregation of the mutant protein, and those intercepting the toxic effects of the polyQ protein such as mitochondrial dysfunction and oxidative stress, transcriptional abnormalities, UPS impairment, excitotoxicity, or apoptotic pathways (Bauer and Nukina, 2009).

Therapeutic strategies that directly target the polyQ proteins include: i) **gene silencing** that leads to decreasing levels of the mutant protein. It has been shown in conditional mouse models of HD, SCA1 and MJD that the blockade of mutant protein expression leads to a disappearance of inclusions and an amelioration of the behavioral phenotype (Yamamoto et al., 2000; Zu et al., 2004; Boy et al., 2009). Two different approaches have been considered for the treatment of CNS disorders: nonallele-specific silencing, which does not discriminate between the wild-type and mutant alleles, silencing both simultaneously; and allele-specific silencing, that allows the selective silencing of the mutant allele whereas the expression of the normal is maintained (Reynolds et al., 2004). Importantly, and although the RNA interference (RNAi) technology has progressed remarkably, gene silencing delivery in the CNS is still a big challenge; ii) **enhancement of protein degradation by modulating cellular degradation pathways.** Autophagy clearance of mutant Htt has been shown to reduce protein toxicity in mouse, Drosophila and zebrafish models of HD (Sarkar and Rubinsztein, 2008; Williams et al., 2008). Moreover, the mammalian target of rapamycin- (mTOR-) dependent (e.g. by rapamycin, CCI-779) or –independent (e.g. by lithium, calpain inhibitors, etc.) autophagy activation was beneficial and the combination of both resulted in an additive protection in a HD fly model (Sarkar et al., 2008). On the other hand, even though the regulation of the UPS enzymatic activity is not well understood, its modulation has been pointed as a good candidate for therapy in polyQ diseases. However, in contrast with the wide range of UPS inhibitors, no chemical



## Chapter 1. Introduction

compound that activates the UPS activity was available. More recently, amiloride and its derivative, benzamil, have been reported to reduce the polyQ aggregation and toxicity in HD models (Wong et al., 2008). Another compound shown to increase UPS enzymatic activity is Y-27632, leading to a reduction of polyQ toxicity in a *Drosophila* model of HD (Pollitt et al., 2003). Interestingly, this compound also enhanced macroautophagy, and this particular effect of modulating both main cellular degradation pathways led to reduced levels and reduced aggregation of mutant Htt, ATXN3, AR, and ATN1 in cell systems (Bauer et al., 2009); iii) **inhibition of aggregation**. Several studies have been published showing the ability of small molecules (e.g. Congo red, trehalose) to prevent directly the formation of polyQ aggregates and to improve survival and motor phenotype in a transgenic mouse model for HD (Sanchez et al., 2003; Tanaka et al., 2004). The treatment of a *Drosophila* model of HD with PolyQ Binding Peptide 1 (QBP1) was shown to prevent conversion of the expanded polyQ into its aggregation-prone  $\beta$ -sheet conformation, resulting in a neuroprotective effect (Nagai et al., 2003; Nagai et al., 2007). Cystamine may reduce expanded polyQ aggregation and survival by inhibition of transglutaminase, which is thought to crosslink expanded polyQ proteins and facilitate their aggregation (Dedeoglu et al., 2002). Another approach to reduce the misfolding, oligomerization, and aggregation of polyQ proteins is to increase the cellular levels of molecular chaperones such as heat shock protein 70 (Hsp70) (Katsuno et al., 2005). Besides the effect in the aggregation process, chaperone up-regulation might also enhance the degradation of the mutant protein through the UPS.

In addition to these attempts of preventing the polyQ pathology at the level of the mRNA or polyQ protein itself, several strategies targeting the downstream pathogenic events has been conceived, namely: i) **transcription normalization**. The modulation of the deregulated gene transcription, in particular by targeting histone methylation and acetylation using different compounds, has been tested in different models of polyQ diseases. Histone deacetylase inhibitors such as suberoylanilide hydroxamic acid (SAHA) and sodium butyrate (SB) have been demonstrated to improve the motor phenotype in mouse models of HD, DRPLA, SBMA (Ferrante et al., 2003; Hockly et al., 2003; Minamiyama et al., 2004; Ying et al., 2006). Another histone deacetylase inhibitor, phenylbutyrate, improved survival, and attenuated gross brain atrophy and ventricular enlargement in N171-82Q HD transgenic mice (Gardian et al., 2005). On the other hand, inhibition of histone H3 methylation by mithramycin lead to an increase of the R6/2 mice lifespan and improvement in motor performance and striatal pathology (Ferrante et al., 2004). Another drug shown to alleviate the transcriptional dysbalance is the phosphodiesterase type IV inhibitor rolipram, by increasing the phosphorylation

and activity of CREB. R6/2 HD mice treated with rolipram have an extension in lifespan as well as an improvement of the neuropathology and a slowed progression of neurological phenotype. Interestingly, the expression of brain-derived neurotrophic factor (BDNF) which is impaired in HD (Zuccato et al., 2003), was induced in treated mice through restored function of CREB (DeMarch et al., 2008). In another study, it was shown that rolipram also prevented the sequestration of CBP into nuclear aggregates (Giampa et al., 2009); ii) **improvement of the mitochondrial metabolism and reduction of oxidative stress.** Reduced concentrations of creatine and phosphocreatine have been observed in the basal ganglia of HD patients, reinforcing the idea that oxidative stress and mitochondrial dysfunction could be implicated in polyQ pathogenesis (Sanchez-Pernaute et al., 1999). Creatine treatment stabilized the mitochondrial membrane permeability transition (MPT), prevented ATP depletion and increased the protein synthesis. In two different mouse models of HD creatine treatment has been ameliorate the brain pathology and motor symptoms (Ferrante et al., 2000; Andreassen et al., 2001). Moreover, antioxidants such as  $\alpha$ -lipoic acid, coenzyme Q10, clioquinol, tauroursodeoxycholic acid (also with antiapoptotic effect), or BN82451 have proven to be effective in R6/2 mouse lines (Giampa et al., 2009); iii) **excitotoxicity blockade.** Excessive activation of N-methyl D-aspartate (NMDA) glutamate receptors and the subsequent excitotoxicity in neurons of the striatum, leading to their death, has been implicated in the pathogenesis of HD (Cepeda et al., 2003). Interestingly, the use of compounds that block the excessive glutamate release, like riluzole, has been significantly effective in a HD mouse model (Schiefer et al., 2002). Similar to riluzole, two drugs affecting the levels of glutamate in the synaptic cleft, LY379268 and 2-methyl-6-(phenylethynyl)-pyridine, have significantly increased the lifespan of R6/2 mice (Schiefer et al., 2004). In one study, the administration of remacemide (NMDA antagonist) or coenzyme Q10 prolonged the survival of R6/2 mice by 15.5% and 14.5%, respectively, while combined, the survival was extended by 31.8% (Ferrante et al., 2002). This combination was not so effective in N171-82Q mice but the lifespan was still improved by more than 20% (Schilling et al., 2001). The clinical trial using either of these drugs or in combination, however displayed no significant effects in HD patients (HuntingtonStudyGroup, 2001); iv) **apoptosis inhibition.** Treatment with minocycline, an antiapoptotic drug, was shown to extend the lifespan of R6/2 mice by 13.5% (Chen et al., 2000) and the combination of minocycline and coenzyme Q10 has improved survival, neuropathology and phenotype of R6/2 mice when compared with separate treatments (Stack et al., 2006). Although the results of the clinical studies using minocycline produced promising data (Bonelli et al., 2004) a long-term clinical trial should be conducted to clearly evaluate the benefits of minocycline in HD

patients. Another strategy for apoptosis blockade is the inhibition of caspases that could have a second beneficial effect by decreased generation of caspase-cleaved fragments of mutant proteins. Indeed, a broad caspase inhibitor, z-Val-Ala-Asp-fluoromethylketone, was shown to improve the rotarod performance of R6/2 mice and extended the lifespan by 25% (Ona et al., 1999), and the co-administration of caspases 1 and 3 inhibitors, Tyr-Val-Ala-Asp-chloromethylketone and Asp-Glu-Val-Asp-aldehyde-fluoromethylketone, respectively, increased the survival by 17.3% (Chen et al., 2000).

### 1.5. Machado-Joseph disease

The official history of MJD begins in the 70th decade with the description of North-American families with Azorean ancestry. In 1972 Nakano and co-authors reported a family descendent from William Machado, a native from São Miguel in Azores, presenting progressive hereditary ataxia. They named this disorder “Machado disease” (Nakano et al., 1972). In the same year, Woods and Schaumburg observed another family of Azorean ancestry, the Thomas family, which although showing similar clinical features to the Machado disease, presented some particular clinical and pathological signs that led them to define this disorder as a novel clinical entity – “nigro-spino-dentatal degeneration” (Woods and Schaumburg, 1972). A few years later, Rosenberg and collaborators defined a “new” hereditary neurological disease different from the previous two, by observation of the Joseph family, originated from Flores Island, which they named “Joseph disease” (Rosenberg et al., 1976). In this report no importance was given to the cerebellar ataxia and only a few years later Rosenberg did accept this as an important element of the clinical picture (Rosenberg, 1983). A fourth Azorean family was reported to carry an “Azorean disease of the nervous system” in 1977 (Romanul et al., 1977). Finally, starting in 1976, Coutinho and Andrade studied the first 15 families from the Azorean Islands and proposed that the above mentioned diseases were indeed variations of the same clinical disease (Coutinho and Andrade, 1978). They defined this as “Machado-Joseph disease”, a single disorder characterized by a high clinical variability, proposing the clinical classification of patients into three types that accommodated all this variability. In our days, MJD, now also called SCA3, is known to be the most common dominantly inherited ataxia worldwide (15- 45% of all forms in different countries and ethnic populations) (Margolis, 2002; Schols et al., 2004; Paulson, 2007).

### 1.5.1. Clinical symptoms and progression of MJD

MJD is a progressive neurodegenerative disease, affecting mainly the motor function. Patients usually present ataxia, pyramidal and extrapyramidal signs, progressive external ophthalmoplegia, peripheral amyotrophies, intention fasciculation-like movements of facial and lingual muscles, rigidity, and bulging eyes (Coutinho and Andrade, 1978; Lima and Coutinho, 1980; Barbeau et al., 1984; Coutinho, 1992). Although the first cases described came from families with a common origin and shared similar clinical features and transmission pattern, the individuality of each of the described entities was always defended by the authors. This difficulty to accommodate all disease presentations in a unique identity lasted for several years. This could be partially justified by the phenotypic variability of MJD that lead to the organization of the disease sub-types, sorted by the age of clinical onset and major symptoms of the disorder (Lima and Coutinho, 1980). **MJD type I** includes the MJD forms with early age at onset (10-30 years of age), faster progression and more intense pyramidal and extra-pyramidal signs. **MJD type II** is the most frequent, and is characterized by intermediate age-at-onset (20-50 years of age) and progression, with patients exhibiting the usual ataxia and ophthalmoplegia. MJD patients with **MJD type III** present the latest age at onset (40-70 years of age), slow disease progression and more peripheral signs. In 1983, Roger Rosenberg added a **fourth type**, which is the most rare and includes MJD patients exhibiting Parkinsonic symptoms associated with the most typical symptoms of MJD (Rosenberg, 1983; Margolis, 2002).

### 1.5.2. MJD neuropathology

The majority of the neuropathological MJD studies performed so far have suggested that central nervous neurodegeneration was restricted to very specific brain regions, such as cerebellar dentate nucleus, pallidum, substantia nigra, subthalamic, red and pontine nuclei, select cranial nerve nuclei and the anterior horn and Clarke's column of the spinal cord (Robitaille et al., 1997; Schmidt et al., 1998; Iwabuchi et al., 1999; Gilman, 2000; Yamada et al., 2004; Koeppen, 2005) (Figure 6). According to these studies central nervous white matter lesions are restricted to the medial lemniscus, spinocerebellar tracts and dorsal columns. In addition, the majority of the brains of MJD patients with disease duration of more than 15 years have showed a lower weight than those individuals without medical histories of neurological or psychiatric diseases (Iwabuchi et al., 1999). In contrast to previous conventional neuropathological studies, recent pathoanatomical investigations using unconventional thick serial tissue sections of 100µm (that display considerably more nerve

## Chapter 1. Introduction

cells than the conventional 4–6 $\mu$ m single sections normally used by neuropathologists) demonstrated widespread damage to the cerebellum, thalamus, midbrain, pons, medulla oblongata and spinal cord in MJD, providing suitable explanations for a variety of less understood clinical MJD symptoms (Rub et al., 2003a; Rub et al., 2003b; Rub et al., 2003c; Rub et al., 2004; Rub et al., 2005; Rub et al., 2006a; Rub et al., 2006b; Rub et al., 2007). According to these studies the gray matter components affected in MJD patients include: nuclei of the motor cerebellothalamocortical loop (i.e., cerebellar dentate nucleus, pontine nuclei, thalamic ventral lateral nucleus) and the basal ganglia-thalamocortical loop (i.e., pallidum, subthalamic nucleus, thalamic ventral anterior nucleus), the substantia nigra and ventral tegmental area, select non-motor thalamic nuclei (thalamic reticular nucleus, lateral geniculate body, pulvinar), subcortical components of the somatosensory system (i.e., ventral posterior lateral and ventral posterior medial thalamic nuclei, trigeminal, cuneate, external cuneate, and gracile nuclei, Clarke's columns), all of the vestibular nuclei, select oculomotor brainstem nuclei (i.e., oculomotor, trochlear, abducens and raphe interpositus nuclei, rostral interstitial nucleus of the medial longitudinal fascicle, reticulotegmental nucleus of the pons), all ingestion-related brainstem nuclei (i.e., trigeminal, facial, ambiguus, dorsal motor vagal, and solitary nuclei, as well as associated nuclei of the reticular formation), and the rest of the proposed precerebellar nuclei in the midbrain and brain stem (i.e., red, arcuate, prepositus hypoglossal, and lateral reticular nuclei, inferior olive) (Table 3) (Riess et al., 2008; Rub et al., 2008). While the distribution pattern of CNS affected regions of MJD widely overlaps with those observed in SCA2 and SCA7 patients, there are particular features of MJD which included the sparing of the cortical and subcortical components of the limbic system and the less severe involvement of central white matter components (Iwabuchi et al., 1999; Rub et al., 2006b; Rub et al., 2007). The peripheral nerves, cranial nerves, trapezoid body, cerebellar peduncles, vestibulospinal and spinocerebellar tracts, as well as the medial longitudinal, cuneate and gracile fascicles are the peripheral and central white matter components affected in MJD (Iwabuchi et al., 1999; Gilman, 2000; Rub et al., 2004; Schols et al., 2004; Rub et al., 2007). Although no cross-sectional studies have been performed in MJD, preliminary observations have suggested that the early targets of the degenerative process of MJD include the cerebellar dentate nucleus, the substantia nigra and a subset of vestibular (i.e., medial and superior vestibular nuclei), oculomotor (i.e., abducens nucleus, reticulotegmental nucleus of the pons) and precerebellar nuclei (i.e., red, lateral reticular and external cuneate nuclei), while the thalamus, ingestion-related brainstem nuclei and the rest of the cranial nerve nuclei (e.g., dorsal

motor vagal and ambiguous nuclei) and precerebellar nuclei (e.g., pontine nuclei, inferior olive) are affected only later during the course of the disease (Iwabuchi et al., 1999; Rub et al., 2005).

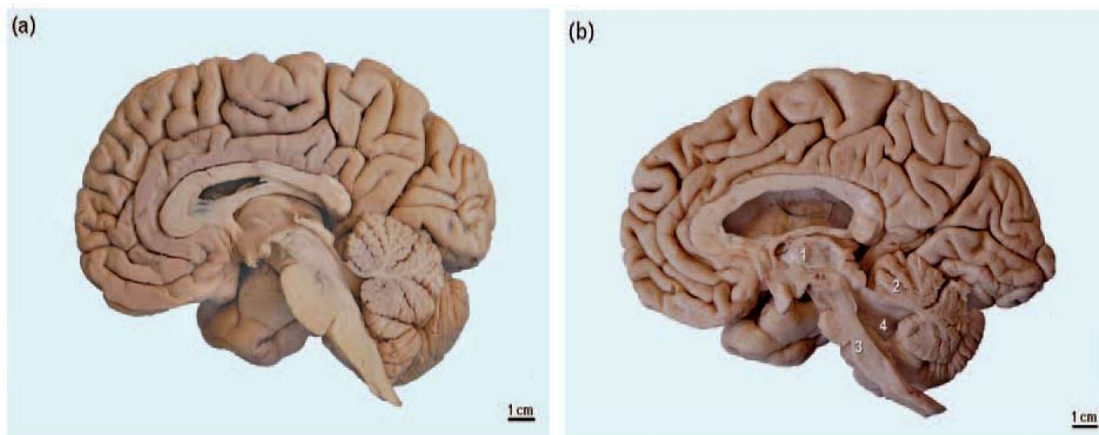


**Figure 6.** Macroscopic aspects in MJD. Comparison between the right cerebral hemisphere, cerebellum and brainstem of a representative control individual without medical history of neurological or psychiatric diseases (a) and a genetically confirmed MJD (age at death 85 years; 64 CAG-repeats in the mutated *ATXN3* allele; onset of MJD, 59 years). Note the atrophic thalamus (1), cerebellum (2), midbrain, pons and medulla oblongata (3), as well as the widened fourth ventricle (4). (Rub U, 2008).

**Table 3.** Summary of the central nervous loops and systems that undergo neurodegeneration during the progression of MJD. Adapted from (Rub et al., 2008).

| Affected central nervous component       | Major lesions   |
|--|---|
| Cerebellothalamocortical motor loop      | Cerebellar cortex, dentate and fastigial nuclei; pontine nuclei; thalamic ventral lateral nucleus; giant Betz pyramidal cells of the primary motor cortex; anterior horn motoneurons of the spinal cord   |
| Basal ganglia–thalamocortical motor loop | Pallidum; subthalamic nucleus; thalamic ventral lateral and reticular nuclei  |
| Visual system                            | Lateral and inferior nuclei of the pulvinar; lateral geniculate body of the thalamus  |
| Auditory system                          | Colliculus inferior; nuclei of the lateral lemniscus; superior olive; cochlear nuclei   |
| Somatosensory system                     | All somatosensory nuclei of the thalamus, pons and medulla oblongata; Clarke’s column of the spinal cord  |
| Vestibular system                        | Superior, lateral, medial, spinal and interstitial vestibular nuclei  |
| Oculomotor system                        | Oculomotor, trochlear, and abducens nuclei; rostral interstitial nucleus of the medial longitudinal fascicle; reticulotegmental nucleus of the pons; area of the excitatory burst neurons for horizontal saccades; raphe interpositus nucleus; prepositus hypoglossal nucleus |
| Ingestion-related brainstem system       | All somatosensory, somatomotor, viscerosensory and visceromotor ingestion-related brainstem nuclei; ingestion-related regions of the brainstem reticular formation  |
| Precerebellar brainstem system           | Arcuate nucleus; red nucleus; pontine nuclei; reticulotegmental nucleus of the pons; vestibular nuclei; lateral reticular nucleus; external cuneate nucleus; prepositus hypoglossal nucleus; dorsal paramedian reticular nucleus; nucleus Roller; inferior olive              |
| Midbrain dopaminergic system             | Mesostratial dopaminergic system (substantia nigra); mesolimbic dopaminergic system (nuclei of the ventral tegmental area)  |
| Midbrain cholinergic system              | Pedunculopontine nucleus  |
| Pontine noradrenergic system             | Locus coeruleus   |

**1.5.3. The *MJD/ATXN3* gene**

The MJD locus was first localized to the long arm of chromosome 14 (14q24.3-q32) (Takiyama et al., 1993). In 1994, Kawaguchi et al. isolated and characterized a cDNA clone designated as MJD1a, identifying the causative mutation as an expansion of a CAG repeat, located in the coding region of the *ataxin-3* gene (*ATXN3*) (14q32.1) (Kawaguchi et al., 1994). In this manner, the molecular diagnosis of MJD became possible, and the mutation was then confirmed in families of diverse origins (Maciel et al., 1995; Higgins et al., 1996; Lopes-Cendes et al., 1996; Gaspar et al., 2001)

The gene was described as consisting of having 11 exons, spanning a genomic region of about 48 kilobases (kb), with the (CAG)<sub>n</sub> tract being located at the 5'-end of exon 10 (Ichikawa et al., 2001). In the normal alleles the CAG repeat ranged between 12-44 and expanded alleles with full penetrance the CAG repeat range between 52-86 (Maciel et al., 2001; Padiath et al., 2005). Although the range of repeat lengths with reduced penetrance is not firmly established in MJD as in other SCAs, individuals with alleles carrying a CAG repeat between 45-51 have been described that may or may not manifest the disorder during their lifetime (Maciel et al., 2001; Gu et al., 2004; Padiath et al., 2005).

Northern blot analysis have revealed ubiquitous *ATXN3* expression and the existence of four different transcripts (1.4, 1.8, 4.5 and 7.5 Kb), thought to result from alternative splicing (occurring in exons 2, 10, and 11), and from different polyadenylation signals (Ichikawa et al., 2001). Five cDNA variants were described: MJD1a, MJD1-1, MJD5-1, MJD2-1 and H2 (Kawaguchi et al., 1994; Goto et al., 1997); the latter lacks exon 2, but maintains the open reading frame (ORF), identical to variant MJD1-1 (Ichikawa et al., 2001). The MJD1-1 and MJD5-1 variants only differ in the size of their 3' UTR. More recently, the occurrence of alternative splicing at the *ATXN3* gene was analysed by sequencing a total of 415 cDNAs clones from 20 MJD patients and 14 controls. Two novel exons were described for the *ATXN3* gene and fifty-six alternative splicing variants were observed, generated by four types of splicing events. From those variants, 50 were not previously described, and 26 were only found in MJD patients' samples. Most of the variants (85.7%) presented frameshift, which lead to the appearance of premature stop codons. Thirty-seven of the observed variants constituted good targets to nonsense-mediated decay, but the remaining were likely to be translated into at least 20 different protein isoforms (Bettencourt et al., 2010). The physiological and clinical relevance of these isoforms remains to be determined.

#### 1.5.4. The ATXN3 protein(s)

Among the proteins associated with polyQ expansion diseases, ataxin-3 is the smallest one, with 42 KDa. The human *ATXN3* gene product, ataxin-3, is a ubiquitously expressed protein, containing a conserved N-terminal Josephin domain (JD) (1-198 aa), containing the putative catalytic triad aminoacids cysteine (C14), histidine (H119) and asparagine (N134). The Josephin domain, the name of which derives from the name of the disease, is followed by two ubiquitin interaction motifs (UIMs, 223-240 aa and 243-260 aa) domains, the polyQ repeat region, and a third UIM (334-351) in some ATXN3 variants (isoform 1 and 4) (Albrecht et al., 2003; Masino et al., 2003; Albrecht et al., 2004). Ataxin-3 also has a conserved NLS upstream of the polyQ tract, which may determine the rate of ataxin-3 transport into the nucleus (Goto et al., 1997; Doss-Pepe et al., 2003; Macedo-Ribeiro et al., 2009). The UIM domain is a highly conserved amino acidic sequence that was initially found in the proteasome S5a subunit, but then found in several proteins participating in pathways as diverse as ubiquitylation, Ub metabolism and endocytosis (Young et al., 1998; Hofmann and Falquet, 2001; Miller et al., 2007). The UIMs can act either to bind Ub or ubiquitylated proteins, or to promote ubiquitylation (mono-, oligo- and polyubiquitylation) (Miller et al., 2004).

The *ATXN3* gene is present in distinct organisms, including plants, nematodes and human. Sequence analysis revealed that there is a high degree of conservation, at the DNA level, between human ataxin-3 and the corresponding orthologues in rat (Schmitt et al., 1997), mouse (Costa et al., 2004) (88%), chicken (82%) (Linhartova et al., 1999) and *Caenorhabditis elegans* (*C.elegans*) (38%) (Rodrigues et al., 2007), suggesting evolutionary conserved functions and properties (Albrecht et al., 2003). Interestingly, the polyQ tract seems to be human-specific because it is absent in other species such as mouse and worms that have only six and one glutamines in the ataxin-3 homologue, respectively.

Due to the lack of ATXN3 isoform functional studies, it is only possible to speculate from the different cloned cDNA variants, the existence of the correspondent four protein isoforms (Figure 7). These proteins were designated in 2003 (Albrecht et al., 2003): **ATXN3-v1**, constituted by 361 amino acids (aa), is encoded by the MJD1-1 and MJD5-1 cDNAs, carries three UIMs and possesses an hydrophilic C-terminal (Goto et al., 1997); **ATXN3-v2** is the longest variant (364 aa), the corresponding protein of MJD2-1, contains two UIMs before the polyQ tract and an hydrophobic C-terminal (Goto et al., 1997); **ATXN3-v3** (348 aa) is the protein encoded by the cDNA variant cloned for the first time, MJD1a, corresponding to a truncated variant of ATXN3-v2 in 16 aa due to a premature stop codon that is the result of the TAA<sup>1118</sup>/TAC<sup>1118</sup> single-nucleotide polymorphism (SNP)



## Chapter 1. Introduction

(Kawaguchi et al., 1994); and **ATXN3-v4** (306 aa) is 55 aa shorter than ATXN3-v1 due to the absence of the residues encoded by exon 2 in the H2 cDNA variant, carrying an incomplete JD which lacks the catalytic cysteine 14 (C14) (Ichikawa et al., 2001) (Figure 7).

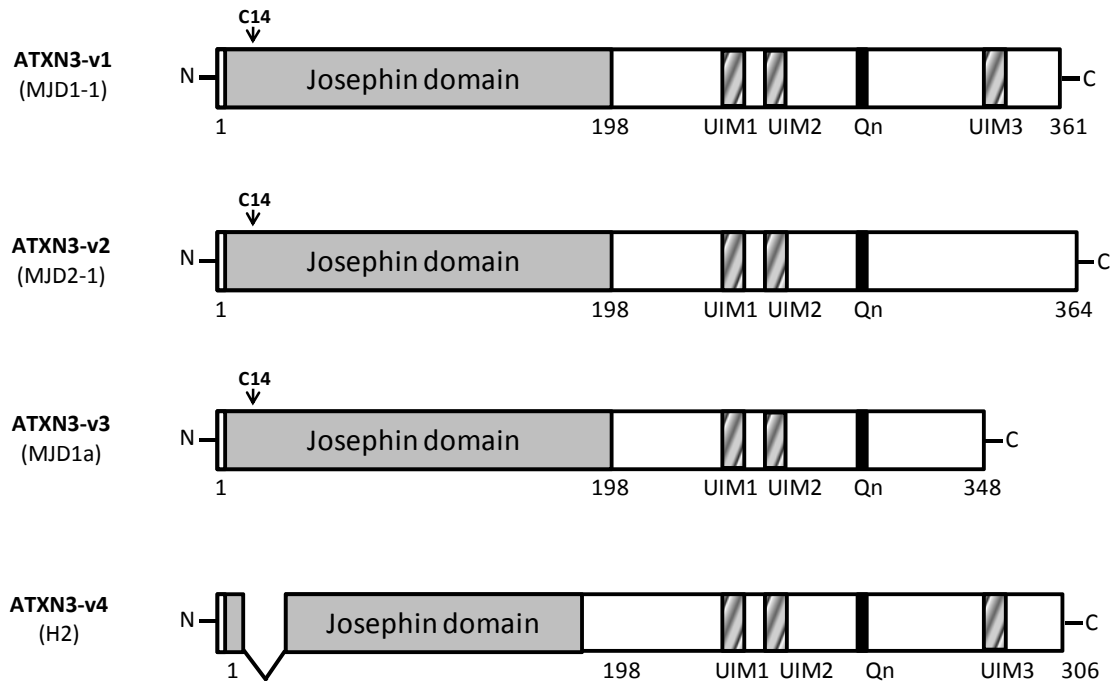


**Figure 7.** Schematic representation of the four ataxin-3 protein variants initially described. The accession numbers of the proteins are the following: for ATXN3-v1, Q96TC4; ATXN3-v2, Q96TC3; ATXN3-v3, AAB33571.1; and ATXN3-v4, BAB18798. The corresponding cDNA variants are indicated in parenthesis.

Using bioinformatic analyses, Scheel and collaborators (2003) demonstrated that the JD, comprising the first 198 aa of ataxin-3, was a highly evolutionarily conserved domain that possessed the predictive catalytic triad (C14-H119-N134) typical of ubiquitin C-terminal hydrolases (UCHs), and thus, might have a role as a ubiquitin-specific cysteine protease (USP) (Scheel et al., 2003). Using the same approach, Donaldson and co-workers (2003) suggested that ataxin-3 could be an ubiquitin-interacting protein, localising to polyQ aggregates in a UIM-dependent manner, with partial modulation by the JD (Donaldson et al., 2003). Soon, these observations were confirmed *in vitro*, by the binding of ataxin-3 to K48-linked Ub chains, hydrolysing preferentially protein chains containing more than four Ub's. This deubiquitylating (DUB) activity of ataxin-3 was shown to be dependent on the conserved cysteine 14 (C14) *in vitro* (Burnett et al., 2003; Chai et al., 2004). Moreover, over-expression of inactive C14A-mutated protein in neural cell lines led to an evident accumulation of ubiquitylated proteins, comparable only to proteasome-inhibited conditions. The authors also

suggested that ataxin-3 is able of self-ubiquitylation (dependent of the UIMs) and self-deubiquitylating processing, showing a possible auto-regulation of its participation in the protein quality control pathways (Berke and Paulson, 2003). More recently, it was shown that ataxin-3 catalytic activity is able to regulate its own cellular turnover, ubiquitylation, and subcellular distribution (Todi et al., 2007). ataxin-3 has also been found to bind ubiquitylated proteins in a manner that is regulated by its UIM domains (Berke et al., 2005), and interestingly the ataxin-3 UIMs were shown to be capable of inhibiting the aggregation of expanded huntingtin (Miller et al., 2007).

Although the three-dimensional structure of the entire ataxin-3 is still unavailable, studies using limited proteolysis and NMR assays, revealed the existence of a 20 kDa region resistant to proteolysis (comprising a region later defined as the JD), and a flexible C-terminal region, that includes the polyQ domain (Masino et al., 2003). NMR analysis of the JD, confirmed that this is the only constitutively folded region in ataxin-3, rich in  $\alpha$ -helices and adopting an open semi-elongated L-structure, compatible with its cysteinic protease activity (Nicastro et al., 2005; Nicastro et al., 2006).

## **1.6. Animal models for MJD**

Since the identification of the disease-causing genes, particularly the mutant *ATXN3* gene in MJD, *in vitro* (Evert et al., 1999; Yoshizawa et al., 2000; Yoshizawa et al., 2001) and *in vivo* models (Ikeda et al., 1996; Cemal et al., 2002; Riess et al., 2008) have been developed, in order to elucidate the molecular mechanism underlying the pathogenesis and to assess potential therapeutic strategies. So far, several MJD animal models have been developed using mice, rat, *Drosophila* and *C.elegans*. A brief description of those models will follow.

### **1.6.1. MJD knockout model in *C. elegans* and *M. musculus***

The first knockout (KO) model for ataxin-3 was generated in *C.elegans* by the Caenorhabditis Genetics Center (CGC) and the characterization of these animals was performed in our group (Rodrigues et al., 2007) in order to contribute for the understanding of the normal function of this protein. No overt phenotype was observed at 20°C in the KO animals, which were viable and showed no obvious abnormalities. The lifespan, size of KO strains as well as locomotion and basic behaviors such as feeding and defecation were similar to wild-type strains. Nevertheless, gene expression analysis uncovered a molecular phenotype with significant dysregulation of genes involved in the ubiquitin-proteasome pathway, structure/motility and signal transduction (Rodrigues

## Chapter 1. Introduction

et al., 2007). More recently, our group has found that at 25°C ataxin-3 KOs do present an uncoordination phenotype (Rodrigues et al., 2009), and, most intriguingly, that these animals have an increased resistance to heat stress (Rodrigues et al., unpublished data).

A mouse strain lacking ataxin-3 was also generated, to provide information on the normal function of ataxin-3 and to test the hypothesis that loss of ataxin-3 contributes to the pathology in SCA3 (Schmitt et al., 2007). Ataxin-3 null mice are viable, fertile and display a normal lifespan and somatic development, with no major coordination problems. Although no morphological signs of pathogenesis were found in several areas of the CNS of mice lacking ataxin-3 up to 1 year of age, researchers found increased levels of ubiquitylated proteins in *Atxn3* KO tissues, providing for the first time *in vivo* evidence of the deubiquitylating function of ataxin-3. These observations clearly support the idea that MJD is not caused by the loss of function of ataxin-3, but do not rule out a possible contribution of wild-type ataxin-3 in MJD pathogenesis.

### 1.6.2. *Drosophila melanogaster* MJD model

The first MJD model in *Drosophila* expressing a fragment of the ataxin-3 protein carrying an expanded polyQ repeat, has demonstrated NI formation and late-onset cell degeneration. Interestingly, different sensitivity to the expanded protein has been observed among different cell types, the neurons being particularly susceptible (Warrick et al., 1998). The same group also showed that directed overexpression of the molecular chaperone HSP70 suppressed polyQ-induced neurodegeneration *in vivo*, without a visible effect on NI formation, indicating that polyQ toxicity can be dissociated from the formation of large aggregates. Indeed, it has been demonstrated in different animal models that over-expression of molecular chaperones has a neuroprotective effect, reinforcing the idea that modulation of chaperone expression could be a therapeutic strategy for treating MJD and other neurodegenerative diseases associated with abnormal protein conformation and toxicity (Warrick et al., 1999; Adachi et al., 2003; Adachi et al., 2009).

More recently, the same group, using the *Drosophila* model, has established a direct link between both protein function and disease pathogenesis to ubiquitin pathways in MJD. Indeed, they showed that normal human ataxin-3, is a prominent suppressor of polyQ neurodegeneration *in vivo* that requires its ubiquitin-associated activities and is dependent upon proteasome function. This finding highlights the importance of the normal function of ataxin-3 in MJD pathogenesis and suggests a potential therapeutic role of ataxin-3 activity for polyQ disorders (Warrick et al., 2005).

### 1.6.3. MJD transgenic mice

In contrast with the results obtained in KO models, mice over expressing truncated or full-length expanded human ataxin-3 have demonstrated a neurological phenotype and pathological features. Kakizuka's group was the first to demonstrate neurodegeneration and a neurological phenotype in transgenic mice with a CAG trinucleotide repeat in the ataxin-3 cDNA. They generated transgenic lines in which a 79Q tract was expressed in the context of the full-length mutant ataxin-3 cDNA (*mjd1a* isoform), of the truncated form of the protein, or alone, under the control of a Purkinje cell specific promoter (L7). No ataxic phenotype was observed at 23 weeks of age in animals expressing the full-length ataxin-3 with 79Q whereas animals expressing the polyQ fragment displayed an ataxic behavior at 4 weeks of age and presented considerable degeneration in the three layers of the cerebellum at 8 weeks (Ikeda et al., 1996).

Some years later, Cemal and co-workers, generated transgenic mouse models using the yeast artificial chromosome (YAC) technology. A vector containing the full-length human *MJD1* gene was used, potentially coding for all alternative spliced isoforms of mutant ataxin-3, with 64 and up to 84 CAG repeats, under the control of the endogenous (human) *MJD1* promoter (Cemal et al., 1999). Animals with the expanded alleles developed a very mild and slowly progressive cerebellar deficit, manifesting as early as 4 weeks of age. Nlls and cell loss were prominent in the pontine and dentate nuclei, with variable cell loss in the cerebellar cortex and Purkinje cells (Cemal et al., 2002). These mice also displayed peripheral nerve degeneration and axonal loss at 26 weeks of age, nevertheless, premature death was not observed. This mouse was the first model described expressing the full-length *MJD1* gene under the control of its own regulatory elements. Even so, there is a concern regarding the existence of two other genes flanking the *MJD1* gene (*TRP1*, *URA3*) whose over expression could influence the results obtained.

A much more severe phenotype was observed in a mouse model expressing *MJD1* under control of a mouse prion promoter (moPrP) (Goti et al., 2004). Nlls were found in homozygous mice with 8 months of age, predominantly in the deep cerebellar nuclei and in pontine nuclei, but also in the spinal cord and olfactory bulb, and only occasionally in the thalamus or cerebellar cortex. No qualitative morphological differences were observed in the brains of this transgenic mouse, in which apoptosis and astrogliosis were absent. Using unbiased stereology, the researchers looked for differences in the number of neurons in dentate nuclei and dopaminergic (Tyrosine hydroxylase-(TH)-positive) neurons in the substantia nigra. No significant differences were found in the total numbers of neurons in the dentate nucleus, whereas a reduction of TH-positive cells was found in

## Chapter 1. Introduction

the substantia nigra, a region which is also affected in humans. In contrast, heterozygous Q71 mice displayed normal behavior at 15 months, which does not mimic the autosomal dominant feature of MJD. Interestingly, however, a C-terminal cleavage fragment of the transgene product has been revealed in this model, which the researchers also observed in human patients' post-mortem brains (Goti et al., 2004). Cleavage fragments had also been described in transfected cells (Paulson et al., 1997a; Perez et al., 1998; Pozzi et al., 2008).

In 2007, the group of Olaf Riess developed another MJD transgenic mouse model expressing the full-length ataxin-3 with 15, 70 or 148 CAG repeats under the control of the moPrP (Bichelmeier et al., 2007). Transgenic mice for ataxin-3 with 15 CAG repeats were normal with no signs of neurodegeneration, while mice expressing mutant ataxin-3 with (70 and 148 CAG repeats) displayed a neurological phenotype including reduced motor and exploratory activity, tremor and premature death by 3 to 6 months. Ataxin-3 and Ub-positive inclusions were observed in almost all brain with the exception of Purkinje cells. Interestingly, the cell body of these cells was atrophic but no significant loss was observed. Q148 mice displayed a more severe neurological phenotype with more inclusions and earlier death when compared with mice expressing mutant ataxin-3 with 70 CAG repeats. In addition, the authors proved that the nuclear localization of the mutant protein is crucial for pathogenesis to occur, by the manipulation of the ataxin-3 cellular localization with NLS or nuclear export signal (NES).

More recently, a new transgenic mouse model was generated expressing the human ataxin-3 cDNA containing 79 CAG repeats, under the moPrP (Chou et al., 2008). These mice displayed motor dysfunction at an age of 5-6 months and the severity of neurological symptoms progressively increased in the following months. A robust neuronal loss was observed in the cerebellum of 10-11 months old mice expressing mutant ataxin-3. Behavioral analysis revealed motor coordination impairment, deficit in the ability to correct the body posture, ataxic gait, reduced locomotor activity and weight loss. Intranuclear inclusions were observed in the dentate and pontine nuclei, and in the substantia nigra.

In order to analyze whether symptoms caused by ataxin-3 with an expanded repeat are reversible *in vivo*, a conditional mouse model of SCA3 with the full-length human ataxin-3 cDNA with 77 repeats was created using the Tet-Off system (Boy et al., 2009). When the expression of the expanded ataxin-3 was induced, transgenic mice developed a progressive neurological phenotype characterized by neuronal dysfunction in the cerebellum, reduced anxiety, hyperactivity, impaired Rotarod performance and decreased gain of body weight. On the other hand, when ataxin-3

expression was turned off at an early symptomatic stage of the disease, the transgenic mice were indistinguishable from negative controls after 5 months of treatment. In the same year, the same group published another MJD transgenic mice model expressing ataxin-3 with 148 CAG repeats under the control of the huntingtin promoter, resulting in ubiquitous expression throughout the whole brain (Boy et al., 2010). The model resembles many features of the disease in humans, including a late onset of symptoms and CAG repeat instability in transmission to offspring. They observed a biphasic progression of the disease, with hyperactivity during the first months (not seen in human patients) and a decline of motor coordination after about 1 year of age; however, intranuclear aggregates were not visible at this age, but only at the age of 18 months.

The MJD transgenic mouse models referred above suggest that despite the expression of mutant ataxin-3 in the brain, there are considerable differences in the affected brains regions and cell types. So far, no model has yet completely reproduced the pathological and clinical symptoms observed in MJD patients. Several factors might explain the differences between these models and the human pathology (Yamada et al., 2008). First, the short lifespan associated to the high metabolic activity of mice could play a role; then the different transgenic models have been generated with the introduction of proteins with expanded polyQ stretches under the control of different promoters and variations in the number of transgene copy number. Moreover, one should not discard the effects of the ectopic expression of transgenic human ataxin-3 in mouse brain regions, which also express the endogenous homologous protein. These models have also suggested that in order to reproduce specific MJD neurodegeneration in mice, it may be necessary to express a much higher level of the expanded protein with the appropriate spatio-temporal pattern in the brain. Even so, these mice models have provided further insights into the mechanisms involved in MJD pathogenesis.

**1.7. Aims of the study**

The overall objective of this thesis was the generation and characterization of new transgenic mouse models for MJD.

Specifically, we intended to:

- Study the intergenerational and somatic instability pattern of the expanded CAG tract in MJD transgenic mice;
- Perform a correlation study between the somatic mosaicism observed in different regions of the brain and the pathological findings observed in our mice;
- Evaluate the behavioral profile of MJD mice, comparing it to MJD symptoms in patients;
- Analyze the pathological changes in the CNS of transgenic mice displaying motor behavioral deficits;
- Evaluate the activation of autophagy as a therapeutic strategy in MJD.

## 1.8. References

- Adachi, H., Kume, A., Li, M., Nakagomi, Y., Niwa, H., Do, J., Sang, C., Kobayashi, Y., Doyu, M. and Sobue, G. 2001. Transgenic mice with an expanded CAG repeat controlled by the human AR promoter show polyglutamine nuclear inclusions and neuronal dysfunction without neuronal cell death. *Hum Mol Genet.* 10, 1039-1048.
- Adachi, H., Katsuno, M., Minamiyama, M., Sang, C., Pagoulatos, G., Angelidis, C., Kusakabe, M., Yoshiki, A., Kobayashi, Y., Doyu, M. and Sobue, G. 2003. Heat shock protein 70 chaperone overexpression ameliorates phenotypes of the spinal and bulbar muscular atrophy transgenic mouse model by reducing nuclear-localized mutant androgen receptor protein. *J Neurosci.* 23, 2203-2211.
- Adachi, H., Katsuno, M., Waza, M., Minamiyama, M., Tanaka, F. and Sobue, G. 2009. Heat shock proteins in neurodegenerative diseases: pathogenic roles and therapeutic implications. *Int J Hyperthermia.* 25, 647-654.
- Al-Mahdawi, S., Pinto, R. M., Ruddle, P., Carroll, C., Webster, Z. and Pook, M. 2004. GAA repeat instability in Friedreich ataxia YAC transgenic mice. *Genomics.* 84, 301-310.
- Al-Ramahi, I., Perez, A. M., Lim, J., Zhang, M., Sorensen, R., de Haro, M., Branco, J., Pulst, S. M., Zoghbi, H. Y. and Botas, J. 2007. dAtaxin-2 mediates expanded Ataxin-1-induced neurodegeneration in a *Drosophila* model of SCA1. *PLoS Genet.* 3, e234.
- Albrecht, M., Hoffmann, D., Evert, B. O., Schmitt, I., Wullner, U. and Lengauer, T. 2003. Structural modeling of ataxin-3 reveals distant homology to adaptins. *Proteins.* 50, 355-370.
- Albrecht, M., Golatta, M., Wullner, U. and Lengauer, T. 2004. Structural and functional analysis of ataxin-2 and ataxin-3. *Eur J Biochem.* 271, 3155-3170.
- Andreassen, O. A., Dedeoglu, A., Ferrante, R. J., Jenkins, B. G., Ferrante, K. L., Thomas, M., Friedlich, A., Browne, S. E., Schilling, G., Borchelt, D. R., Hersch, S. M., Ross, C. A. and Beal, M. F. 2001. Creatine increase survival and delays motor symptoms in a transgenic animal model of Huntington's disease. *Neurobiol Dis.* 8, 479-491.
- Ansved, T., Lundin, A. and Anvret, M. 1998. Larger CAG expansions in skeletal muscle compared with lymphocytes in Kennedy disease but not in Huntington disease. *Neurology.* 51, 1442-1444.
- Apostolinas, S., Rajendren, G., Dobrjansky, A. and Gibson, M. J. 1999. Androgen receptor immunoreactivity in specific neural regions in normal and hypogonadal male mice: effect of androgens. *Brain Res.* 817, 19-24.
- Arrasate, M., Mitra, S., Schweitzer, E. S., Segal, M. R. and Finkbeiner, S. 2004. Inclusion body formation reduces levels of mutant huntingtin and the risk of neuronal death. *Nature.* 431, 805-810.
- Barbeau, A., Roy, M., Cunha, L., de Vincente, A. N., Rosenberg, R. N., Nyhan, W. L., MacLeod, P. L., Chazot, G., Langston, L. B., Dawson, D. M. and et al. 1984. The natural history of Machado-Joseph disease. An analysis of 138 personally examined cases. *Can J Neurol Sci.* 11, 510-525.
- Bates, G. P., Mangiarini, L. and Davies, S. W. 1998. Transgenic mice in the study of polyglutamine repeat expansion diseases. *Brain Pathol.* 8, 699-714.
- Bauer, P. O. and Nukina, N. 2009. The pathogenic mechanisms of polyglutamine diseases and current therapeutic strategies. *J Neurochem.* 110, 1737-1765.
- Bauer, P. O., Wong, H. K., Oyama, F., Goswami, A., Okuno, M., Kino, Y., Miyazaki, H. and Nukina, N. 2009. Inhibition of Rho kinases enhances the degradation of mutant huntingtin. *J Biol Chem.* 284, 13153-13164.
- Becher, M. W., Kotzuc, J. A., Sharp, A. H., Davies, S. W., Bates, G. P., Price, D. L. and Ross, C. A. 1998. Intranuclear neuronal inclusions in Huntington's disease and dentatorubral and



## Chapter 1. Introduction

- pallidolusian atrophy: correlation between the density of inclusions and IT15 CAG triplet repeat length. *Neurobiol Dis.* 4, 387-397.
- Becher, M. W. and Ross, C. A. 1998. Intranuclear neuronal inclusions in DRPLA. *Mov Disord.* 13, 852-853.
- Berke, S. J. and Paulson, H. L. 2003. Protein aggregation and the ubiquitin proteasome pathway: gaining the UPPer hand on neurodegeneration. *Curr Opin Genet Dev.* 13, 253-261.
- Berke, S. J., Schmied, F. A., Brunt, E. R., Ellerby, L. M. and Paulson, H. L. 2004. Caspase-mediated proteolysis of the polyglutamine disease protein ataxin-3. *J Neurochem.* 89, 908-918.
- Berke, S. J., Chai, Y., Marrs, G. L., Wen, H. and Paulson, H. L. 2005. Defining the role of ubiquitin-interacting motifs in the polyglutamine disease protein, ataxin-3. *J Biol Chem.* 280, 32026-32034.
- Bettencourt, C., Santos, C., Montiel, R., Costa Mdo, C., Cruz-Morales, P., Santos, L. R., Simoes, N., Kay, T., Vasconcelos, J., Maciel, P. and Lima, M. 2010. Increased transcript diversity: novel splicing variants of Machado-Joseph disease gene (ATXN3). *Neurogenetics.* 11, 193-202.
- Bichelmeier, U., Schmidt, T., Hubener, J., Boy, J., Ruttiger, L., Habig, K., Poths, S., Bonin, M., Knipper, M., Schmidt, W. J., Wilbertz, J., Wolburg, H., Laccone, F. and Riess, O. 2007. Nuclear localization of ataxin-3 is required for the manifestation of symptoms in SCA3: in vivo evidence. *J Neurosci.* 27, 7418-7428.
- Bogdanov, M. B., Andreassen, O. A., Dedeoglu, A., Ferrante, R. J. and Beal, M. F. 2001. Increased oxidative damage to DNA in a transgenic mouse model of Huntington's disease. *J Neurochem.* 79, 1246-1249.
- Bonelli, R. M., Hodl, A. K., Hofmann, P. and Kapfhammer, H. P. 2004. Neuroprotection in Huntington's disease: a 2-year study on minocycline. *Int Clin Psychopharmacol.* 19, 337-342.
- Boy, J., Schmidt, T., Wolburg, H., Mack, A., Nuber, S., Bottcher, M., Schmitt, I., Holzmann, C., Zimmermann, F., Servadio, A. and Riess, O. 2009. Reversibility of symptoms in a conditional mouse model of spinocerebellar ataxia type 3. *Hum Mol Genet.* 18, 4282-4295.
- Boy, J., Schmidt, T., Schumann, U., Grasshoff, U., Unser, S., Holzmann, C., Schmitt, I., Karl, T., Laccone, F., Wolburg, H., Ibrahim, S. and Riess, O. 2010. A transgenic mouse model of spinocerebellar ataxia type 3 resembling late disease onset and gender-specific instability of CAG repeats. *Neurobiol Dis.* 37, 284-293.
- Brignull, H. R., Moore, F. E., Tang, S. J. and Morimoto, R. I. 2006. Polyglutamine proteins at the pathogenic threshold display neuron-specific aggregation in a pan-neuronal *Caenorhabditis elegans* model. *J Neurosci.* 26, 7597-7606.
- Burnett, B., Li, F. and Pittman, R. N. 2003. The polyglutamine neurodegenerative protein ataxin-3 binds polyubiquitylated proteins and has ubiquitin protease activity. *Hum Mol Genet.* 12, 3195-3205.
- Burright, E. N., Clark, H. B., Servadio, A., Matilla, T., Feddersen, R. M., Yunis, W. S., Duvick, L. A., Zoghbi, H. Y. and Orr, H. T. 1995. SCA1 transgenic mice: a model for neurodegeneration caused by an expanded CAG trinucleotide repeat. *Cell.* 82, 937-948.
- Cancel, G., Gourfinkel-An, I., Stevanin, G., Didierjean, O., Abbas, N., Hirsch, E., Agid, Y. and Brice, A. 1998. Somatic mosaicism of the CAG repeat expansion in spinocerebellar ataxia type 3/Machado-Joseph disease. *Hum Mutat.* 11, 23-27.
- Caramins, M., Halliday, G., McCusker, E. and Trent, R. J. 2003. Genetically confirmed clinical Huntington's disease with no observable cell loss. *J Neurol Neurosurg Psychiatry.* 74, 968-970.
- Cemal, C. K., Huxley, C. and Chamberlain, S. 1999. Insertion of expanded CAG trinucleotide repeat motifs into a yeast artificial chromosome containing the human Machado-Joseph disease gene. *Gene.* 236, 53-61.
- Cemal, C. K., Carroll, C. J., Lawrence, L., Lowrie, M. B., Ruddle, P., Al-Mahdawi, S., King, R. H., Pook, M. A., Huxley, C. and Chamberlain, S. 2002. YAC transgenic mice carrying pathological

- alleles of the MJD1 locus exhibit a mild and slowly progressive cerebellar deficit. *Hum Mol Genet.* 11, 1075-1094.
- Cepeda, C., Hurst, R. S., Calvert, C. R., Hernandez-Echeagaray, E., Nguyen, O. K., Jocoy, E., Christian, L. J., Ariano, M. A. and Levine, M. S. 2003. Transient and progressive electrophysiological alterations in the corticostriatal pathway in a mouse model of Huntington's disease. *J Neurosci.* 23, 961-969.
- Cha, J. H. and Dure, L. S. t. 1994. Trinucleotide repeats in neurologic diseases: an hypothesis concerning the pathogenesis of Huntington's disease, Kennedy's disease, and spinocerebellar ataxia type I. *Life Sci.* 54, 1459-1464.
- Chai, Y., Wu, L., Griffin, J. D. and Paulson, H. L. 2001. The role of protein composition in specifying nuclear inclusion formation in polyglutamine disease. *J Biol Chem.* 276, 44889-44897.
- Chai, Y., Berke, S. S., Cohen, R. E. and Paulson, H. L. 2004. Poly-ubiquitin binding by the polyglutamine disease protein ataxin-3 links its normal function to protein surveillance pathways. *J Biol Chem.* 279, 3605-3611.
- Chen, H. K., Fernandez-Funez, P., Acevedo, S. F., Lam, Y. C., Kaytor, M. D., Fernandez, M. H., Aitken, A., Skoulakis, E. M., Orr, H. T., Botas, J. and Zoghbi, H. Y. 2003. Interaction of Akt-phosphorylated ataxin-1 with 14-3-3 mediates neurodegeneration in spinocerebellar ataxia type 1. *Cell.* 113, 457-468.
- Chen, M., Ona, V. O., Li, M., Ferrante, R. J., Fink, K. B., Zhu, S., Bian, J., Guo, L., Farrell, L. A., Hersch, S. M., Hobbs, W., Vonsattel, J. P., Cha, J. H. and Friedlander, R. M. 2000. Minocycline inhibits caspase-1 and caspase-3 expression and delays mortality in a transgenic mouse model of Huntington disease. *Nat Med.* 6, 797-801.
- Chong, S. S., McCall, A. E., Cota, J., Subramony, S. H., Orr, H. T., Hughes, M. R. and Zoghbi, H. Y. 1995. Gametic and somatic tissue-specific heterogeneity of the expanded SCA1 CAG repeat in spinocerebellar ataxia type 1. *Nat Genet.* 10, 344-350.
- Chou, A. H., Yeh, T. H., Kuo, Y. L., Kao, Y. C., Jou, M. J., Hsu, C. Y., Tsai, S. R., Kakizuka, A. and Wang, H. L. 2006. Polyglutamine-expanded ataxin-3 activates mitochondrial apoptotic pathway by upregulating Bax and downregulating Bcl-xL. *Neurobiol Dis.* 21, 333-345.
- Chou, A. H., Yeh, T. H., Ouyang, P., Chen, Y. L., Chen, S. Y. and Wang, H. L. 2008. Polyglutamine-expanded ataxin-3 causes cerebellar dysfunction of SCA3 transgenic mice by inducing transcriptional dysregulation. *Neurobiol Dis.* 31, 89-101.
- Cooper, J. K., Schilling, G., Peters, M. F., Herring, W. J., Sharp, A. H., Kaminsky, Z., Masone, J., Khan, F. A., Delanoy, M., Borchelt, D. R., Dawson, V. L., Dawson, T. M. and Ross, C. A. 1998. Truncated N-terminal fragments of huntingtin with expanded glutamine repeats form nuclear and cytoplasmic aggregates in cell culture. *Hum Mol Genet.* 7, 783-790.
- Costa, C., Gomes-da-Silva, J., Miranda, C. J., Sequeiros, J., Santos, M. M. and Maciel, P. 2004. Genomic structure, promoter activity, and developmental expression of the mouse homologue of the Machado-Joseph disease (MJD) gene. *Genomics.* 84, 361-373.
- Coutinho, M. 1992. [Not Available]. *Estud Hist Saude.* 4, 1-23.
- Coutinho, P. and Andrade, C. 1978. Autosomal dominant system degeneration in Portuguese families of the Azores Islands. A new genetic disorder involving cerebellar, pyramidal, extrapyramidal and spinal cord motor functions. *Neurology.* 28, 703-709.
- Cummings, C. J., Mancini, M. A., Antalffy, B., DeFranco, D. B., Orr, H. T. and Zoghbi, H. Y. 1998. Chaperone suppression of aggregation and altered subcellular proteasome localization imply protein misfolding in SCA1. *Nat Genet.* 19, 148-154.
- Cummings, C. J., Sun, Y., Opal, P., Antalffy, B., Mestril, R., Orr, H. T., Dillmann, W. H. and Zoghbi, H. Y. 2001. Over-expression of inducible HSP70 chaperone suppresses neuropathology and improves motor function in SCA1 mice. *Hum Mol Genet.* 10, 1511-1518.
- Davies, S. W., Turmaine, M., Cozens, B. A., DiFiglia, M., Sharp, A. H., Ross, C. A., Scherzinger, E., Wanker, E. E., Mangiarini, L. and Bates, G. P. 1997. Formation of neuronal intranuclear inclusions underlies the neurological dysfunction in mice transgenic for the HD mutation. *Cell.* 90, 537-548.

## Chapter 1. Introduction

- Davies, S. W., Beardsall, K., Turmaine, M., DiFiglia, M., Aronin, N. and Bates, G. P. 1998. Are neuronal intranuclear inclusions the common neuropathology of triplet-repeat disorders with polyglutamine-repeat expansions? *Lancet*. 351, 131-133.
- de Chiara, C., Menon, R. P., Dal Piaz, F., Calder, L. and Pastore, A. 2005. Polyglutamine is not all: the functional role of the AXH domain in the ataxin-1 protein. *J Mol Biol*. 354, 883-893.
- Dedeoglu, A., Kubilus, J. K., Jeitner, T. M., Matson, S. A., Bogdanov, M., Kowall, N. W., Matson, W. R., Cooper, A. J., Ratan, R. R., Beal, M. F., Hersch, S. M. and Ferrante, R. J. 2002. Therapeutic effects of cystamine in a murine model of Huntington's disease. *J Neurosci*. 22, 8942-8950.
- DeMarch, Z., Giampa, C., Patassini, S., Bernardi, G. and Fusco, F. R. 2008. Beneficial effects of rolipram in the R6/2 mouse model of Huntington's disease. *Neurobiol Dis*. 30, 375-387.
- Desplats, P. A., Kass, K. E., Gilmartin, T., Stanwood, G. D., Woodward, E. L., Head, S. R., Sutcliffe, J. G. and Thomas, E. A. 2006. Selective deficits in the expression of striatal-enriched mRNAs in Huntington's disease. *J Neurochem*. 96, 743-757.
- Di Prospero, N. A. and Fischbeck, K. H. 2005. Therapeutics development for triplet repeat expansion diseases. *Nat Rev Genet*. 6, 756-765.
- DiFiglia, M., Sapp, E., Chase, K. O., Davies, S. W., Bates, G. P., Vonsattel, J. P. and Aronin, N. 1997. Aggregation of huntingtin in neuronal intranuclear inclusions and dystrophic neurites in brain. *Science*. 277, 1990-1993.
- DiFiglia, M. 2002. Huntingtin fragments that aggregate go their separate ways. *Mol Cell*. 10, 224-225.
- Donaldson, K. M., Li, W., Ching, K. A., Batalov, S., Tsai, C. C. and Joazeiro, C. A. 2003. Ubiquitin-mediated sequestration of normal cellular proteins into polyglutamine aggregates. *Proc Natl Acad Sci U S A*. 100, 8892-8897.
- Doss-Pepe, E. W., Stenroos, E. S., Johnson, W. G. and Madura, K. 2003. Ataxin-3 interactions with rad23 and valosin-containing protein and its associations with ubiquitin chains and the proteasome are consistent with a role in ubiquitin-mediated proteolysis. *Mol Cell Biol*. 23, 6469-6483.
- Dunah, A. W., Jeong, H., Griffin, A., Kim, Y. M., Standaert, D. G., Hersch, S. M., Mouradian, M. M., Young, A. B., Tanese, N. and Krainc, D. 2002. Sp1 and TAFII130 transcriptional activity disrupted in early Huntington's disease. *Science*. 296, 2238-2243.
- Duyao, M., Ambrose, C., Myers, R., Novelletto, A., Persichetti, F., Frontali, M., Folstein, S., Ross, C., Franz, M., Abbott, M. and et al. 1993. Trinucleotide repeat length instability and age of onset in Huntington's disease. *Nat Genet*. 4, 387-392.
- Duyao, M. P., Auerbach, A. B., Ryan, A., Persichetti, F., Barnes, G. T., McNeil, S. M., Ge, P., Vonsattel, J. P., Gusella, J. F., Joyner, A. L. and et al. 1995. Inactivation of the mouse Huntington's disease gene homolog Hdh. *Science*. 269, 407-410.
- Ellerby, L. M., Hackam, A. S., Propp, S. S., Ellerby, H. M., Rabizadeh, S., Cashman, N. R., Trifiro, M. A., Pinsky, L., Wellington, C. L., Salvesen, G. S., Hayden, M. R. and Bredesen, D. E. 1999. Kennedy's disease: caspase cleavage of the androgen receptor is a crucial event in cytotoxicity. *J Neurochem*. 72, 185-195.
- Emamian, E. S., Kaytor, M. D., Duvick, L. A., Zu, T., Tousey, S. K., Zoghbi, H. Y., Clark, H. B. and Orr, H. T. 2003. Serine 776 of ataxin-1 is critical for polyglutamine-induced disease in SCA1 transgenic mice. *Neuron*. 38, 375-387.
- Everett, C. M. and Wood, N. W. 2004. Trinucleotide repeats and neurodegenerative disease. *Brain*. 127, 2385-2405.
- Evert, B. O., Wullner, U., Schulz, J. B., Weller, M., Groscurth, P., Trottier, Y., Brice, A. and Klockgether, T. 1999. High level expression of expanded full-length ataxin-3 in vitro causes cell death and formation of intranuclear inclusions in neuronal cells. *Hum Mol Genet*. 8, 1169-1176.

- Fei, E., Jia, N., Zhang, T., Ma, X., Wang, H., Liu, C., Zhang, W., Ding, L., Nukina, N. and Wang, G. 2007. Phosphorylation of ataxin-3 by glycogen synthase kinase 3 $\beta$  at serine 256 regulates the aggregation of ataxin-3. *Biochem Biophys Res Commun.* 357, 487-492.
- Ferrante, R. J., Andreassen, O. A., Jenkins, B. G., Dedeoglu, A., Kuemmerle, S., Kubilus, J. K., Kaddurah-Daouk, R., Hersch, S. M. and Beal, M. F. 2000. Neuroprotective effects of creatine in a transgenic mouse model of Huntington's disease. *J Neurosci.* 20, 4389-4397.
- Ferrante, R. J., Andreassen, O. A., Dedeoglu, A., Ferrante, K. L., Jenkins, B. G., Hersch, S. M. and Beal, M. F. 2002. Therapeutic effects of coenzyme Q10 and remacemide in transgenic mouse models of Huntington's disease. *J Neurosci.* 22, 1592-1599.
- Ferrante, R. J., Kubilus, J. K., Lee, J., Ryu, H., Beesen, A., Zucker, B., Smith, K., Kowall, N. W., Ratan, R. R., Luthi-Carter, R. and Hersch, S. M. 2003. Histone deacetylase inhibition by sodium butyrate chemotherapy ameliorates the neurodegenerative phenotype in Huntington's disease mice. *J Neurosci.* 23, 9418-9427.
- Ferrante, R. J., Ryu, H., Kubilus, J. K., D'Mello, S., Sugars, K. L., Lee, J., Lu, P., Smith, K., Browne, S., Beal, M. F., Kristal, B. S., Stavrovskaya, I. G., Hewett, S., Rubinsztein, D. C., Langley, B. and Ratan, R. R. 2004. Chemotherapy for the brain: the antitumor antibiotic mithramycin prolongs survival in a mouse model of Huntington's disease. *J Neurosci.* 24, 10335-10342.
- Fleischer, B. 1918. Über myotonische Dystrophie mit Katarakt: eine hereditäre, familiäre Degeneration. *Arch Ophthalmol.* 96, 91-133.
- Forman, M. S., Trojanowski, J. Q. and Lee, V. M. 2004. Neurodegenerative diseases: a decade of discoveries paves the way for therapeutic breakthroughs. *Nat Med.* 10, 1055-1063.
- Fortune, M. T., Vassilopoulos, C., Coolbaugh, M. I., Siciliano, M. J. and Monckton, D. G. 2000. Dramatic, expansion-biased, age-dependent, tissue-specific somatic mosaicism in a transgenic mouse model of triplet repeat instability. *Hum Mol Genet.* 9, 439-445.
- Fu, Y. H., Kuhl, D. P., Pizzuti, A., Pieretti, M., Sutcliffe, J. S., Richards, S., Verkerk, A. J., Holden, J. J., Fenwick, R. G., Jr., Warren, S. T. and et al. 1991. Variation of the CGG repeat at the fragile X site results in genetic instability: resolution of the Sherman paradox. *Cell.* 67, 1047-1058.
- Fujigasaki, H., Uchihara, T., Koyano, S., Iwabuchi, K., Yagishita, S., Makifuchi, T., Nakamura, A., Ishida, K., Toru, S., Hirai, S., Ishikawa, K., Tanabe, T. and Mizusawa, H. 2000. Ataxin-3 is translocated into the nucleus for the formation of intranuclear inclusions in normal and Machado-Joseph disease brains. *Exp Neurol.* 165, 248-256.
- Gafni, J., Hermel, E., Young, J. E., Wellington, C. L., Hayden, M. R. and Ellerby, L. M. 2004. Inhibition of calpain cleavage of huntingtin reduces toxicity: accumulation of calpain/caspase fragments in the nucleus. *J Biol Chem.* 279, 20211-20220.
- Gardian, G., Browne, S. E., Choi, D. K., Klivenyi, P., Gregorio, J., Kubilus, J. K., Ryu, H., Langley, B., Ratan, R. R., Ferrante, R. J. and Beal, M. F. 2005. Neuroprotective effects of phenylbutyrate in the N171-82Q transgenic mouse model of Huntington's disease. *J Biol Chem.* 280, 556-563.
- Gaspar, C., Lopes-Cendes, I., Hayes, S., Goto, J., Arvidsson, K., Dias, A., Silveira, I., Maciel, P., Coutinho, P., Lima, M., Zhou, Y. X., Soong, B. W., Watanabe, M., Giunti, P., Stevanin, G., Riess, O., Sasaki, H., Hsieh, M., Nicholson, G. A., Brunt, E., Higgins, J. J., Lauritzen, M., Tranebjaerg, L., Volpini, V., Wood, N., Ranum, L., Tsuji, S., Brice, A., Sequeiros, J. and Rouleau, G. A. 2001. Ancestral origins of the Machado-Joseph disease mutation: a worldwide haplotype study. *Am J Hum Genet.* 68, 523-528.
- Gatchel, J. R. and Zoghbi, H. Y. 2005. Diseases of unstable repeat expansion: mechanisms and common principles. *Nat Rev Genet.* 6, 743-755.
- Gervais, F. G., Singaraja, R., Xanthoudakis, S., Gutekunst, C. A., Leavitt, B. R., Metzler, M., Hackam, A. S., Tam, J., Vaillancourt, J. P., Houtzager, V., Rasper, D. M., Roy, S., Hayden, M. R. and Nicholson, D. W. 2002. Recruitment and activation of caspase-8 by the Huntingtin-interacting protein Hip-1 and a novel partner Hipp1. *Nat Cell Biol.* 4, 95-105.

## Chapter 1. Introduction

- Ghosh, S. and Feany, M. B. 2004. Comparison of pathways controlling toxicity in the eye and brain in *Drosophila* models of human neurodegenerative diseases. *Hum Mol Genet.* 13, 2011-2018.
- Giampa, C., Middei, S., Patassini, S., Borreca, A., Marullo, F., Laurenti, D., Bernardi, G., Ammassari-Teule, M. and Fusco, F. R. 2009. Phosphodiesterase type IV inhibition prevents sequestration of CREB binding protein, protects striatal parvalbumin interneurons and rescues motor deficits in the R6/2 mouse model of Huntington's disease. *Eur J Neurosci.* 29, 902-910.
- Gilman, S. 2000. The spinocerebellar ataxias. *Clin Neuropharmacol.* 23, 296-303.
- Goldberg, Y. P., Nicholson, D. W., Rasper, D. M., Kalchman, M. A., Koide, H. B., Graham, R. K., Bromm, M., Kazemi-Esfarjani, P., Thornberry, N. A., Vaillancourt, J. P. and Hayden, M. R. 1996. Cleavage of huntingtin by apopain, a proapoptotic cysteine protease, is modulated by the polyglutamine tract. *Nat Genet.* 13, 442-449.
- Goti, D., Katzen, S. M., Mez, J., Kurtis, N., Kiluk, J., Ben-Haiem, L., Jenkins, N. A., Copeland, N. G., Kakizuka, A., Sharp, A. H., Ross, C. A., Mouton, P. R. and Colomer, V. 2004. A mutant ataxin-3 putative-cleavage fragment in brains of Machado-Joseph disease patients and transgenic mice is cytotoxic above a critical concentration. *J Neurosci.* 24, 10266-10279.
- Goto, J., Watanabe, M., Ichikawa, Y., Yee, S. B., Ihara, N., Endo, K., Igarashi, S., Takiyama, Y., Gaspar, C., Maciel, P., Tsuji, S., Rouleau, G. A. and Kanazawa, I. 1997. Machado-Joseph disease gene products carrying different carboxyl termini. *Neurosci Res.* 28, 373-377.
- Graham, R. K., Deng, Y., Slow, E. J., Haigh, B., Bissada, N., Lu, G., Pearson, J., Shehadeh, J., Bertram, L., Murphy, Z., Warby, S. C., Doty, C. N., Roy, S., Wellington, C. L., Leavitt, B. R., Raymond, L. A., Nicholson, D. W. and Hayden, M. R. 2006. Cleavage at the caspase-6 site is required for neuronal dysfunction and degeneration due to mutant huntingtin. *Cell.* 125, 1179-1191.
- Gu, W., Ma, H., Wang, K., Jin, M., Zhou, Y., Liu, X., Wang, G. and Shen, Y. 2004. The shortest expanded allele of the MJD1 gene in a Chinese MJD kindred with autonomic dysfunction. *Eur Neurol.* 52, 107-111.
- Gusella, J. F. and MacDonald, M. E. 2000. Molecular genetics: unmasking polyglutamine triggers in neurodegenerative disease. *Nat Rev Neurosci.* 1, 109-115.
- Hackam, A. S., Hodgson, J. G., Singaraja, R., Zhang, T., Gan, L., Gutekunst, C. A., Hersch, S. M. and Hayden, M. R. 1999. Evidence for both the nucleus and cytoplasm as subcellular sites of pathogenesis in Huntington's disease in cell culture and in transgenic mice expressing mutant huntingtin. *Philos Trans R Soc Lond B Biol Sci.* 354, 1047-1055.
- Hashida, H., Goto, J., Kurisaki, H., Mizusawa, H. and Kanazawa, I. 1997. Brain regional differences in the expansion of a CAG repeat in the spinocerebellar ataxias: dentatorubral-pallidoluysian atrophy, Machado-Joseph disease, and spinocerebellar ataxia type 1. *Ann Neurol.* 41, 505-511.
- Hashida, H., Goto, J., Suzuki, T., Jeong, S., Masuda, N., Ooie, T., Tachiiri, Y., Tsuchiya, H. and Kanazawa, I. 2001. Single cell analysis of CAG repeat in brains of dentatorubral-pallidoluysian atrophy (DRPLA). *J Neurol Sci.* 190, 87-93.
- Hay, D. G., Sathasivam, K., Tobaben, S., Stahl, B., Marber, M., Mestril, R., Mahal, A., Smith, D. L., Woodman, B. and Bates, G. P. 2004. Progressive decrease in chaperone protein levels in a mouse model of Huntington's disease and induction of stress proteins as a therapeutic approach. *Hum Mol Genet.* 13, 1389-1405.
- Hebert, L. E., Scherr, P. A., Bienias, J. L., Bennett, D. A. and Evans, D. A. 2003. Alzheimer disease in the US population: prevalence estimates using the 2000 census. *Arch Neurol.* 60, 1119-1122.
- Heng, M. Y., Duong, D. K., Albin, R. L., Tallaksen-Greene, S. J., Hunter, J. M., Lesort, M. J., Osmand, A., Paulson, H. L. and Detloff, P. J. 2010. Early autophagic response in a novel knock-in model of Huntington disease. *Hum Mol Genet.* 19, 3702-3720.

- Higgins, J. J., Nee, L. E., Vasconcelos, O., Ide, S. E., Lavedan, C., Goldfarb, L. G. and Polymeropoulos, M. H. 1996. Mutations in American families with spinocerebellar ataxia (SCA) type 3: SCA3 is allelic to Machado-Joseph disease. *Neurology*. 46, 208-213.
- Hockly, E., Richon, V. M., Woodman, B., Smith, D. L., Zhou, X., Rosa, E., Sathasivam, K., Ghazi-Noori, S., Mahal, A., Lowden, P. A., Steffan, J. S., Marsh, J. L., Thompson, L. M., Lewis, C. M., Marks, P. A. and Bates, G. P. 2003. Suberoylanilide hydroxamic acid, a histone deacetylase inhibitor, ameliorates motor deficits in a mouse model of Huntington's disease. *Proc Natl Acad Sci U S A*. 100, 2041-2046.
- Hodgson, J. G., Agopyan, N., Gutekunst, C. A., Leavitt, B. R., LePiane, F., Singaraja, R., Smith, D. J., Bissada, N., McCutcheon, K., Nasir, J., Jamot, L., Li, X. J., Stevens, M. E., Rosemond, E., Roder, J. C., Phillips, A. G., Rubin, E. M., Hersch, S. M. and Hayden, M. R. 1999. A YAC mouse model for Huntington's disease with full-length mutant huntingtin, cytoplasmic toxicity, and selective striatal neurodegeneration. *Neuron*. 23, 181-192.
- Hoffner, G., Island, M. L. and Djian, P. 2005. Purification of neuronal inclusions of patients with Huntington's disease reveals a broad range of N-terminal fragments of expanded huntingtin and insoluble polymers. *J Neurochem*. 95, 125-136.
- Hofmann, K. and Falquet, L. 2001. A ubiquitin-interacting motif conserved in components of the proteasomal and lysosomal protein degradation systems. *Trends Biochem Sci*. 26, 347-350.
- Holmberg, M., Duyckaerts, C., Durr, A., Cancel, G., Gourfinkel-An, I., Damier, P., Faucheux, B., Trottier, Y., Hirsch, E. C., Agid, Y. and Brice, A. 1998. Spinocerebellar ataxia type 7 (SCA7): a neurodegenerative disorder with neuronal intranuclear inclusions. *Hum Mol Genet*. 7, 913-918.
- Hoshino, M., Tagawa, K., Okuda, T. and Okazawa, H. 2004. General transcriptional repression by polyglutamine disease proteins is not directly linked to the presence of inclusion bodies. *Biochem Biophys Res Commun*. 313, 110-116.
- Huen, N. Y. and Chan, H. Y. 2005. Dynamic regulation of molecular chaperone gene expression in polyglutamine disease. *Biochem Biophys Res Commun*. 334, 1074-1084.
- Humbert, S., Bryson, E. A., Cordelieres, F. P., Connors, N. C., Datta, S. R., Finkbeiner, S., Greenberg, M. E. and Saudou, F. 2002. The IGF-1/Akt pathway is neuroprotective in Huntington's disease and involves huntingtin phosphorylation by Akt. *Dev Cell*. 2, 831-837.
- Humbert, S. and Saudou, F. 2002. Toward cell specificity in SCA1. *Neuron*. 34, 669-670.
- HuntingtonStudyGroup. 2001. A randomized, placebo-controlled trial of coenzyme Q10 and remacemide in Huntington's disease. *Neurology*. 57, 397-404.
- Huynh, D. P., Figueroa, K., Hoang, N. and Pulst, S. M. 2000. Nuclear localization or inclusion body formation of ataxin-2 are not necessary for SCA2 pathogenesis in mouse or human. *Nat Genet*. 26, 44-50.
- Ichikawa, Y., Goto, J., Hattori, M., Toyoda, A., Ishii, K., Jeong, S. Y., Hashida, H., Masuda, N., Ogata, K., Kasai, F., Hirai, M., Maciel, P., Rouleau, G. A., Sakaki, Y. and Kanazawa, I. 2001. The genomic structure and expression of MJD, the Machado-Joseph disease gene. *J Hum Genet*. 46, 413-422.
- Igarashi, S., Koide, R., Shimohata, T., Yamada, M., Hayashi, Y., Takano, H., Date, H., Oyake, M., Sato, T., Sato, A., Egawa, S., Ikeuchi, T., Tanaka, H., Nakano, R., Tanaka, K., Hozumi, I., Inuzuka, T., Takahashi, H. and Tsuji, S. 1998. Suppression of aggregate formation and apoptosis by transglutaminase inhibitors in cells expressing truncated DRPLA protein with an expanded polyglutamine stretch. *Nat Genet*. 18, 111-117.
- Ikeda, H., Yamaguchi, M., Sugai, S., Aze, Y., Narumiya, S. and Kakizuka, A. 1996. Expanded polyglutamine in the Machado-Joseph disease protein induces cell death in vitro and in vivo. *Nat Genet*. 13, 196-202.
- Ishihara, K., Yamagishi, N., Saito, Y., Adachi, H., Kobayashi, Y., Sobue, G., Ohtsuka, K. and Hatayama, T. 2003. Hsp105alpha suppresses the aggregation of truncated androgen receptor with expanded CAG repeats and cell toxicity. *J Biol Chem*. 278, 25143-25150.

## Chapter 1. Introduction

- Iwabuchi, K., Tsuchiya, K., Uchihara, T. and Yagishita, S. 1999. Autosomal dominant spinocerebellar degenerations. Clinical, pathological, and genetic correlations. *Rev Neurol (Paris)*. 155, 255-270.
- Jana, N. R., Tanaka, M., Wang, G. and Nukina, N. 2000. Polyglutamine length-dependent interaction of Hsp40 and Hsp70 family chaperones with truncated N-terminal huntingtin: their role in suppression of aggregation and cellular toxicity. *Hum Mol Genet*. 9, 2009-2018.
- Katsuno, M., Sang, C., Adachi, H., Minamiyama, M., Waza, M., Tanaka, F., Doyu, M. and Sobue, G. 2005. Pharmacological induction of heat-shock proteins alleviates polyglutamine-mediated motor neuron disease. *Proc Natl Acad Sci U S A*. 102, 16801-16806.
- Kawaguchi, Y., Okamoto, T., Taniwaki, M., Aizawa, M., Inoue, M., Katayama, S., Kawakami, H., Nakamura, S., Nishimura, M., Akiguchi, I. and et al. 1994. CAG expansions in a novel gene for Machado-Joseph disease at chromosome 14q32.1. *Nat Genet*. 8, 221-228.
- Kazemi-Esfarjani, P. and Benzer, S. 2000. Genetic suppression of polyglutamine toxicity in *Drosophila*. *Science*. 287, 1837-1840.
- Kennedy, L., Evans, E., Chen, C. M., Craven, L., Detloff, P. J., Ennis, M. and Shelbourne, P. F. 2003. Dramatic tissue-specific mutation length increases are an early molecular event in Huntington disease pathogenesis. *Hum Mol Genet*. 12, 3359-3367.
- Klement, I. A., Skinner, P. J., Kaytor, M. D., Yi, H., Hersch, S. M., Clark, H. B., Zoghbi, H. Y. and Orr, H. T. 1998. Ataxin-1 nuclear localization and aggregation: role in polyglutamine-induced disease in SCA1 transgenic mice. *Cell*. 95, 41-53.
- Kobayashi, Y., Miwa, S., Merry, D. E., Kume, A., Mei, L., Doyu, M. and Sobue, G. 1998. Caspase-3 cleaves the expanded androgen receptor protein of spinal and bulbar muscular atrophy in a polyglutamine repeat length-dependent manner. *Biochem Biophys Res Commun*. 252, 145-150.
- Koeppen, A. H. 2005. The pathogenesis of spinocerebellar ataxia. *Cerebellum*. 4, 62-73.
- Kouroku, Y., Fujita, E., Jimbo, A., Kikuchi, T., Yamagata, T., Momoi, M. Y., Kominami, E., Kuida, K., Sakamaki, K., Yonehara, S. and Momoi, T. 2002. Polyglutamine aggregates stimulate ER stress signals and caspase-12 activation. *Hum Mol Genet*. 11, 1505-1515.
- Koyano, S., Iwabuchi, K., Yagishita, S., Kuroiwa, Y. and Uchihara, T. 2002. Paradoxical absence of nuclear inclusion in cerebellar Purkinje cells of hereditary ataxias linked to CAG expansion. *J Neurol Neurosurg Psychiatry*. 73, 450-452.
- La Spada, A. R., Wilson, E. M., Lubahn, D. B., Harding, A. E. and Fischbeck, K. H. 1991. Androgen receptor gene mutations in X-linked spinal and bulbar muscular atrophy. *Nature*. 352, 77-79.
- Lang, A. E., Rogaeva, E. A., Tsuda, T., Hutterer, J. and St George-Hyslop, P. 1994. Homozygous inheritance of the Machado-Joseph disease gene. *Ann Neurol*. 36, 443-447.
- Leegwater-Kim, J. and Cha, J. H. 2004. The paradigm of Huntington's disease: therapeutic opportunities in neurodegeneration. *NeuroRx*. 1, 128-138.
- Lerer, I., Merims, D., Abeliovich, D., Zlotogora, J. and Gadoth, N. 1996. Machado-Joseph disease: correlation between the clinical features, the CAG repeat length and homozygosity for the mutation. *Eur J Hum Genet*. 4, 3-7.
- Li, F., Macfarlan, T., Pittman, R. N. and Chakravarti, D. 2002a. Ataxin-3 is a histone-binding protein with two independent transcriptional corepressor activities. *J Biol Chem*. 277, 45004-45012.
- Li, J. Y., Plomann, M. and Brundin, P. 2003. Huntington's disease: a synaptopathy? *Trends Mol Med*. 9, 414-420.
- Li, M., Chevalier-Larsen, E. S., Merry, D. E. and Diamond, M. I. 2007. Soluble androgen receptor oligomers underlie pathology in a mouse model of spinobulbar muscular atrophy. *J Biol Chem*. 282, 3157-3164.
- Li, S. H., Cheng, A. L., Zhou, H., Lam, S., Rao, M., Li, H. and Li, X. J. 2002b. Interaction of Huntington disease protein with transcriptional activator Sp1. *Mol Cell Biol*. 22, 1277-1287.

- Lia, A. S., Seznec, H., Hofmann-Radvanyi, H., Radvanyi, F., Duros, C., Saquet, C., Blanche, M., Junien, C. and Gourdon, G. 1998. Somatic instability of the CTG repeat in mice transgenic for the myotonic dystrophy region is age dependent but not correlated to the relative intertissue transcription levels and proliferative capacities. *Hum Mol Genet.* 7, 1285-1291.
- Lima, L. and Coutinho, P. 1980. Clinical criteria for diagnosis of Machado-Joseph disease: report of a non-Azorena Portuguese family. *Neurology.* 30, 319-322.
- Lin, X., Antalffy, B., Kang, D., Orr, H. T. and Zoghbi, H. Y. 2000. Polyglutamine expansion down-regulates specific neuronal genes before pathologic changes in SCA1. *Nat Neurosci.* 3, 157-163.
- Linhartova, I., Repitz, M., Draber, P., Nemec, M., Wiche, G. and Propst, F. 1999. Conserved domains and lack of evidence for polyglutamine length polymorphism in the chicken homolog of the Machado-Joseph disease gene product ataxin-3. *Biochim Biophys Acta.* 1444, 299-305.
- Lopes-Cendes, I., Maciel, P., Kish, S., Gaspar, C., Robitaille, Y., Clark, H. B., Koeppen, A. H., Nance, M., Schut, L., Silveira, I., Coutinho, P., Sequeiros, J. and Rouleau, G. A. 1996. Somatic mosaicism in the central nervous system in spinocerebellar ataxia type 1 and Machado-Joseph disease. *Ann Neurol.* 40, 199-206.
- Lunkes, A. and Mandel, J. L. 1998. A cellular model that recapitulates major pathogenic steps of Huntington's disease. *Hum Mol Genet.* 7, 1355-1361.
- Lunkes, A., Trottier, Y., Fagart, J., Schultz, P., Zeder-Lutz, G., Moras, D. and Mandel, J. L. 1999. Properties of polyglutamine expansion in vitro and in a cellular model for Huntington's disease. *Philos Trans R Soc Lond B Biol Sci.* 354, 1013-1019.
- Lunkes, A., Lindenberg, K. S., Ben-Haiem, L., Weber, C., Devys, D., Landwehrmeyer, G. B., Mandel, J. L. and Trottier, Y. 2002. Proteases acting on mutant huntingtin generate cleaved products that differentially build up cytoplasmic and nuclear inclusions. *Mol Cell.* 10, 259-269.
- Luo, S., Vacher, C., Davies, J. E. and Rubinsztein, D. C. 2005. Cdk5 phosphorylation of huntingtin reduces its cleavage by caspases: implications for mutant huntingtin toxicity. *J Cell Biol.* 169, 647-656.
- Luthi-Carter, R., Strand, A., Peters, N. L., Solano, S. M., Hollingsworth, Z. R., Menon, A. S., Frey, A. S., Spektor, B. S., Penney, E. B., Schilling, G., Ross, C. A., Borchelt, D. R., Tapscott, S. J., Young, A. B., Cha, J. H. and Olson, J. M. 2000. Decreased expression of striatal signaling genes in a mouse model of Huntington's disease. *Hum Mol Genet.* 9, 1259-1271.
- Macedo-Ribeiro, S., Cortes, L., Maciel, P. and Carvalho, A. L. 2009. Nucleocytoplasmic shuttling activity of ataxin-3. *PLoS One.* 4, e5834.
- Maciel, P., Gaspar, C., DeStefano, A. L., Silveira, I., Coutinho, P., Radvanyi, J., Dawson, D. M., Sudarsky, L., Guimaraes, J., Loureiro, J. E. and et al. 1995. Correlation between CAG repeat length and clinical features in Machado-Joseph disease. *Am J Hum Genet.* 57, 54-61.
- Maciel, P., Lopes-Cendes, I., Kish, S., Sequeiros, J. and Rouleau, G. A. 1997. Mosaicism of the CAG repeat in CNS tissue in relation to age at death in spinocerebellar ataxia type 1 and Machado-Joseph disease patients. *Am J Hum Genet.* 60, 993-996.
- Maciel, P., Costa, M. C., Ferro, A., Rousseau, M., Santos, C. S., Gaspar, C., Barros, J., Rouleau, G. A., Coutinho, P. and Sequeiros, J. 2001. Improvement in the molecular diagnosis of Machado-Joseph disease. *Arch Neurol.* 58, 1821-1827.
- Mangiarini, L., Sathasivam, K., Seller, M., Cozens, B., Harper, A., Hetherington, C., Lawton, M., Trottier, Y., Lehrach, H., Davies, S. W. and Bates, G. P. 1996. Exon 1 of the HD gene with an expanded CAG repeat is sufficient to cause a progressive neurological phenotype in transgenic mice. *Cell.* 87, 493-506.
- Mangiarini, L., Sathasivam, K., Mahal, A., Mott, R., Seller, M. and Bates, G. P. 1997. Instability of highly expanded CAG repeats in mice transgenic for the Huntington's disease mutation. *Nat Genet.* 15, 197-200.



## Chapter 1. Introduction

- Margolis, R. L. 2002. The spinocerebellar ataxias: order emerges from chaos. *Curr Neurol Neurosci Rep.* 2, 447-456.
- Marsh, J. L., Walker, H., Theisen, H., Zhu, Y. Z., Fielder, T., Purcell, J. and Thompson, L. M. 2000. Expanded polyglutamine peptides alone are intrinsically cytotoxic and cause neurodegeneration in *Drosophila*. *Hum Mol Genet.* 9, 13-25.
- Marsh, J. L., Lukacsovich, T. and Thompson, L. M. 2009. Animal models of polyglutamine diseases and therapeutic approaches. *J Biol Chem.* 284, 7431-7435.
- Martin, J. B. 1999. Molecular basis of the neurodegenerative disorders. *N Engl J Med.* 340, 1970-1980.
- Martindale, D., Hackam, A., Wieczorek, A., Ellerby, L., Wellington, C., McCutcheon, K., Singaraja, R., Kazemi-Esfarjani, P., Devon, R., Kim, S. U., Bredesen, D. E., Tufaro, F. and Hayden, M. R. 1998. Length of huntingtin and its polyglutamine tract influences localization and frequency of intracellular aggregates. *Nat Genet.* 18, 150-154.
- Masino, L., Musi, V., Menon, R. P., Fusi, P., Kelly, G., Frenkiel, T. A., Trottier, Y. and Pastore, A. 2003. Domain architecture of the polyglutamine protein ataxin-3: a globular domain followed by a flexible tail. *FEBS Lett.* 549, 21-25.
- Matsuyama, Z., Wakamori, M., Mori, Y., Kawakami, H., Nakamura, S. and Imoto, K. 1999. Direct alteration of the P/Q-type Ca<sup>2+</sup> channel property by polyglutamine expansion in spinocerebellar ataxia 6. *J Neurosci.* 19, RC14.
- McCampbell, A., Taylor, J. P., Taye, A. A., Robitschek, J., Li, M., Walcott, J., Merry, D., Chai, Y., Paulson, H., Sobue, G. and Fischbeck, K. H. 2000. CREB-binding protein sequestration by expanded polyglutamine. *Hum Mol Genet.* 9, 2197-2202.
- Merry, D. E., Kobayashi, Y., Bailey, C. K., Taye, A. A. and Fischbeck, K. H. 1998. Cleavage, aggregation and toxicity of the expanded androgen receptor in spinal and bulbar muscular atrophy. *Hum Mol Genet.* 7, 693-701.
- Miller, S. L., Malotky, E. and O'Bryan, J. P. 2004. Analysis of the role of ubiquitin-interacting motifs in ubiquitin binding and ubiquitylation. *J Biol Chem.* 279, 33528-33537.
- Miller, S. L., Scappini, E. L. and O'Bryan, J. 2007. Ubiquitin-interacting motifs inhibit aggregation of polyQ-expanded huntingtin. *J Biol Chem.* 282, 10096-10103.
- Minamiyama, M., Katsuno, M., Adachi, H., Waza, M., Sang, C., Kobayashi, Y., Tanaka, F., Doyu, M., Inukai, A. and Sobue, G. 2004. Sodium butyrate ameliorates phenotypic expression in a transgenic mouse model of spinal and bulbar muscular atrophy. *Hum Mol Genet.* 13, 1183-1192.
- Mirkin, S. M. 2006. DNA structures, repeat expansions and human hereditary disorders. *Curr Opin Struct Biol.* 16, 351-358.
- Mirkin, S. M. 2007. Expandable DNA repeats and human disease. *Nature.* 447, 932-940.
- Mitsui, K., Nakayama, H., Akagi, T., Nekooki, M., Ohtawa, K., Takio, K., Hashikawa, T. and Nukina, N. 2002. Purification of polyglutamine aggregates and identification of elongation factor-1 $\alpha$  and heat shock protein 84 as aggregate-interacting proteins. *J Neurosci.* 22, 9267-9277.
- Mizuno, H., Shibayama, H., Tanaka, F., Doyu, M., Sobue, G., Iwata, H., Kobayashi, H., Yamada, K., Iwai, K., Takeuchi, T., Hashimoto, N., Ishihara, R., Ibuki, Y., Ogasawara, S. and Ozeki, M. 2000. An autopsy case with clinically and molecular genetically diagnosed Huntington's disease with only minimal non-specific neuropathological findings. *Clin Neuropathol.* 19, 94-103.
- Morley, J. F., Brignull, H. R., Weyers, J. J. and Morimoto, R. I. 2002. The threshold for polyglutamine-expansion protein aggregation and cellular toxicity is dynamic and influenced by aging in *Caenorhabditis elegans*. *Proc Natl Acad Sci U S A.* 99, 10417-10422.
- Mueller, T., Breuer, P., Schmitt, I., Walter, J., Evert, B. O. and Wullner, U. 2009. CK2-dependent phosphorylation determines cellular localization and stability of ataxin-3. *Hum Mol Genet.* 18, 3334-3343.

- Nagai, Y., Fujikake, N., Ohno, K., Higashiyama, H., Popiel, H. A., Rahadian, J., Yamaguchi, M., Strittmatter, W. J., Burke, J. R. and Toda, T. 2003. Prevention of polyglutamine oligomerization and neurodegeneration by the peptide inhibitor QBP1 in *Drosophila*. *Hum Mol Genet.* 12, 1253-1259.
- Nagai, Y., Inui, T., Popiel, H. A., Fujikake, N., Hasegawa, K., Urade, Y., Goto, Y., Naiki, H. and Toda, T. 2007. A toxic monomeric conformer of the polyglutamine protein. *Nat Struct Mol Biol.* 14, 332-340.
- Nakano, K. K., Dawson, D. M. and Spence, A. 1972. Machado disease. A hereditary ataxia in Portuguese emigrants to Massachusetts. *Neurology.* 22, 49-55.
- Nicastro, G., Menon, R. P., Masino, L., Knowles, P. P., McDonald, N. Q. and Pastore, A. 2005. The solution structure of the Josephin domain of ataxin-3: structural determinants for molecular recognition. *Proc Natl Acad Sci U S A.* 102, 10493-10498.
- Nicastro, G., Habeck, M., Masino, L., Svergun, D. I. and Pastore, A. 2006. Structure validation of the Josephin domain of ataxin-3: conclusive evidence for an open conformation. *J Biomol NMR.* 36, 267-277.
- Nucifora, F. C., Jr., Sasaki, M., Peters, M. F., Huang, H., Cooper, J. K., Yamada, M., Takahashi, H., Tsuji, S., Troncoso, J., Dawson, V. L., Dawson, T. M. and Ross, C. A. 2001. Interference by huntingtin and atrophin-1 with cbp-mediated transcription leading to cellular toxicity. *Science.* 291, 2423-2428.
- Obrietan, K. and Hoyt, K. R. 2004. CRE-mediated transcription is increased in Huntington's disease transgenic mice. *J Neurosci.* 24, 791-796.
- Ogryzko, V. V., Schiltz, R. L., Russanova, V., Howard, B. H. and Nakatani, Y. 1996. The transcriptional coactivators p300 and CBP are histone acetyltransferases. *Cell.* 87, 953-959.
- Okazawa, H. 2003. Polyglutamine diseases: a transcription disorder? *Cell Mol Life Sci.* 60, 1427-1439.
- Ona, V. O., Li, M., Vonsattel, J. P., Andrews, L. J., Khan, S. Q., Chung, W. M., Frey, A. S., Menon, A. S., Li, X. J., Stieg, P. E., Yuan, J., Penney, J. B., Young, A. B., Cha, J. H. and Friedlander, R. M. 1999. Inhibition of caspase-1 slows disease progression in a mouse model of Huntington's disease. *Nature.* 399, 263-267.
- Ordway, J. M., Tallaksen-Greene, S., Gutekunst, C. A., Bernstein, E. M., Cearley, J. A., Wiener, H. W., Dure, L. S. t., Lindsey, R., Hersch, S. M., Jope, R. S., Albin, R. L. and Detloff, P. J. 1997. Ectopically expressed CAG repeats cause intranuclear inclusions and a progressive late onset neurological phenotype in the mouse. *Cell.* 91, 753-763.
- Orr, H. T. 2001. Beyond the Qs in the polyglutamine diseases. *Genes Dev.* 15, 925-932.
- Orr, H. T. and Zoghbi, H. Y. 2001. SCA1 molecular genetics: a history of a 13 year collaboration against glutamines. *Hum Mol Genet.* 10, 2307-2311.
- Orr, H. T. and Zoghbi, H. Y. 2007. Trinucleotide repeat disorders. *Annu Rev Neurosci.* 30, 575-621.
- Padiath, Q. S., Srivastava, A. K., Roy, S., Jain, S. and Brahmachari, S. K. 2005. Identification of a novel 45 repeat unstable allele associated with a disease phenotype at the MJD1/SCA3 locus. *Am J Med Genet B Neuropsychiatr Genet.* 133B, 124-126.
- Pardo, R., Colin, E., Regulier, E., Aebischer, P., Deglon, N., Humbert, S. and Saudou, F. 2006. Inhibition of calcineurin by FK506 protects against polyglutamine-huntingtin toxicity through an increase of huntingtin phosphorylation at S421. *J Neurosci.* 26, 1635-1645.
- Paulson, H. L., Das, S. S., Crino, P. B., Perez, M. K., Patel, S. C., Gotsdiner, D., Fischbeck, K. H. and Pittman, R. N. 1997a. Machado-Joseph disease gene product is a cytoplasmic protein widely expressed in brain. *Ann Neurol.* 41, 453-462.
- Paulson, H. L., Perez, M. K., Trottier, Y., Trojanowski, J. Q., Subramony, S. H., Das, S. S., Vig, P., Mandel, J. L., Fischbeck, K. H. and Pittman, R. N. 1997b. Intranuclear inclusions of expanded polyglutamine protein in spinocerebellar ataxia type 3. *Neuron.* 19, 333-344.
- Paulson, H. L. 1999. Protein fate in neurodegenerative proteinopathies: polyglutamine diseases join the (mis)fold. *Am J Hum Genet.* 64, 339-345.

## Chapter 1. Introduction

- Paulson, H. L., Bonini, N. M. and Roth, K. A. 2000. Polyglutamine disease and neuronal cell death. *Proc Natl Acad Sci U S A.* 97, 12957-12958.
- Paulson, H. L. 2007. Dominantly inherited ataxias: lessons learned from Machado-Joseph disease/spinocerebellar ataxia type 3. *Semin Neurol.* 27, 133-142.
- Pearson, C. E., Nichol Edamura, K. and Cleary, J. D. 2005. Repeat instability: mechanisms of dynamic mutations. *Nat Rev Genet.* 6, 729-742.
- Perez, M. K., Paulson, H. L., Pendse, S. J., Saionz, S. J., Bonini, N. M. and Pittman, R. N. 1998. Recruitment and the role of nuclear localization in polyglutamine-mediated aggregation. *J Cell Biol.* 143, 1457-1470.
- Peters, M. F., Nucifora, F. C., Jr., Kushi, J., Seaman, H. C., Cooper, J. K., Herring, W. J., Dawson, V. L., Dawson, T. M. and Ross, C. A. 1999. Nuclear targeting of mutant Huntingtin increases toxicity. *Mol Cell Neurosci.* 14, 121-128.
- Pollitt, S. K., Pallos, J., Shao, J., Desai, U. A., Ma, A. A., Thompson, L. M., Marsh, J. L. and Diamond, M. I. 2003. A rapid cellular FRET assay of polyglutamine aggregation identifies a novel inhibitor. *Neuron.* 40, 685-694.
- Pozzi, C., Valtorta, M., Tedeschi, G., Galbusera, E., Pastori, V., Bigi, A., Nonnis, S., Grassi, E. and Fusi, P. 2008. Study of subcellular localization and proteolysis of ataxin-3. *Neurobiol Dis.* 30, 190-200.
- Rebec, G. V., Conroy, S. K. and Barton, S. J. 2006. Hyperactive striatal neurons in symptomatic Huntington R6/2 mice: variations with behavioral state and repeated ascorbate treatment. *Neuroscience.* 137, 327-336.
- Reddy, P. H., Williams, M., Charles, V., Garrett, L., Pike-Buchanan, L., Whetsell, W. O., Jr., Miller, G. and Tagle, D. A. 1998. Behavioural abnormalities and selective neuronal loss in HD transgenic mice expressing mutated full-length HD cDNA. *Nat Genet.* 20, 198-202.
- Reynolds, A., Leake, D., Boese, Q., Scaringe, S., Marshall, W. S. and Khvorova, A. 2004. Rational siRNA design for RNA interference. *Nat Biotechnol.* 22, 326-330.
- Riess, O., Rub, U., Pastore, A., Bauer, P. and Schols, L. 2008. SCA3: neurological features, pathogenesis and animal models. *Cerebellum.* 7, 125-137.
- Riley, B. E., Zoghbi, H. Y. and Orr, H. T. 2005. SUMOylation of the polyglutamine repeat protein, ataxin-1, is dependent on a functional nuclear localization signal. *J Biol Chem.* 280, 21942-21948.
- Riley, B. E. and Orr, H. T. 2006. Polyglutamine neurodegenerative diseases and regulation of transcription: assembling the puzzle. *Genes Dev.* 20, 2183-2192.
- Robitaille, Y., Lopes-Cendes, I., Becher, M., Rouleau, G. and Clark, A. W. 1997. The neuropathology of CAG repeat diseases: review and update of genetic and molecular features. *Brain Pathol.* 7, 901-926.
- Rodrigues, A. J., Coppola, G., Santos, C., Costa Mdo, C., Ailion, M., Sequeiros, J., Geschwind, D. H. and Maciel, P. 2007. Functional genomics and biochemical characterization of the *C. elegans* orthologue of the Machado-Joseph disease protein ataxin-3. *Faseb J.* 21, 1126-1136.
- Rodrigues, A. J., Neves-Carvalho, A., Ferro, A., Rokka, A., Corthals, G., Logarinho, E. and Maciel, P. 2009. ATX-3, CDC-48 and UBXN-5: a new trimolecular complex in *Caenorhabditis elegans*. *Biochem Biophys Res Commun.* 386, 575-581.
- Rolfs, A., Koeppen, A. H., Bauer, I., Bauer, P., Buhlmann, S., Topka, H., Schols, L. and Riess, O. 2003. Clinical features and neuropathology of autosomal dominant spinocerebellar ataxia (SCA17). *Ann Neurol.* 54, 367-375.
- Romanul, F. C., Fowler, H. L., Radvany, J., Feldman, R. G. and Feingold, M. 1977. Azorean disease of the nervous system. *N Engl J Med.* 296, 1505-1508.
- Rosenberg, R. N., Nyhan, W. L. and Bay, C. 1976. Autosomal dominant striatonigral degeneration: a clinical, pathological, and biochemical study of a new genetic disorder. *Trans Am Neurol Assoc.* 101, 78-80.
- Rosenberg, R. N. 1983. Dominant ataxias. *Res Publ Assoc Res Nerv Ment Dis.* 60, 195-213.

- Ross, C. A. 1997. Intranuclear neuronal inclusions: a common pathogenic mechanism for glutamine-repeat neurodegenerative diseases? *Neuron*. 19, 1147-1150.
- Ross, C. A., Wood, J. D., Schilling, G., Peters, M. F., Nucifora, F. C., Jr., Cooper, J. K., Sharp, A. H., Margolis, R. L. and Borchelt, D. R. 1999. Polyglutamine pathogenesis. *Philos Trans R Soc Lond B Biol Sci*. 354, 1005-1011.
- Rub, U., Brunt, E. R., Del Turco, D., de Vos, R. A., Gierga, K., Paulson, H. and Braak, H. 2003a. Guidelines for the pathoanatomical examination of the lower brain stem in ingestive and swallowing disorders and its application to a dysphagic spinocerebellar ataxia type 3 patient. *Neuropathol Appl Neurobiol*. 29, 1-13.
- Rub, U., Brunt, E. R., Gierga, K., Schultz, C., Paulson, H., de Vos, R. A. and Braak, H. 2003b. The nucleus raphe interpositus in spinocerebellar ataxia type 3 (Machado-Joseph disease). *J Chem Neuroanat*. 25, 115-127.
- Rub, U., Del Turco, D., Del Tredici, K., de Vos, R. A., Brunt, E. R., Reifenberger, G., Seifried, C., Schultz, C., Auburger, G. and Braak, H. 2003c. Thalamic involvement in a spinocerebellar ataxia type 2 (SCA2) and a spinocerebellar ataxia type 3 (SCA3) patient, and its clinical relevance. *Brain*. 126, 2257-2272.
- Rub, U., Brunt, E. R., de Vos, R. A., Del Turco, D., Del Tredici, K., Gierga, K., Schultz, C., Ghebremedhin, E., Burk, K., Auburger, G. and Braak, H. 2004. Degeneration of the central vestibular system in spinocerebellar ataxia type 3 (SCA3) patients and its possible clinical significance. *Neuropathol Appl Neurobiol*. 30, 402-414.
- Rub, U., Gierga, K., Brunt, E. R., de Vos, R. A., Bauer, M., Schols, L., Burk, K., Auburger, G., Bohl, J., Schultz, C., Vuksic, M., Burbach, G. J., Braak, H. and Deller, T. 2005. Spinocerebellar ataxias types 2 and 3: degeneration of the pre-cerebellar nuclei isolates the three phylogenetically defined regions of the cerebellum. *J Neural Transm*. 112, 1523-1545.
- Rub, U., Brunt, E. R., Petrasch-Parwez, E., Schols, L., Theegarten, D., Auburger, G., Seidel, K., Schultz, C., Gierga, K., Paulson, H., van Broeckhoven, C., Deller, T. and de Vos, R. A. 2006a. Degeneration of ingestion-related brainstem nuclei in spinocerebellar ataxia type 2, 3, 6 and 7. *Neuropathol Appl Neurobiol*. 32, 635-649.
- Rub, U., de Vos, R. A., Brunt, E. R., Sebesteny, T., Schols, L., Auburger, G., Bohl, J., Ghebremedhin, E., Gierga, K., Seidel, K., den Dunnen, W., Heinsen, H., Paulson, H. and Deller, T. 2006b. Spinocerebellar ataxia type 3 (SCA3): thalamic neurodegeneration occurs independently from thalamic ataxin-3 immunopositive neuronal intranuclear inclusions. *Brain Pathol*. 16, 218-227.
- Rub, U., Seidel, K., Ozerden, I., Gierga, K., Brunt, E. R., Schols, L., de Vos, R. A., den Dunnen, W., Schultz, C., Auburger, G. and Deller, T. 2007. Consistent affection of the central somatosensory system in spinocerebellar ataxia type 2 and type 3 and its significance for clinical symptoms and rehabilitative therapy. *Brain Res Rev*. 53, 235-249.
- Rub, U., Brunt, E. R. and Deller, T. 2008. New insights into the pathoanatomy of spinocerebellar ataxia type 3 (Machado-Joseph disease). *Curr Opin Neurol*. 21, 111-116.
- Sanchez-Pernaute, R., Garcia-Segura, J. M., del Barrio Alba, A., Viano, J. and de Yébenes, J. G. 1999. Clinical correlation of striatal 1H MRS changes in Huntington's disease. *Neurology*. 53, 806-812.
- Sanchez, I., Xu, C. J., Juo, P., Kakizaka, A., Blenis, J. and Yuan, J. 1999. Caspase-8 is required for cell death induced by expanded polyglutamine repeats. *Neuron*. 22, 623-633.
- Sanchez, I., Mahlke, C. and Yuan, J. 2003. Pivotal role of oligomerization in expanded polyglutamine neurodegenerative disorders. *Nature*. 421, 373-379.
- Sarkar, S., Krishna, G., Imarisio, S., Saiki, S., O'Kane, C. J. and Rubinsztein, D. C. 2008. A rational mechanism for combination treatment of Huntington's disease using lithium and rapamycin. *Hum Mol Genet*. 17, 170-178.
- Sarkar, S. and Rubinsztein, D. C. 2008. Small molecule enhancers of autophagy for neurodegenerative diseases. *Mol Biosyst*. 4, 895-901.

## Chapter 1. Introduction

- Sathasivam, K., Woodman, B., Mahal, A., Bertaux, F., Wanker, E. E., Shima, D. T. and Bates, G. P. 2001. Centrosome disorganization in fibroblast cultures derived from R6/2 Huntington's disease (HD) transgenic mice and HD patients. *Hum Mol Genet.* 10, 2425-2435.
- Sato, T., Oyake, M., Nakamura, K., Nakao, K., Fukusima, Y., Onodera, O., Igarashi, S., Takano, H., Kikugawa, K., Ishida, Y., Shimohata, T., Koide, R., Ikeuchi, T., Tanaka, H., Futamura, N., Matsumura, R., Takayanagi, T., Tanaka, F., Sobue, G., Komure, O., Takahashi, M., Sano, A., Ichikawa, Y., Goto, J., Kanazawa, I. and et al. 1999. Transgenic mice harboring a full-length human mutant DRPLA gene exhibit age-dependent intergenerational and somatic instabilities of CAG repeats comparable with those in DRPLA patients. *Hum Mol Genet.* 8, 99-106.
- Saudou, F., Finkbeiner, S., Devys, D. and Greenberg, M. E. 1998. Huntingtin acts in the nucleus to induce apoptosis but death does not correlate with the formation of intranuclear inclusions. *Cell.* 95, 55-66.
- Scheel, H., Tomiuk, S. and Hofmann, K. 2003. Elucidation of ataxin-3 and ataxin-7 function by integrative bioinformatics. *Hum Mol Genet.* 12, 2845-2852.
- Schiefer, J., Landwehrmeyer, G. B., Luesse, H. G., Sprunken, A., Puls, C., Milkereit, A., Milkereit, E. and Kosinski, C. M. 2002. Riluzole prolongs survival time and alters nuclear inclusion formation in a transgenic mouse model of Huntington's disease. *Mov Disord.* 17, 748-757.
- Schiefer, J., Sprunken, A., Puls, C., Luesse, H. G., Milkereit, A., Milkereit, E., Johann, V. and Kosinski, C. M. 2004. The metabotropic glutamate receptor 5 antagonist MPEP and the mGluR2 agonist LY379268 modify disease progression in a transgenic mouse model of Huntington's disease. *Brain Res.* 1019, 246-254.
- Schilling, B., Gafni, J., Torcassi, C., Cong, X., Row, R. H., LaFevre-Bernt, M. A., Cusack, M. P., Ratovitski, T., Hirschhorn, R., Ross, C. A., Gibson, B. W. and Ellerby, L. M. 2006. Huntingtin phosphorylation sites mapped by mass spectrometry. Modulation of cleavage and toxicity. *J Biol Chem.* 281, 23686-23697.
- Schilling, G., Wood, J. D., Duan, K., Slunt, H. H., Gonzales, V., Yamada, M., Cooper, J. K., Margolis, R. L., Jenkins, N. A., Copeland, N. G., Takahashi, H., Tsuji, S., Price, D. L., Borchelt, D. R. and Ross, C. A. 1999. Nuclear accumulation of truncated atrophin-1 fragments in a transgenic mouse model of DRPLA. *Neuron.* 24, 275-286.
- Schilling, G., Coonfield, M. L., Ross, C. A. and Borchelt, D. R. 2001. Coenzyme Q10 and remacemide hydrochloride ameliorate motor deficits in a Huntington's disease transgenic mouse model. *Neurosci Lett.* 315, 149-153.
- Schmidt, T., Landwehrmeyer, G. B., Schmitt, I., Trottier, Y., Auburger, G., Laccone, F., Klockgether, T., Volpel, M., Epplen, J. T., Schols, L. and Riess, O. 1998. An isoform of ataxin-3 accumulates in the nucleus of neuronal cells in affected brain regions of SCA3 patients. *Brain Pathol.* 8, 669-679.
- Schmidt, T., Lindenberg, K. S., Krebs, A., Schols, L., Laccone, F., Herms, J., Rechsteiner, M., Riess, O. and Landwehrmeyer, G. B. 2002. Protein surveillance machinery in brains with spinocerebellar ataxia type 3: redistribution and differential recruitment of 26S proteasome subunits and chaperones to neuronal intranuclear inclusions. *Ann Neurol.* 51, 302-310.
- Schmitt, I., Brattig, T., Gossen, M. and Riess, O. 1997. Characterization of the rat spinocerebellar ataxia type 3 gene. *Neurogenetics.* 1, 103-112.
- Schmitt, I., Linden, M., Khazneh, H., Evert, B. O., Breuer, P., Klockgether, T. and Wuellner, U. 2007. Inactivation of the mouse *Atxn3* (ataxin-3) gene increases protein ubiquitination. *Biochem Biophys Res Commun.* 362, 734-739.
- Schols, L., Bauer, P., Schmidt, T., Schulte, T. and Riess, O. 2004. Autosomal dominant cerebellar ataxias: clinical features, genetics, and pathogenesis. *Lancet Neurol.* 3, 291-304.
- Seidel, K., den Dunnen, W. F., Schultz, C., Paulson, H., Frank, S., de Vos, R. A., Brunt, E. R., Deller, T., Kampinga, H. H. and Rub, U. 2010. Axonal inclusions in spinocerebellar ataxia type 3. *Acta Neuropathol.* 120, 449-460.

- Seo, H., Sonntag, K. C. and Isacson, O. 2004. Generalized brain and skin proteasome inhibition in Huntington's disease. *Ann Neurol.* 56, 319-328.
- Serra, H. G., Byam, C. E., Lande, J. D., Tousey, S. K., Zoghbi, H. Y. and Orr, H. T. 2004. Gene profiling links SCA1 pathophysiology to glutamate signaling in Purkinje cells of transgenic mice. *Hum Mol Genet.* 13, 2535-2543.
- Shao, J. and Diamond, M. I. 2007. Polyglutamine diseases: emerging concepts in pathogenesis and therapy. *Hum Mol Genet.* 16 Spec No. 2, R115-123.
- Shelbourne, P. F., Killeen, N., Hevner, R. F., Johnston, H. M., Tecott, L., Lewandoski, M., Ennis, M., Ramirez, L., Li, Z., Iannicola, C., Littman, D. R. and Myers, R. M. 1999. A Huntington's disease CAG expansion at the murine *Hdh* locus is unstable and associated with behavioural abnormalities in mice. *Hum Mol Genet.* 8, 763-774.
- Silva-Fernandes, A., Costa Mdo, C., Duarte-Silva, S., Oliveira, P., Botelho, C. M., Martins, L., Mariz, J. A., Ferreira, T., Ribeiro, F., Correia-Neves, M., Costa, C. and Maciel, P. 2010. Motor uncoordination and neuropathology in a transgenic mouse model of Machado-Joseph disease lacking intranuclear inclusions and ataxin-3 cleavage products. *Neurobiol Dis.* 40, 163-176.
- Sisodia, S. S. 1998. Nuclear inclusions in glutamine repeat disorders: are they pernicious, coincidental, or beneficial? *Cell.* 95, 1-4.
- Smith, R., Brundin, P. and Li, J. Y. 2005. Synaptic dysfunction in Huntington's disease: a new perspective. *Cell Mol Life Sci.* 62, 1901-1912.
- Sobue, G., Doyu, M., Nakao, N., Shimada, N., Mitsuma, T., Maruyama, H., Kawakami, S. and Nakamura, S. 1996. Homozygosity for Machado-Joseph disease gene enhances phenotypic severity. *J Neurol Neurosurg Psychiatry.* 60, 354-356.
- Soto, C. 2003. Unfolding the role of protein misfolding in neurodegenerative diseases. *Nat Rev Neurosci.* 4, 49-60.
- Stack, E. C., Smith, K. M., Ryu, H., Cormier, K., Chen, M., Hagerty, S. W., Del Signore, S. J., Cudkowicz, M. E., Friedlander, R. M. and Ferrante, R. J. 2006. Combination therapy using minocycline and coenzyme Q10 in R6/2 transgenic Huntington's disease mice. *Biochim Biophys Acta.* 1762, 373-380.
- Steffan, J. S., Kazantsev, A., Spasic-Boskovic, O., Greenwald, M., Zhu, Y. Z., Gohler, H., Wanker, E. E., Bates, G. P., Housman, D. E. and Thompson, L. M. 2000. The Huntington's disease protein interacts with p53 and CREB-binding protein and represses transcription. *Proc Natl Acad Sci U S A.* 97, 6763-6768.
- Steffan, J. S., Bodai, L., Pallos, J., Poelman, M., McCampbell, A., Apostol, B. L., Kazantsev, A., Schmidt, E., Zhu, Y. Z., Greenwald, M., Kurokawa, R., Housman, D. E., Jackson, G. R., Marsh, J. L. and Thompson, L. M. 2001. Histone deacetylase inhibitors arrest polyglutamine-dependent neurodegeneration in *Drosophila*. *Nature.* 413, 739-743.
- Steffan, J. S., Agrawal, N., Pallos, J., Rockabrand, E., Trotman, L. C., Slepko, N., Illes, K., Lukacsovich, T., Zhu, Y. Z., Cattaneo, E., Pandolfi, P. P., Thompson, L. M. and Marsh, J. L. 2004. SUMO modification of Huntingtin and Huntington's disease pathology. *Science.* 304, 100-104.
- Stenoien, D. L., Cummings, C. J., Adams, H. P., Mancini, M. G., Patel, K., DeMartino, G. N., Marcelli, M., Weigel, N. L. and Mancini, M. A. 1999. Polyglutamine-expanded androgen receptors form aggregates that sequester heat shock proteins, proteasome components and SRC-1, and are suppressed by the HDJ-2 chaperone. *Hum Mol Genet.* 8, 731-741.
- Stenoien, D. L., Mielke, M. and Mancini, M. A. 2002. Intranuclear ataxin1 inclusions contain both fast- and slow-exchanging components. *Nat Cell Biol.* 4, 806-810.
- Strom, A. L., Forsgren, L. and Holmberg, M. 2005. A role for both wild-type and expanded ataxin-7 in transcriptional regulation. *Neurobiol Dis.* 20, 646-655.
- Sun, J., Xu, H., Negi, S., Subramony, S. H. and Hebert, M. D. 2007. Differential effects of polyglutamine proteins on nuclear organization and artificial reporter splicing. *J Neurosci Res.* 85, 2306-2317.

## Chapter 1. Introduction

- Tabrizi, S. J., Workman, J., Hart, P. E., Mangiarini, L., Mahal, A., Bates, G., Cooper, J. M. and Schapira, A. H. 2000. Mitochondrial dysfunction and free radical damage in the Huntington R6/2 transgenic mouse. *Ann Neurol.* 47, 80-86.
- Takano, H., Onodera, O., Takahashi, H., Igarashi, S., Yamada, M., Oyake, M., Ikeuchi, T., Koide, R., Tanaka, H., Iwabuchi, K. and Tsuji, S. 1996. Somatic mosaicism of expanded CAG repeats in brains of patients with dentatorubral-pallidoluysian atrophy: cellular population-dependent dynamics of mitotic instability. *Am J Hum Genet.* 58, 1212-1222.
- Takiyama, Y., Nishizawa, M., Tanaka, H., Kawashima, S., Sakamoto, H., Karube, Y., Shimazaki, H., Soutome, M., Endo, K., Ohta, S. and et al. 1993. The gene for Machado-Joseph disease maps to human chromosome 14q. *Nat Genet.* 4, 300-304.
- Tanaka, F., Ito, Y. and Sobue, G. 1999. [Somatic mosaicism of expanded CAG trinucleotide repeat in spinal and bulbar muscular atrophy (SBMA)]. *Nippon Rinsho.* 57, 862-868.
- Tanaka, M., Machida, Y., Niu, S., Ikeda, T., Jana, N. R., Doi, H., Kurosawa, M., Nekooki, M. and Nukina, N. 2004. Trehalose alleviates polyglutamine-mediated pathology in a mouse model of Huntington disease. *Nat Med.* 10, 148-154.
- Taylor, J. P., Taye, A. A., Campbell, C., Kazemi-Esfarjani, P., Fischbeck, K. H. and Min, K. T. 2003. Aberrant histone acetylation, altered transcription, and retinal degeneration in a *Drosophila* model of polyglutamine disease are rescued by CREB-binding protein. *Genes Dev.* 17, 1463-1468.
- Todi, S. V., Laco, M. N., Winborn, B. J., Travis, S. M., Wen, H. M. and Paulson, H. L. 2007. Cellular turnover of the polyglutamine disease protein ataxin-3 is regulated by its catalytic activity. *J Biol Chem.* 282, 29348-29358.
- Toru, S., Murakoshi, T., Ishikawa, K., Saegusa, H., Fujigasaki, H., Uchihara, T., Nagayama, S., Osanai, M., Mizusawa, H. and Tanabe, T. 2000. Spinocerebellar ataxia type 6 mutation alters P-type calcium channel function. *J Biol Chem.* 275, 10893-10898.
- Tsuda, H., Jafar-Nejad, H., Patel, A. J., Sun, Y., Chen, H. K., Rose, M. F., Venken, K. J., Botas, J., Orr, H. T., Bellen, H. J. and Zoghbi, H. Y. 2005. The AXH domain of Ataxin-1 mediates neurodegeneration through its interaction with Gfi-1/Senseless proteins. *Cell.* 122, 633-644.
- Turmaine, M., Raza, A., Mahal, A., Mangiarini, L., Bates, G. P. and Davies, S. W. 2000. Nonapoptotic neurodegeneration in a transgenic mouse model of Huntington's disease. *Proc Natl Acad Sci U S A.* 97, 8093-8097.
- Usdin, K. and Grabczyk, E. 2000. DNA repeat expansions and human disease. *Cell Mol Life Sci.* 57, 914-931.
- van den Broek, W. J., Nelen, M. R., Wansink, D. G., Coerwinkel, M. M., te Riele, H., Groenen, P. J. and Wieringa, B. 2002. Somatic expansion behaviour of the (CTG)<sub>n</sub> repeat in myotonic dystrophy knock-in mice is differentially affected by Msh3 and Msh6 mismatch-repair proteins. *Hum Mol Genet.* 11, 191-198.
- Wancata, J., Musalek, M., Alexandrowicz, R. and Krautgartner, M. 2003. Number of dementia sufferers in Europe between the years 2000 and 2050. *Eur Psychiatry.* 18, 306-313.
- Warby, S. C., Doty, C. N., Graham, R. K., Shively, J., Singaraja, R. R. and Hayden, M. R. 2009. Phosphorylation of huntingtin reduces the accumulation of its nuclear fragments. *Mol Cell Neurosci.* 40, 121-127.
- Warrick, J. M., Paulson, H. L., Gray-Board, G. L., Bui, Q. T., Fischbeck, K. H., Pittman, R. N. and Bonini, N. M. 1998. Expanded polyglutamine protein forms nuclear inclusions and causes neural degeneration in *Drosophila*. *Cell.* 93, 939-949.
- Warrick, J. M., Chan, H. Y., Gray-Board, G. L., Chai, Y., Paulson, H. L. and Bonini, N. M. 1999. Suppression of polyglutamine-mediated neurodegeneration in *Drosophila* by the molecular chaperone HSP70. *Nat Genet.* 23, 425-428.
- Warrick, J. M., Morabito, L. M., Bilen, J., Gordesky-Gold, B., Faust, L. Z., Paulson, H. L. and Bonini, N. M. 2005. Ataxin-3 suppresses polyglutamine neurodegeneration in *Drosophila* by a ubiquitin-associated mechanism. *Mol Cell.* 18, 37-48.

- Watanabe, H., Tanaka, F., Doyu, M., Riku, S., Yoshida, M., Hashizume, Y. and Sobue, G. 2000. Differential somatic CAG repeat instability in variable brain cell lineage in dentatorubral pallidoluysian atrophy (DRPLA): a laser-captured microdissection (LCM)-based analysis. *Hum Genet.* 107, 452-457.
- Watase, K., Venken, K. J., Sun, Y., Orr, H. T. and Zoghbi, H. Y. 2003. Regional differences of somatic CAG repeat instability do not account for selective neuronal vulnerability in a knock-in mouse model of SCA1. *Hum Mol Genet.* 12, 2789-2795.
- Weiss, A., Klein, C., Woodman, B., Sathasivam, K., Bibel, M., Regulier, E., Bates, G. P. and Paganetti, P. 2008. Sensitive biochemical aggregate detection reveals aggregation onset before symptom development in cellular and murine models of Huntington's disease. *J Neurochem.* 104, 846-858.
- Wellington, C. L., Ellerby, L. M., Hackam, A. S., Margolis, R. L., Trifiro, M. A., Singaraja, R., McCutcheon, K., Salvesen, G. S., Propp, S. S., Bromm, M., Rowland, K. J., Zhang, T., Rasper, D., Roy, S., Thornberry, N., Pinsky, L., Kakizuka, A., Ross, C. A., Nicholson, D. W., Bredesen, D. E. and Hayden, M. R. 1998. Caspase cleavage of gene products associated with triplet expansion disorders generates truncated fragments containing the polyglutamine tract. *J Biol Chem.* 273, 9158-9167.
- Wellington, C. L. and Hayden, M. R. 2000. Caspases and neurodegeneration: on the cutting edge of new therapeutic approaches. *Clin Genet.* 57, 1-10.
- Wellington, C. L., Ellerby, L. M., Gutekunst, C. A., Rogers, D., Warby, S., Graham, R. K., Loubser, O., van Raamsdonk, J., Singaraja, R., Yang, Y. Z., Gafni, J., Bredesen, D., Hersch, S. M., Leavitt, B. R., Roy, S., Nicholson, D. W. and Hayden, M. R. 2002. Caspase cleavage of mutant huntingtin precedes neurodegeneration in Huntington's disease. *J Neurosci.* 22, 7862-7872.
- Wexler, N. S., Young, A. B., Tanzi, R. E., Travers, H., Starosta-Rubinstein, S., Penney, J. B., Snodgrass, S. R., Shoulson, I., Gomez, F., Ramos Arroyo, M. A. and et al. 1987. Homozygotes for Huntington's disease. *Nature.* 326, 194-197.
- Wheeler, V. C., Lebel, L. A., Vrbanac, V., Teed, A., te Riele, H. and MacDonald, M. E. 2003. Mismatch repair gene Msh2 modifies the timing of early disease in Hdh(Q111) striatum. *Hum Mol Genet.* 12, 273-281.
- Williams, A., Sarkar, S., Cuddon, P., Ttofi, E. K., Saiki, S., Siddiqi, F. H., Jahreiss, L., Fleming, A., Pask, D., Goldsmith, P., O'Kane, C. J., Floto, R. A. and Rubinsztein, D. C. 2008. Novel targets for Huntington's disease in an mTOR-independent autophagy pathway. *Nat Chem Biol.* 4, 295-305.
- Wong, H. K., Bauer, P. O., Kurosawa, M., Goswami, A., Washizu, C., Machida, Y., Tosaki, A., Yamada, M., Knopfel, T., Nakamura, T. and Nukina, N. 2008. Blocking acid-sensing ion channel 1 alleviates Huntington's disease pathology via an ubiquitin-proteasome system-dependent mechanism. *Hum Mol Genet.* 17, 3223-3235.
- Woods, B. T. and Schaumburg, H. H. 1972. Nigro-spino-dentatal degeneration with nuclear ophthalmoplegia. A unique and partially treatable clinico-pathological entity. *J Neurol Sci.* 17, 149-166.
- Xuereb, J. H., MacMillan, J. C., Snell, R., Davies, P. and Harper, P. S. 1996. Neuropathological diagnosis and CAG repeat expansion in Huntington's disease. *J Neurol Neurosurg Psychiatry.* 60, 78-81.
- Yamada, M., Tan, C. F., Inenaga, C., Tsuji, S. and Takahashi, H. 2004. Sharing of polyglutamine localization by the neuronal nucleus and cytoplasm in CAG-repeat diseases. *Neuropathol Appl Neurobiol.* 30, 665-675.
- Yamada, M., Sato, T., Tsuji, S. and Takahashi, H. 2008. CAG repeat disorder models and human neuropathology: similarities and differences. *Acta Neuropathol.* 115, 71-86.
- Yamamoto, A., Lucas, J. J. and Hen, R. 2000. Reversal of neuropathology and motor dysfunction in a conditional model of Huntington's disease. *Cell.* 101, 57-66.



## Chapter 1. Introduction

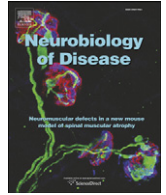
- Yang, W., Dunlap, J. R., Andrews, R. B. and Wetzel, R. 2002. Aggregated polyglutamine peptides delivered to nuclei are toxic to mammalian cells. *Hum Mol Genet.* 11, 2905-2917.
- Ying, M., Xu, R., Wu, X., Zhu, H., Zhuang, Y., Han, M. and Xu, T. 2006. Sodium butyrate ameliorates histone hypoacetylation and neurodegenerative phenotypes in a mouse model for DRPLA. *J Biol Chem.* 281, 12580-12586.
- Yoshizawa, T., Yamagishi, Y., Koseki, N., Goto, J., Yoshida, H., Shibasaki, F., Shoji, S. and Kanazawa, I. 2000. Cell cycle arrest enhances the in vitro cellular toxicity of the truncated Machado-Joseph disease gene product with an expanded polyglutamine stretch. *Hum Mol Genet.* 9, 69-78.
- Yoshizawa, T., Yoshida, H. and Shoji, S. 2001. Differential susceptibility of cultured cell lines to aggregate formation and cell death produced by the truncated Machado-Joseph disease gene product with an expanded polyglutamine stretch. *Brain Res Bull.* 56, 349-352.
- Young, P., Deveraux, Q., Beal, R. E., Pickart, C. M. and Rechsteiner, M. 1998. Characterization of two polyubiquitin binding sites in the 26 S protease subunit 5a. *J Biol Chem.* 273, 5461-5467.
- Yu, Z. X., Li, S. H., Nguyen, H. P. and Li, X. J. 2002. Huntingtin inclusions do not deplete polyglutamine-containing transcription factors in HD mice. *Hum Mol Genet.* 11, 905-914.
- Yvert, G., Lindenberg, K. S., Picaud, S., Landwehrmeyer, G. B., Sahel, J. A. and Mandel, J. L. 2000. Expanded polyglutamines induce neurodegeneration and trans-neuronal alterations in cerebellum and retina of SCA7 transgenic mice. *Hum Mol Genet.* 9, 2491-2506.
- Zander, C., Takahashi, J., El Hachimi, K. H., Fujigasaki, H., Albanese, V., Lebre, A. S., Stevanin, G., Duyckaerts, C. and Brice, A. 2001. Similarities between spinocerebellar ataxia type 7 (SCA7) cell models and human brain: proteins recruited in inclusions and activation of caspase-3. *Hum Mol Genet.* 10, 2569-2579.
- Zoghbi, H. Y. 1996. The expanding world of ataxins. *Nat Genet.* 14, 237-238.
- Zoghbi, H. Y. and Orr, H. T. 2000. Glutamine repeats and neurodegeneration. *Annu Rev Neurosci.* 23, 217-247.
- Zoghbi, H. Y. and Botas, J. 2002. Mouse and fly models of neurodegeneration. *Trends Genet.* 18, 463-471.
- Zu, T., Duvick, L. A., Kaytor, M. D., Berlinger, M. S., Zoghbi, H. Y., Clark, H. B. and Orr, H. T. 2004. Recovery from polyglutamine-induced neurodegeneration in conditional SCA1 transgenic mice. *J Neurosci.* 24, 8853-8861.
- Zuccato, C., Tartari, M., Crotti, A., Goffredo, D., Valenza, M., Conti, L., Cataudella, T., Leavitt, B. R., Hayden, M. R., Timmusk, T., Rigamonti, D. and Cattaneo, E. 2003. Huntingtin interacts with REST/NRSF to modulate the transcription of NRSE-controlled neuronal genes. *Nat Genet.* 35, 76-83.

## **Chapter 2**

---

Motor uncoordination and neuropathology in a transgenic mouse model of Machado-Joseph disease lacking intranuclear inclusions and ataxin-3 cleavage products





## Motor uncoordination and neuropathology in a transgenic mouse model of Machado–Joseph disease lacking intranuclear inclusions and ataxin-3 cleavage products

Anabela Silva-Fernandes<sup>a,1</sup>, Maria do Carmo Costa<sup>a,b,1</sup>, Sara Duarte-Silva<sup>a,1</sup>, Pedro Oliveira<sup>c</sup>,  
Claudia M. Botelho<sup>a</sup>, Luís Martins<sup>a</sup>, José António Mariz<sup>a</sup>, Tiago Ferreira<sup>d</sup>, Filipa Ribeiro<sup>a</sup>,  
Margarida Correia-Neves<sup>a</sup>, Cristina Costa<sup>e</sup>, Patrícia Maciel<sup>a,\*</sup>

<sup>a</sup> Life and Health Sciences Research Institute (ICVS), School of Health Sciences, University of Minho, Campus de Gualtar, 4710-057 Braga, Portugal

<sup>b</sup> Department of Neurology, University of Michigan, Ann Arbor, USA

<sup>c</sup> Department of Production and Systems Engineering, School of Engineering, University of Minho, Braga, Portugal

<sup>d</sup> Centre for Research in Neuroscience, McGill University, Quebec, Canada

<sup>e</sup> Department of Neurology, Hospital Prof. Fernando Fonseca, E.P.E., Amadora, Portugal

### ARTICLE INFO

#### Article history:

Received 6 February 2010

Revised 30 April 2010

Accepted 17 May 2010

Available online 25 May 2010

#### Keywords:

Polyglutamine  
Neuronal atrophy  
Pathogenesis  
Neuroinflammation  
Spinocerebellar ataxia  
Neurodegeneration  
Genetic instability  
Triplet repeats

### ABSTRACT

Machado–Joseph disease (MJD) is a late-onset neurodegenerative disorder caused by a polyglutamine (polyQ) expansion in the ataxin-3 protein. We generated two transgenic mouse lineages expressing the expanded human ataxin-3 under the control of the CMV promoter: CMVMJD83 and CMVMJD94, carrying Q83 and Q94 stretches, respectively. Behavioral analysis revealed that the CMVMJD94 transgenic mice developed motor uncoordination, intergenerational instability of the CAG repeat and a tissue-specific increase in the somatic mosaicism of the repeat with aging. Histopathological analysis of MJD mice at early and late stages of the disease revealed neuronal atrophy and astrogliosis in several brain regions; however, we found no signs of microglial activation or neuroinflammatory response prior to the appearance of an overt phenotype. In our model, the appearance of MJD-like symptoms was also not associated with the presence of ataxin-3 cleavage products or intranuclear aggregates. We propose the transgenic CMVMJD94 mice as a useful model to study the early stages in the pathogenesis of MJD and to explore the molecular mechanisms involved in CAG repeat instability.

© 2010 Elsevier Inc. All rights reserved.

### Introduction

Machado–Joseph disease (MJD), also known as Spinocerebellar Ataxia type 3 (SCA3), is an autosomal dominant neurodegenerative disorder caused by the expansion of a polyglutamine tract (polyQ) in the C-terminus of the *ATXN3* gene product, ataxin-3 (*ATXN3*) (Kawaguchi et al., 1994). In this gene, the polyQ tract length ranges between 12 and 44 in the normal population and between 53 and 87 in patients (Maciel et al., 2001; van Alfen et al., 2001).

Clinically, MJD is characterized by a late-onset spinocerebellar ataxia, ophthalmoplegia and spasticity associated to variable degree with amyotrophy or extrapyramidal features (Coutinho and Andrade, 1978). The pathological hallmark of the disease is the presence of nuclear inclusions of aggregation-prone expanded

*ATXN3* in the patients' brains. Although *ATXN3* is ubiquitously expressed (Paulson et al., 1997), only restricted neuronal populations of the central nervous system (CNS) are classically described as affected, namely the cerebellar dentate nucleus, pallidum, substantia nigra, thalamus, subthalamic, red, and pontine nuclei, cranial nerve nuclei and the anterior horn and Clarke's column of the spinal cord (Romanul et al., 1977; Rosenberg et al., 1976; Woods and Schaumburg, 1972). Recent pathological studies have suggested that the extension of CNS degeneration in MJD patients at end stages may be more widespread, including the visual, auditory, vestibular, somatosensory, ingestion-related, dopaminergic and cholinergic systems (Rub et al., 2008).

Fifteen years have passed since the cloning of the MJD causative gene (Kawaguchi et al., 1994), and to date the mechanism of cell demise taking place in specific regions of the brains of MJD patients remains largely ignored. However, the numerous studies of polyQ and other neurodegenerative diseases undertaken during these years have raised important questions: i) How are neurons dying: is active cell death occurring, or is necrosis the main pathway of death? ii) What is the contribution of somatic mosaicism in cell-specific vulnerability?

\* Corresponding author. Fax: +351 253604820.

E-mail address: [pmaciel@eicsaude.uminho.pt](mailto:pmaciel@eicsaude.uminho.pt) (P. Maciel).

<sup>1</sup> These authors contributed equally to this work.

Available online on ScienceDirect ([www.sciencedirect.com](http://www.sciencedirect.com)).

iii) Which are the toxic species: the aggregated, cleaved or soluble forms of ataxin-3? iv) What is the role of neuroinflammation in the disease process?

To attempt to answer these questions, several transgenic mouse models of MJD were created using different promoters to drive the expression of the human cDNA/gene: the L7 specific Purkinje cell promoter (Ikeda et al., 1996); the *ATXN3* promoter (Cemal et al., 2002); the *HD* promoter (Boy et al., 2009a); and different portions of the *PrP* promoter (which originates high brain expression levels) (Bichelmeier et al., 2007; Chou et al., 2008; Goti et al., 2004). More recently, a conditional MJD mouse model using the Tet-Off system was described showing reversibility of the phenotype (Boy et al., 2009b).

Although the most central questions still remain unanswered, these mouse models provide excellent mammalian systems to be used in the study of MJD pathogenesis. In this study, we have generated and characterized a new transgenic mouse model in which the human cDNA is ubiquitously expressed under the regulation of the cytomegalovirus promoter (pCMV). This mouse model mimics some key features of MJD including the ataxia and the dynamics of the CAG repeat, and we used it to study the cellular pathway(s) involved in cell death and the potential role of neuroinflammation in MJD pathogenesis.

## Methods

### Generation of CMVMJD transgenic mice

To generate transgenic MJD mice, the cDNA *ATXN3c* variant (GenBank accession no. U64820.1) (Goto et al., 1997) carrying a repeat tract  $(CAG)_2CAAAGCAGCAA(CAG)_{77}$  coding for 83 glutamines was amplified by PCR, introducing 5' and 3' flanking *NotI* restriction sites, and then cloned into the pCMV vector (kindly provided by Dr. Mónica Sousa, Univ. Porto). This plasmid, designated as pCMVMJD1-1E, was linearized by partial digestion with *PstI* (Fermentas), the fragment of interest (3150 bp) was then purified from an agarose gel using the QiaQuick gel extraction system (Qiagen, Hamburg, Germany) and microinjected into fertilized murine oocytes of the FVB/N mouse strain (Eurogentec, Seraing, Belgium). Two female founders were obtained from two different microinjections, establishing the transgenic CMVMJD94 and CMVMJD83 mouse lineages, which were backcrossed with C57Bl/6 mice (Harlan Iberica, Barcelona, Spain) over nine and seven generations, respectively. Hemizygous, homozygous CMVMJD transgenic mice (hemi CMVMJD and homo CMVMJD, respectively) and control littermates were obtained from colony inbreeding.

### Animals

All animals were maintained under standard laboratory conditions: an artificial 12 h light/dark cycle (lights on from 8:00 to 20:00 h), with an ambient temperature of  $21 \pm 1$  °C and a relative humidity of 50–60%; the mice were given a standard diet (4RF25 during the gestation and postnatal periods, and 4RF21 after weaning, Mucedola SRL, Settimo Milanese, Italy) and water *ad libitum*. Health monitoring was performed according to FELASA guidelines (Nicklas et al., 2002), confirming the *Specified Pathogen Free* health status of sentinel animals maintained in the same animal room. All procedures were conducted in accordance with European regulations (European Union Directive 86/609/EEC). Animal facilities and the people directly involved in animal experiments (ASF, MCC, SS, CB) were certified by the Portuguese regulatory entity – Direção Geral de Veterinária. All of the protocols performed were approved by the joint Animal Ethics Committee of the Life and Health Sciences Research Institute, University of Minho, and the Institute for Molecular and Cell Biology, University of Porto.

### Mouse genotyping

DNA was isolated from tail biopsy using the Puregene DNA isolation kit (Gentra Systems, Minneapolis, MN). In this single PCR genotyping tube, the primers TR1 (5'-GAAGACACCGGGACCGATCCAG-3') and TR2 (5'-CCAGAAGGCTGCTGTAACACGTC-3') were used to amplify the transgene (454 bp), and the primers mmMJD8 (5'-CAAAGTAGGCTTCTCGTCTCTCT-3') and mmMJD24 (5'-AGTGCTGA-GAACTCCAAG-3') to amplify the mouse homologous *Atxn3* gene (800 bp) as an internal control for the PCR. Hemizygoty/homozygoty and the transgene copy number were discriminated by semi-quantitative PCR, in which the transgene was amplified using the pair of primers TR1/TR2, and an intronic fragment (546 bp) of the mouse homologous gene *Atxn3* was amplified, as a reference gene (number of copies), using the primers mmMJD89 (5'-GCTAGCTAGAGCTACT-TATTG-3') and mmMJD54 (5'-GACTCCAGAGAGCACCTG-3'). Briefly, to determine the number of cycles in which the amplification was at the middle of the exponential phase, a sequential series of PCRs using both pairs of primers were performed for each lineage of transgenic mice. Gels were visualized with AlphaImager 2200 (AlphaInnotech, San Leandro, CA, USA) and analyzed by densitometry with the corresponding AlphaEase software.

### Molecular analysis of the $(CAG)_n$ repeat

The analysis of the intergenerational instability of the repeat was assessed in two different genetic backgrounds, FVB/N and C57Bl/6, in male ( $n = 22$ ,  $n = 32$ ) and female meioses ( $n = 24$ ,  $n = 18$ ). The repeat tract  $(CAG)_2CAAAGCAGCAA(CAG)_x$  and a 75-bp flanking region of the *ATXN3* gene were amplified by PCR using the primers MJD25a (5'-GGCTGGCCTTTCACATGGAT-3') and MJDcDNA (5'-CGGAAGAGACGA-GAAGCCTAC-3').

The relative  $(CAG)_n$  size variation across generations was studied by PCR amplification of DNA extracted from tail biopsies using the primers described above and incorporation of [<sup>35</sup>S] dATP (Amersham). PCR products were loaded in a denaturing 6% polyacrylamide gel as previously described (Maciel et al., 2001). The major allele size was determined by densitometry using AlphaEase software to detect the peak with the highest height in the AlphaImager 2200 (AlphaInnotech). CAG repeat length variation was determined by comparison with the highest height peak band from PCR products generated from progenitor DNAs.

For the analysis of the repeat in different tissues, hemi CMVMJD94 transgenic males with 5 ( $n = 3$ ), 24 ( $n = 5$ ), 60 ( $n = 6$ ) and 72 ( $n = 4$ ) weeks of age, were transcardially perfused with PBS under anaesthesia (ketamine hydrochloride (150 mg/kg) plus medetomidine (0.3 mg/kg)) and tissues were rapidly removed, frozen in dry ice and stored at  $-80$  °C. DNA extraction from brain regions (cerebellar cortex, deep cerebellar nuclei, motor cortex, hippocampus, amygdala, hypothalamus, substantia nigra, striatum and pontine nuclei) and peripheral tissues (heart, skeletal muscle, testis, kidney, liver and tail) was performed using the Puregene DNA isolation kit (Gentra Systems). Somatic mosaicism was studied in the transgenic mice by determination of the CAG repeat number using the same PCR strategy as described above, except for the usage of a 6-FAM fluorescently labeled MJDcDNA primer. Products were displayed in an ABI 310 automated DNA sequencer (Applied Biosystems, Foster City, CA). The degree of mosaicism of different tissues of mutant mice was analyzed by calculating the mosaicism index (MI). In order to avoid inclusion of PCR artifacts, only bands larger than the major bands were taken into account (Cancel et al., 1998). The number of bands with peak areas of at least 10% of the major band was counted and their surfaces summed. MI was defined as the ratio between this sum and the area of the major size band. The CAG tract length of the major size band was determined using an equation from the calibration curve obtained

with cloned alleles containing known numbers of CAG repeats (Williams et al., 1999).

#### Transgene expression analysis

Anaesthetized animals ( $n=3$  or  $4$  for each genotype) were euthanized by transcardial perfusion with PBS, tissues were collected, frozen in dry ice and stored at  $-80^{\circ}\text{C}$ . For protein isolation, mouse tissues were homogenized in 5 volumes of cold resuspension buffer (RB):  $0.1\text{ M Tris-HCl}$ ,  $\text{pH } 7.5$ ,  $0.1\text{ M EDTA}$ ,  $0.4\text{ mM PMSF}$  and a mixture of protease inhibitors (Roche, Indianapolis, IN). Protein concentrations were determined using the Bradford protein assay (Bio-Rad, Hercules, CA, USA), and samples were diluted in RB and Laemmli sample buffer at a final concentration of  $2.5\text{ mg/ml}$ . Samples were sonicated for  $10\text{ s}$ , heated for  $3\text{ min}$  at  $100^{\circ}\text{C}$  and centrifuged for  $10\text{ s}$  before loading  $20\text{ }\mu\text{l}$  per sample in  $10\%$  SDS-PAGE minigels. The blots were blocked in  $5\%$  dry milk/PBS before incubation overnight at  $4^{\circ}\text{C}$  with the primary antibody: serum anti-ataxin-3 (kindly provided by Dr. Henry Paulson) ( $1:20,000$ ), 1H9 ( $1:2000$ ) or anti-GAPDH (Advanced ImmunoChemical, Inc., Long Beach, CA, USA) ( $1:500$ ). Bound primary antibodies were visualized with goat anti-mouse or goat anti-rabbit HRP-conjugated secondary antibodies at  $1:500$  (PIERCE, Rockford, IL), chemiluminescent substrate (PIERCE), and exposure on autoradiography films (Amersham, Uppsala, Sweden). Signal bands were quantified using the ImageJ Software.

Total RNA from wild-type or CMVMJD mice ( $n=4$  or  $5$ ) brain tissue was isolated using TRIZOL (Invitrogen, Carlsbad, CA, USA) according to the manufacturer's protocol. First-strand cDNA synthesized using oligo-dT was amplified by quantitative reverse-transcriptase PCR (qRT-PCR) using primers in the  $3'$  UTR region to detect specifically human and mouse ataxin-3 mRNA (MJD\_UTR1b\_r:  $5'$  GCCCTAACTTTAGACATGTTAC3'; MJD\_UTR3\_F:  $5'$  GGAACAATGCGTCGGTTG3'; mjd\_3UTR\_2r:  $5'$  GTTACAAGAACAGAGCTGACT3'; mjd\_3UTR\_1f:  $5'$  TGTCTGTTCAGAAAGATCAG3'). Primer specificity was controlled by two negative PCR reaction controls: one with the primers for mouse ataxin-3 mRNA using the pCMVMJD1-1E plasmid (carrying the human cDNA) as template; and the other with the primers for human ataxin-3 mRNA and a total cDNA template from a wild-type mouse.

#### Immunohistochemistry

Transgenic (hemi and homozygotes) and control non-transgenic littermate mice ( $n=4$  or  $5$  for each group) at different ages ( $16$ ,  $49$  and  $84$  weeks) were deeply anaesthetized and transcardially perfused with PBS followed by  $4\%$  paraformaldehyde (PFA) in PBS. Brains were post-fixed overnight in fixative solution and embedded in paraffin. Slides with  $4\text{-}\mu\text{m}$ -thick paraffin sections were steamed for antigen retrieval and then incubated with rabbit GFAP antibody (DAKO Corporation, Carpinteria, CA) ( $1:500$ ) or rabbit anti-MJD1.1 (Ferro et al., 2007) ( $1:40$ ). A biotinylated secondary antibody was applied, followed by ABC coupled to horseradish peroxidase (DAKO) and DAB substrate (Vector Laboratories Inc., Burlingame, CA, USA). The slides were counterstained with hematoxylin according to standard procedures and analyzed with an optical microscope (Olympus, Hamburg, Germany). For morphological brain analysis, we performed hematoxylin & eosin and cresyl violet staining. The stereological analysis of GFAP-positive cells was performed in the vestibular region and in the substantia nigra using StereoInvestigator software (MicroBrightField, Williston/VT, USA). From each set of serial sections,  $2$  photomicrographs of the areas of interest were obtained at a primary magnification of  $\times 25$  and analyzed at a final magnification of  $\times 1000$ . Measurements were performed on regions randomly selected by the software. The densitometric analysis was performed in Purkinje cells, locus coeruleus, dentate nuclei and substantia nigra using a Zeiss light microscope coupled to a PC, using NIH Image 1.52 software. Density

levels were quantified and, for all sections, background density measurements were subtracted to these values.

For anti-Iba-1 immunohistochemistry, brains from hemi CMVMJD94 mice and littermates at  $10$  and  $25$  weeks of age ( $n=3$  per group) were fixed in a  $4\%$  PFA/PBS solution for  $3$  days, after which they were kept in an  $8\%$  sucrose solution. Forty-micron-thick vibratome sections were incubated with rabbit anti-Iba-1 (Wako chemicals, 019-19741) ( $1:250$ ). The antibodies were detected as above, as was the counterstaining and visualization of the slides.

Apoptosis was analyzed using the TUNEL assay. *In situ* DNA end-labeling was accomplished using the Apoptag Peroxidase *In situ* Apoptosis Detection Kit (Chemicon International, USA) according to the manufacturer's instructions. Mice were deeply anaesthetized, transcardially perfused with PBS and brains were removed and frozen at  $-80^{\circ}\text{C}$  embedded in OCT. Frozen brain sections ( $10\text{ }\mu\text{m}$ ) of transgenic CMVMJD94 and wild-type mice ( $n=4$  for each genotype) with  $86$  to  $100$  weeks of age, were fixed in  $1\%$  PFA/PBS for  $30\text{ min}$  and post-fixed in pre-cooled ethanol:acetic acid ( $2:1$ ) at  $-20^{\circ}\text{C}$  for  $5\text{ min}$ . Endogenous peroxidase was inactivated by immersing the tissue sections in  $3\%$   $\text{H}_2\text{O}_2$  in PBS solution for  $30\text{ min}$  and rinsing several times with water and PBS.

For caspase-3 detection, frozen sections of the same experimental group used for TUNEL assay, were fixed in  $4\%$  PFA/PBS and incubated with rabbit anti-active-caspase-3 (R&D systems AF835,  $1:250$ , diluted in TBS) overnight at  $4^{\circ}\text{C}$ . The detection of active-caspase-3 was assessed according to the streptavidin-biotin peroxidase complex system (Ultra Vision Large Volume Detection System Anti-Polyvalent, HRP; Lab Vision Corporation, Fremont, CA, USA) according to the manufacturer's instructions.

Fluoro-jade B staining was also performed in the animals group described above, to evaluate the presence of non-apoptotic cell death according to the manufacturer's instructions (Chemicon International).

#### Phenotype analysis

Behavioral analysis was performed during the diurnal period in groups of  $5$  animals per cage of CMVMJD83 and CMVMJD94 transgenic mice (hemi and homo) and wild-type littermates ( $n=10$  per genotype and gender). Animals were evaluated at  $16$ ,  $24$ ,  $36$ ,  $48$ ,  $60$ ,  $72$  and  $84$  weeks of age in the Rotarod followed by the SHIRPA protocol.

#### SHIRPA protocol

We established a protocol for phenotypic assessment based on the primary screen of the SHIRPA protocol, which mimics the diagnostic process of general neurological and psychiatric examination in humans (Rogers et al., 1997). Each mouse was placed in a viewing jar ( $15\text{ cm}$  diameter) for  $5\text{ min}$ , transferred to a  $15$ -labeled-squares arena ( $55\times 33\times 18\text{ cm}$ ), and then a series of anatomical and neurological measures were determined. The full details of the SHIRPA protocol are available at the site: [http://www.mgu.har.mrc.ac.uk/facilities/mutagenesis/mutabase/shirpa\\_summary.html](http://www.mgu.har.mrc.ac.uk/facilities/mutagenesis/mutabase/shirpa_summary.html).

In addition, we included the vertical pole test (Wallace et al., 1980), the footprint pattern test (Carter et al., 1999) and the counting of rears over  $5\text{ min}$  in the viewing jar as a measure of spontaneous exploratory activity. The protocol was adjusted in order to minimize animal handling and to generate uniformity in waiting times between the tests (Rafael et al., 2000).

#### Vertical pole test

This test was performed on a wood pole of approximately two cm in diameter and  $40\text{-cm}$  long, wrapped with cloth tape for improved traction. The mouse was placed in the center of the pole, held horizontally, and then the pole was gradually lifted to a vertical



position. Latency to fall off the pole was recorded with a maximum time of 1 min.

#### Footprint pattern

The footprint test was used to evaluate the gait of the animals. To obtain footprints, the hind- and forepaws of the mice were coated with black and red non-toxic paints, respectively. A clean sheet was placed on the floor of the runway for each run. The animals were then allowed to walk along a 100-cm-long  $\times$  4.2 cm width  $\times$  10 cm height corridor in the direction of an enclosed black box. Each animal was allowed to achieve one valid trial per age. The footprint patterns were analyzed for four step parameters (all measured in cm): the front- and hind-base width, the foot step uniformity and the length of the step. For each step parameter, three values were measured for three consecutive steps, with the exclusion of the first four steps to allow for habituation.

#### Rotarod

Mice were tested in a rotarod apparatus (TSE systems, Bad Homburg, Germany) to evaluate their motor performance. The protocol consisted of 3 days of training at a constant speed (15 rpm) for a maximum of 60 s in four trials, with a 10 min interval between each trial. On the fourth day, animals were tested for each of 6 different speeds (5 rpm, 8 rpm, 15 rpm, 20 rpm, 24 rpm and 31 rpm) for a maximum of 60 s in two trials, with a 10-min-long interval between each trial. After a one-hour rest period, the animals were subjected to four trials on an acceleration rod (4–40 rpm, 5 min) with a 10–15-long interval between each trial.

#### RT<sup>2</sup> Profiler™ PCR Array (Superarray) analysis of neuroinflammation

The mRNA expression level of 84 key genes involved in the inflammatory response, 5 house-keeping genes and controls for DNA contamination, reverse transcription and PCR efficiency were determined simultaneously using Superarray technology (SABiosciences™). For this experiment, animals were euthanized by decapitation, and the cerebellum was collected and immediately snap frozen and stored at  $-80^{\circ}\text{C}$ . RNA samples extracted from the cerebellum of CMVMJD94 transgenic and wild-type animals at 8 and 24 weeks of age ( $n = 10$  or 12) were pooled onto individual Superarrays with 3–4 samples per array for a total of 3 arrays per condition. The RNA was first converted into first-strand cDNA using the RT<sup>2</sup> First Strand Kit following the manufacturer's guidelines. In addition, we analyzed the expression levels of the tumor necrosis factor (*Tnfx*), interleukin 6 (*Il6*), interleukin 1 beta (*Il1 $\beta$* ) and ionized calcium-binding adapter molecule 1 (*Iba-1*) genes by the qRT-PCR assay using the following primers, respectively: mu *Tnfa* Sy F (5'GCCACCACGCTCTTCTGTCT3'); mu *Tnfa* Sy R (5'TGAGGGTCTGGCCATAGAAC3'); mu *Il-6* Sy F (5'ACACATGTTCTCTGGGAAATCGT3'); mu *Il-6* Sy R (5'AAGTGCATCATCGTTTCATACA3'); SP\_II-1b (5'ACCTCCAGGATGAGGACATGA3'); AS\_II-1b (5'AACGTCA-CACACCAGCAGGTTA3'); *Iba-1\_f* (5'GAAGCGAATGCTGGAGAAAC3'); *Iba-1\_r* (5'CTCATACATCAGAATCATTCTC3').

#### Statistical analysis

Behavioral data were subjected to the non-parametric Mann-Whitney *U*-test when variables were non-continuous or when a continuous variable did not present a normal distribution (Kolmogorov-Smirnov test  $p < 0.05$ ). Continuous variables with normal distributions (*K-S* test  $p > 0.05$ ) were analyzed with the Student *t*-test or ANOVA. All statistical analyses were performed using SPSS 16.0 (SPSS Inc., Chicago, IL). A critical value for significance of  $p < 0.05$  was used throughout the study.

## Results and discussion

We have created a novel transgenic mouse model of MJD expressing an expanded version of the human MJD1-1 cDNA (the 3 UIMs-containing variant of ATXN3, previously used in the mouse models described by Bichelmeier et al., 2007; Boy et al., 2009a,b), under the regulation of the CMV promoter. This model displays some important features that mirror the human disease. Transgenic CMVMJD94 mice (94 CAGs) showed: i) a motor uncoordination phenotype that, manifested in hemizygous mice, is in agreement with the dominant mode of transmission of this spinocerebellar ataxia; ii) a direct correlation between CAG repeat length and disease manifestation; iii) intergenerational instability of the (CAG)<sub>n</sub> tract; iv) somatic mosaicism of the repetitive CAG stretch in neuronal and non-neuronal tissues; and v) neuropathologic alterations in specific regions such as the thalamus, the dentate and pontine nuclei, the substantia nigra and the vestibular nuclei, that parallel the human disorder. Importantly, the detailed study of this model allowed us to exclude events such as ATXN3 cleavage and intranuclear aggregation as key factors to the onset of disease and revealed that neurodegeneration occurs in the absence of apoptosis or necrosis. Neuroinflammation was also not evident at the early stages of the disease.

#### Generation of MJD transgenic mice

In order to generate MJD transgenic mice, we subcloned the mutant human cDNA ATXN3c variant carrying a (CAG)<sub>2</sub>CAAAAGCAGCAA (CAG)<sub>77</sub> repeat tract, coding for 83 polyQs, into the pCMV vector, which is a strong and general expression promoter (Fig. 1A). Two founders were obtained from two different microinjections: founder CMVMJD94 and CMVMJD83, carrying 94 and 83 CAGs, respectively (Fig. 1B). This indicates that the CAG repeat tract from founder CMVMJD94 suffered an expansion of 11 CAG repeats from the injected construct, probably occurring during early embryonic mitosis events. Our analysis of the transmission of the transgene revealed an adequate fit to Mendelian expectations, with no decrease of the proportion of homozygotes (Fig. 1B). Although a Mendelian segregation distortion for the expanded CAG allele (with a higher transmission of the mutant allele) has been described by some authors in human MJD families (Ikeuchi et al., 1996; Iughetti et al., 1998; Riess et al., 1997; Takiyama et al., 1997), this is a controversial finding that, according to others, can be explained by observational bias in families selected for genetic lineage studies due to a large number of affected individuals (Grewal et al., 1999). Our analysis of the transmission of the CMVMJD94 and CMVMJD83 transgenic lineages excluded a "meiotic drive" effect of the expanded allele in these mice (Fig. 1B).

#### Expression of expanded human ataxin-3

As expected from the general expression features of the pCMV promoter, the human ataxin-3 (ATXN3) was detected in the CNS (Fig. 1C) and peripheral tissues of transgenic mice in both lineages by anti-ataxin-3 western blot and immunohistochemistry (IHC). This is comparable to the ubiquitous expression of ATXN3 reported in human tissues (Kawaguchi et al., 1994; Paulson et al., 1997). The ATXN3 mRNA expression was also confirmed in both lineages by qRT-PCR (data not shown).

In the immunoblots for both lineages endogenous mouse ataxin-3 protein (*Atxn3*) was observed at 42 kDa, as previously described (Costa et al., 2004), while ATXN3 was detected at approximately 70 kDa; due to the CAG tract length difference it was possible to observe a slight variation in the ATXN3 protein size between CMVMJD94 and CMVMJD83 transgenic mice (Fig. 1C). No SDS-resistant species or cleaved products of ATXN3 were observed in the brains of mice from either transgenic lineage (Fig. 1D). Quantitative measurement of these immunoblots confirmed that CMVMJD94

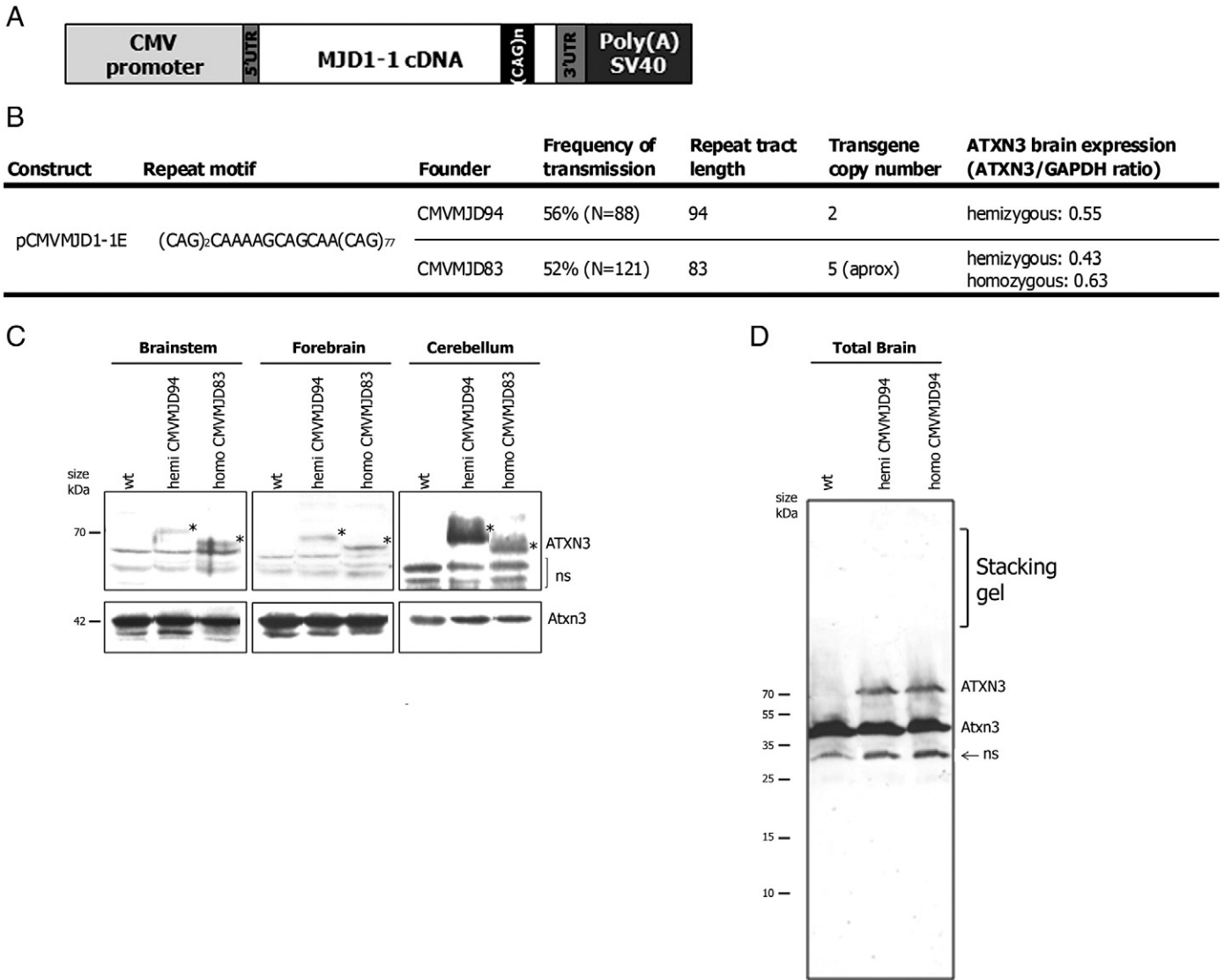


**Fig. 1.** Mendelian transmission of the transgene and ubiquitous brain expression of ATXN3 in CMVMJD transgenic mice. (A) Schematic diagram of the plasmid CMVMJD1-1E used for the generation of cDNA MJD transgenic mice. (B) Descriptive summary of the transgenic mouse lineages generated. (C) Western blot analysis of human ataxin-3 (ATXN3) in different CNS regions of CMVMJD83 and CMVMJD94 mice with approximately 86 weeks of age. In all lanes, the endogenous mouse ataxin-3 (Atxn3) is detected at about 42 kDa. An approximately 70-kDa protein (asterisks) corresponding to expanded ATXN3 is detected in transgenic animal lysates from the cerebellum, forebrain and brainstem. Hemi CMVMJD94 animals and homo CMVMJD83 express approximately equal levels of ATXN3. (D) Western blot using 1H9 antibody for CMVMJD94 mice at advanced ages (84 weeks of age) did not reveal the presence of ATXN3 fragments or insoluble protein in the stacking gel. wt, wild-type; hemi, hemizygous; homo, homozygous; ns, non-specific bands.

hemizygotes and CMVMJD83 homozygotes mice expressed approximately equal levels of ATXN3 in total brain (Fig. 1B). As a control result, we observed that ATXN3 expression in homozygous mice was double that of hemizygous mice (Fig. 1D). In addition, ATXN3 was also detected in peripheral tissues and organs such as skeletal muscle, pancreas, heart and testis of both mutant lines (data not shown).

Anti-ataxin-3 IHC revealed increased ATXN3 expression in transgenic MJD mice brains, both in terms of intensity and number of stained cells, in comparison with non-transgenic littermates (Fig. 2; Supp. Figure 1). In addition, mutant ATXN3 was detected in several brain regions including areas involved in MJD, namely, the cerebellum (cerebellar cortex and deep cerebellar nuclei), the pontine nuclei, the locus coeruleus and the substantia nigra, among others (Fig. 2).

*Parental gender and genetic background-dependent pattern of CAG intergenerational instability*

A common feature of polyQ disorders is the dynamic behavior of CAG expansions, which are thought to be responsible for the

anticipation observed in human patients. This phenomenon reflects the global tendency of expanded repeats to become larger when transmitted from one generation to the next. CAG repeat length variation is observed not only throughout generations – intergenerational instability – but also among several tissues of individual patients – somatic mosaicism. To investigate whether MJD transgenic mice, like human patients, displayed intergenerational instability of the expanded triplet repeat, we determined the (CAG)<sub>n</sub> tract length in maternal and paternal meioses of transgenic CMVMJD94 animals. This lineage was chosen for the study because amplification of the CAG repeat produces a single major peak. This finding means that the two copies of the transgene integrated in these transgenic mice carry the same CAG repeat number, allowing the analysis of (CAG)<sub>n</sub> length variation. When amplified by PCR, the DNA extracted from transgenic mouse tissues exhibited a pattern of bands very similar to that observed in heterozygous human patients (Maciel et al., 1997).

These mice were generated by breeding between either hemi CMVMJD94 males or females with the correspondent non-transgenic breeder in two different genetic backgrounds, C57Bl/6 and FVB/N,



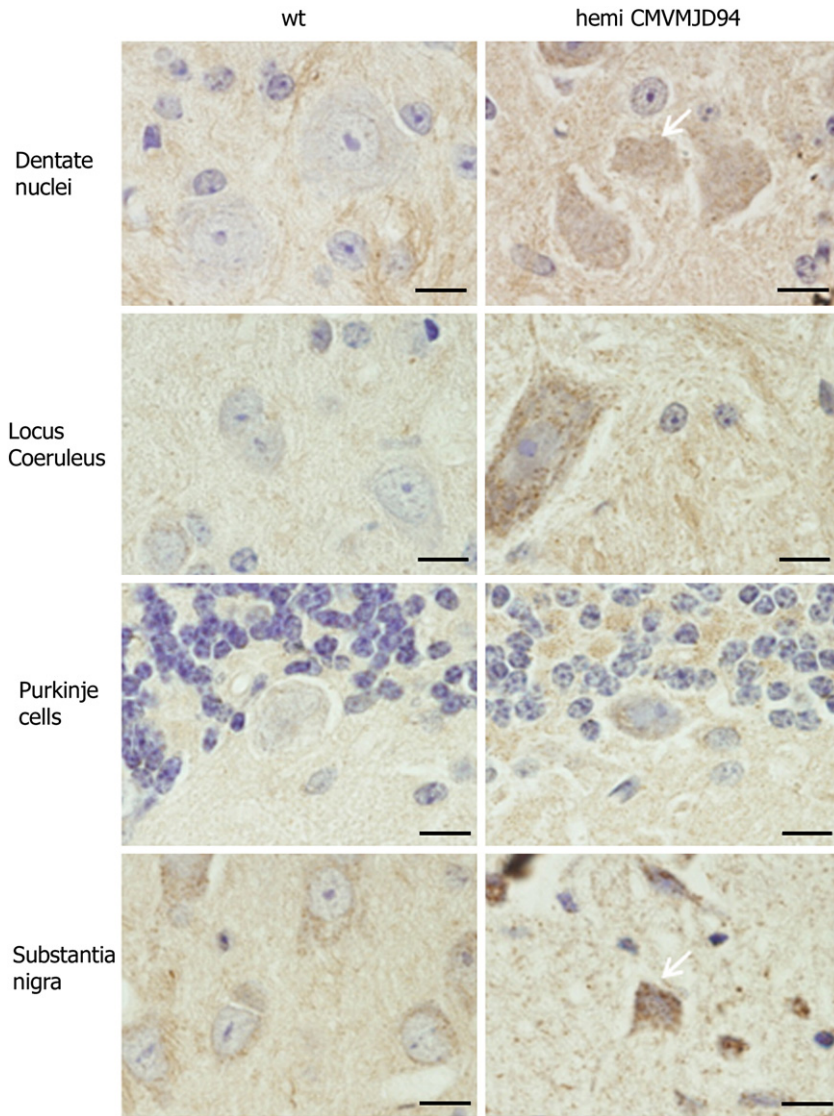


**Fig. 2.** Absence of large intranuclear inclusions in transgenic mice with motor impairment. Anti-ataxin-3 immunohistochemistry (rabbit anti-MJD1.1) of wild-type and transgenic CMVMJD94 mice at late stages of the disease (49 weeks). Ataxin-3 presents a cytoplasmic localization in special forming small-punctate structures in the perinuclear region. Examples of scattered dark and shrunken cells positive for ataxin-3 can be observed in dentate nuclei and substantia nigra (arrows). wt, wild-type; hemi, hemizygous. Scale bar: 10  $\mu$ m.

which allowed us to identify genetic background effects on repeat instability. We observed, for both backgrounds, that the CAG repeat length varied through generations in more than 50% of the transmissions: the expanded allele had the tendency to expand when transmitted through the male progenitor and to contract when transmitted from the female progenitor (Figs. 3A,B). This observation reached statistical significance in the C57Bl/6 background ( $p < 0.05$ ) (Fig. 3B). The differential distribution of CAG repeat length variation in the two congenic strains suggests that background-specific modifier loci might affect the pattern of instability of this CAG tract.

Our results are in agreement with previous results described in MJD patients regarding the mild instability of the CAG tract length and the difference in  $(CAG)_n$  instability between male and female transmissions (Maciel et al., 1995).

#### CAG length-dependent motor phenotype

During the behavioral analysis period, some animals with different genotypes died, without bias. Behavioral studies revealed a number of

findings in the CMVMJD94 transgenic mice, which differed from non-transgenic and transgenic hemizygous or homozygous mice from lineage CMVMJD83. The rotarod test performed either at constant speeds or using an acceleration protocol revealed that both hemi and homo CMVMJD94 mice presented a motor coordination impairment beginning at 16 weeks of age (Fig. 4A). In MJD, a gene-dosage effect has been proposed in individuals who are homozygous for the mutation, showing a juvenile onset and more rapid progression of the disease (Sobue et al., 1996). Interestingly, in our model, homozygous animals also spent less time on the rod in comparison with hemizygous animals, although this difference did not reach statistical significance (Fig. 4A).

Additionally, transgenic CMVMJD94 mice presented a trend towards a decrease of locomotor activity, given by the number of squares traveled in the arena in the SHIRPA protocol (Fig. 4B). This reduced locomotor activity only reached significance for homozygous animals at 48 weeks of age (Fig. 4B). No differences were found for the other parameters evaluated, including the vertical pole test and the footprinting pattern (Supp. Figure 2). Hemi or homo CMVMJD83 mice, differing from the CMVMJD94 in the CAG tract, which was only 11

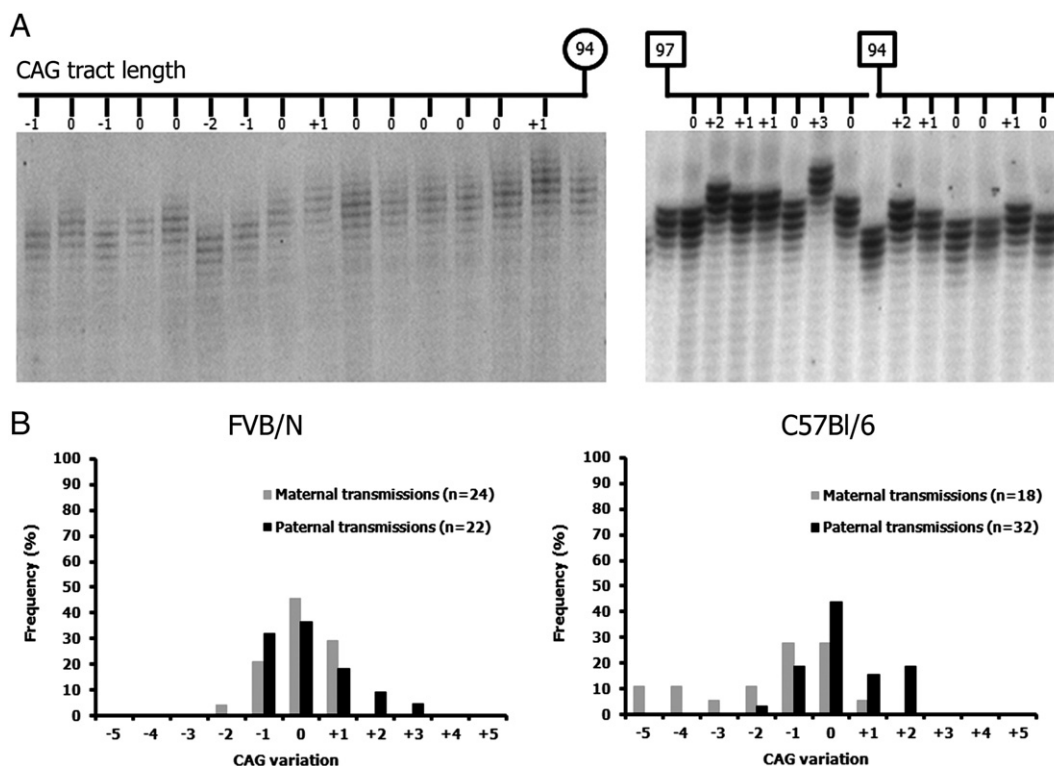


**Fig. 3.** Intergenerational instability of the expanded CAG repeat in transgenic CMVMJD94 mice. (A) Polyacrylamide gels showing the variation of the CAG repeat tract length of male and female hemi CMVMJD94 progenitors and their respective descendants in the FVB/N genetic background. (B) Differential pattern of CAG repeat variation in transgenic CMVMJD94 male and female meioses, in the FVB/N and C57Bl/6 genetic backgrounds.

units shorter, did not present any behavioral differences in comparison with control littermates (Figs. 4A,B).

Although the expression of normal ATXN3 in mouse could in theory give rise to some pathological consequences, other transgenic mice expressing the same protein were indistinguishable from wild-type mice, even when considering mouse lines with strong expression and mice of older ages (between 12 and 22 months) (Bichelmeier et al., 2007; Cemal et al., 2002; Chou et al., 2008; Goti et al., 2004). In view of these findings, we used wild-type littermates as controls. Furthermore, homo CMVMJD83 mice did not present motor phenotype or brain pathology (see below) although they expressed levels of expanded ATXN3 similar to those of hemi CMVMJD94 mice. Since transgenic CMVMJD83 mice carried a shorter CAG tract than the CMVMJD94 ones (83 vs. 94 CAGs), these data allowed us to conclude that at this level of expression of expanded ATXN3, the minimum CAG tract length to induce an altered phenotype in the transgenic mice is between 84 and 94 CAG repeats.

Interestingly, the usage of two different study groups, including hemi CMVMJD94 mice and their non-transgenic littermates for phenotype assessment, revealed that although, at 16 weeks of age, the first group of hemizygous animals displayed a significant decrease in the time spent on the accelerating rod (mean of 4 trials, 4–40 rpm), the hemizygous mice from the second group did not replicate this motor deficit at the same age (Fig. 5A). Since transgenic mice displayed CAG instability across generations, we hypothesized that CAG repeat length differences could have influenced the manifestation of the disease at early stages. In fact, we observed that hemizygous animals from group II carried lower CAG repeat lengths (mean  $95.85 \pm 1.73$ ) than animals from group I (mean  $97.61 \pm 2.00$ ) (Fig. 5B). Additionally, when analyzing all of the data, we found an inverse correlation between the CAG tract length and the time spent on the rod at 16 weeks of age ( $p < 0.05$ ): animals carrying longer CAG repeats spent less time on the rod (Fig. 5B). This genotype–phenotype correlation is in agreement with that observed in MJD patients

(Maciel et al., 1995) and with the anticipation phenomenon, in which longer repeat lengths in successive generations are associated with a more severe and earlier onset of symptoms.

#### Neuronal atrophy and astrogliosis in transgenic CMVMJD94 mice

Histopathological observations of brain sections of transgenic CMVMJD94 mice revealed the presence of scattered dark, shrunken cells with basophilic cytoplasm (Fig. 6) (H&E staining) in several regions, such as the dentate, pontine nuclei and thalamus, in comparison with normal cells observed in wild-type animals (Fig. 6). Globally, these findings are consistent with the pathological findings reported in MJD patients, where the degeneration involves atrophy and gliosis (Kanda et al., 1989; Rub et al., 2008). To further investigate the molecular mechanism of neurodegeneration, we performed a TUNEL assay, as well as caspase-3 IHC and fluoro-jade staining in brain sections of CMVMJD94 mice with no positive results (data not shown). These results suggest that the dark neurons observed in such areas, as the thalamus and pontine and dentate nuclei could be dying via another cell death process, or, alternatively, that their morphology could be associated with a dysfunctional but not a dying cell status. Nevertheless, CMVMJD94 transgenic mice with 49 weeks of age displayed an increase in GFAP immunostaining (within reactive astrocytes) in specific areas, such as the vestibular nuclei (Ve) and substantia nigra (SN), indicative of an abnormal increase in the number of astrocytes in these areas, a phenomenon normally associated with neuronal demise (Figs. 7A–F; Supp. Figure 3). The analysis of CMVMJD94 mice brains at early stages of the disease (16 weeks) revealed the presence of a milder neuronal atrophy in areas such as the pontine and dentate nuclei (Fig. 6) and the absence of the astrogliosis observed at late stages. Our results direct us to a different concept of neurodegeneration, encompassing a progressive degradation of neuronal function and structure that may include cellular changes, such as loss of synaptic contacts, disruption

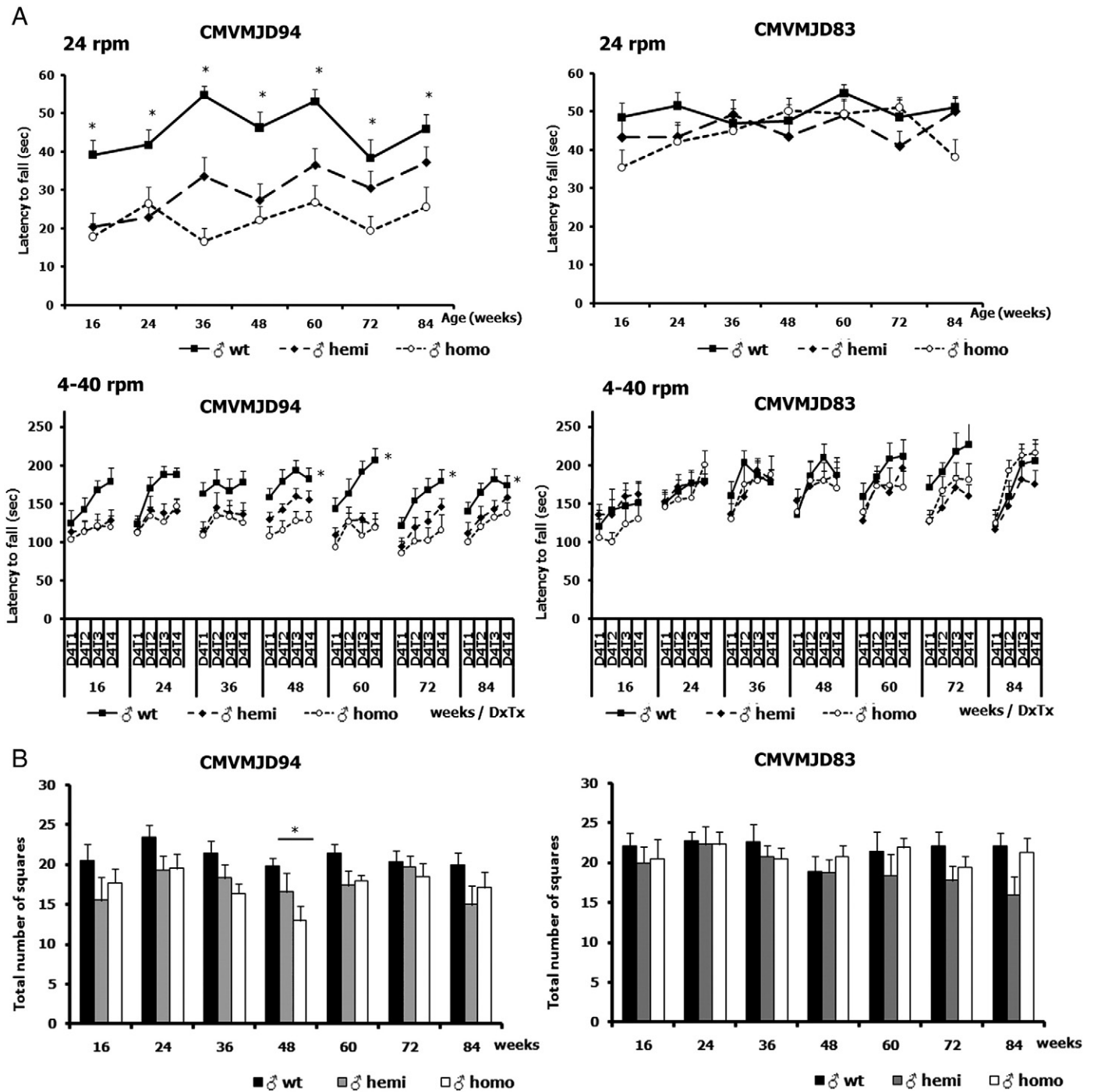


**Fig. 4.** Motor phenotype of CMVMJD transgenic mice. (A) The rotarod test ( $n = 10$  for each tested group) demonstrated that hemi and homo CMVMJD94 mice displayed a significant decrease in the latency to fall at 24 rpm (one-way ANOVA; factor: genotype) and in the accelerating rod (4–40 rpm) (Repeated measures; factor: genotype) in comparison with wild-type animals. Transgenic CMVMJD83 mice (hemi and homo) did not display a motor coordination deficit in the rotarod paradigm until 84 weeks of age. (B) Spontaneous locomotor activity decrease in transgenic CMVMJD94 mice. CMVMJD94 mice displayed a tendency to travel less squares during the 30 seconds of observation in the arena. wt, wild-type; hemi, hemizygous; homo, homozygous. \*Statistical significance  $p < 0.05$ .

of axonal transport, blockage of autophagy and mitochondrial dysfunction, among others. Although this process can eventually lead to cell death through different pathways, it is by itself sufficient to cause neurological disease.

Although it has been suggested that a cleavage product of mutant ATXN3 is critical for the induction of MJD pathogenesis (Wellington et al., 1998), western blot analysis of brains from symptomatic transgenic CMVMJD94 mice, did not reveal the presence of the 36 kDa cleavage product of ATXN3, described previously in human (end-stage) patients and in another mouse model (Goti et al., 2004).

Additionally, anti-ataxin-3 IHC in the brain of these MJD transgenic mice demonstrated that the protein was mainly localized in punctuate structures in the perinuclear region of neurons (Fig. 2), and no large intranuclear inclusions were found even at late stages (84 weeks of age). These results suggest that the disease manifestation in our transgenic mice is not dependent on the formation of nuclear inclusions. In fact, although cytoplasmic and/or nuclear inclusions in neurons of the CNS represent a pathological hallmark of polyQs diseases (Yamada et al., 2000), several studies have demonstrated a dissociation between the presence of large protein inclusions and



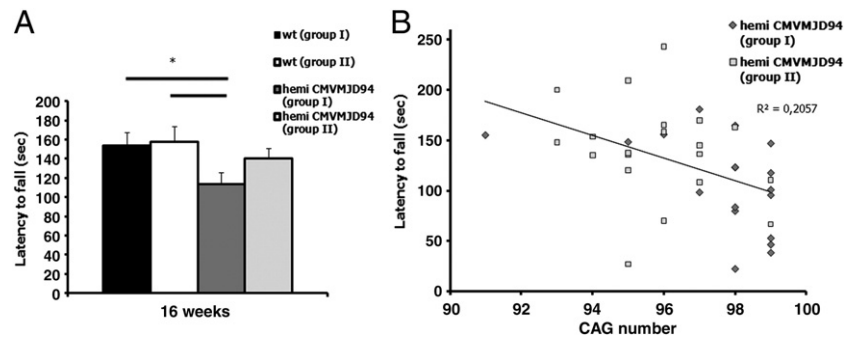


**Fig. 5.** Genotype–phenotype correlation. (A) At 16 weeks, hemi CMVMJD94 mice from group I ( $n = 18$ ) revealed a motor phenotype deficit, whereas hemi CMVMJD94 animals from group II ( $n = 20$ ) did not manifest significant differences in rotarod performance when compared to wild-type littermates ( $t$ -test student; mean of four consecutive trials in the accelerating rod). Hemi CMVMJD94 mice from group I developed a motor phenotype earlier than group II because the first was enriched with animals carrying higher CAG repeat lengths. (B) Genotype–phenotype correlation in hemi CMVMJD94 transgenic mice (groups I and II). wt, wild-type; hemi, hemizygous. \*Statistical significance  $p < 0.05$ ; Pearson correlation  $R^2 = 0.2057$ ;  $p = 0.004$ .

toxicity *in vivo* (Klement et al., 1998; Reiner et al., 2007; Slow et al., 2005) and *in vitro* (Arrasate et al., 2004; Saudou et al., 1998). Furthermore, recent findings using a Spinal and Bulbar Muscular Atrophy (SBMA) mouse model have implicated the species corresponding to the earlier stages of polyQ protein aggregate formation – oligomers – in the disease progression (Li et al., 2007).

#### Tissue- and age-dependent somatic mosaicism of the CAG repeat

The hypothesis that somatic mosaicism of the CAG repeat may contribute to the specificity of neurodegeneration (Telenius et al., 1994) was previously tested by determining the mosaicism index of the CAG repeat tract in various brain regions of MJD patients (Cancel et al., 1998; Lopes-Cendes et al., 1996; Tanaka et al., 1999). Our analysis of the CAG repeat size in several brain regions and different peripheral tissues of the CMVMJD94 mice showed the existence of

somatic mosaicism of the expanded allele – several bands larger and smaller than the major band were observed (Fig. 8A). The mosaicism index (MI) of the (CAG)<sub>n</sub> tract in different brain regions (cerebellar cortex, deep cerebellar nuclei, motor cortex, hippocampus, amygdala, hypothalamus, substantia nigra, striatum and pontine nuclei) and peripheral tissues (heart, skeletal muscle, testis, kidney, liver and tail) was determined with aging (Fig. 8). An age-dependent increase in the mosaicism index (ANOVA, factor age,  $p < 0.05$ ) was observed in all tissues that were analyzed, except for the heart (Fig. 8B). In addition, it was possible to observe the MI increase during aging in successive tail DNA samples from the same animal (Fig. 8A). Our results are in accordance with those obtained in animal models of different polyQ diseases, in which age has been described as a CAG repeat instability modifier (Clark et al., 2007; Ishiguro et al., 2001; Sato et al., 1999). Interestingly, we also observed that different tissues exhibited different patterns of MI increase with age. The cells from the liver,

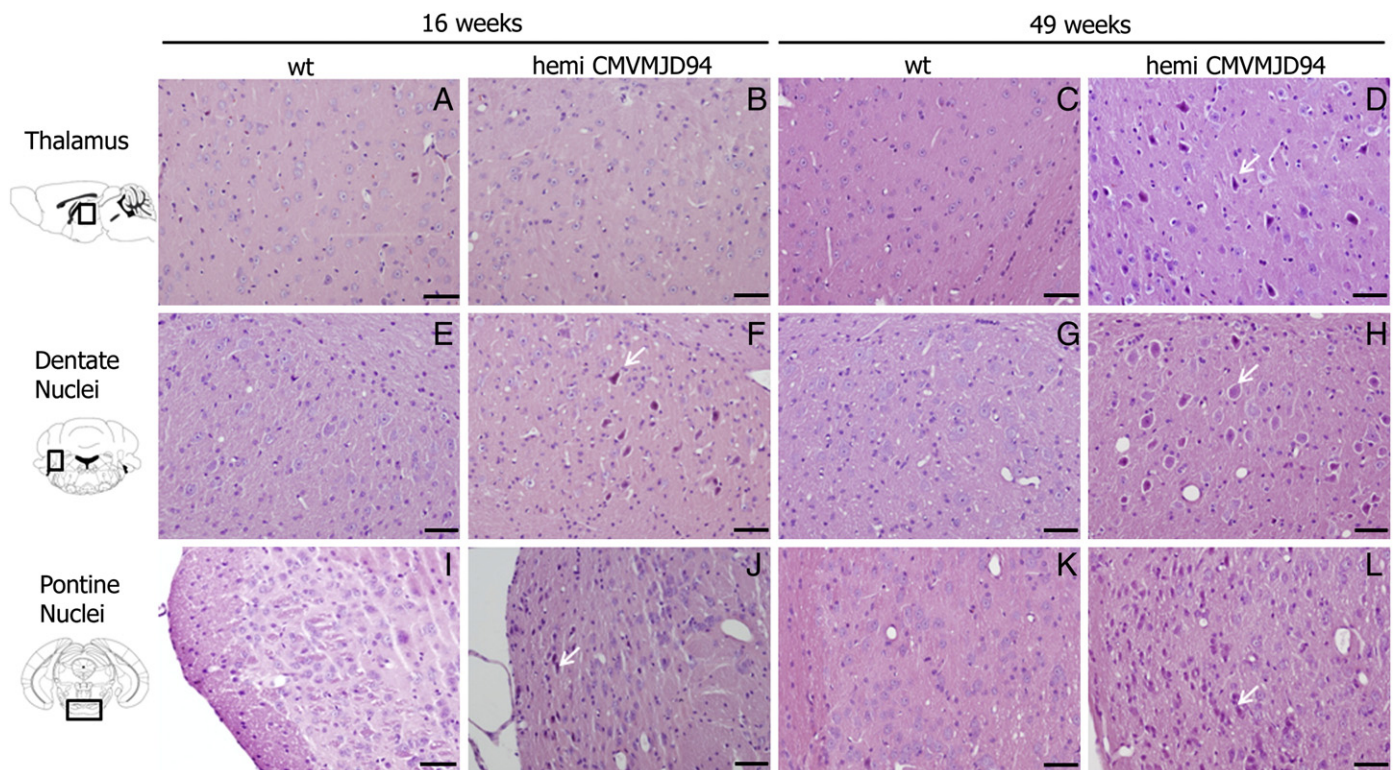


**Fig. 6.** Neuropathology of CMVMJD94 mice. Comparative sections stained with H&E of wild-type and hemi CMVMJD94 mice thalami (A–D), dentate nuclei (E–H) and pontine nuclei (I–L) at 16 and 49 weeks of age. Transgenic CMVMJD94 mouse neurons in the thalamus and dentate nuclei were observed by H&E staining as scattered dark, shrunken cells with pyknotic nuclei and a basophilic cytoplasm (arrows) in comparison with normal cells observed in wild-type animals. wt, wild-type; hemi, hemizygous. Scale bar: 50  $\mu$ m.

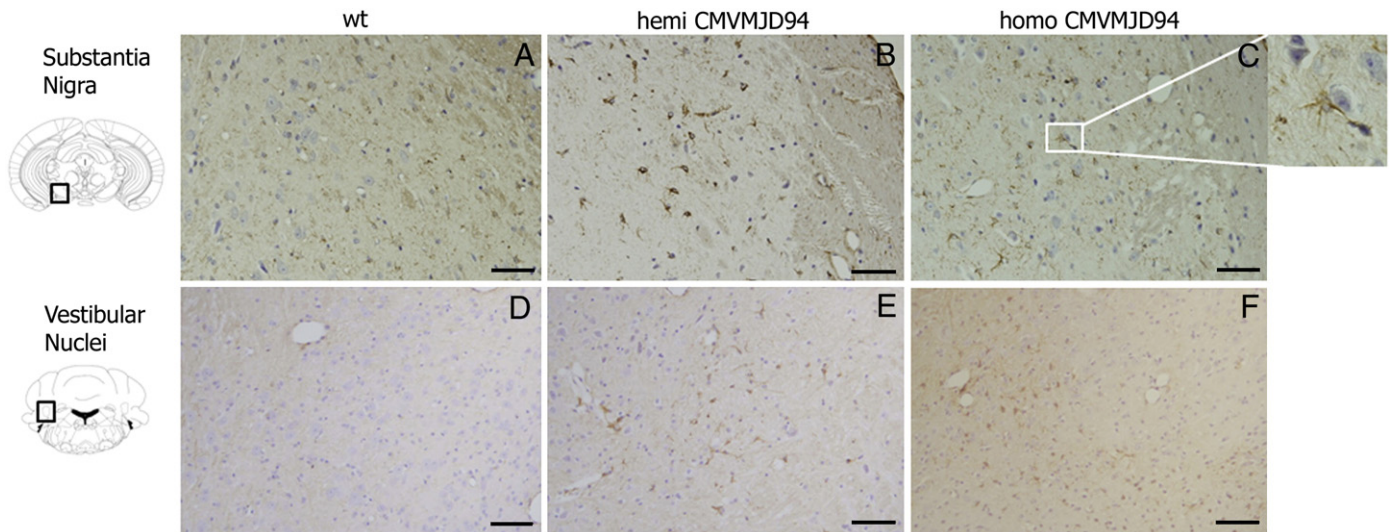


**Fig. 7.** Astrogliosis in the brain of CMVMJD94 mice. GFAP immunostaining of the substantia nigra (A–C) and the vestibular nuclei (D–F) at 49 weeks of age. Transgenic hemizygous and homozygous mice showed increased immunostaining (\*,  $p < 0.05$ ) and the presence of reactive astrocytes, relative to wild-type animals. The insets represent a higher magnification demonstrating both atrophic neurons and reactive astrocytes. wt, wild-type; hemi, hemizygous; homo, homozygous. Scale bar: 50  $\mu\text{m}$ .

pontine nuclei, substantia nigra and striatum displayed the highest MI increase, and the cells from the cerebellar cortex and skeletal muscle showed the lowest MI increase during aging. These results are in agreement with the behavior of the mutant allele in the human patients, in which the cerebellar cortex and skeletal muscle exhibited a lesser degree of CAG instability, while the liver displayed a greater diversity of bands (Tanaka et al., 1999). Although mitotic turnover may contribute largely to the tissue-specific pattern of mosaicism in MJD, the absence of a direct correlation of the MI with the mitotic rate of the cells of the tissues analyzed (e.g., liver and pontine nuclei) suggests that other unknown cell-specific factors should be taken into consideration to understand the mechanism of somatic mosaicism in CAG repeat diseases.

Among the brain regions analyzed, the pontine nuclei, substantia nigra and striatum were the areas with the highest MI increase during aging; of these, we observed pathological involvement in the pontine nuclei and substantia nigra (described above) but not in the striatum, which led us to conclude that, in this mouse model, the specific increase of somatic mosaicism was not clearly correlated with neuronal vulnerability. Although a correlation between somatic mosaicism and the pathology of different brain regions was not evident, our results concerning the  $(\text{CAG})_n$  size variation pattern in CMVMJD94 transgenic mice revealed that this mouse model can be useful for the study of the molecular basis of the CAG repeat instability as well as of MJD pathogenesis.

#### Absence of neuroinflammation in CMVMJD94 mice before the onset of the disease and at early symptomatic stages

The idea of chronic and detrimental microglial neuroinflammation as a cause of neurodegeneration has been studied extensively in the context of neurodegenerative diseases, notably in Alzheimer's disease (Streit et al., 2004), but nothing is known about the role of neuroinflammation in MJD pathogenesis. According to this theory, activated microglia, as the main cellular source of inflammatory

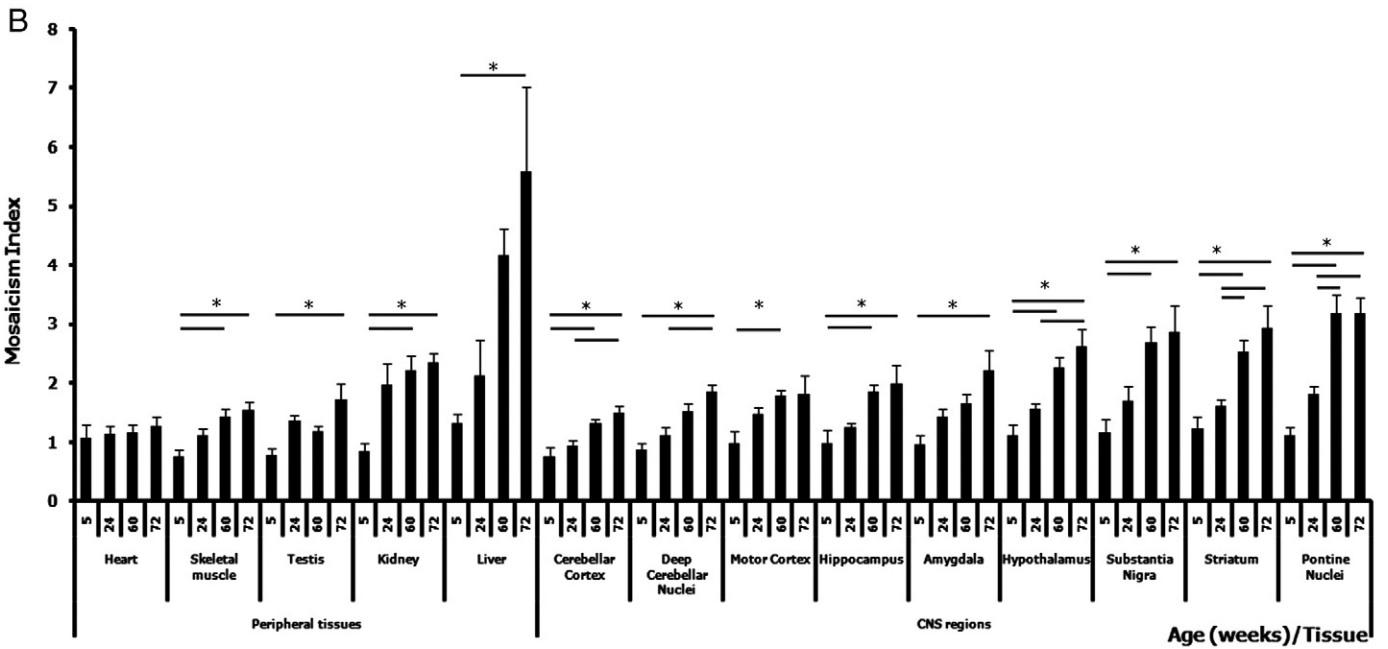
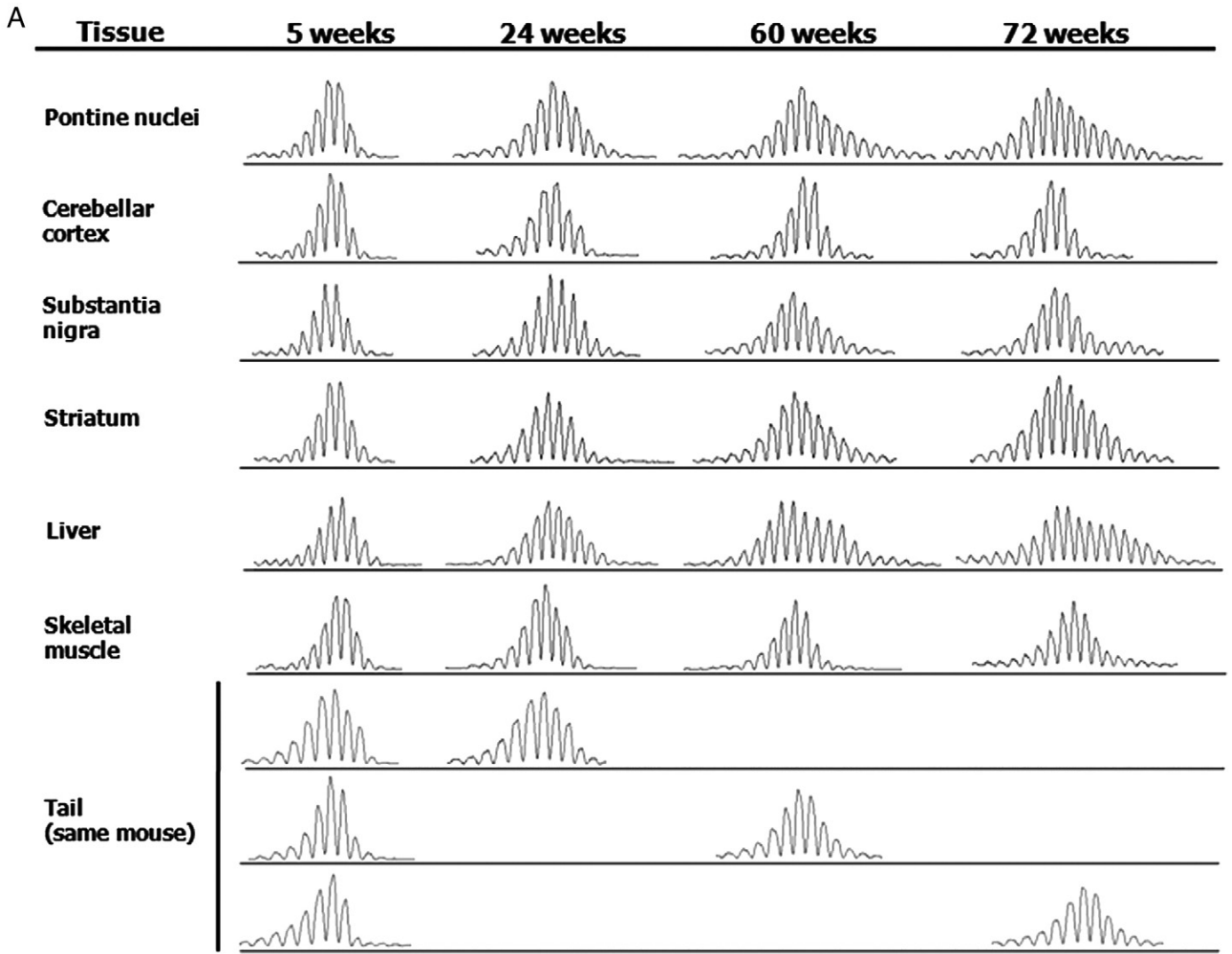
mediators in the CNS, gain neurotoxic properties leading to neuronal death (McGeer and McGeer, 2001, 2002).

Previous results demonstrated that genes associated with inflammation are upregulated in expanded ataxin-3-expressing cell lines and in *post-mortem* MJD brains (Evert et al., 2001). However, the authors discussed the difficulty associated with deciding whether this inflammation is an essential step in the pathogenesis, or whether it is a compensatory response to maintain cellular function and integrity. Moreover, they suggested that it is unlikely that the reported changes represent an early event in the pathophysiology of MJD, because upregulation of pro-inflammatory genes was observed at a time when NIs were already present.

In order to clarify the role of neuroinflammation in the pathogenesis of MJD, we evaluated microglial cell morphology in the cerebellum of wild-type and CMVMJD94 transgenic mice prior to the onset of the disease manifestation (10 weeks), at early (25 weeks) and late stages of disease (109 weeks). We did not find any differences in Iba-1 staining at any studied age between transgenic and control groups (Fig. 9A; Supp. Figure 4A). In agreement, the *Iba-1* expression levels as measured by qRT-PCR in the cerebellum of transgenic animals did not differ from wild-type animals, as expected if microglia cells were activated (Fig. 9B; Supp. Figure 4B). Additionally, the gene expression levels of TNF, interleukin-1 $\beta$  and interleukin-6 did not differ between control and transgenic mice (Fig. 9B; Supp. Figure 4B). Among the additional 84 genes related to the inflammatory response that we analyzed in the cerebella of CMVMJD94 and control mice at 8 and 24 weeks of age, only six were significantly (but very slightly) altered in the transgenic mice: at 8 weeks we observed a downregulation of integrin 1 $\beta$  (0.66 fold change;  $p = 0.026$ ) and at 24 weeks an upregulation of the chemokines Ccl4 (2.31 fold change;  $p = 0.041$ ) and CxCl10 (2.02 fold change;  $p = 0.015$ ) and a downregulation of IL13 receptor  $\alpha 1$  (0.83 fold change;  $p = 0.043$ ), IL10 receptor  $\alpha 1$  (0.73 fold change;  $p = 0.034$ ) and Lymphotoxin B (0.60 fold change;  $p = 0.047$ ) (Supplementary table). The biological relevance of these subtle changes is not clear, but we conclude that an overall pro-inflammatory pattern is not present

**Fig. 8.** Age-dependent somatic mosaicism of the expanded CAG repeat in neuronal and non-neuronal tissues of hemi CMVMJD94 mice. (A) Representative Genescan tract diagrams of the CAG repeat pattern of neuronal and non-neuronal tissues from CMVMJD94 mice at different ages. (B) Differential pattern of the mosaicism index (MI) increase through aging for transgenic CMVMJD94 mice. The average of the MI for at least three mouse samples of each tissue is represented ( $\pm$  SEM). \*Statistical significance  $p < 0.05$ .





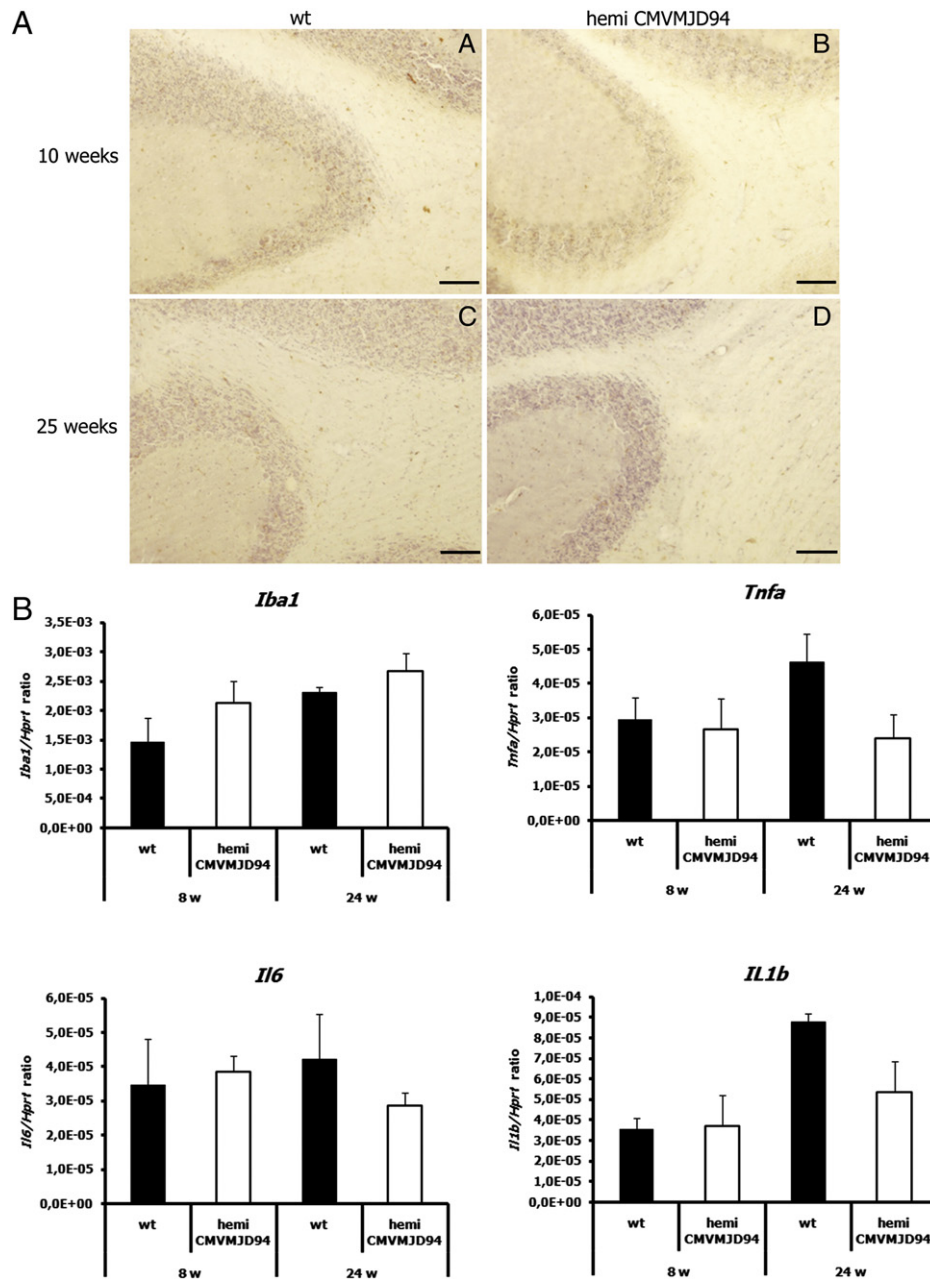


**Fig. 9.** Inflammatory profile of the cerebellum of CMVMJD94 mice. (A) Iba-1 immunostaining in sections of cerebellum of hemi CMVMJD94 mice and wild-type animals at 10 and 25 weeks of age (A–D). Transgenic mice did not exhibit differences in the morphology of microglial cells in the cerebellum when compared to control littermates at asymptomatic and symptomatic ages. Scale bar 100  $\mu$ m. (B) qRT-PCR analysis of mRNA *Iba-1*, *Tnfa*, *Il1b*, *Il6* expression levels in the cerebellum of hemi CMVMJD94 and wild-type mice. All values were normalized for the *Hprt1* gene. wt, wild-type; hemi, hemizygous.

at these early stages in the cerebellum of CMVMJD94 transgenic mice. Our results thus suggest that microglial cells are not primed for activation before the onset of the MJD disease, which implies that the microglial activation observed in *post-mortem* tissues (Evert et al., 2001) could be a consequence rather than a cause of the long neurodegeneration process undergone by human patients.

In summary, this work provides evidence for a dominant CAG length-dependent neurological phenotype in the novel CMVMJD94 transgenic mouse model, in agreement with that observed in human patients. Moreover, we show that this mouse model recapitulates key features of the human disorder: CAG repeat instability, neurological dysfunction and brain pathology. The neuronal dysfunction occurs in the absence of ATXN3 cleavage products, intranuclear inclusions, or any evidence of programmed cell death, necrosis or neuroinflamma-

tion, which might occur at later stages of the disease. We propose that this model is useful for dissecting the initial cellular and molecular events in the pathogenesis of MJD.

#### Acknowledgments

We would like to thank to Dr. Henry Paulson for providing the anti-ataxin-3 serum, Dr. Mónica Sousa for the pCMV vector and to Eng. Lucília Goreti Pinto for technical assistance. A.S-F., M.C.C., S.S. and C.B. received FCT fellowships (SFRH/BD/15910/2005; SFRH/BPD/28560/2006; PTDC/SAU-GMG/64076/2006; SFRH/BPD/20987/2004). This research was funded by Fundação para a Ciência e Tecnologia through projects FEDER/FCT, POCI/SAU-MMO/60412/2004, PTDC/SAU-GMG/64076/2006; and Ataxia MJD Research Project.

## Appendix A. Supplementary data

Supplementary data associated with this article can be found in the online version, at doi:10.1016/j.nbd.2010.05.021.

## References

- Arrasate, M., Mitra, S., Schweitzer, E.S., Segal, M.R., Finkbeiner, S., 2004. Inclusion body formation reduces levels of mutant huntingtin and the risk of neuronal death. *Nature* 431, 805–810.
- Bichelmeier, U., Schmidt, T., Hubener, J., Boy, J., Ruttiger, L., Habig, K., Poths, S., Bonin, M., Knipper, M., Schmidt, W.J., Wilbertz, J., Wolburg, H., Lacccone, F., Riess, O., 2007. Nuclear localization of ataxin-3 is required for the manifestation of symptoms in SCA3: in vivo evidence. *J. Neurosci.* 27, 7418–7428.
- Boy, J., Schmidt, T., Schumann, U., Grasshoff, U., Unser, S., Holzmann, C., Schmitt, I., Karl, T., Lacccone, F., Wolburg, H., Ibrahim, S., Riess, O., 2009a. A transgenic mouse model of Spinocerebellar Ataxia Type 3 resembling late disease onset and gender-specific instability of CAG repeats. *Neurobiol. Dis.* 37, 284–293.
- Boy, J., Schmidt, T., Wolburg, H., Mack, A., Nuber, S., Bottcher, M., Schmitt, I., Holzmann, C., Zimmermann, F., Servadio, A., Riess, O., 2009b. Reversibility of symptoms in a conditional mouse model of Spinocerebellar Ataxia Type 3. *Hum. Mol. Genet.* 18, 4282–4295.
- Cancel, G., Gourfinkel-An, I., Stevanin, G., Didierjean, O., Abbas, N., Hirsch, E., Agid, Y., Brice, A., 1998. Somatic mosaicism of the CAG repeat expansion in spinocerebellar ataxia type 3/Machado–Joseph disease. *Hum. Mutat.* 11, 23–27.
- Carter, R.J., Lione, L.A., Humby, T., Mangiarini, L., Mahal, A., Bates, G.P., Dunnett, S.B., Morton, A.J., 1999. Characterization of progressive motor deficits in mice transgenic for the human Huntington's disease mutation. *J. Neurosci.* 19, 3248–3257.
- Cemal, C.K., Carroll, C.J., Lawrence, L., Lowrie, M.B., Ruddle, P., Al-Mahdawi, S., King, R.H., Pook, M.A., Huxley, C., Chamberlain, S., 2002. YAC transgenic mice carrying pathological alleles of the MJD1 locus exhibit a mild and slowly progressive cerebellar deficit. *Hum. Mol. Genet.* 11, 1075–1094.
- Chou, A.H., Yeh, T.H., Ouyang, P., Chen, Y.L., Chen, S.Y., Wang, H.L., 2008. Polyglutamine-expanded ataxin-3 causes cerebellar dysfunction of SCA3 transgenic mice by inducing transcriptional dysregulation. *Neurobiol. Dis.* 31, 89–101.
- Clark, R.M., De Biase, I., Malykhina, A.P., Al-Mahdawi, S., Pook, M., Bidichandani, S.I., 2007. The GAA triplet-repeat is unstable in the context of the human FXN locus and displays age-dependent expansions in cerebellum and DRG in a transgenic mouse model. *Hum. Genet.* 120, 633–640.
- Costa, M.C., Gomes-da-Silva, J., Miranda, C.J., Sequeiros, J., Santos, M.M., Maciel, P., 2004. Genomic structure, promoter activity, and developmental expression of the mouse homologue of the Machado–Joseph disease (MJD) gene. *Genomics* 84, 361–373.
- Coutinho, P., Andrade, C., 1978. Autosomal dominant system degeneration in Portuguese families of the Azores Islands. A new genetic disorder involving cerebellar, pyramidal, extrapyramidal and spinal cord motor functions. *Neurology* 28, 703–709.
- Evert, B.O., Vogt, I.R., Kindermann, C., Ozimek, L., de Vos, R.A., Brunt, E.R., Schmitt, I., Klockgether, T., Wullner, U., 2001. Inflammatory genes are upregulated in expanded ataxin-3-expressing cell lines and spinocerebellar ataxia type 3 brains. *J. Neurosci.* 21, 5389–5396.
- Ferro, A., Carvalho, A.L., Teixeira-Castro, A., Almeida, C., Tome, R.J., Cortes, L., Rodrigues, A.J., Logarinho, E., Sequeiros, J., Macedo-Ribeiro, S., Maciel, P., 2007. NEDD8: a new ataxin-3 interactor. *Biochim. Biophys. Acta* 1773, 1619–1627.
- Goti, D., Katzen, S.M., Mez, J., Kurtis, N., Kiluk, J., Ben-Haiem, L., Jenkins, N.A., Copeland, N.G., Kalkizuka, A., Sharp, A.H., Ross, C.A., Mouton, P.R., Colomer, V., 2004. A mutant ataxin-3 putative-cleavage fragment in brains of Machado–Joseph disease patients and transgenic mice is cytotoxic above a critical concentration. *J. Neurosci.* 24, 10266–10279.
- Goto, J., Watanabe, M., Ichikawa, Y., Yee, S.B., Ihara, N., Endo, K., Igarashi, S., Takiyama, Y., Gaspar, C., Maciel, P., Tsuji, S., Rouleau, G.A., Kanazawa, I., 1997. Machado–Joseph disease gene products carrying different carboxyl termini. *Neurosci. Res.* 28, 373–377.
- Grewal, R.P., Cancel, G., Leeflang, E.P., Durr, A., McPeck, M.S., Draghinis, D., Yao, X., Stevanin, G., Alnot, M.O., Brice, A., Arnheim, N., 1999. French Machado–Joseph disease patients do not exhibit gametic segregation distortion: a sperm typing analysis. *Hum. Mol. Genet.* 8, 1779–1784.
- Ikeda, H., Yamaguchi, M., Sugai, S., Aze, Y., Narumiya, S., Kakizuka, A., 1996. Expanded polyglutamine in the Machado–Joseph disease protein induces cell death in vitro and in vivo. *Nat. Genet.* 13, 196–202.
- Ikeuchi, T., Igarashi, S., Takiyama, Y., Onodera, O., Oyake, M., Takano, H., Koide, R., Tanaka, H., Tsuji, S., 1996. Non-Mendelian transmission in dentatorubral-pallidolusian atrophy and Machado–Joseph disease: the mutant allele is preferentially transmitted in male meiosis. *Am. J. Hum. Genet.* 58, 730–733.
- Ishiguro, H., Yamada, K., Sawada, H., Nishii, K., Ichino, N., Sawada, M., Kurosawa, Y., Matsushita, N., Kobayashi, K., Goto, J., Hashida, H., Masuda, N., Kanazawa, I., Nagatsu, T., 2001. Age-dependent and tissue-specific CAG repeat instability occurs in mouse knock-in for a mutant Huntington's disease gene. *J. Neurosci. Res.* 65, 289–297.
- Iughetti, P., Otto, P.A., Zatz, M., Passos Bueno, M.R., Marie, S.K., 1998. Different behavior in the paternally vs. maternally inherited mutated allele in Brazilian Machado–Joseph (MJD1) families. *Am. J. Med. Genet.* 77, 246–248.
- Kanda, T., Isozaki, E., Kato, S., Tanabe, H., Oda, M., 1989. Type III Machado–Joseph disease in a Japanese family: a clinicopathological study with special reference to the peripheral nervous system. *Clin. Neuropathol.* 8, 134–141.
- Kawaguchi, Y., Okamoto, T., Taniwaki, M., Aizawa, M., Inoue, M., Katayama, S., Kawakami, H., Nakamura, S., Nishimura, M., Akiguchi, I., 1994. CAG expansions in a novel gene for Machado–Joseph disease at chromosome 14q32.1. *Nat. Genet.* 8, 221–228.
- Klement, I.A., Skinner, P.J., Kaytor, M.D., Yi, H., Hersch, S.M., Clark, H.B., Zoghbi, H.Y., Orr, H.T., 1998. Ataxin-1 nuclear localization and aggregation: role in polyglutamine-induced disease in SCA1 transgenic mice. *Cell* 95, 41–53.
- Li, M., Chevalier-Larsen, E.S., Merry, D.E., Diamond, M.L., 2007. Soluble androgen receptor oligomers underlie pathology in a mouse model of spinobulbar muscular atrophy. *J. Biol. Chem.* 282, 3157–3164.
- Lopes-Cendes, I., Maciel, P., Kish, S., Gaspar, C., Robitaille, Y., Clark, H.B., Koeppe, A.H., Nance, M., Schut, L., Silveira, I., Coutinho, P., Sequeiros, J., Rouleau, G.A., 1996. Somatic mosaicism in the central nervous system in spinocerebellar ataxia type 1 and Machado–Joseph disease. *Ann. Neurol.* 40, 199–206.
- Maciel, P., Gaspar, C., DeStefano, A.L., Silveira, I., Coutinho, P., Radvany, J., Dawson, D.M., Sudarsky, L., Guimaraes, J., Loureiro, J.E., et al., 1995. Correlation between CAG repeat length and clinical features in Machado–Joseph disease. *Am. J. Hum. Genet.* 57, 54–61.
- Maciel, P., Lopes-Cendes, I., Kish, S., Sequeiros, J., Rouleau, G.A., 1997. Mosaicism of the CAG repeat in CNS tissue in relation to age at death in spinocerebellar ataxia type 1 and Machado–Joseph disease patients. *Am. J. Hum. Genet.* 60, 993–996.
- Maciel, P., Costa, M.C., Ferro, A., Rousseau, M., Santos, C.S., Gaspar, C., Barros, J., Rouleau, G.A., Coutinho, P., Sequeiros, J., 2001. Improvement in the molecular diagnosis of Machado–Joseph disease. *Arch. Neurol.* 58, 1821–1827.
- McGeer, P.L., McGeer, E.G., 2001. Inflammation, autotoxicity and Alzheimer disease. *Neurobiol. Aging* 22, 799–809.
- McGeer, P.L., McGeer, E.G., 2002. Inflammatory processes in amyotrophic lateral sclerosis. *Muscle Nerve* 26, 459–470.
- Nicklas, W., Baneux, P., Boot, R., Decelle, T., Deeny, A.A., Fumanelli, M., Illgen-Wilcke, B., 2002. Recommendations for the health monitoring of rodent and rabbit colonies in breeding and experimental units. *Lab Anim.* 36, 20–42.
- Paulson, H.L., Das, S.S., Crino, P.B., Perez, M.K., Patel, S.C., Gotsdiner, D., Fischbeck, K.H., Pittman, R.N., 1997. Machado–Joseph disease gene product is a cytoplasmic protein widely expressed in brain. *Ann. Neurol.* 41, 453–462.
- Rafael, J.A., Nitta, Y., Peters, J., Davies, K.E., 2000. Testing of SHIRPA, a mouse phenotypic assessment protocol, on Dmd(mdx) and Dmd(mdx3cv) dystrophin-deficient mice. *Mamm. Genome* 11, 725–728.
- Reiner, A., Del Mar, N., Deng, Y.P., Meade, C.A., Sun, Z., Goldowitz, D., 2007. R6/2 neurons with intranuclear inclusions survive for prolonged periods in the brains of chimeric mice. *J. Comp. Neurol.* 505, 603–629.
- Riess, O., Epplen, J.T., Amoiridis, G., Przuntek, H., Schols, L., 1997. Transmission distortion of the mutant alleles in spinocerebellar ataxia. *Hum. Genet.* 99, 282–284.
- Rogers, D.C., Fisher, E.M., Brown, S.D., Peters, J., Hunter, A.J., Martin, J.E., 1997. Behavioral and functional analysis of mouse phenotype: SHIRPA, a proposed protocol for comprehensive phenotype assessment. *Mamm. Genome* 8, 711–713.
- Romanul, F.C., Fowler, H.L., Radvany, J., Feldman, R.G., Feingold, M., 1977. Azorean disease of the nervous system. *N Engl J. Med.* 296, 1505–1508.
- Rosenberg, R.N., Nyhan, W.L., Bay, C., 1976. Autosomal dominant striatonigral degeneration: a clinical, pathological, and biochemical study of a new genetic disorder. *Trans. Am. Neurol. Assoc.* 101, 78–80.
- Rub, U., Brunt, E.R., Deller, T., 2008. New insights into the pathoanatomy of spinocerebellar ataxia type 3 (Machado–Joseph disease). *Curr. Opin. Neurol.* 21, 111–116.
- Sato, T., Oyake, M., Nakamura, K., Nakao, K., Fukusima, Y., Onodera, O., Igarashi, S., Takano, H., Kikugawa, K., Ishida, Y., Shimohata, T., Koide, R., Ikeuchi, T., Tanaka, H., Futamura, N., Matsumura, R., Takayanagi, T., Tanaka, F., Sobue, G., Komure, O., Takahashi, M., Sano, A., Ichikawa, Y., Goto, J., Kanazawa, I., et al., 1999. Transgenic mice harboring a full-length human mutant DRPLA gene exhibit age-dependent intergenerational and somatic instabilities of CAG repeats comparable with those in DRPLA patients. *Hum. Mol. Genet.* 8, 99–106.
- Saudou, F., Finkbeiner, S., Devys, D., Greenberg, M.E., 1998. Huntingtin acts in the nucleus to induce apoptosis but death does not correlate with the formation of intranuclear inclusions. *Cell* 95, 55–66.
- Slow, E.J., Graham, R.K., Osmand, A.P., Devon, R.S., Lu, G., Deng, Y., Pearson, J., Vaid, K., Bissada, N., Wetzel, R., Leavitt, B.R., Hayden, M.R., 2005. Absence of behavioral abnormalities and neurodegeneration in vivo despite widespread neuronal huntingtin inclusions. *Proc. Natl. Acad. Sci. U. S. A.* 102, 11402–11407.
- Sobue, G., Doyu, M., Nakao, N., Shimada, N., Mitsuma, T., Maruyama, H., Kawakami, S., Nakamura, S., 1996. Homozygosity for Machado–Joseph disease gene enhances phenotypic severity. *J. Neurol. Neurosurg. Psychiatry* 60, 354–356.
- Streit, W.J., Mrak, R.E., Griffin, W.S., 2004. Microglia and neuroinflammation: a pathological perspective. *J. Neuroinflammation* 1, 14.
- Takiyama, Y., Sakoe, K., Soutome, M., Namekawa, M., Ogawa, T., Nakano, I., Igarashi, S., Oyake, M., Tanaka, H., Tsuji, S., Nishizawa, M., 1997. Single sperm analysis of the CAG repeats in the gene for Machado–Joseph disease (MJD1): evidence for non-Mendelian transmission of the MJD1 gene and for the effect of the intragenic CCG/GGG polymorphism on the intergenerational instability. *Hum. Mol. Genet.* 6, 1063–1068.
- Tanaka, F., Ito, Y., Sobue, G., 1999. Somatic mosaicism of expanded CAG trinucleotide repeat in the neural and nonneural tissues of Machado–Joseph disease (MJD). *Nippon Rinsho* 57, 838–842.
- Telenius, H., Kremer, B., Goldberg, Y.P., Theilmann, J., Andrew, S.E., Zeisler, J., Adam, S., Greenberg, C., Ives, E.J., Clarke, L.A., et al., 1994. Somatic and gonadal mosaicism of the Huntington disease gene CAG repeat in brain and sperm. *Nat. Genet.* 6, 409–414.
- van Alfen, N., Sinke, R.J., Zwarts, M.J., Gabreels-Festen, A., Praamstra, P., Kremer, B.P., Horstink, M.W., 2001. Intermediate CAG repeat lengths (53, 54) for MJD/SCA3 are associated with an abnormal phenotype. *Ann. Neurol.* 49, 805–807.

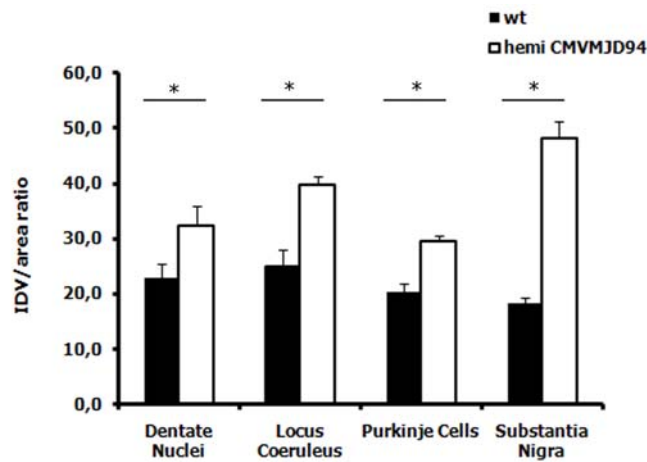


- Wallace, J.E., Krauter, E.E., Campbell, B.A., 1980. Motor and reflexive behavior in the aging rat. *J. Gerontol.* 35, 364–370.
- Wellington, C.L., Ellerby, L.M., Hackam, A.S., Margolis, R.L., Trifiro, M.A., Singaraja, R., McCutcheon, K., Salvesen, G.S., Propp, S.S., Bromm, M., Rowland, K.J., Zhang, T., Rasper, D., Roy, S., Thornberry, N., Pinsky, L., Kakizuka, A., Ross, C.A., Nicholson, D.W., Bredesen, D.E., Hayden, M.R., 1998. Caspase cleavage of gene products associated with triplet expansion disorders generates truncated fragments containing the polyglutamine tract. *J. Biol. Chem.* 273, 9158–9167.
- Williams, L.C., Hegde, M.R., Herrera, G., Stapleton, P.M., Love, D.R., 1999. Comparative semi-automated analysis of (CAG) repeats in the Huntington disease gene: use of internal standards. *Mol. Cell. Probes* 13, 283–289.
- Woods, B.T., Schaumburg, H.H., 1972. Nigro-spino-dentatal degeneration with nuclear ophthalmoplegia. A unique and partially treatable clinico-pathological entity. *J. Neurol. Sci.* 17, 149–166.
- Yamada, M., Tsuji, S., Takahashi, H., 2000. Pathology of CAG repeat diseases. *Neuropathology* 20, 319–325.

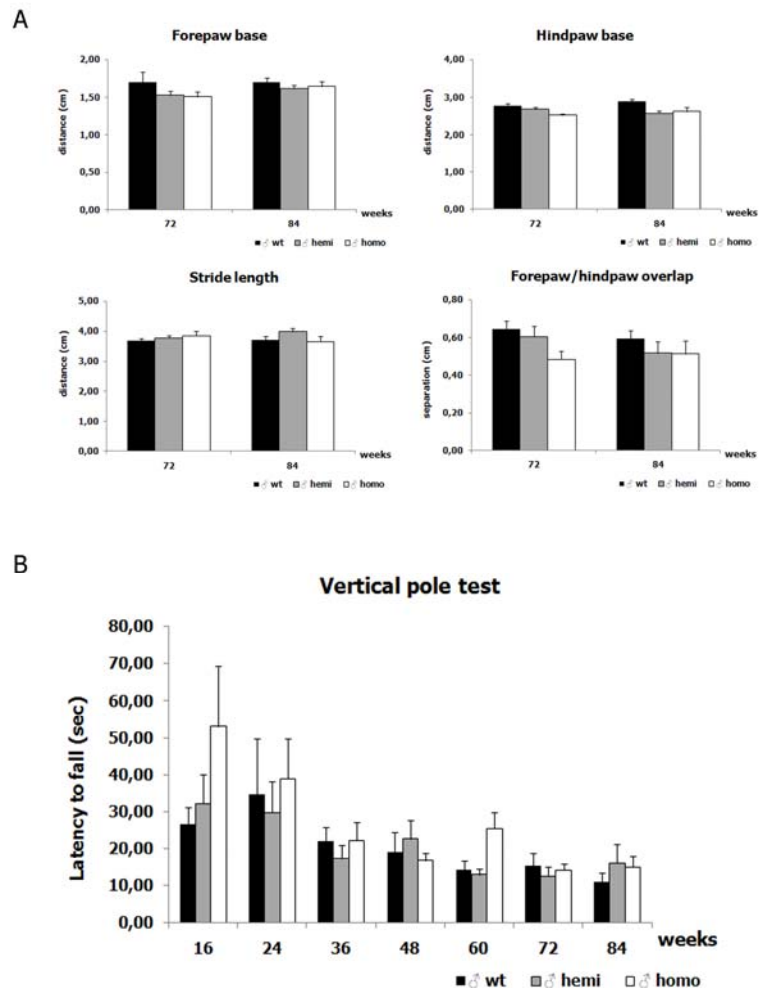
## **Supplementary material**

---

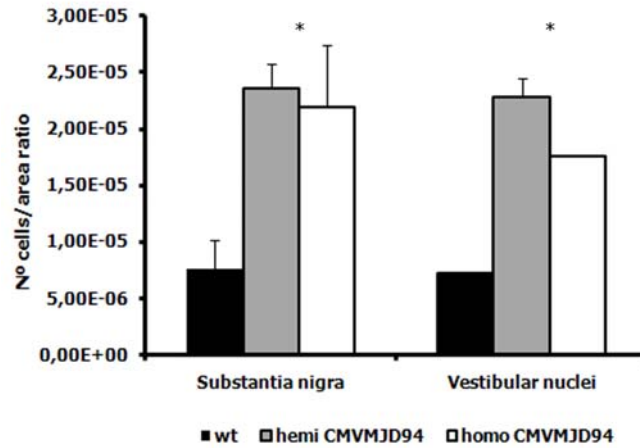




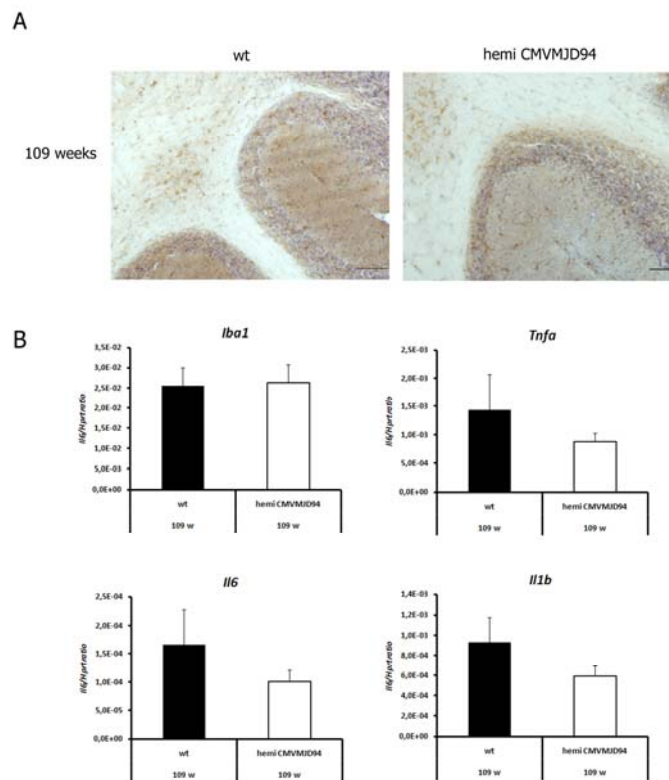
**Supplementary Figure 1.** Increased AT3 expression in CMVMJD mice. Quantification of the expression of ataxin-3 in neurons of different brain regions of hemizygous CMVMJD94 mice in comparison with control animals. (\* statistical significance  $p < 0.05$ ).



**Supplementary Figure 2.** No difference in the gait pattern and limb strength between transgenic and control animals. (A) Analysis of footprinting pattern data from CMVMJD94 mice at 72 and 84 weeks of age. (B) Vertical pole test results in CMVMJD94 mice from 16 to 84 weeks of age.



**Supplementary Figure 3.** Increased GFAP-immunoreactivity in CMVMJD94 mice. Quantification of GFAP-positive cells in the Substantia Nigra and Vestibular Nuclei of CMVMJD94 mice. (\* statistical significance  $p < 0.05$ ).



**Supplementary Figure 4.** Inflammatory profile of the cerebellum of CMVMJD94 mice at late stage. (A) Iba-1 immunostaining in sections of cerebellum of hemi CMVMJD94 mice and wild-type animals at 109 weeks of age. Transgenic mice did not exhibit differences in the morphology of microglial cells in the cerebellum when compared to control littermates. Scale bar 100  $\mu\text{m}$ . (B) qRT-PCR analysis of mRNA *Iba-1*, *Tnfa*, *Il1b*, *Il6* expression levels in the cerebellum of hemi CMVMJD94 and wild-type mice. All values were normalized for the *Hprt1* gene. wt, wild-type; hemi, hemizygous.

| Position | Unigene   | GeneBank  | Symbol  | Description  | Gene Name                   | Age/weeks |           |           |               |               |               | p     | 8 W       |           |           |               |               |               | p     | 24 W      |           |           |               |               |               | p |
|----------|-----------|-----------|---------|--|-----------------------------|-----------|-----------|-----------|---------------|---------------|---------------|-------|-----------|-----------|-----------|---------------|---------------|---------------|-------|-----------|-----------|-----------|---------------|---------------|---------------|---|
|          |           |           |         |  |                             | pool_1 wt | pool_2 wt | pool_3 wt | pool_1 hemi A | pool_2 hemi A | pool_3 hemi A |       | pool_1 wt | pool_2 wt | pool_3 wt | pool_1 hemi A | pool_2 hemi A | pool_3 hemi A |       | pool_1 wt | pool_2 wt | pool_3 wt | pool_1 hemi A | pool_2 hemi A | pool_3 hemi A |   |
| A01      | Mm.329022 | NM_013854 | Ablf1   | ATP-binding cassette, sub-family F (GCN20), member 1 | AU041969/Abc50              | 27,87     | 29,45     | 28,65     | 27,46         | 28,26         | 29,71         | 0,875 | 27,84     | 27,80     | 27,45     | 27,19         | 27,02         | 26,82         | 0,369 |           |           |           |               |               |               |   |
| A02      | Mm.347398 | NM_009744 | Bcl6    | B-cell leukemia/lymphoma 6                           | Bcl5                        | 25,54     | 26,98     | 26,61     | 24,97         | 25,54         | 27,56         | 0,620 | 25,72     | 26,00     | 25,69     | 25,79         | 25,32         | 25,53         | 0,066 |           |           |           |               |               |               |   |
| A03      | Mm.6246   | NM_007551 | Cxcr5   | Chemokine (C-X-C motif) receptor 5                   | Blr1/CXC-R5                 | N/C       | N/C       | N/A       | N/C           | N/C           | N/C           | -     | N/A       | N/C       | N/A       | N/C           | N/C           | N/C           | -     |           |           |           |               |               |               |   |
| A04      | Mm.19131  | NM_009778 | C3      | Complement component 3                               | A1255234/ASP                | 32,01     | N/C       | 31,66     | 31,98         | 32,06         | 33,74         | 0,124 | 32,04     | 31,73     | 31,25     | 31,27         | 30,98         | N/C           | 0,902 |           |           |           |               |               |               |   |
| A05      | Mm.1051   | NM_009807 | Casp1   | Caspase 1  | ICE/II1bc                   | 30,78     | 32,46     | 30,84     | 30,57         | 30,35         | 32,23         | 0,819 | 29,66     | 29,91     | 29,17     | 29,23         | 28,76         | 28,84         | 0,602 |           |           |           |               |               |               |   |
| A06      | Mm.1283   | NM_011329 | Ccl1    | Chemokine (C-C motif) ligand 1                       | BF534335/I-309              | N/A       | N/A       | N/A       | N/A           | N/A           | N/A           | -     | N/A       | N/A       | N/A       | N/A           | N/A           | N/A           | -     |           |           |           |               |               |               |   |
| A07      | Mm.4686   | NM_011330 | Ccl11   | Small chemokine (C-C motif) ligand 11                | Scya11/eotaxin              | N/A       | N/C       | N/C       | N/C           | 37,01         | N/C           | -     | 35,91     | N/C       | N/C       | N/C           | N/C           | 35,67         | N/C   | -         |           |           |               |               |               |   |
| A08      | Mm.867    | NM_011331 | Ccl12   | Chemokine (C-C motif) ligand 12                      | MCP-5/Scya12                | 32,08     | N/C       | 32,56     | 31,78         | 31,41         | 32,93         | 0,349 | 31,65     | 32,08     | N/C       | 30,82         | 31,36         | 30,66         | 0,458 |           |           |           |               |               |               |   |
| A09      | Mm.41988  | NM_011332 | Ccl17   | Chemokine (C-C motif) ligand 17                      | ABCD-2/Scya17               | 34,83     | 34,65     | 34,87     | N/C           | 34,28         | 36,82         | 0,343 | 35,14     | 33,89     | N/C       | N/C           | 33,58         | 33,29         | 0,661 |           |           |           |               |               |               |   |
| A10      | Mm.424740 | NM_011888 | Ccl19   | Chemokine (C-C motif) ligand 19                      | Ckb11/ELC                   | 31,84     | 32,90     | 32,53     | 31,31         | 31,56         | 32,91         | 0,266 | 31,12     | 31,22     | 30,59     | 30,72         | 30,38         | 30,03         | 0,730 |           |           |           |               |               |               |   |
| A11      | Mm.290320 | NM_011333 | Ccl2    | Chemokine (C-C motif) ligand 2                       | A1323594/HC11               | N/C       | N/C       | 35,27     | 35,31         | 34,26         | 34,87         | -     | 33,47     | 34,05     | 33,97     | 33,38         | 33,52         | 33,56         | 0,534 |           |           |           |               |               |               |   |
| A12      | Mm.116739 | NM_016960 | Ccl20   | Chemokine (C-C motif) ligand 20                      | Ckb4/LARC                   | N/A       | N/A       | N/A       | N/A           | 36,63         | 37,85         | -     | N/A       | N/A       | N/A       | N/A           | N/A           | N/C           | -     |           |           |           |               |               |               |   |
| B01      | Mm.12895  | NM_009137 | Ccl22   | Chemokine (C-C motif) ligand 22                      | ABCD-1/DCBCK                | N/C       | N/C       | N/C       | N/C           | 34,91         | N/A           | -     | N/C       | N/A       | N/C       | N/C           | 34,04         | N/C           | -     |           |           |           |               |               |               |   |
| B02      | Mm.31505  | NM_019577 | Ccl24   | Chemokine (C-C motif) ligand 24                      | Ckb-6/MPIF-2                | 33,73     | N/C       | N/C       | 33,42         | 33,28         | 35,05         | -     | 33,93     | N/C       | N/C       | 32,64         | 33,35         | 33,11         | -     |           |           |           |               |               |               |   |
| B03      | Mm.7275   | NM_009138 | Ccl25   | Chemokine (C-C motif) ligand 25                      | A1852536/Ckb15              | 28,93     | 29,41     | 29,15     | 28,64         | 28,84         | 29,64         | 0,989 | 28,90     | 29,09     | 28,88     | 28,32         | 28,37         | 28,58         | 0,883 |           |           |           |               |               |               |   |
| B04      | Mm.1282   | NM_011337 | Ccl3    | Chemokine (C-C motif) ligand 3                       | A1323804/GDS19-1            | N/A       | N/A       | N/A       | N/A           | N/A           | N/A           | -     | N/A       | N/A       | N/A       | N/A           | N/C           | N/A           | -     |           |           |           |               |               |               |   |
| B05      | Mm.244263 | NM_013652 | Ccl4    | Chemokine (C-C motif) ligand 4                       | Act-2/MIP-1B                | 37,61     | 35,65     | 34,77     | 35,30         | 35,75         | 35,65         | 0,905 | 35,23     | 36,50     | 34,89     | 33,66         | 33,59         | 34,18         | 0,041 |           |           |           |               |               |               |   |
| B06      | Mm.284248 | NM_013653 | Ccl5    | Chemokine (C-C motif) ligand 5                       | MuRantes/RANTES             | 32,86     | N/C       | 33,04     | 31,98         | 32,64         | 32,55         | 0,282 | 32,66     | 31,96     | 31,64     | 31,76         | 31,19         | 31,60         | 0,968 |           |           |           |               |               |               |   |
| B07      | Mm.137    | NM_009139 | Ccl6    | Chemokine (C-C motif) ligand 6                       | MRP-1/Scya6                 | N/C       | N/C       | N/C       | N/C           | N/C           | N/C           | -     | N/C       | N/C       | N/C       | N/C           | N/C           | N/C           | -     |           |           |           |               |               |               |   |
| B08      | Mm.341574 | NM_013654 | Ccl7    | Chemokine (C-C motif) ligand 7                       | MCP-3/Scya7                 | 32,05     | 33,45     | 32,78     | 32,69         | 31,75         | 33,00         | 0,718 | 31,99     | 32,22     | 32,07     | 32,00         | 31,98         | 31,35         | 0,618 |           |           |           |               |               |               |   |
| B09      | Mm.42029  | NM_021443 | Ccl8    | Chemokine (C-C motif) ligand 8                       | 1810063B20Rik/AB023418      | 34,56     | N/A       | N/C       | N/C           | 36,80         | 36,09         | -     | 34,84     | N/C       | 32,67     | 33,77         | 33,45         | 33,90         | 0,618 |           |           |           |               |               |               |   |
| B10      | Mm.416125 | NM_011338 | Ccl9    | Chemokine (C-C motif) ligand 9                       | CCF18/MRP-2                 | 32,61     | 33,07     | 32,73     | 31,96         | 32,98         | 33,81         | 0,707 | N/A       | 32,81     | 32,29     | 32,21         | 32,18         | 31,96         | 0,887 |           |           |           |               |               |               |   |
| B11      | Mm.274927 | NM_009912 | Ccl9    | Chemokine (C-C motif) receptor 1                     | Cmkbr1/Mip-1a-R             | N/C       | 33,83     | 32,84     | N/C           | N/C           | N/C           | -     | 32,91     | 32,96     | 32,78     | 32,12         | 31,97         | 31,98         | 0,101 |           |           |           |               |               |               |   |
| B12      | Mm.6272   | NM_009915 | Ccr2    | Chemokine (C-C motif) receptor 2                     | Cc-ckr-2/Ccr2a              | 32,96     | N/C       | N/C       | N/A           | 33,72         | 34,05         | -     | 33,15     | N/C       | N/C       | N/C           | 33,02         | 33,03         | -     |           |           |           |               |               |               |   |
| C01      | Mm.57050  | NM_009914 | Ccr3    | Chemokine (C-C motif) receptor 3                     | CC-CKR3/CKR3                | N/C       | N/C       | 31,87     | 32,33         | 31,88         | 32,71         | -     | 30,96     | 31,20     | 30,60     | 30,82         | 30,65         | 31,03         | 0,059 |           |           |           |               |               |               |   |
| C02      | Mm.1337   | NM_009916 | Ccr4    | Chemokine (C-C motif) receptor 4                     | CHEMR1/Cmkbr4               | N/A       | N/A       | N/C       | 35,68         | N/C           | N/C           | -     | N/A       | N/C       | N/C       | N/C           | N/C           | N/C           | -     |           |           |           |               |               |               |   |
| C03      | Mm.14302  | NM_009917 | Ccr5    | Chemokine (C-C motif) receptor 5                     | AM4-7/CD195                 | 30,71     | 31,82     | 31,11     | 30,94         | 30,98         | 31,91         | 0,371 | 30,26     | 30,46     | 29,75     | 29,42         | 29,51         | 29,52         | 0,527 |           |           |           |               |               |               |   |
| C04      | Mm.8007   | NM_009835 | Ccr6    | Chemokine (C-C motif) receptor 6                     | Cmkbr6                      | N/A       | N/A       | N/A       | N/A           | N/A           | N/A           | -     | N/A       | N/A       | N/A       | N/A           | N/A           | N/A           | -     |           |           |           |               |               |               |   |
| C05      | Mm.2932   | NM_007719 | Ccr7    | Chemokine (C-C motif) receptor 7                     | CD197/Cdw197                | N/A       | N/A       | N/A       | N/A           | N/A           | N/C           | -     | N/A       | N/C       | 35,59     | N/A           | N/A           | N/A           | -     |           |           |           |               |               |               |   |
| C06      | Mm.442098 | NM_007720 | Ccr8    | Chemokine (C-C motif) receptor 8                     | Cmkbr8/mCCR8                | N/A       | N/A       | N/A       | N/C           | N/A           | N/A           | -     | N/A       | N/C       | N/C       | N/A           | N/C           | N/A           | -     |           |           |           |               |               |               |   |
| C07      | Mm.440604 | NM_009913 | Ccr9    | Chemokine (C-C motif) receptor 9                     | Cmkbr10/GPR-9-6             | 32,18     | N/C       | N/C       | 31,64         | 32,14         | 32,82         | -     | 31,34     | 31,69     | N/C       | N/C           | 31,07         | 31,05         | 0,479 |           |           |           |               |               |               |   |
| C08      | Mm.28767  | NM_007768 | Ccrp    | C-reactive protein, pentraxin-related                | A1255847                    | N/C       | N/C       | N/C       | N/C           | N/A           | N/C           | -     | N/A       | N/C       | N/C       | N/C           | N/C           | N/A           | -     |           |           |           |               |               |               |   |
| C09      | Mm.103711 | NM_009142 | Cx3cl1  | Chemokine (C-X3-C motif) ligand 1                    | AB030188/ABCD-3             | 27,11     | 28,67     | 27,90     | 26,77         | 27,28         | 28,99         | 0,833 | 26,77     | 26,90     | 26,68     | 26,43         | 26,19         | 26,68         | 0,217 |           |           |           |               |               |               |   |
| C10      | Mm.21013  | NM_008176 | Cxcl1   | Chemokine (C-X-C motif) ligand 1                     | Fsp/Gro1                    | N/C       | 37,09     | N/C       | 36,38         | 37,84         | N/A           | -     | 34,85     | N/C       | 33,53     | N/C           | 34,16         | 34,70         | 0,423 |           |           |           |               |               |               |   |
| C11      | Mm.877    | NM_021274 | Cxcl10  | Chemokine (C-X-C motif) ligand 10                    | C7/CRG-2                    | 33,03     | N/C       | N/C       | 33,51         | N/A           | 33,67         | -     | 32,78     | 33,22     | 32,27     | 31,18         | 30,93         | 31,55         | 0,015 |           |           |           |               |               |               |   |
| C12      | Mm.131723 | NM_019494 | Cxcl11  | Chemokine (C-X-C motif) ligand 11                    | CXC11/H174                  | 35,12     | N/C       | N/C       | 34,42         | 32,79         | 35,13         | -     | 35,02     | N/C       | N/C       | 32,20         | 34,65         | N/C           | -     |           |           |           |               |               |               |   |
| D01      | Mm.303231 | NM_021704 | Cxcl12  | Chemokine (C-X-C motif) ligand 12                    | A1174028/PBSF               | 27,12     | 27,68     | 27,22     | 26,90         | 26,65         | 28,17         | 0,940 | 26,82     | 26,79     | 26,53     | 26,11         | 26,04         | 26,09         | 0,381 |           |           |           |               |               |               |   |
| D02      | Mm.10116  | NM_018866 | Cxcl13  | Chemokine (C-X-C motif) ligand 13                    | ANGIE2/Angie                | N/A       | N/A       | N/A       | N/A           | 33,86         | N/A           | -     | N/A       | N/A       | N/A       | N/A           | 35,16         | 35,41         | -     |           |           |           |               |               |               |   |
| D03      | Mm.64326  | NM_011339 | Cxcl15  | Chemokine (C-X-C motif) ligand 15                    | Scyb15/lungkine             | N/A       | N/A       | N/A       | N/A           | N/A           | N/A           | -     | N/A       | N/A       | N/A       | N/A           | N/A           | N/A           | -     |           |           |           |               |               |               |   |
| D04      | Mm.332490 | NM_019932 | Pf4     | Platelet factor 4                                    | Cxcl4/Scyb4                 | 30,26     | 31,06     | 30,32     | 29,96         | 29,84         | 30,81         | 0,252 | 30,02     | 30,15     | 30,18     | 29,59         | 29,27         | 29,18         | 0,218 |           |           |           |               |               |               |   |
| D05      | Mm.4660   | NM_009141 | Cxcl5   | Chemokine (C-X-C motif) ligand 5                     | AMCF-1/ENA-78               | N/A       | N/A       | N/A       | N/A           | N/A           | N/A           | -     | N/A       | N/A       | N/A       | N/A           | N/A           | N/A           | -     |           |           |           |               |               |               |   |
| D06      | Mm.766    | NM_008599 | Cxcl9   | Chemokine (C-X-C motif) ligand 9                     | BB139920/CMK                | 36,68     | N/C       | 33,56     | 34,47         | 34,28         | 34,53         | 0,942 | 35,04     | 34,73     | N/C       | 34,19         | 33,58         | 34,11         | 0,080 |           |           |           |               |               |               |   |
| D07      | Mm.12876  | NM_009910 | Cxcr3   | Chemokine (C-X-C motif) receptor 3                   | Cd183/Cmkar3                | N/C       | N/A       | N/C       | N/C           | N/A           | 36,81         | -     | N/C       | N/A       | N/C       | N/C           | 36,06         | N/A           | -     |           |           |           |               |               |               |   |
| D08      | Mm.8021   | NM_007721 | Ccr10   | Chemokine (C-C motif) receptor 10                    | Cmkbr9/Gpr2                 | 31,16     | 32,58     | 32,59     | 31,62         | 31,57         | 33,20         | 0,671 | 30,76     | 31,04     | 30,68     | 30,68         | 30,52         | 30,31         | 0,364 |           |           |           |               |               |               |   |
| D09      | Mm.240327 | NM_008337 | Ifng    | Interferon gamma                                     | IFN-g/IFN-gamma             | N/A       | N/A       | N/A       | N/A           | N/A           | N/A           | -     | N/A       | N/A       | N/A       | N/A           | N/A           | N/A           | -     |           |           |           |               |               |               |   |
| D10      | Mm.874    | NM_010548 | Il10    | Interleukin 10                                       | CSIF/Il-10                  | N/C       | N/A       | N/C       | N/C           | N/C           | N/A           | -     | N/C       | N/A       | N/C       | N/A           | N/A           | N/C           | -     |           |           |           |               |               |               |   |
| D11      | Mm.26658  | NM_008348 | Il10ra  | Interleukin 10 receptor, alpha                       | AW553859/CDw210             | 30,35     | 31,43     | 31,17     | 29,72         | 29,88         | 31,89         | 0,384 | 29,86     | 29,98     | 29,74     | 29,82         | 29,84         | 29,72         | 0,034 |           |           |           |               |               |               |   |
| D12      | Mm.4154   | NM_008349 | Il10rb  | Interleukin 10 receptor, beta                        | 6620401D04Rik/A1528744      | 29,33     | 30,62     | 30,30     | 29,14         | 29,93         | 30,92         | 0,947 | 28,53     | 28,68     | 28,60     | 28,65         | 28,37         | 28,23         | 0,113 |           |           |           |               |               |               |   |
| E01      | Mm.35814  | NM_008350 | Il11    | Interleukin 11                                       | IL-11                       | 33,17     | 33,97     | 34,01     | 33,14         | 33,68         | 34,29         | 0,678 | 33,59     | 32,73     | 32,46     | 32,50         | 31,96         | 32,89         | 0,821 |           |           |           |               |               |               |   |
| E02      | Mm.1284   | NM_008355 | Il13    | Interleukin 13                                       | Il-13                       | N/C       | N/C       | N/A       | N/A           | N/A           | N/A           | -     | N/A       | N/A       | N/A       | N/A           | N/A           | N/A           | -     |           |           |           |               |               |               |   |
| E03      | Mm.24208  | NM_133990 | Il13ra1 | Interleukin 13 receptor, alpha 1                     | A1882074/CD213a1            | 29,44     | 29,90     | 29,88     | 29,23         | 29,18         | 30,37         | 0,837 | 29,84     | 29,53     | 29,54     | 29,60         | 29,10         | 29,47         | 0,043 |           |           |           |               |               |               |   |
| E04      | Mm.4392   | NM_008357 | Il15    | Interleukin 15                                       | A1503618                    | 31,65     | 33,03     | 32,81     | 32,01         | 31,63         | 34,06         | 0,782 | 31,79     | 31,22     | 30,85     | 30,86         | 30,50         | 31,09         | 0,763 |           |           |           |               |               |               |   |
| E05      | Mm.10137  | NM_010551 | Il16    | Interleukin 16                                       | mk1AA4048                   | 26,07     | 27,11     | 26,90     | 25,95         | 26,02         | 27,61         | 0,888 | 26,00     | 26,27     | 25,99     | 25,90         | 25,68         | 25,99         | 0,070 |           |           |           |               |               |               |   |
| E06      | Mm.59313  | NM_019508 | Il17b   | Interleukin 17B                                      | 1110006O16Rik/1700006N07Rik | N/C       | N/A       | N/A       | N/C           | N/C           | N/C           | -     | N/C       | N/C       | N/C       | N/C           | N/C           | N/A           | -     |           |           |           |               |               |               |   |
| E07      | Mm.1410   | NM_008360 | Il18    | Interleukin 18                                       | Igll/Il-18                  | 28,91     | 29,58     | 29,46     | 28,83         | 29,08         | 29,88         | 0,628 | 28,94     | 29,27     | 28,81     | 28,73         | 28,03         | 28,47         | 0,585 |           |           |           |               |               |               |   |
| E08      | Mm.15534  | NM_010554 | Il1a    | Interleukin 1 alpha                                  | Il-1a                       | N/A       | N/A       | N/A       | N/C           | N/C           | N/C           | -     | N/C       | N/C       | N/A       | N/C           | N/C           | N/C           | -     |           |           |           |               |               |               |   |

Supplementary Table. (continued)

| Position | Unigene   | GeneBank  | Symbol   | Description  | Gene Name                   | 8 W       |           |           |               |               |               | p     | 24 W      |           |           |               |               |               | p     |
|----------|-----------|-----------|----------|--|-----------------------------|-----------|-----------|-----------|---------------|---------------|---------------|-------|-----------|-----------|-----------|---------------|---------------|---------------|-------|
|          |           |           |          |  |                             | pool_1 wt | pool_2 wt | pool_3 wt | pool_1 hemi A | pool_2 hemi A | pool_3 hemi A |       | pool_1 wt | pool_2 wt | pool_3 wt | pool_1 hemi A | pool_2 hemi A | pool_3 hemi A |       |
| E09      | Mm.222830 | NM_008361 | Il1b     | Interleukin 1 beta   | IL-1beta/Il-1b              | 35,65     | N/A       | N/C       | 33,86         | N/C           | N/C           | -     | 34,69     | 33,84     | 33,45     | 34,64         | 33,82         | 33,60         | 0,252 |
| E10      | Mm.133095 | NM_019450 | Il1f6    | Interleukin 1 family, member 6                               | Il1f1/IL-1H1                | N/A       | N/A       | N/C       | 33,89         | N/A           | N/C           | -     | N/A       | N/C       | N/A       | N/C           | N/A           | N/A           | -     |
| E11      | Mm.45901  | NM_027163 | Il1f8    | Interleukin 1 family, member 8                               | 231004N20Rik                | N/C       | N/A       | N/A       | N/C           | N/A           | N/C           | -     | N/A       | N/A       | N/C       | N/A           | 35,93         | N/A           | -     |
| E12      | Mm.896    | NM_008362 | Il1r1    | Interleukin 1 receptor, type I                               | CD121a/CD121b               | 29,89     | 30,77     | 30,40     | 30,32         | 29,02         | 30,74         | 0,544 | 29,46     | 29,77     | 29,35     | 29,34         | 29,11         | 29,28         | 0,124 |
| F01      | Mm.1349   | NM_010555 | Il1r2    | Interleukin 1 receptor, type II                              | CD121b/Il1r-2               | N/C       | N/A       | N/C       | N/A           | 32,83         | N/C           | -     | 32,36     | N/C       | N/A       | N/A           | N/A           | N/C           | -     |
| F02      | Mm.103794 | NM_021380 | Il20     | Interleukin 20   | Zcymo10                     | N/A       | N/A       | N/C       | N/C           | N/A           | N/A           | -     | N/A       | N/A       | N/C       | N/A           | N/A           | N/C           | -     |
| F03      | Mm.35287  | NM_008368 | Il2rb    | Interleukin 2 receptor, beta chain                           | CD122/IL-15Rbeta            | 36,13     | N/A       | N/C       | N/C           | N/C           | 35,79         | -     | 36,89     | 34,13     | 34,84     | 34,26         | N/A           | 34,18         | 0,693 |
| F04      | Mm.2923   | NM_013563 | Il2rg    | Interleukin 2 receptor, gamma chain                          | CD132/Il2g[c                | 31,27     | 32,03     | 31,84     | 31,38         | 31,22         | 32,53         | 0,457 | 30,92     | 31,07     | 30,83     | 30,48         | 30,65         | 31,39         | 0,260 |
| F05      | Mm.983    | NM_010556 | Il3      | Interleukin 3  | BPA/Csfm3                   | N/A       | N/A       | N/C       | N/A           | N/A           | N/A           | -     | N/A       | 37,39     | N/A       | N/A           | 36,33         | N/A           | -     |
| F06      | Mm.276360 | NM_021283 | Il4      | Interleukin 4  | IgG1/Il-4                   | N/A       | N/A       | N/A       | N/A           | N/A           | N/A           | -     | N/A       | N/A       | N/A       | N/A           | N/A           | N/A           | -     |
| F07      | Mm.3448   | NM_008370 | Il5ra    | Interleukin 5 receptor, alpha                                | CD125/CDw125                | 36,89     | N/A       | N/A       | N/A           | N/A           | N/A           | -     | N/A       | N/A       | 37,62     | N/A           | N/A           | N/A           | -     |
| F08      | Mm.2856   | NM_010559 | Il6ra    | Interleukin 6 receptor, alpha                                | CD126/IL-6R                 | 30,50     | 32,01     | 32,14     | 30,05         | 30,35         | 32,42         | 0,469 | 29,79     | 30,40     | 29,73     | 29,82         | 29,75         | 30,08         | 0,137 |
| F09      | Mm.4364   | NM_010560 | Il6st    | Interleukin 6 signal transducer                              | 5133400A03Rik/AA389424      | 25,99     | 27,56     | 27,13     | 25,82         | 26,12         | 28,06         | 0,838 | 25,58     | 25,88     | 25,48     | 25,49         | 25,04         | 25,37         | 0,143 |
| F10      | Mm.234466 | NM_009909 | Il8rb    | Interleukin 8 receptor, beta                                 | CD128/CDw128                | 34,02     | N/C       | 34,27     | 36,02         | 35,68         | 34,70         | 0,239 | 35,43     | N/A       | N/A       | N/A           | N/A           | 35,36         | -     |
| F11      | Mm.262106 | NM_008401 | Itgam    | Integrin alpha M   | CD11b/CD118                 | 31,35     | 33,88     | 32,12     | 32,01         | 31,30         | 34,28         | 0,760 | 30,74     | 31,10     | 30,61     | 30,61         | 30,09         | 30,72         | 0,268 |
| F12      | Mm.1137   | NM_008404 | Itgb2    | Integrin beta 2  | 2E6/AI528527                | 32,71     | 33,05     | 32,71     | 32,96         | 32,65         | 34,24         | 0,026 | 31,80     | 31,80     | 31,62     | 31,63         | 31,26         | 32,29         | 0,131 |
| G01      | Mm.87787  | NM_010735 | Lta      | Lymphotoxin A  | LT/LT-[a]                   | N/A       | N/A       | N/A       | 36,79         | N/C           | N/A           | -     | 37,91     | N/A       | N/A       | N/A           | N/A           | N/A           | -     |
| G02      | Mm.1715   | NM_008518 | Ltb      | Lymphotoxin B  | AI662801/LTbeta             | 34,83     | 33,64     | 34,86     | 34,90         | 34,61         | 34,62         | 0,534 | 33,23     | 33,48     | 33,16     | N/C           | 33,53         | 33,29         | 0,047 |
| G03      | Mm.2326   | NM_010798 | Mif      | Macrophage migration inhibitory factor                       | GIF/Glif                    | 23,91     | 24,90     | 24,48     | 23,64         | 23,72         | 24,92         | 0,373 | 23,84     | 23,91     | 23,78     | 23,76         | 23,34         | 23,48         | 0,059 |
| G04      | Mm.235137 | NM_007926 | Scyc1    | Small inducible cytokine subfamily E, member 1               | 9830137A06Rik/AIMP1         | 25,52     | 26,70     | 26,05     | 25,58         | 25,55         | 26,72         | 0,945 | 25,29     | 25,59     | 25,09     | 24,87         | 24,57         | 24,85         | 0,778 |
| G05      | Mm.288474 | NM_009263 | Spp1     | Secreted phosphoprotein 1                                    | AA960535/AI790405           | 27,47     | 28,69     | 28,07     | 27,07         | 27,88         | 28,58         | 0,758 | 27,40     | 27,65     | 26,89     | 26,91         | 26,45         | 26,72         | 0,651 |
| G06      | Mm.248380 | NM_011577 | Tgfb1    | Transforming growth factor, beta 1                           | TGF-beta1/TGFBeta1          | 30,10     | 31,50     | 30,95     | 29,77         | 30,09         | 31,91         | 0,737 | 29,69     | 29,97     | 30,01     | 29,47         | 29,40         | 30,05         | 0,358 |
| G07      | Mm.1293   | NM_013693 | Tnf      | Tumor necrosis factor  | DIF/TNF-alpha               | N/A       | N/A       | N/A       | N/C           | N/A           | N/C           | -     | N/A       | N/A       | N/C       | N/C           | N/A           | N/A           | -     |
| G08      | Mm.1258   | NM_011609 | Tnfrsf1a | Tumor necrosis factor receptor superfamily, member 1a        | CD120a/FFP                  | 29,93     | N/C       | N/C       | 29,10         | 29,55         | 31,52         | -     | 29,38     | 29,36     | 28,93     | 28,93         | 29,03         | 28,81         | 0,350 |
| G09      | Mm.235328 | NM_011610 | Tnfrsf1b | Tumor necrosis factor receptor superfamily, member 1b        | CD120b/TNF-R-II             | 32,67     | N/C       | 31,71     | 31,81         | 31,74         | 33,35         | 0,773 | 31,09     | 31,49     | 31,34     | 30,76         | 31,18         | 31,34         | 0,430 |
| G10      | Mm.4861   | NM_011616 | Cd40lg   | CD40 ligand  | CD154/Cd40l                 | N/A       | N/A       | N/A       | N/A           | N/A           | N/A           | -     | N/A       | N/A       | N/A       | N/A           | N/A           | N/A           | -     |
| G11      | Mm.103551 | NM_023764 | Tollip   | Toll interacting protein                                     | 4930403G24Rik/4931428G15Rik | 27,00     | 28,46     | 27,63     | 26,36         | 26,68         | 28,73         | 0,498 | 26,76     | 26,87     | 26,64     | 26,36         | 26,19         | 26,47         | 0,366 |
| G12      | Mm.390241 | NM_011798 | Xcr1     | Chemokine (C motif) receptor 1                               | Cxcr1/GPRS                  | N/C       | N/A       | N/A       | 36,11         | N/A           | N/A           | -     | N/A       | N/A       | N/C       | N/A           | N/A           | 33,84         | -     |
| H01      | Mm.3317   | NM_010368 | Gusb     | Glucuronidase, beta  | A1747421/Gur                | 29,61     | 31,56     | 31,05     | 29,52         | 29,80         | 31,32         | -     | 28,86     | 29,31     | 28,90     | 28,99         | 28,63         | 28,78         | -     |
| H02      | Mm.299381 | NM_013556 | Hprt1    | Hypoxanthine guanine phosphoribosyl transferase 1            | C81579/HPGRT                | 23,19     | 23,60     | 23,42     | 23,01         | 22,92         | 23,90         | -     | 23,04     | 23,02     | 22,84     | 22,64         | 22,17         | 22,53         | -     |
| H03      | Mm.2180   | NM_008302 | Hsp90ab1 | Heat shock protein 90kDa alpha (cytosolic), class B member 1 | 90kDa/AL022974              | 22,24     | 23,36     | 22,98     | 21,88         | 22,05         | 23,54         | -     | 22,58     | 22,62     | 22,18     | 22,14         | 21,70         | 21,89         | -     |
| H04      | Mm.343110 | NM_008084 | Gapdh    | Glyceraldehyde-3-phosphate dehydrogenase                     | Gapd                        | 20,39     | 21,78     | 21,00     | 20,08         | 19,95         | 21,41         | -     | 20,20     | 20,17     | 19,99     | 20,01         | 19,58         | 19,84         | -     |
| H05      | Mm.328431 | NM_007393 | Actb     | Actin, beta, cytoplasmic                                     | Actb/E430023M04Rik          | 21,87     | 23,13     | 22,75     | 21,31         | 21,43         | 23,16         | -     | 21,76     | 21,82     | 21,50     | 21,40         | 21,06         | 21,43         | -     |
| H06      | N/A       | SA_00106  | MGDC     | Mouse Genomic DNA Contamination                              | MIGX1B                      | N/A       | N/A       | N/A       | N/A           | N/A           | N/A           | -     | N/A       | N/A       | N/A       | N/A           | N/A           | N/A           | -     |
| H07      | N/A       | SA_00104  | RTC      | Reverse Transcription Control                                | RTC                         | 22,79     | 23,69     | 23,31     | 23,00         | 22,69         | 23,58         | -     | 22,65     | 22,67     | 22,60     | 22,48         | 22,37         | 22,66         | -     |
| H08      | N/A       | SA_00104  | RTC      | Reverse Transcription Control                                | RTC                         | 22,87     | 23,76     | 23,65     | 22,86         | 22,74         | 23,78         | -     | 22,66     | 22,79     | 22,65     | 22,66         | 22,40         | 22,84         | -     |
| H09      | N/A       | SA_00104  | RTC      | Reverse Transcription Control                                | RTC                         | 23,02     | 23,86     | 23,66     | 23,16         | 23,07         | 24,31         | -     | 22,85     | 23,01     | 22,92     | 22,75         | 22,66         | 22,86         | -     |
| H10      | N/A       | SA_00103  | PPC      | Positive PCR Control   | PPC                         | 20,38     | 20,04     | 20,58     | 20,76         | 19,99         | 20,55         | -     | 19,84     | 20,32     | 20,20     | 19,98         | 20,05         | 19,77         | -     |
| H11      | N/A       | SA_00103  | PPC      | Positive PCR Control   | PPC                         | 20,34     | 20,23     | 20,12     | 20,69         | 19,72         | 20,62         | -     | 19,75     | 20,15     | 20,13     | 19,76         | 19,69         | 19,83         | -     |
| H12      | N/A       | SA_00103  | PPC      | Positive PCR Control   | PPC                         | 20,62     | 20,16     | 20,22     | 21,00         | 20,02         | 20,62         | -     | 20,06     | 20,35     | 20,36     | 19,92         | 19,91         | 19,94         | -     |

N/C Not considered due to insufficient melting curve quality  
N/A Not amplifiable  
- Insufficient data to perform statistical analysis

**Supplementary Table.** Gene expression profile of the cerebellum of CMVMJD94 transgenic mice in comparison with control animals at 8 and 24 weeks of age using the Mouse Inflammatory Cytokines & Receptors RT2 Profiler™ PCR Array (SABioscience).

## **Chapter 3**

---

Behavioral and pathological analysis of a novel transgenic mouse model of Machado-Joseph disease expressing full-length ataxin-3 with 135 CAGs





**Behavioral and pathological analysis of a novel transgenic mouse model of Machado-Joseph disease expressing full-length ataxin-3 with 135 CAGs**

Silva-Fernandes A<sup>1</sup>, Duarte-Silva S<sup>1</sup>, Carvalho A<sup>1</sup>, Oliveira P<sup>2</sup>, Maciel P<sup>1</sup>

<sup>1</sup>Life and Health Sciences Research Institute (ICVS), School of Health Sciences, University of Minho, Campus Gualtar, 4710-057 Braga, Portugal; <sup>2</sup>Department of Neurology, Hospital Prof. Fernando Fonseca, E.P.E., Amadora, Portugal.

<sup>2</sup>Department of Production and Systems Engineering, School of Engineering, University of Minho, Braga, Portugal

Corresponding author: Patrícia Maciel. Life and Health Sciences Research Institute (ICVS), School of Health Sciences, University of Minho, Campus Gualtar, 4710-057 Braga, Portugal.

Telephone: 351-253-604824, Fax: 351-253-604820. E-mail: [pmaciel@ecsaude.uminho.pt](mailto:pmaciel@ecsaude.uminho.pt)

#### **Abstract**

Machado-Joseph disease (MJD), also known as spinocerebellar ataxia type 3 (SCA3) is a polyglutamine (polyQ) disorder caused by a CAG/polyQ tract expansion in the ataxin-3 gene. Our previous results in the CMVMJD94 mice have shown that animals with a range of 91-99 glutamines developed a mild phenotype correlated with the CAG number. In order to establish an animal model with more severe symptoms we have generated a transgenic mouse expressing ataxin-3 with 135 glutamines under the control of the CMV (cytomegalovirus) promoter. CMVMJD135 mice manifest MJD-like motor symptoms beginning at two months, when they present a loss of limb strength, given by a significant decrease in the time in the hanging-wire-grip and in the vertical pole test. At 3 months of age animals developed a balance deficit in the beam test and at 4-5 months of age they displayed motor uncoordination in the Rotarod, in addition to tremors and limb claspings. At this age the gait analysis demonstrated that transgenic animals exhibited foot dragging and at more advanced ages (7 months) an enlargement of the base width and a shorted step. Locomotor and exploratory activity was decreased in transgenic mice at this stage. During the gradual appearance of disease symptoms (at approximately 16 weeks of age) it becomes easy to identify transgenic mice visually due to the abnormal gait, however they do not die prematurely. Pathologic evaluation of CMVMJD135 brains revealed the presence of intranuclear inclusions positive for ataxin-3 and ubiquitin in several brain regions, including the pontine nuclei, lateral reticular nuclei and deep cerebellar nuclei. Our results demonstrate that this animal model presents many phenotypic and pathological features of MJD that could be of great value as objective and quantifiable traits/biomarkers in therapeutic trials.

**Introduction**

Machado-Joseph disease (MJD) belongs to the group of polyQ diseases, that includes SCA1, 2, 6, 7, and 17, dentatorubro-pallidoluysian atrophy (DRPLA), spinobulbar muscular atrophy (SBMA), and Huntington's disease (HD). MJD is caused by a CAG repeat expansion in the protein coding region of the *ATXN3* gene, located in chromosome 14q32.1. CAG tract length ranges between 55-86 in the case of MJD patients and between 12-41 in normal populations (Maciel et al., 2001).

Ataxin-3 harboring the expanded polyQ tract has a strong tendency for aggregation leading to the formation of inclusions in the nucleus and cytoplasm of neuronal cells, including axonal tracts (Paulson et al., 1997; Rub et al., 2006). Interestingly, while ataxin-3 is ubiquitously expressed throughout the brain, specific regions of the CNS are markedly affected in the disease, namely the pontine nuclei, the dentate nucleus, the pallidum, and the spinal cord (Schmidt et al., 1998). The main clinical feature of MJD is ataxia, frequently associated to peripheral neuropathy and distal muscular atrophy in the case of patients with later onset (Coutinho and Andrade, 1978). Due to the highly heterogeneous phenotype of MJD patients, it was necessary to differentiate several clinical subtypes (Paulson, 2007). The most important factor responsible for this wide clinical variability is the diversity of repeat lengths resulting from the genetic instability, a dynamic feature of the CAG repeat expansion.

Although several transgenic mouse models have been generated for the study of MJD (Ikeda et al., 1996; Cemal et al., 2002; Goti et al., 2004; Bichelmeier et al., 2007; Chou et al., 2008; Boy et al., 2009; Boy et al., 2010) it has been difficult to find in one single model the main features of this disorder. For instance, in the first model described, the expression of the full-length ataxin-3 in Purkinje cells (neurons poorly affected in MJD) did not lead to MJD symptoms, whereas the expression of a portion of the mutant ataxin-3 isoform induced neurodegeneration and ataxic behavior (Ikeda et al., 1996). A YAC mouse model expressing the expanded ataxin-3 gene under the regulation of its own promoter demonstrated a mild phenotype and the presence of inclusions and astrogliosis (Cemal et al., 2002). A cDNA transgenic mouse model has been obtained using the PrP promoter (strong brain expression) which only manifested disease in homozygous animals (Goti et al., 2004), not resembling the autosomal dominant mode of transmission of MJD. More recently, a transgenic mouse has been created carrying a CAG repeat tract not observed so far in humans (148Q) that caused a severe phenotype starting at 2 months of age, with a very fast progression and

### **Chapter 3. CMVMJD135 mice**

premature death after one month, which might also not be reflective of MJD (Bichelmeier et al., 2007).

We have previously generated a mouse model of MJD (CMVMJD94) (Silva-Fernandes et al., 2010) that developed a mild motor phenotype (without significant disease progression over time) which was correlated with the CAG repeat tract length (91 to 99 CAGs) in the absence of nuclear inclusions. The principal pathological signs observed in this mouse were the presence of atrophic neurons and astrogliosis. No cell death (apoptosis and necrosis) was observed in the brains of CMVMJD94 mice and no inflammatory response was present. In this manner, this transgenic mouse could be important to study the initial events in the pathogenesis of MJD, but it became crucial to generate a mouse model with more marked signs of the disease, that could be assessed as endpoints for therapeutic trial purposes. With our previous results in mind, we thought it would be necessary to increase the number of CAG repeats, in order to intensify and accelerate the progression of the MJD pathology in a mouse model. We generated a transgenic animal expressing AT3 with 135 glutamines under the control of the CMV promoter. These mice did not die prematurely but showed a progressive phenotype starting at the age of 8 weeks that gradually became more severe, including a coordination deficit, gait ataxia, loss of muscle strength, and decreased locomotor and exploratory activity. CMVMJD135 transgenic mice also display ataxin-3- and ubiquitin-positive neuronal inclusions in different regions of the brain including the pontine nuclei, lateral reticular nuclei and deep cerebellar nuclei.

**Methods*****Generation of transgenic mice***

To generate transgenic MJD mice, we converted the ATXN3a cDNA variant carrying 130 CAGs (plasmid pEGFP-N1-130Q-kindly, provided by Dr Nukina) in the ATXN3c variant. 5' and 3' flanking NotI restriction sites were introduced by PCR, and then the PCR product was digested and cloned into the pCMV vector (kindly provided by Dr Mónica Sousa, Univ. Porto). This plasmid, designated as pCMVAT3Q135\_1.5, was linearized by total digestion with PaeI (Fermentas), the fragment of interest (3150 bp) was then purified from an agarose gel using the QiaQuick gel extraction system (Qiagen, Hamburg, Germany) and microinjected into fertilized murine oocytes of the C57Bl/6 mouse strain (QTRN, Canada). Four founders were obtained: pCMVAT3Q135\_1.5\_C, \_D, \_E, \_F but only lineage C (which we will refer as CMVMJD135) has revealed expression of the mutant protein (Figure 1B) and was used for further studies.

All animal procedures were conducted in accordance with European regulations (European Union Directive 86/609/EEC). Health monitoring was performed according to FELASA guidelines (Nicklas et al., 2002), confirming the Specified Pathogen Free health status of sentinel animals maintained in the same animal room.

***Genotyping and CAG repeat sizing***

DNA from mouse tail biopsy was isolated using a Puregene Kit (Citogene). Animal genotyping was performed by PCR as previously described (Silva-Fernandes et al., 2010).

To determine the CAG repeat number the repeat tract (CAG)<sub>2</sub>CAAAAGCAGCAA(CAG)<sub>X</sub> and a 75-bp flanking region of the ATXN3 gene were amplified by PCR using the primer MJD25a (5'-GGCTGGCCTTTCACATGGAT-3') and a 6-FAM fluorescently-labeled MJDcDNA primer (5'-CGGAAGAGACGAGAAGCCTAC-3'). Products were displayed in an ABI 310 automated DNA sequencer (Applied Biosystems, Foster City, CA). The CAG tract length of the major size band (higher height) was determined by comparison with the fragment size obtained from the clone pCMVAT3Q135\_1.5 carrying 135 repeats sequenced.

***Transgene expression analysis***

Anesthetized animals (n=4) were euthanized by transcardial perfusion with PBS. Brainstem, cerebellum and forebrain from left and right hemisphere were separately collected, frozen in dry ice

### **Chapter 3. CMVMJD135 mice**

and stored at -80°C. For protein isolation, brainstem, cerebellum and forebrain (right hemisphere) were homogenized in 5 volumes of cold resuspension buffer (RB): 0.1 M Tris-HCl, pH 7.5, 0.1 M EDTA, 0.4 mM PMSF and a mixture of protease inhibitors (Roche, Indianapolis, IN). Protein concentrations were determined using the Bradford protein assay (Bio-Rad, Hercules, CA, USA), and samples were diluted in RB and Laemmli sample buffer at a final concentration of 3,3 mg/ml. Samples were sonicated for 10 sec, heated for 3 min at 100°C and centrifuged for 10 sec before loading 30 µl per sample in 10% SDS-PAGE minigels. The blots were blocked in 5% dry milk/ PBS before incubation overnight at 4°C with the primary antibody: serum anti-ataxin-3 (kindly provided by Dr. Henry Paulson) (1:10000). Bound primary antibody were visualized with goat anti-rabbit HRP-conjugated secondary antibodies at 1:10000 (Santa Cruz), chemiluminescent substrate (PIERCE), and exposure on autoradiography films (Amersham, Uppsala, Sweden). Signal bands were quantified using the ImageJ Software.

Total RNA from CMVMJD135 mice (n=4) brainstem, cerebellum and forebrain tissue (left hemisphere) was isolated using TRIZOL (Invitrogen, Calrsbad, CA, USA) according to the manufacturer's protocol. First-strand cDNA, synthesized using oligo-dT (Bio-rad), was amplified by quantitative reverse-transcriptase PCR (qRT-PCR) using primers in the 3'UTR region to detect specifically human and mouse ataxin-3 mRNA (MJD\_UTR1b\_r: 5'GCCCTAACTTTAGACATGTTAC3'; MJD\_UTR3\_F: 5'GGAACAATGCGTCGGTTG3'; mjd\_3UTR\_2r: 5'GTTACAAGAACAGAGCTGACT3'; mjd\_3UTR\_1f: 5'TGTCTTGTTACAGAAAGATCAG3'). Primer specificity was controlled by two negative PCR reaction controls: one with the primers for mouse ataxin-3 mRNA using the pCMVMJD1-1E plasmid (carrying the human cDNA) as template; and the other with the primers for human ataxin-3 mRNA and a total cDNA template from a wild-type mouse.

#### ***Phenotype analysis***

Behavioral analysis was performed during the diurnal period in groups of 5 animals per cage of CMVMJD135 hemizygous transgenic mice and wild-type littermates (n=11-15 per genotype and gender). Animals were evaluated monthly in the Rotarod (beginning at 4 weeks of age), by the modified SHIRPA protocol (at 7 and 19 weeks of age), using the balance beam test (at 10 weeks of age) and the motor swimming test (between 22-25 weeks of age. Rotarod tests were performed as previously described (Silva-Fernandes et al., 2010) as well as the SHIRPA protocol with the addition of the hanging wire grip test.

### **Hanging wire grip test**

Each mouse was placed on a wire cage top, which was slowly inverted and suspended at approximately 30 cm to the floor. The time it took each mouse to fall from the cage top was recorded. Any mouse still gripping the cage top after 60 seconds was removed.

### **Balance Beam test**

Motor coordination and balance of mice were assessed by measuring the ability of the mice to traverse a graded series of narrow beams to reach an enclosed safety platform (Carter et al., 1999). The beams consisted of long strips of PVC (1 m) with a 27- and 11-square cross-section or a 28, 15, or 10 mm round diameter. During training, mice were placed at the start of the 11-mm square beam and trained over 3 d (4 trials per day) to traverse the beam to the enclosed box. Once the mice were trained (traversed the 11-mm square beam in less than 20 sec) they received two consecutive trials on each of the square beams and each of the round beams, in each case progressing from the widest to the narrowest beam. Mice were allowed up to 60 sec to traverse each beam. The latency to traverse each beam and the number of times the hind feet slipped off each beam were recorded for each trial. Analysis of each measure was based on the mean scores of the two trials for each beam.

### **Motor Swimming test**

To monitor swimming movements, mice were trained for 3 days to swim from one end of a water-filled glass tank to a visible escape platform at the opposite end (Carter et al., 1999). After training, mice were given two trials per day for 3 consecutive days. Mice were videotaped from both sides, and the number of forelimb kicks, the number of hindlimb kicks, and the latency to swim the 60 cm distance was recorded. Analysis was based on the mean scores of the two trials for each measure.

### ***Immunohistochemistry***

Transgenic and control non-transgenic littermate mice (n=4 for each group) with approximately 24 weeks of age were deeply anaesthetized and transcardially perfused with PBS followed by 4% paraformaldehyde (PFA) in PBS. Brains were postfixed overnight in fixative solution and embedded in paraffin. Slides with 4- $\mu$ m-thick paraffin sections were steamed for antigen retrieval and then incubated with rabbit GFAP antibody (DAKO Corporation, Carpinteria, CA) (1:500) or rabbit anti-MJD1.1 (Ferro et al., 2007) (1:40) or anti-ubiquitin (1:500). A biotinylated secondary antibody was



### **Chapter 3. CMVMJD135 mice**

applied, followed by ABC coupled to horseradish peroxidase (DAKO) and DAB substrate (Vector Laboratories Inc., Burlingame, CA, USA). The slides were counterstained with hematoxylin according to standard procedures and analyzed with an optical microscope (Olympus, Hamburg, Germany). For morphological brain analysis, we performed hematoxylin & eosin and cresyl violet staining. Apoptosis was analyzed using the TUNEL assay using the Apoptag Peroxidase In situ Apoptosis Detection Kit (Chemicon International, USA) according to the manufacturer's instructions. Mice were deeply anaesthetized, transcardially perfused with PBS and brains were removed and frozen at -80°C embedded in OCT. Frozen brain sections (10 µm) of transgenic CMVMJD135 and wild-type mice (n=3 for each genotype) with 24 weeks of age, were fixed in 1% PFA/ PBS for 30 min and post-fixed in pre-cooled ethanol:acetic acid (2:1) at -20°C for 5 min. Endogenous peroxidase was inactivated by immersing the tissue sections in 3% H<sub>2</sub>O<sub>2</sub> in PBS solution for 30 min and rinsing several times with water and PBS.

#### **Statistical analysis**

Behavioral data were subjected to the non-parametric Mann-Whitney U-test when variables were non-continuous or when a continuous variable did not present a normal distribution (Kolmogorov-Smirnov test  $p < 0.05$ ). Continuous variables with normal distributions (K-S test  $p > 0.05$ ) were analyzed with the Student's t test or Repeated-Measures ANOVA. All statistical analyses were performed using SPSS 16.0 (SPSS Inc., Chicago, IL). A critical value for significance of  $p < 0.05$  was used throughout the study.

## Results

### Generation of MJD transgenic mice

We have generated a transgenic mouse model of MJD expressing the ATXN3c cDNA variant of the *ATXN3* gene carrying a repeat tract  $(CAG)_2CAAAGCAGCAA(CAG)_{129}$ , coding for 135 glutamines, under the regulation of the CMV promoter. From the microinjection of the transgene four founders were obtained, giving rise to lineages C, D, E and F. PCR amplification of the transgene from founder tail DNA revealed that transgenic mice from lineage F possessed a deletion in the CMV promoter region.

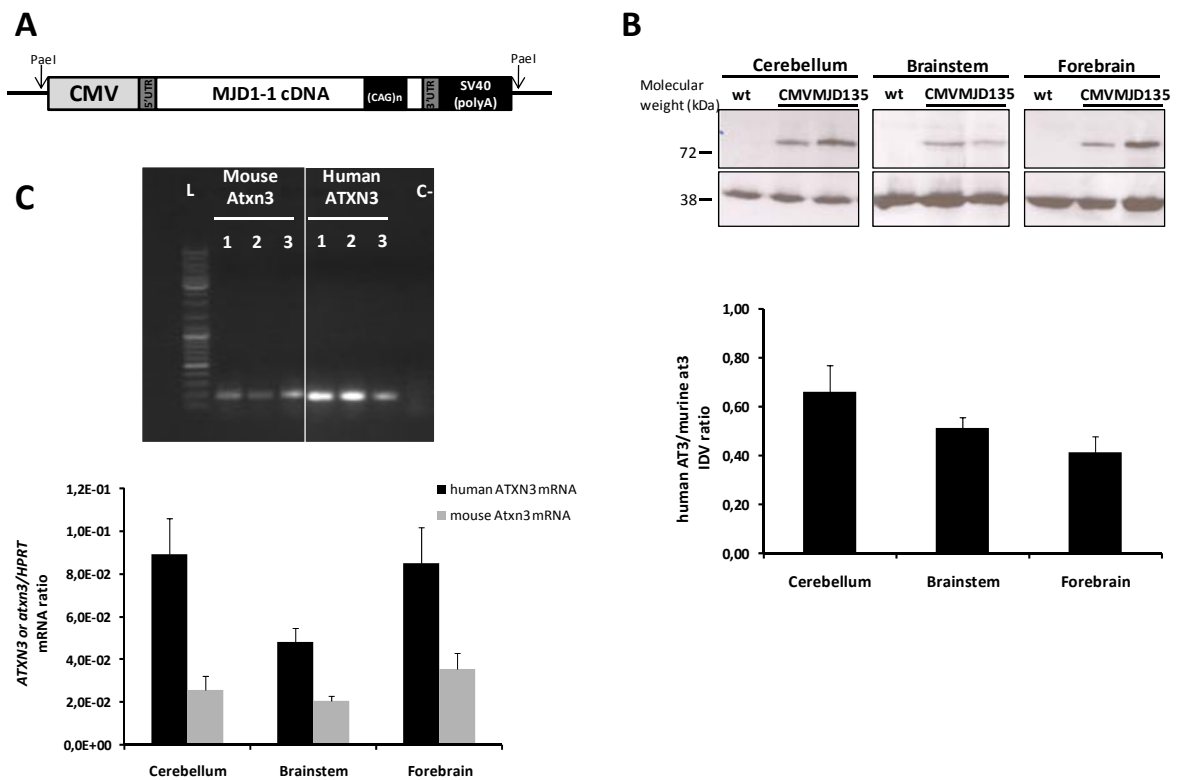


**Figure 1.** Generation of a transgenic mouse model of MJD carrying the expanded AT3 with 135 CAGs. (A) Schematic diagram of the plasmid CMVMJDAT3Q135\_1.5 used for the generation of cDNA MJD transgenic mice. (B) Western blot anti-ATXN3 in different CNS regions (cerebellum, forebrain and brainstem) of CMVMJD135 mice with approximately 16 weeks of age. In all lanes, the endogenous mouse ataxin-3 (Atxn3) is detected at about 42 kDa. An approximately 80-kDa protein corresponding to expanded ATXN3 is detected in transgenic animal lysates. (C) qRT-PCR analysis of human ATXN3 and murine Atxn3 mRNA expression levels. Vertical bars represent mean  $\pm$  SEM. L, Ladder 100 bp; C-, negative control; 1-3, cDNA transgenic mouse samples amplified by qRT-PCR.

### Chapter 3. CMVMJD135 mice

Transgene transmission was not observed in the progeny of founder D. The evaluation of the expression of human mRNA ataxin-3 in the brain of MJD transgenic mice by qRT-PCR demonstrated that only lineage C (hereafter designated CMVMJD135) expressed the human ATXN3 mRNA. Indeed, we observed higher expression levels of human ATXN3 mRNA than of the endogenous murine *Atxn3* in the cerebellum, brainstem and forebrain. Human expanded ATXN3 protein was detected in this lineage by western blot at approximately 80 kDa of molecular weight, the cerebellum being the region with the highest levels of expanded ataxin-3 (Figure 1).

To investigate whether MJD transgenic mice, like human patients, displayed intergenerational instability of the expanded triplet repeat, we determined the (CAG)<sub>n</sub> tract length variation in maternal and paternal meioses of transgenic CMVMJD135 animals. For this purpose, we analysed the CAG tract length of litters obtained by breeding hemizygous CMVMJD135 males or females with a wild-type animal. For both maternal and paternal meioses we observed that CAG repeat length displayed variation between the progenitor and the offspring, mostly towards contraction (maternal meioses (n=6): mean= -3,33±2,42; range=[-7, 0]; paternal meioses (n=28): mean= -2,14±1,74; range=[-6, 0]) (Figure 2).

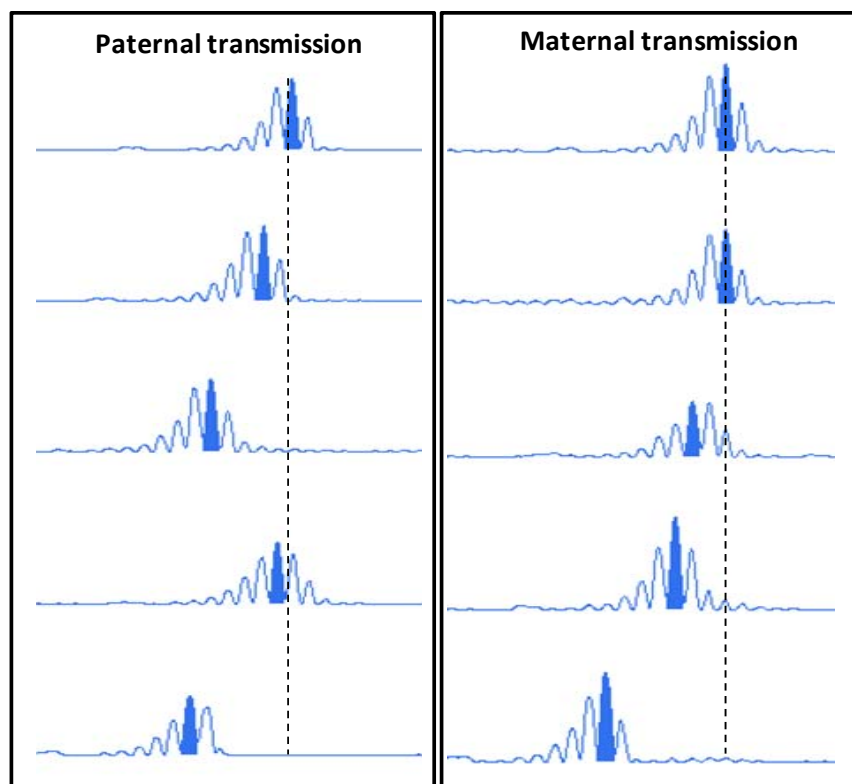


**Figure 2.** Representative genescan tract diagrams showing the variation of the CAG repeat tract in maternal and paternal meioses of CMVMJD135 mice.

### Behavioral deficits in CMVMJD135 transgenic mice: onset and progression

In order to perform the phenotypic characterization of this transgenic animal model we have performed a global evaluation of the animals using the SHIRPA protocol at 7 and 19 weeks of age, that we enriched with more specific tests to assess motor deficits. Since 4 weeks of age we submitted the animals to the Rotarod test monthly, until 20 weeks of age. Body balance was evaluated by the balance beam test at 10 weeks, and the motor swimming test was performed at 22-25 weeks of age (protocol summarized in Figure 3). In parallel, we have analysed other transgenic and wild-type groups for therapeutic trials (see chapter 4) and their behavior was also evaluated. In order to reinforce and give more detail about the beginning of the motor deficits we included some behavioral results of the placebo groups of this parallel therapeutic trial as supplementary material to the current chapter. In this set of experiments wild-type (n=12) and CMVMJD135 (n=10) mice males were injected with a placebo solution (0.15 M NaCl, 5% Tween-20 and 5% PEG 400) three times per week from 5 to 24 weeks of age, except for one week per month, in which animal behavior was evaluated in the Rotarod test and SHIRPA protocol.

#### General health

At 4 weeks of age, transgenic and control littermates were indistinguishable in their home cage; however, at 16 weeks of age transgenic animals clearly showed difficult to walk and an unhealthy look. Concerning growth, both wild-type and CMVMJD135 mice placebo groups showed a similar increase in body weight until around 12 weeks of age, at which point the body weight of the CMVMJD135 mice started to stabilize, while control animals continued to gain weight ( $p=0,009$ ) (supplementary figure 1).

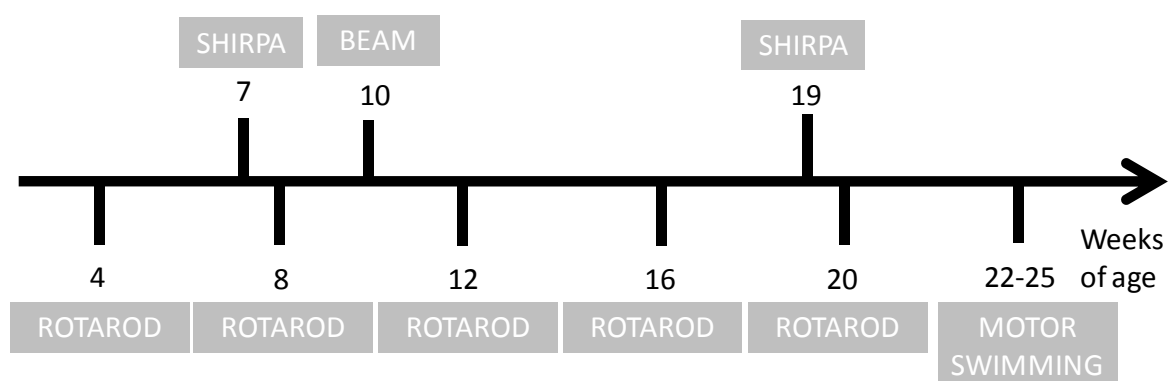


**Figure 3.** Representative diagram of the protocol used for phenotypic evaluation of CMVMJD135 mice. Rotarod test was performed every month since 4 weeks to 20 weeks of age. Animals were evaluated in the SHIRPA protocol at 7 and 19 weeks of age; in the balance beam test at 10 and in the motor swimming test at 22-25 weeks of age.

**SHIRPA protocol**

At the first age of SHIRPA protocol assessment (7 weeks of age) CMVMJD135 transgenic mice demonstrated significant differences in performance in the vertical pole test (♀:  $p=0,002$ ; ♂:  $p=0,073$ ) and in the hanging wire grip test (♀:  $p=0,006$ ; ♂:  $p=0,026$ ) (Figure 4). At 19 weeks of age transgenic mice became more affected, and lowered their performance in both tests (hanging wire: ♀:  $p=4,26 \times 10^{-6}$ , ♂:  $p=1,20 \times 10^{-10}$ , vertical pole test: ♀:  $p=0,001$ ; ♂:  $p=0,149$ ). Although male CMVMJD135 mice showed a similar decrease in the time spent in the vertical pole at 7 and 19 weeks of age as transgenic females, there was no statistically significant difference from wild-type animals, mainly due to the lower performance of the latter. Placebo groups (wt and CMVMJD135 mice) were evaluated for the hanging wire test at 4 weeks, before starting injections, and no differences were detected between groups (supplementary figure 2). The following age of evaluation was at 8 weeks of age, when significant differences were detected, which worsened over time (supplementary figure 2).

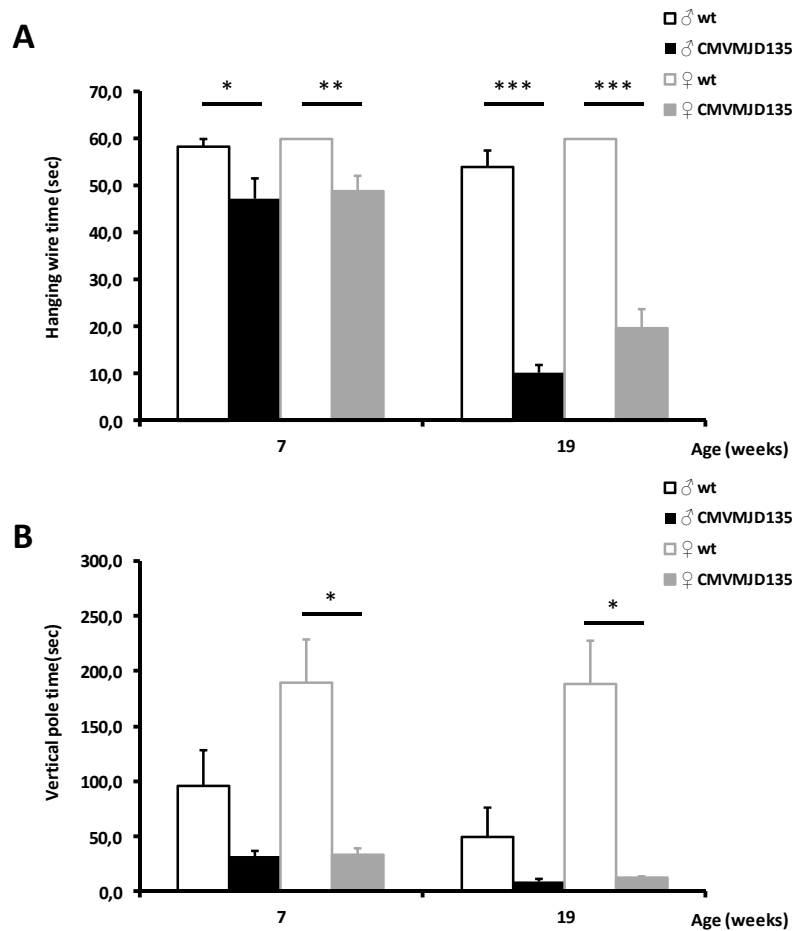


**Figure 4.** Motor evaluation in the hanging wire grip test (A) and vertical pole test (B). CMVMJD135 (♂ n=12; ♀ n=11) and wild-type animals (♂ n=11; ♀ n=12) were tested. Asterisks indicate significant differences between wild-type control and CMVMJD135 transgenic mice (\* $p<0.05$ , \*\* $p<0.01$ , \*\*\* $p<0,001$ ).

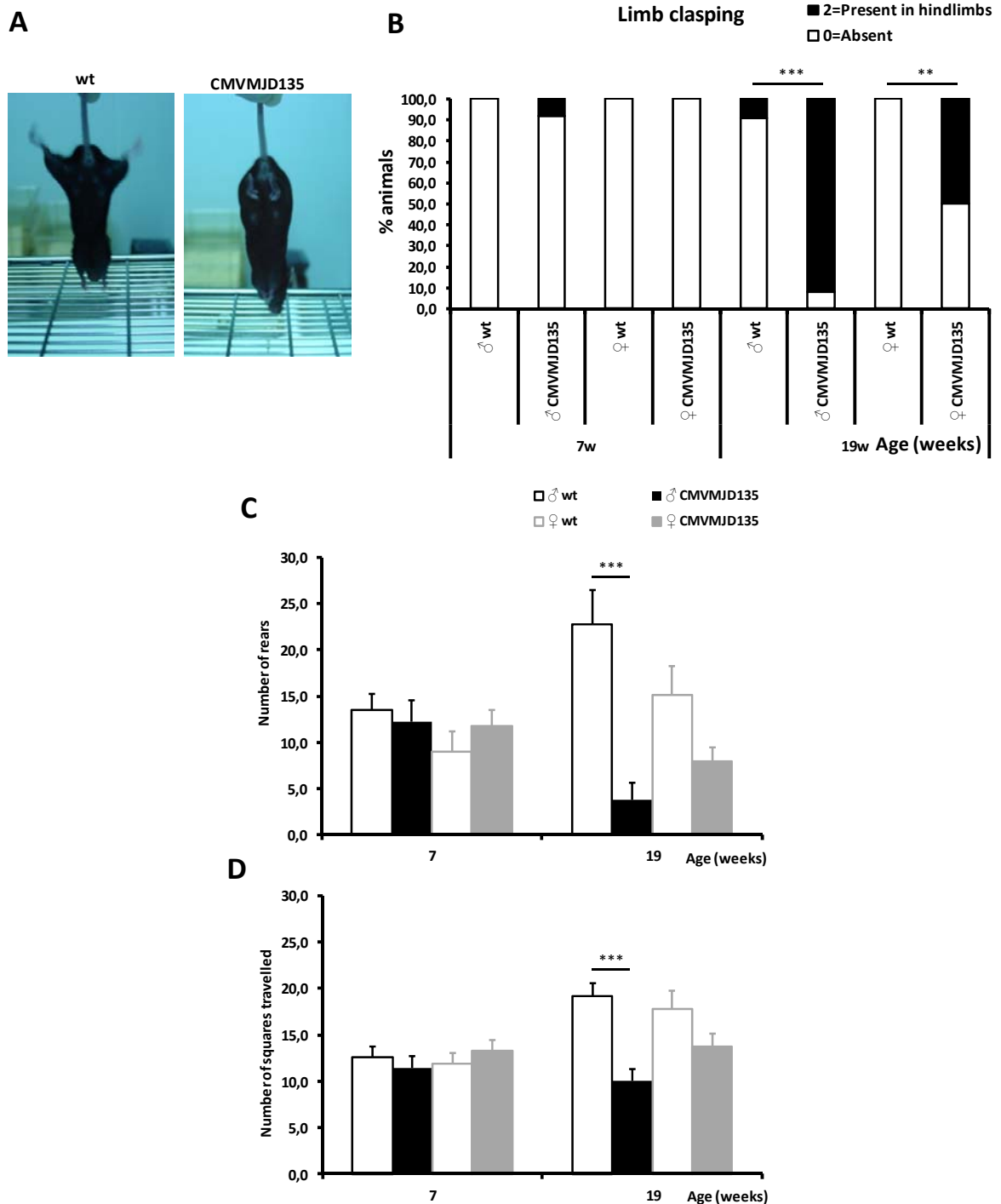
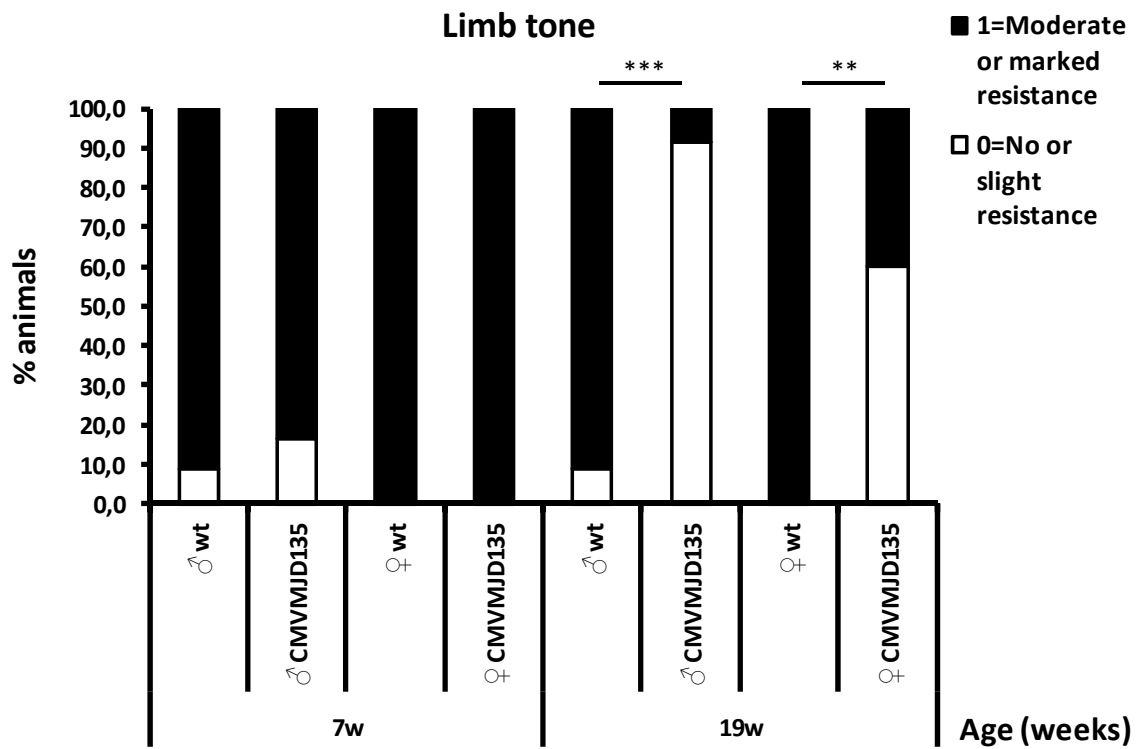


**Figure 5.** Phenotype of CMVMJD135 mice detected in the SHIRPA protocol. (A) Transgenic mice displayed limb claspings since 19 weeks of age. (B) The CMVMJD135 group displayed a higher percentage of animals displaying limb claspings in the hindlimbs than controls at 19 weeks of age. The SHIRPA protocol revealed a deficit in exploratory behavior of CMVMJD135 male mice at 19 weeks of age shown by a decrease in the number of rears in the viewing jar (C) and a decreased locomotor activity given by the number of squares travelled in the arena (D). CMVMJD135 (♂ n=12; ♀ n=11) and wild-type animals (♂ n=11; ♀ n=12) were tested. Vertical bars represent mean ± SEM of the different groups on each test. Asterisks indicate significant differences between wild-type control and CMVMJD135 transgenic mice (\*p<0.05, \*\*p<0.01, \*\*\*p<0,001).

A



B

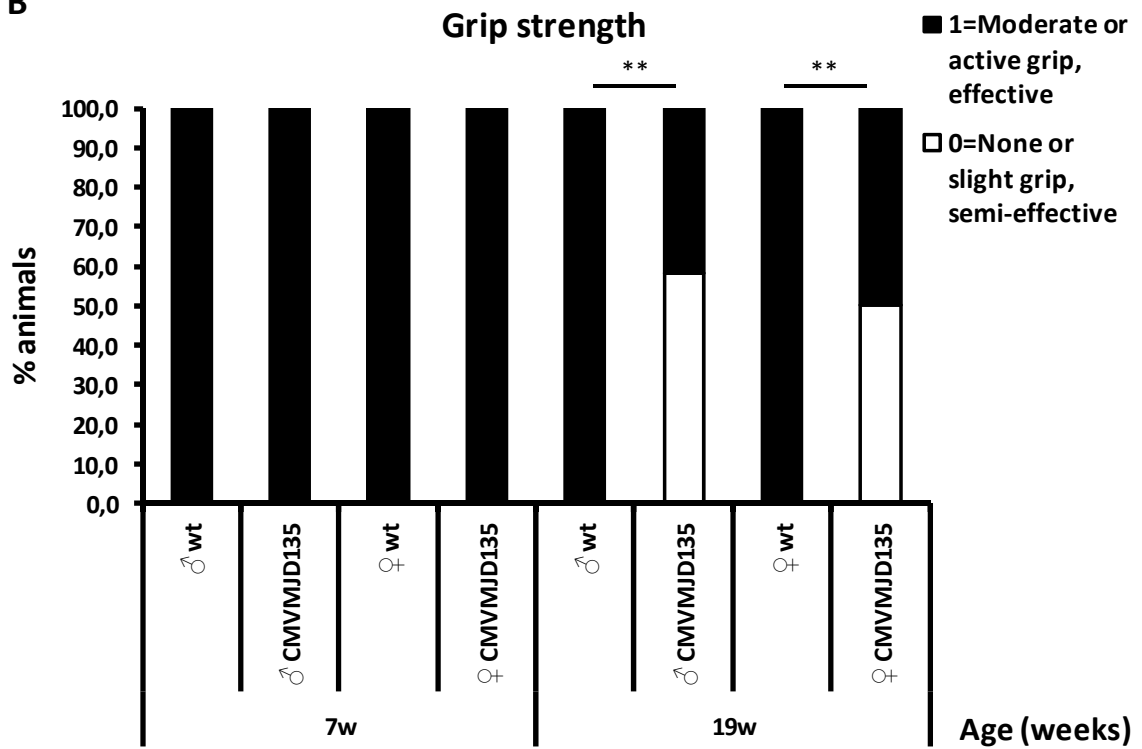
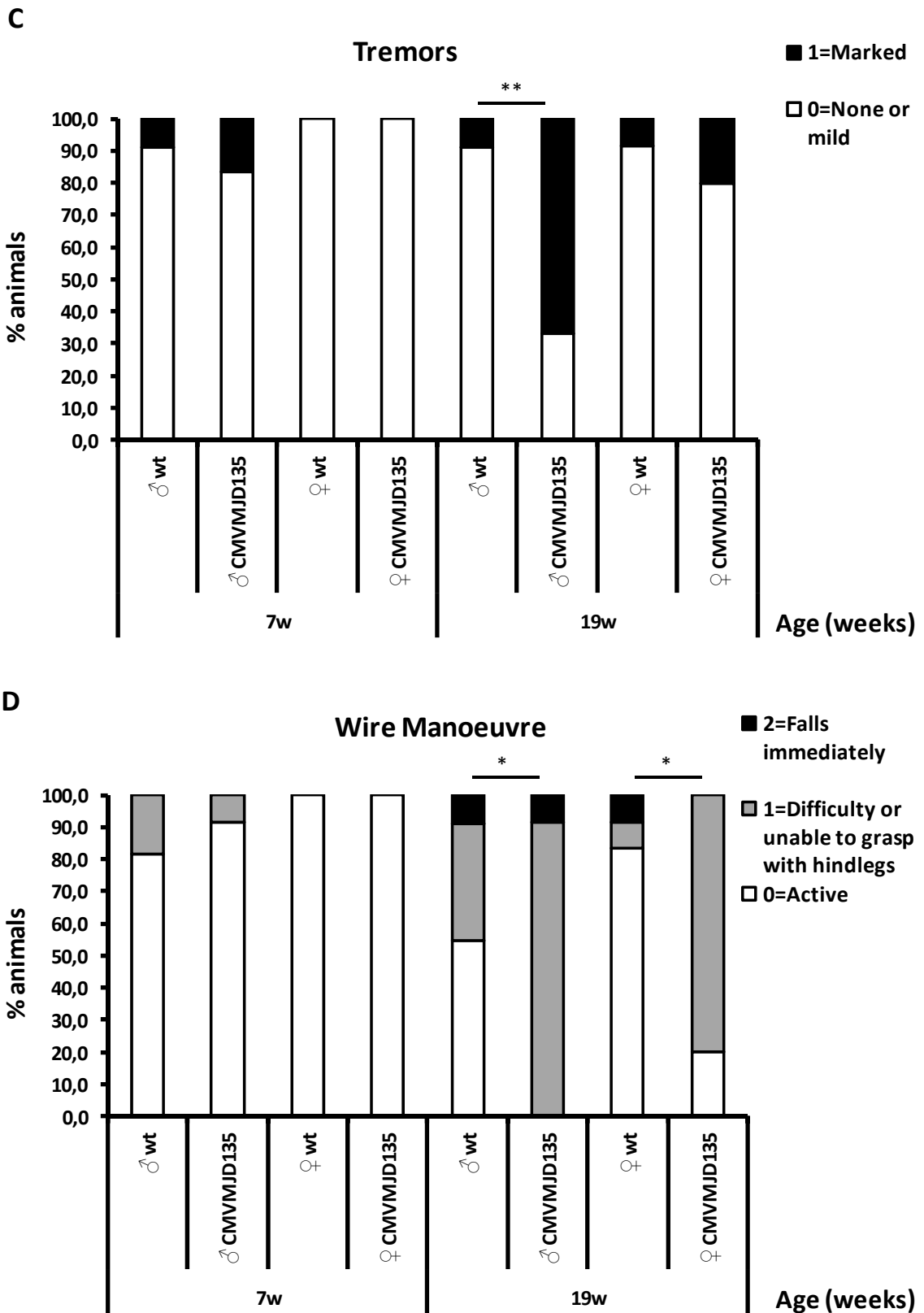


Figure 6. (continued)



**Figure 6.** Phenotype of CMVMJD135 mice detected in the SHIRPA protocol. (A) CMVMJD135 mice show a decrease resistance hindlimb tone in comparison with wild-type animals at 19 weeks of age. (B) Slight or absence grip strength of the forelimbs of CMVMJD135 mice. (C) Increase in the percentage of transgenic animals displaying tremors and (D) difficulty to grasp with hindlegs in the wire manoeuvre. CMVMJD135 (♂ n=12; ♀ n=11) and wild-type animals (♂ n=11; ♀ n=12) were tested.



### **Chapter 3. CMVMJD135 mice**

Locomotor and exploratory activity were also assessed as part of the SHIRPA protocol and shown to be altered in mutant mice at 19 weeks of age, as given by the significant decrease in the number of rears in the viewing jar between transgenic and wild-type males ( $\text{♂}$ :  $p=3,62 \times 10^{-4}$ ) and in the number of squares travelled in the arena ( $\text{♂}$ :  $p=7,28 \times 10^{-5}$ ), respectively (Figure 5C,D). Transgenic CMVMJD135 females also displayed a decrease in these two parameters in comparison to wild-type littermates, however statistical significance was not reached. In addition, at 19 weeks of age, a significant percentage of transgenic animals developed limb claspings in the hindlimbs ( $\text{♀}$ :  $p=0,006$ ;  $\text{♂}$ :  $p=1,07 \times 10^{-4}$ ) (Figure 5 A,B), tremors ( $\text{♀}$ :  $p=0,438$ ;  $\text{♂}$ :  $p=0,003$ ), difficulty in the wire manoeuvre ( $\text{♀}$ :  $p=0,011$ ;  $\text{♂}$ :  $p=0,017$ ), loss of hindlimb tonus resistance ( $\text{♀}$ :  $p=0,006$ ;  $\text{♂}$ :  $p=1,07 \times 10^{-4}$ ) and a decrease in forelimb strength ( $\text{♀}$ :  $p=0,006$ ;  $\text{♂}$ :  $p=0,003$ ) (Figure 6).

In the wire manoeuvre, although the majority of control animals displayed a score 0 (active), at 19 weeks of age there was a percentage of animals that was scored with 1 (difficulty or unable to grasp with hindlegs). These results could be due to the subjectivity of a score evaluation and the variability of the animals' behavior at different time points. Even so, transgenic animals demonstrated a significant increase in the percentage of animals displaying worse performance in these test when compared with wild-type animals ( $\text{♀}$ :  $p=0,011$ ;  $\text{♂}$ :  $p=0,017$ ).

#### ***Balance beam test***

The balance beam test, in which animals have to traverse a graded series of narrow beams to reach an enclosed safety platform, was used to evaluate the fine motor coordination and balance capabilities of animals. Different levels of task difficulty were achieved by varying the shape and cross-section of the beams (Fig. 7). At 10 weeks of age, the control and transgenic mice walked along all the beam types with ease, although the transgenic mice were significantly slower in traversing the 11 mm square beam ( $p=0,030$ ) (Fig. 7).

#### ***Motor swimming test***

The motor swimming test was used to evaluate swimming movement coordination. In this test, mice were evaluated for 3 days, and the task was to swim a distance of 60 cm to reach a visible escape platform at the opposite end (Carter et al., 1999).

CMVMJD135 transgenic mice displayed abnormalities in their swimming movements at the timepoint chosen to perform the swimming test (22-25 weeks of age). When placed in the water, transgenic mice adopted a twisted posture, and kicked in an uncoordinated manner with both hind-

and forelimbs. In contrast, control mice swam instantly and vigorously using mainly their hindlimbs. During the three days of test the CMVMJD135 mice group swam significantly more slowly compared with matched control mice group ( $p=3,81 \times 10^{-4}$ ) (Figure 8).

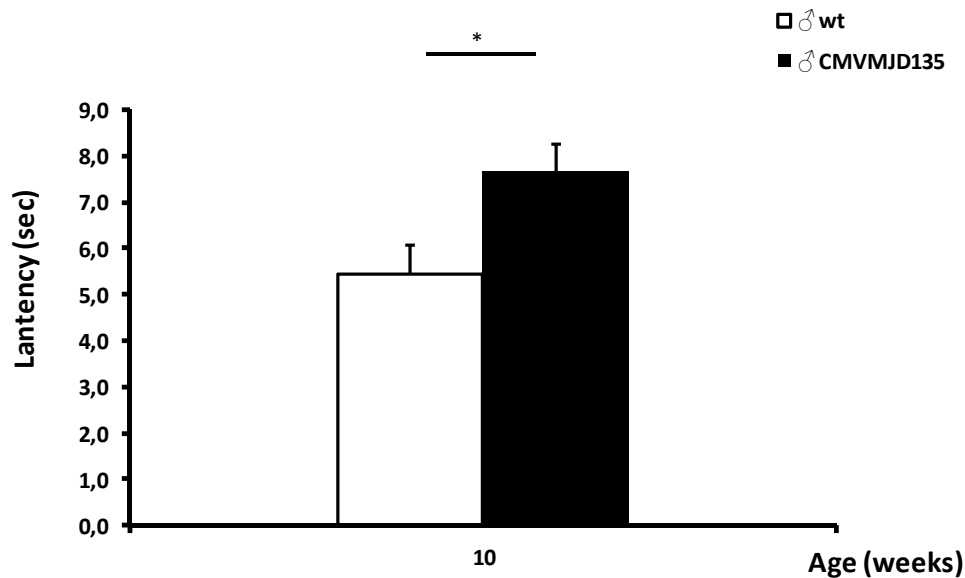


**Figure 7.** Balance assessment in CMVMJD135 male mice. (A) Wild-type (n=8) and CMVMJD135 transgenic (n=10) mice were given two trials on each of the graded square and round beams, in each case progressing from the widest to the narrowest, for 3 consecutive days at 10 weeks of age. Results are shown for the latency to traverse the 11 mm square beam. Vertical bars represent mean  $\pm$  SEM of the different groups on each test.

### ***Footprinting test***

Gait abnormalities were assessed by analyzing the footprint pattern of mice while they walked along a ramp corridor. Footprint patterns of wild-type and CMVMJD135 transgenic mice at 7 and 19 weeks of age are illustrated in Figure 9. At 19 weeks of age the footprinting pattern of CMVMJD135 mice demonstrated a clear foot dragging which was never observed in wild-type animals. Placebo groups (wt and CMVMJD135 mice) were evaluated for footprinting pattern at 4 weeks before starting injections and then monthly, which enabled us to define the onset of foot-dragging manifestation in CMVMJD135 mice more precisely. At 4 and 8 weeks of age foot-dragging was absent in transgenic mice, while at 12 weeks of age 90% of CMVMJD135 mice displayed foot-dragging ( $p=2,96 \times 10^{-5}$ ) and at 20 weeks of age the entire CMVMJD135 group displayed foot-dragging ( $p=4,59 \times 10^{-6}$ ) (supplementary figure 3).

### Chapter 3. CMVMJD135 mice

The resulting footprint patterns were also assessed quantitatively by four measurements: stride length, hindbase width, frontbase width, and front footprint/hind footprint overlap. At 7 and 19 weeks of age we did not find any strong differences in these four parameters. The preliminary gait analysis in transgenic animals (n=2) with approximately 7 months of age demonstrated that, besides the presence of the footdragging, there was an enlargement of the base with and a shortened step length (supplementary figure 4), but this finding needs to be validated in a larger group of animals.

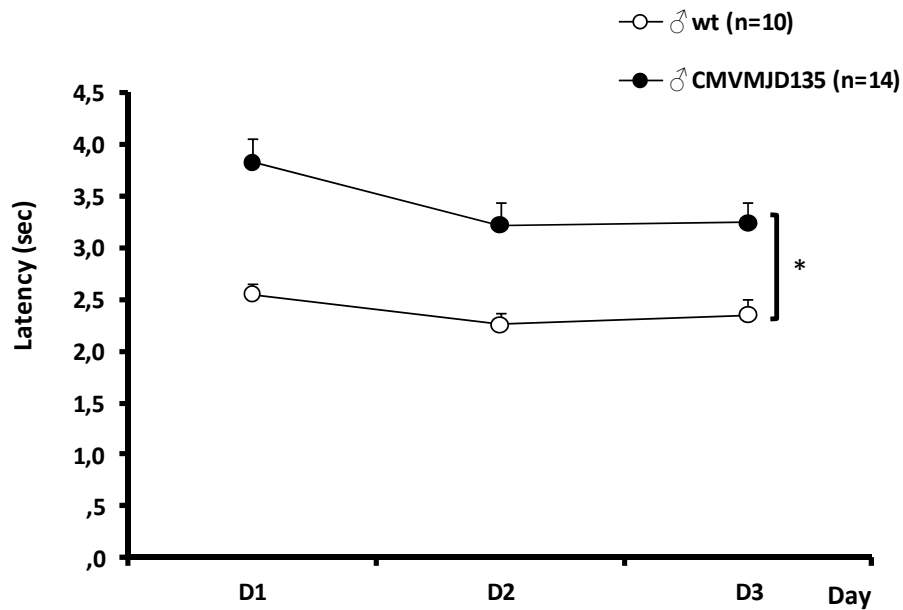


**Figure 8.** Performance of wild-type and CMVMJD135 transgenic mice in the swimming tank. 22-25 weeks old wild-type (n=10) and CMVMJD135 (n=14) male mice were tested in the swimming tank for the latency to swim over a 60 cm distance to a visible escape platform. Individual symbols indicate mean  $\pm$  SEM of each measure across all trials at each day of testing. Transgenic mice displayed swimming impairments given by a significant increase in the time spent to swim the 60 cm distance. Asterisks indicate significant differences between wild-type control and CMVMJD135 transgenic mice (\* $p < 0.05$ , \*\* $p < 0.01$ , \*\*\* $p < 0.001$ ).

### **Rotarod**

Motor coordination and balance of mice were measured using a rotarod paradigm as previously described (Silva-Fernandes et al., 2010). All mice used in this study showed proper learning of the rotarod test and reached a stable level of performance within the three days of training before the day test. At the first age of evaluation (4 weeks of age) CMVMJD135 mice displayed a significant decrease in the time spent in the rod at 24 rpm ( $\text{♀}$ :  $p = 0,011$ ) and at 15 rpm ( $\text{♂}$ :  $p = 0,031$ ) and in the accelerating rod (4-40 rpm) ( $\text{♀}$ :  $p = 0,011$ ). At 8 weeks of age transgenic animals demonstrated a significant decrease in the latency at 24 rpm ( $\text{♀}$ :  $p = 0,006$ ) and also in acceleration ( $\text{♀}$ :  $p = 0,023$ ).

At 12 weeks of age, however, CMVMJD135 mice ameliorated their rotarod performance, becoming statistically indistinguishable from littermate controls. At more advanced ages (16 and 20 weeks of age) CMVMJD135 mice progressively declined in their ability to maintain balance in the rotarod in comparison with wild-type controls (Figure 10). Namely, at 16 weeks of age transgenic mice showed a statistically significant decrease in the latency to fall from the rod at 20 and 24 rpm, when compared with wild-type (♀:  $p=0,024$ ;  $p=0,028$ , respectively). At 20 weeks of age CMVMJD135 animals worsened their performance in the rotarod at 20, 24, and 31 rpm (♀:  $p=0,003$ ;  $p=0,005$ ;  $p=0,013$ , respectively), as well as in the accelerating rod (♀:  $p=0,030$ ) (Figure 10B). Although transgenic male animals had a worse performance in the Rotarod in comparison with female CMVMJD135 mice, there was no statistical significance when compared to male littermate controls at 16 and 20 weeks of age, when female CMVMJD135 mice consistently displayed motor deficits. These results could be explained by a problem (of unknown origin) in the particular control male group being analysed, which behaved significantly worse than usual in mice of this genetic background.

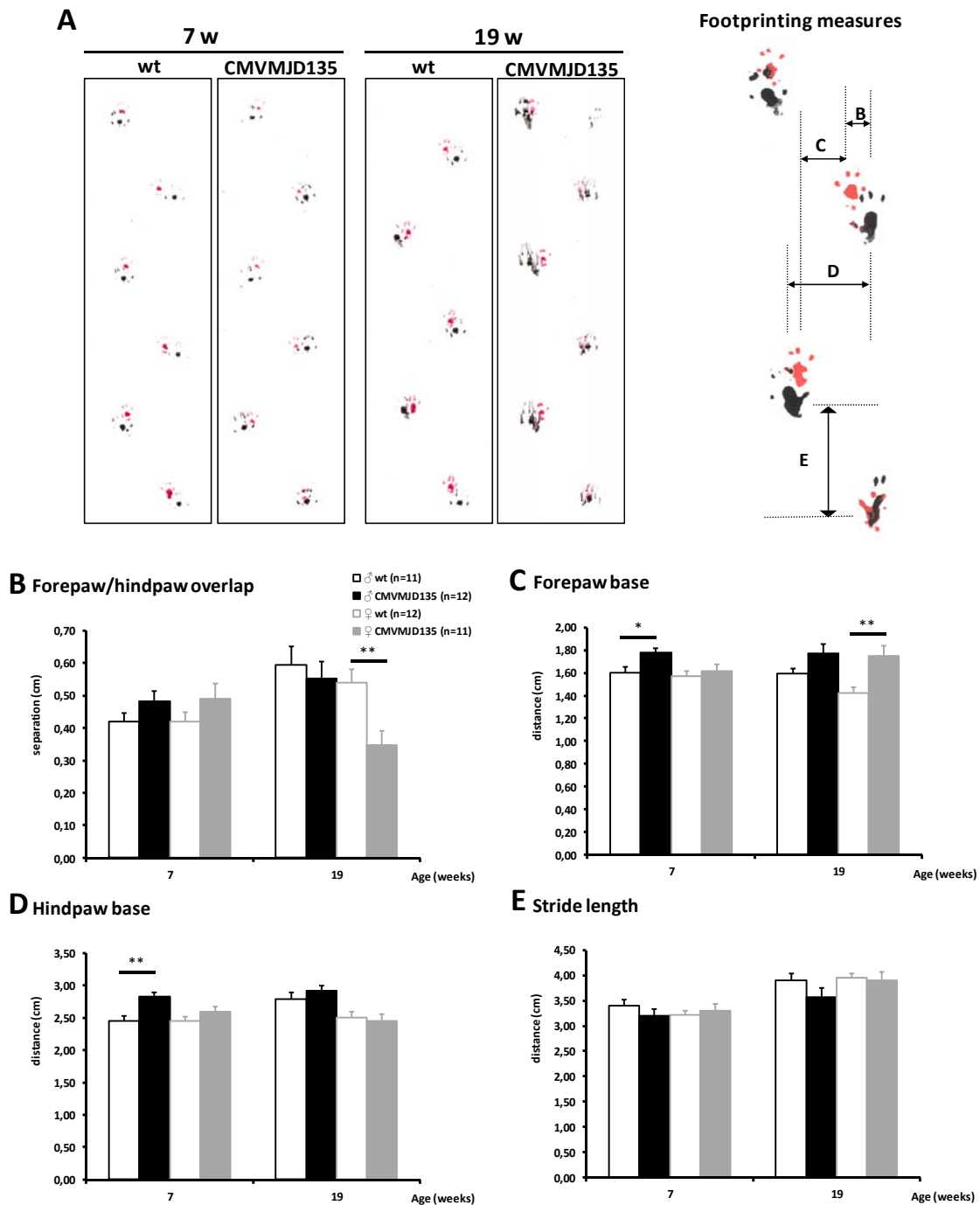


**Figure 9.** Representative walking footprint patterns of 7- to 19-week old wild-type and CMVMJD135 transgenic mice. Qualitatively, the generated patterns clearly differ, showing that CMVMJD135 transgenic mice display irregular foot dragging. Quantitative analysis of the walking footprint patterns produced by wild-type and transgenic mice, based on measurements of stride length (D), hindbase width (C), frontbase width (B), and distance between front and hind footprint placement or overlap (A), showed that at 19 weeks of age the footprint patterns of female CMVMJD135 transgenic mice exhibited a significant enlargement of the frontbase width and a decrease in the overlap of fore- and hindpaws. Vertical bars represent mean  $\pm$  SEM of the different groups on each measure. Asterisks indicate significant differences between wild-type control and CMVMJD135 transgenic mice (\* $p < 0.05$ , \*\* $p < 0.01$ , \*\*\* $p < 0.001$ ).

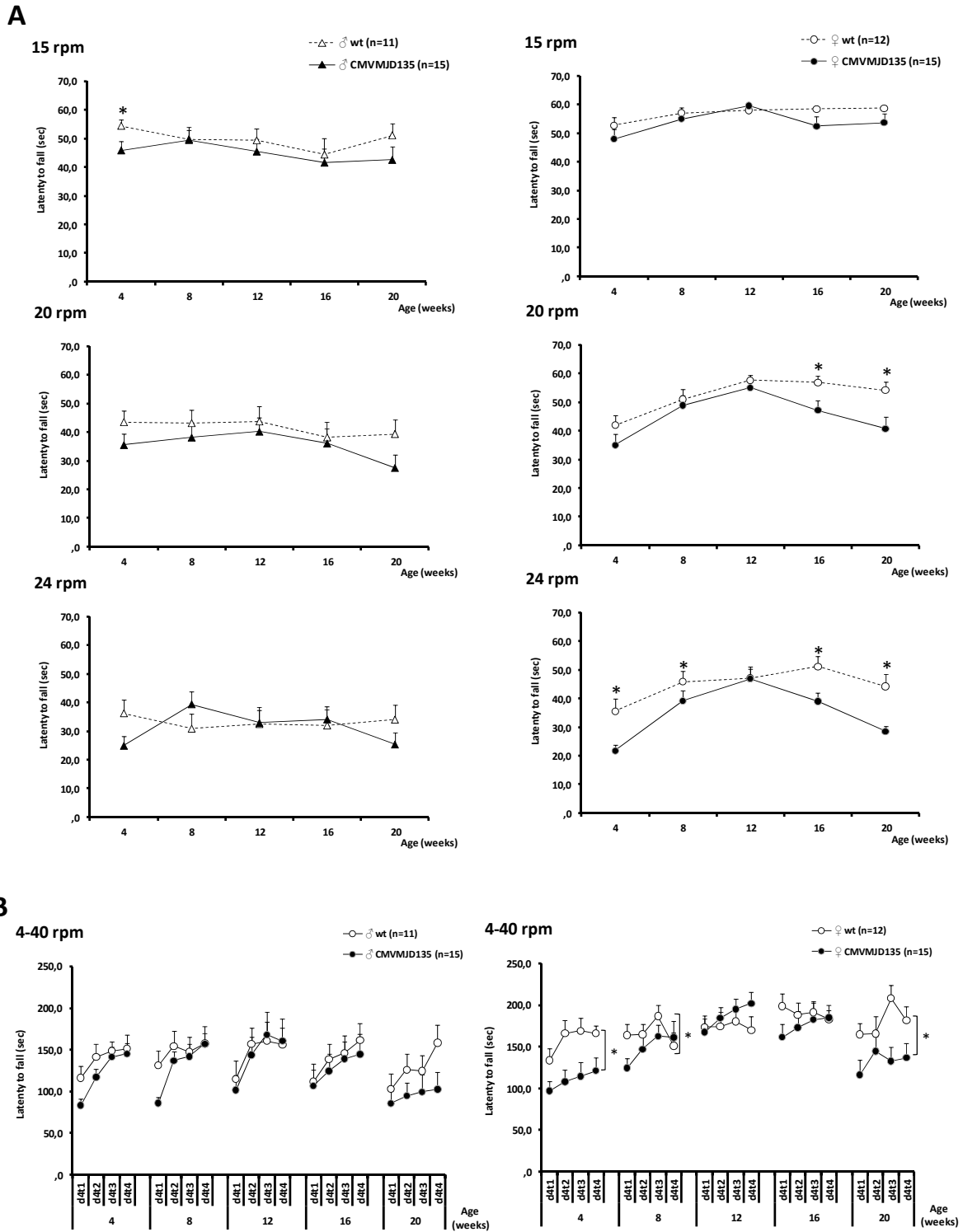


**Figure 10.** Balance and motor coordination on the rotarod. CMVMJD135 and wild-type animals were subjected to constant speeds (A) and an accelerating rod (4-40 rpm) (B). The mean  $\pm$  SEM of the latency to fall at each speed level was recorded. 16 weeks old CMVMJD135 transgenic mice exhibited difficulty maintaining balance on the rotarod at the highest rotation speeds and displayed a progressive decline in performance on the rotarod with increasing rotation speed and age. Asterisks indicate significant differences between wild-type control and CMVMJD135 transgenic mice (\* $p < 0.05$ , \*\* $p < 0.01$ , \*\*\* $p < 0.001$ ).

### Chapter 3. CMVMJD135 mice

A summary of the ages at which the different neurological symptoms were observed in CMVMJD135 mice was depicted in Figure 11.

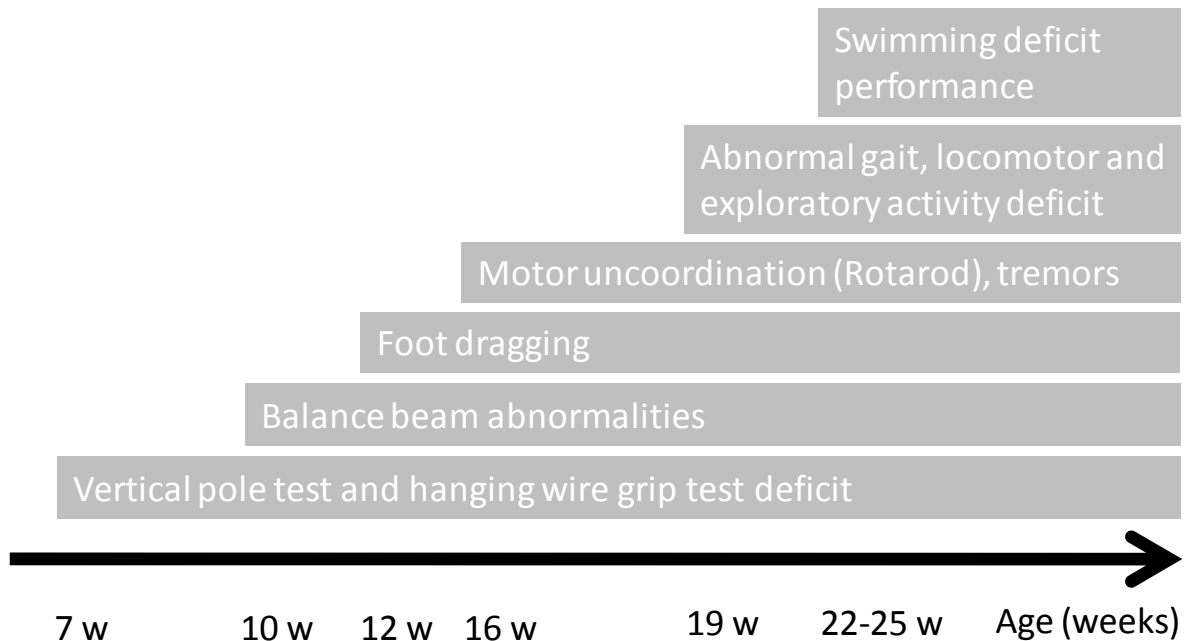


**Figure 11.** Representative timeline diagram of the phenotype abnormalities observed in CMVMJD135 mice.

#### Brain pathology

Histopathological observation of brain sections of transgenic CMVMJD135 mice revealed the presence of shrunken cells (violet cresil staining) in several regions, such as the pontine nuclei, vestibular nuclei and substantia nigra in comparison with normal cells observed in wild-type animals (Figure 12). We did not find apoptotic cells in the affected brain areas of MJD mice by TUNEL assay (data not shown). Immunohistochemistry anti-GFAP revealed the presence of gliosis mainly in the vestibular regions and in the substantia nigra (Figure 12). Immunohistochemistry anti-ataxin-3 and ubiquitin showed the presence of inclusions in the nucleus and cytoplasm of neurons and glial cells in CMVMJD135 mice brains (Figure 13). Inclusions were observed in different regions of the CNS including the pontine nuclei (oral and ventral part), lateral reticular nucleus, deep cerebellar nuclei, as well as in non-affected regions such as the hippocampus and the motor cortex.



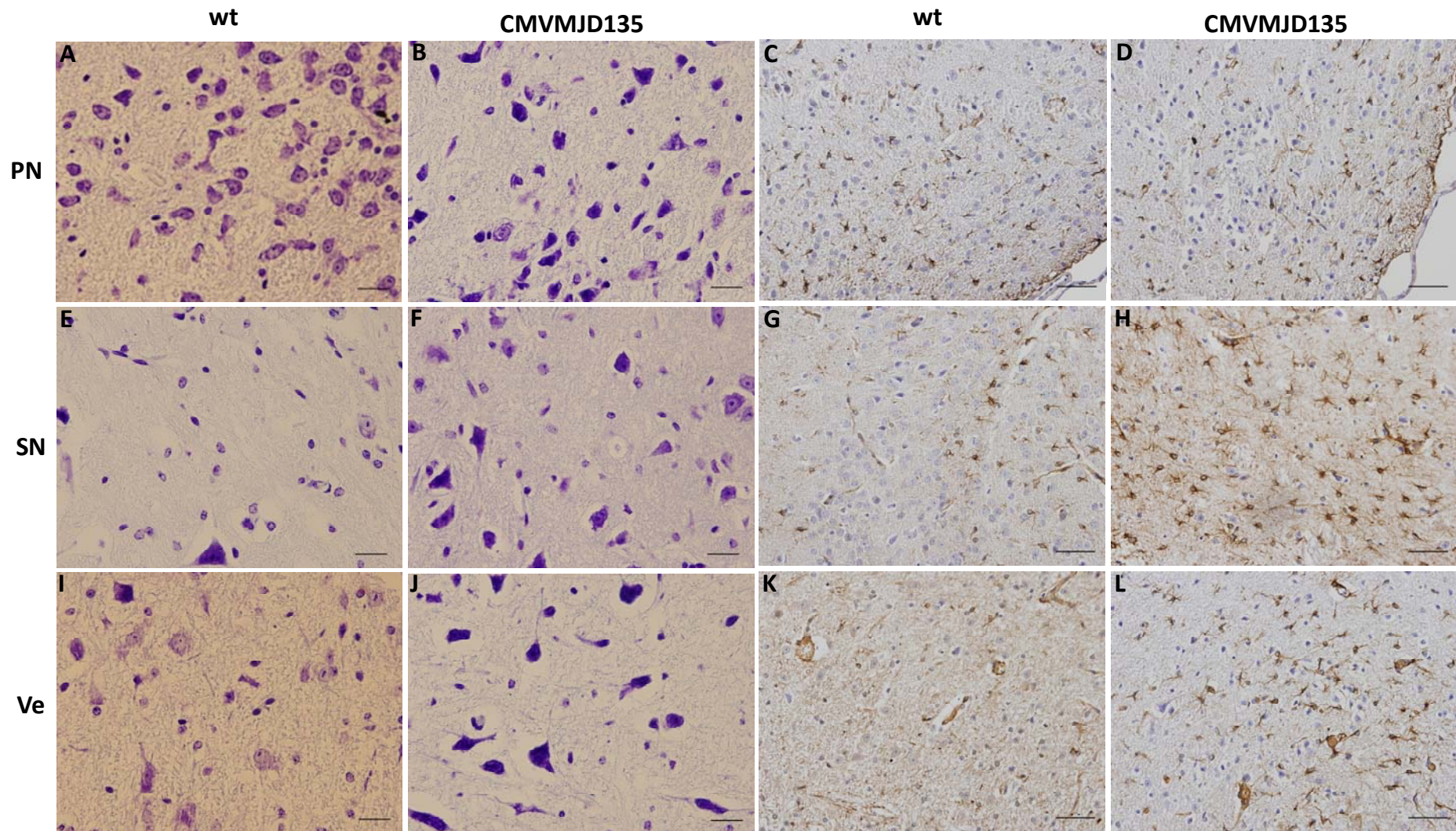


**Figure 12** Neuropathology of CMVMJD135 mice. Comparative sections stained with cresyl violet of wild-type and CMVMJD135 mice pontine (A,B), substantia nigra (E,F) and vestibular nuclei (I,J) at 24 weeks of age; Scale bar: 20  $\mu$ m. GFAP immunohistochemistry in comparative sections of wild-type and CMVMJD135 mice pontine (C,D), substantia nigra (G,H) and vestibular region (K,L) at 24 weeks of age. wt, wild-type; PN, pontine nuclei; SN, substantia nigra; Ve, vestibular nuclei; Scale bar: 50  $\mu$ m.



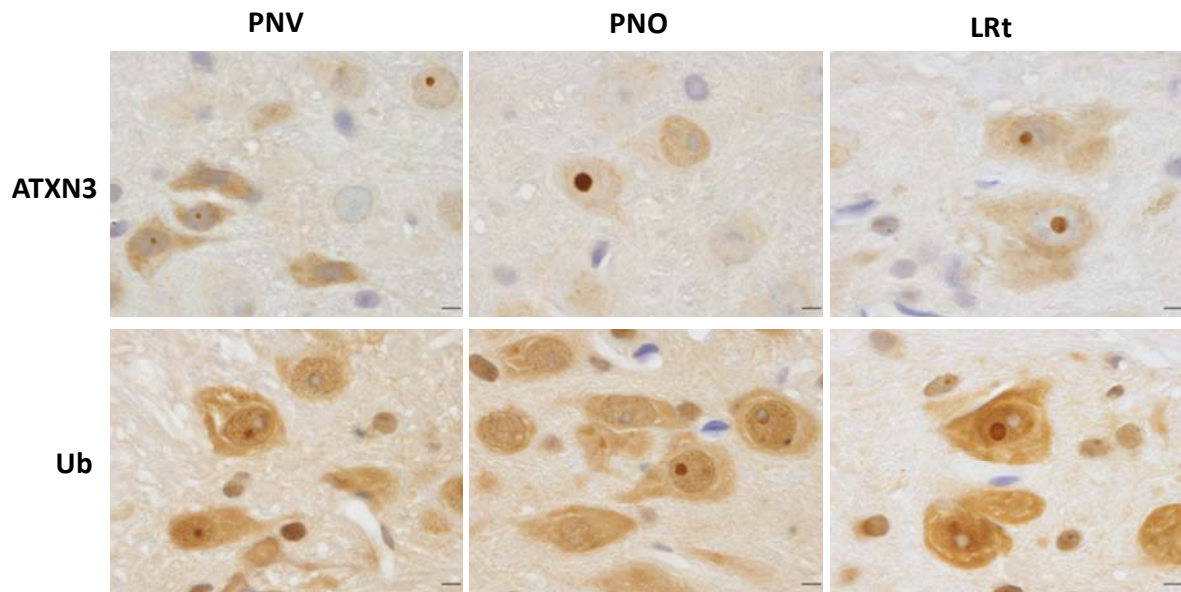


**Figure 13.** Neuronal inclusions in the CNS of CMVMJD135 mice. Anti-ataxin-3 and anti-ubiquitin immunohistochemistry (rabbit anti-MJD1.1) of transgenic CMVMJD135 mice at approximately 36 weeks. CMVMJD135 mice exhibit nuclear and cytoplasmic inclusions positive for both ataxin-3 and ubiquitin in different regions of the CNS. PNV, Pontine Nuclei (ventral); PNO, Pontine Nuclei (oral); LRt, Lateral reticular nucleus; wt, wild-type; hemi, hemizygous. Scale bar: 10  $\mu$ m.

## Discussion

The pathogenic mechanism of MJD, as well as of other polyQ disorders, is not well understood, and they remain incurable to date. For that reason, the establishment of animal models has been a very important field in the research of this disorder, given the need for these valuable tools for the study of the disease process as well as the study of therapeutic strategies. Our previous results have shown that transgenic mice expressing expanded ataxin-3 with 91 to 99 glutamines develop a mild non-progressive motor phenotype that correlates to the repeat length. Although these transgenic animals have a CAG repeat number in the upper limit (or even higher) of what has been described in human patients, we did not observe a dramatic motor phenotype. Other MJD transgenic mouse models have been described with CAG expansions in the range of human patients that did not display phenotype in hemizyosity (Goti et al., 2004) or did present a mild (Cemal et al., 2002) and variable phenotype (Bichelmeier et al., 2007). More recently, a transgenic mouse carrying a CAG repeat tract not observed so far in humans (148Q) was created, displaying a severe phenotype that progresses fastly within one month leading to death (Bichelmeier et al., 2007). In this work, we have created a new transgenic mouse model expressing the same variant of ataxin-3, as in our previous model, in several brain regions but with an increased number of glutamine residues (135Q). Interestingly, we have observed that human *ATXN3* mRNA is more expressed than murine *atxn3* mRNA in the cerebellum, brainstem and forebrain of CMVMJD135 mice, while at the protein level the expression of the endogenous ataxin-3 is higher than the transgene protein. These results could be the consequence of protein synthesis decrease, or highest degradation of the human ataxin-3, or due to its accumulation in inclusions, reducing the levels of the soluble protein.

The behavioral evaluation of CMVMJD135 mice has demonstrated the presence of several phenotypic abnormalities that gradually appear and progress during a lifespan over 1 year of age, namely an apparent loss of limb strength, balance and motor coordination deficits, decreased locomotor and exploratory activity, abnormal gait and tremors. In contrast, our previous results demonstrated that CMVMJD94 mice expressing the ataxin-3 with 91 to 99 glutamines under the regulation of the CMV promoter developed a mild non-progressive motor phenotype. These results could be mostly due to the difference of CAG repeat length between the two expanded ataxin-3 expressed in CMVMJD mice, rather than the protein levels, which did not differ substantially between the two models.

### **Chapter 3. CMVMJD135 mice**

The first sign of neurological disease in the CMVMJD135 model was the presence of balance and grip strength abnormalities at 7 weeks of age, given by the significant decrease in the latency to fall off in the vertical pole test and in the hanging wire. Cerebellar ataxia is one of the first clinical manifestations seen in MJD patients, and is due to unsteadiness or impaired balance. Although behavioral alterations suggestive of loss of coordination in CMVMJD135 mice have been observed at 4 and 8 weeks of age, at these ages animals were indistinguishable from their wild-type littermates by simple observation in their home cage. At 16 weeks of age signs of neurological abnormality in CMVMJD135 mice were observable in the home cage, in particular an abnormal gait. The footprinting pattern evaluation of CMVMJD135 mice clearly demonstrated foot-dragging and, at later stages of the disease, a base-width enlargement, which is a major hallmark of ataxia, as well a shorter step length.

Rotarod testing was initiated at 4 weeks of age, a week after the weaning of mice. Although at this age transgenic animals showed a rotarod deficit at 24 rpm and in the acceleration rod, when compared with wild-type mice, at two subsequent ages of evaluation (8 and 12 weeks of age) an increase in the time spent on the rod was observed, transgenic animals reaching the performance of wild-type littermates. This amelioration of the motor performance in wt mice submitted to the rotarod test followed by a decrease in performance with age has already been described in 1–3-month-old C57Bl/6 mice (Serradj and Jamon, 2007). At 16 weeks of age the positive effect in the motor performance in the rotarod test inherent to age was apparently no longer compensating the motor symptoms observed in our model and for that reason we started to observe significant differences in the latency on the rod in comparison with littermate controls. At the age where mice were evaluated in the motor swimming test, the abnormal posture and inappropriate kicking movements exhibited by CMVMJD135 contrasted markedly with the coordinated, synchronized paddling movements shown by wild-type mice.

The analysis of CAG repeat number through the generations of CMVMJD135 revealed that CAG tract length varied in 80% of the progeny studied, always towards contractions. Intergenerational instability in cDNA transgenic mice for MJD has already been described showing a differential CAG variation pattern between maternal and paternal meioses (Boy et al., 2009; Silva-Fernandes et al., 2010), CAG contractions being more associated with maternal and CAG expansions with paternal transmissions. In the CMVMJD135 mice we observed CAG length contractions for both genders, which could be the result of a protection mechanism of cells or a negative selection of germ cells carrying CAG tract lengths in this upper range. The genescan profile of the CAG tract obtained from

mouse tail tissue has demonstrated that somatic mosaicism was also present. Thus our new model seems to replicate this feature of the human disease as well.

Histopathological evaluation of CMVMJD94 transgenic mouse brains revealed that apoptotic and necrotic events were absent (Silva-Fernandes et al., 2010), however cells with abnormal morphology (shrunken) could be observed in brain regions such as the lateral dentate, vestibular and pontine nuclei, thalamus and substantia nigra. In addition, CMVMJD94 transgenic mouse brains showed astrogliosis in the vestibular nuclei (Ve), substantia nigra (SN) and in the thalamus. In agreement, the CMVMJD135 mouse has been evaluated for the presence of neuronal cell death with the same negative results, although we did observe the presence of neurons with an abnormal morphology in brain regions such as the pontine and vestibular nuclei and substantia nigra as well as gliosis in the vestibular region and in the substantia nigra. The absence of neuronal death has also been described in other MJD transgenic mice with neurological phenotype (Goti et al., 2004; Bichelmeier et al., 2007; Chou et al., 2008). Although other types of cell death have to be evaluated in these mice models (e.g autophagy), it seems possible that the motor phenotype observed in our models is attributable to dysfunction of the brain regions affected in MJD, in the absence of neuronal cell death. A neurochemical evaluation performed in the striatum of transgenic MJD/SCA3 mice (line 70.61) showed a significant reduction of the dopamine metabolites DOPAC and HVA as well as of the turnover rate of both dopamine and serotonin in the striatum compared with wildtype littermates (Bichelmeier et al., 2007). A reduction of dopamine metabolites was also observed in human MJD/SCA3 brains (Higgins et al., 1996), as well as in transgenic mouse models of HD (Reynolds et al., 1999; Duan et al., 2004) and HD patients (Reynolds and Garrett, 1986). We will have to determine if this is also a feature of the CMVMJD135 model.

An important feature of MJD, as well as of other polyQ diseases, is the presence of neuronal inclusions. Our previous results have shown the presence of motor symptoms in a transgenic mouse resembling MJD in the absence of intranuclear inclusions. However, and although we did not find NIs in CMVMJD94 mouse brains, the presence of intermediate species of the aggregation process remains to be elucidated. In this new transgenic mouse, which expresses ataxin-3 under the regulation of same promoter (CMV), the intranuclear inclusions were present in the neuronal and glial cells of affected brain regions such as pontine and deep cerebellar nuclei but also in regions that are spared such as the hippocampus and motor cortex. This is concordant with the situation seen in human MJD patients where neurodegeneration was not clearly correlated with the occurrence of ataxin-3 immunopositive inclusions (Rub et al., 2006).

### **Chapter 3. CMVMJD135 mice**

We provide evidence that transgenic mice expressing human ataxin-3 with 135 glutamines develop a marked phenotype including MJD-like symptoms with a relatively slow progression of the disease and a lifespan over 1 year. This suggests that the CMVMJD135 model may be a good model for the study of the disease process, with more advanced pathology and phenotype being observed at an earlier age. Although the role of intranuclear inclusions, the end-product of the aggregation process in MJD pathogenesis, remains to be clarified, the presence of this pathological hallmark of in disease our model indicates that we were successful in replicating the full aggregation process that happens in humans. It will be interesting to study the impact of different therapeutic strategies upon the phenotypic and pathological manifestations in this model.

## References

- Bichelmeier, U., Schmidt, T., Hubener, J., Boy, J., Ruttiger, L., Habig, K., Poths, S., Bonin, M., Knipper, M., Schmidt, W. J., Wilbertz, J., Wolburg, H., Laccone, F. and Riess, O. 2007. Nuclear localization of ataxin-3 is required for the manifestation of symptoms in SCA3: in vivo evidence. *J Neurosci.* 27, 7418-7428.
- Boy, J., Schmidt, T., Wolburg, H., Mack, A., Nuber, S., Bottcher, M., Schmitt, I., Holzmann, C., Zimmermann, F., Servadio, A. and Riess, O. 2009. Reversibility of symptoms in a conditional mouse model of spinocerebellar ataxia type 3. *Hum Mol Genet.* 18, 4282-4295.
- Boy, J., Schmidt, T., Schumann, U., Grasshoff, U., Unser, S., Holzmann, C., Schmitt, I., Karl, T., Laccone, F., Wolburg, H., Ibrahim, S. and Riess, O. 2010. A transgenic mouse model of spinocerebellar ataxia type 3 resembling late disease onset and gender-specific instability of CAG repeats. *Neurobiol Dis.* 37, 284-293.
- Carter, R. J., Lione, L. A., Humby, T., Mangiarini, L., Mahal, A., Bates, G. P., Dunnett, S. B. and Morton, A. J. 1999. Characterization of progressive motor deficits in mice transgenic for the human Huntington's disease mutation. *J Neurosci.* 19, 3248-3257.
- Cemal, C. K., Carroll, C. J., Lawrence, L., Lowrie, M. B., Ruddle, P., Al-Mahdawi, S., King, R. H., Pook, M. A., Huxley, C. and Chamberlain, S. 2002. YAC transgenic mice carrying pathological alleles of the MJD1 locus exhibit a mild and slowly progressive cerebellar deficit. *Hum Mol Genet.* 11, 1075-1094.
- Chou, A. H., Yeh, T. H., Ouyang, P., Chen, Y. L., Chen, S. Y. and Wang, H. L. 2008. Polyglutamine-expanded ataxin-3 causes cerebellar dysfunction of SCA3 transgenic mice by inducing transcriptional dysregulation. *Neurobiol Dis.* 31, 89-101.
- Coutinho, P. and Andrade, C. 1978. Autosomal dominant system degeneration in Portuguese families of the Azores Islands. A new genetic disorder involving cerebellar, pyramidal, extrapyramidal and spinal cord motor functions. *Neurology.* 28, 703-709.
- Duan, W., Guo, Z., Jiang, H., Ladenheim, B., Xu, X., Cadet, J. L. and Mattson, M. P. 2004. Paroxetine retards disease onset and progression in Huntingtin mutant mice. *Ann Neurol.* 55, 590-594.
- Goti, D., Katzen, S. M., Mez, J., Kurtis, N., Kiluk, J., Ben-Haiem, L., Jenkins, N. A., Copeland, N. G., Kakizuka, A., Sharp, A. H., Ross, C. A., Mouton, P. R. and Colomer, V. 2004. A mutant ataxin-3 putative-cleavage fragment in brains of Machado-Joseph disease patients and transgenic mice is cytotoxic above a critical concentration. *J Neurosci.* 24, 10266-10279.
- Higgins, J. J., Harvey-White, J. D., Nee, L. E., Colli, M. J., Grossi, T. A. and Kopin, I. J. 1996. Brain MRI, lumbar CSF monoamine concentrations, and clinical descriptors of patients with spinocerebellar ataxia mutations. *J Neurol Neurosurg Psychiatry.* 61, 591-595.
- Ikeda, H., Yamaguchi, M., Sugai, S., Aze, Y., Narumiya, S. and Kakizuka, A. 1996. Expanded polyglutamine in the Machado-Joseph disease protein induces cell death in vitro and in vivo. *Nat Genet.* 13, 196-202.
- Maciel, P., Costa, M. C., Ferro, A., Rousseau, M., Santos, C. S., Gaspar, C., Barros, J., Rouleau, G. A., Coutinho, P. and Sequeiros, J. 2001. Improvement in the molecular diagnosis of Machado-Joseph disease. *Arch Neurol.* 58, 1821-1827.
- Nicklas, W., Baneux, P., Boot, R., Decelle, T., Deeny, A. A., Fumanelli, M. and Illgen-Wilcke, B. 2002. Recommendations for the health monitoring of rodent and rabbit colonies in breeding and experimental units. *Lab Anim.* 36, 20-42.
- Paulson, H. L., Perez, M. K., Trottier, Y., Trojanowski, J. Q., Subramony, S. H., Das, S. S., Vig, P., Mandel, J. L., Fischbeck, K. H. and Pittman, R. N. 1997. Intranuclear inclusions of expanded polyglutamine protein in spinocerebellar ataxia type 3. *Neuron.* 19, 333-344.

### Chapter 3. CMVMJD135 mice

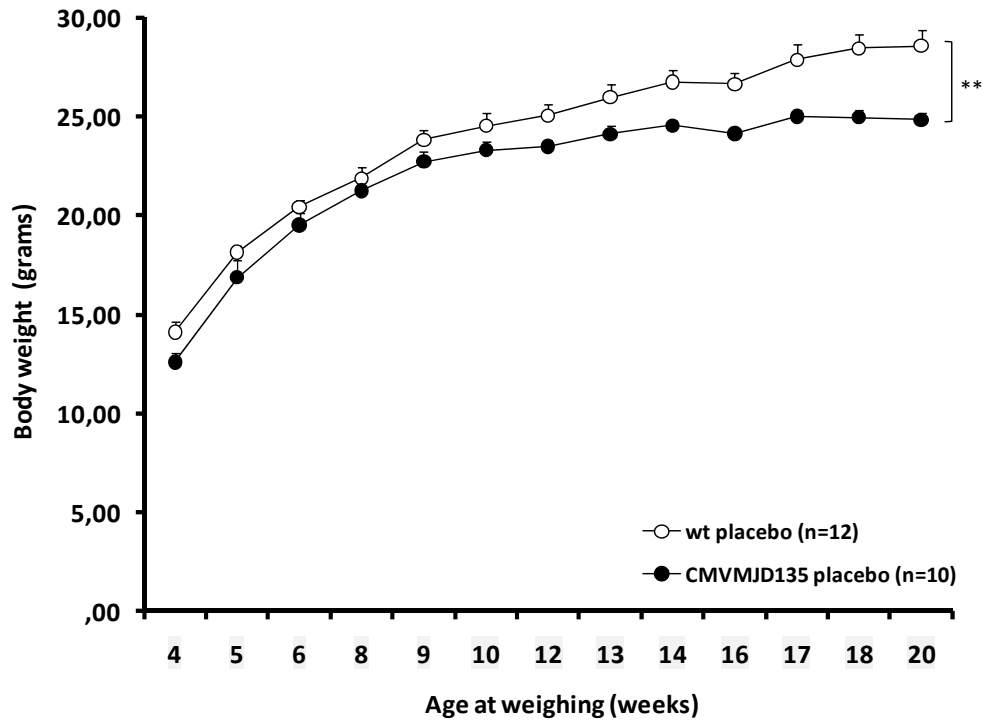
- Paulson, H. L. 2007. Dominantly inherited ataxias: lessons learned from Machado-Joseph disease/spinocerebellar ataxia type 3. *Semin Neurol.* 27, 133-142.
- Reynolds, G. P. and Garrett, N. J. 1986. Striatal dopamine and homovanillic acid in Huntington's disease. *J Neural Transm.* 65, 151-155.
- Reynolds, G. P., Dalton, C. F., Tillery, C. L., Mangiarini, L., Davies, S. W. and Bates, G. P. 1999. Brain neurotransmitter deficits in mice transgenic for the Huntington's disease mutation. *J Neurochem.* 72, 1773-1776.
- Rub, U., de Vos, R. A., Brunt, E. R., Sebesteny, T., Schols, L., Auburger, G., Bohl, J., Ghebremedhin, E., Gierga, K., Seidel, K., den Dunnen, W., Heinsen, H., Paulson, H. and Deller, T. 2006. Spinocerebellar ataxia type 3 (SCA3): thalamic neurodegeneration occurs independently from thalamic ataxin-3 immunopositive neuronal intranuclear inclusions. *Brain Pathol.* 16, 218-227.
- Schmidt, T., Landwehrmeyer, G. B., Schmitt, I., Trottier, Y., Auburger, G., Laccone, F., Klockgether, T., Volpel, M., Epplen, J. T., Schols, L. and Riess, O. 1998. An isoform of ataxin-3 accumulates in the nucleus of neuronal cells in affected brain regions of SCA3 patients. *Brain Pathol.* 8, 669-679.
- Serradj, N. and Jamon, M. 2007. Age-related changes in the motricity of the inbred mice strains 129/sv and C57BL/6j. *Behav Brain Res.* 177, 80-89.
- Silva-Fernandes, A., Costa Mdo, C., Duarte-Silva, S., Oliveira, P., Botelho, C. M., Martins, L., Mariz, J. A., Ferreira, T., Ribeiro, F., Correia-Neves, M., Costa, C. and Maciel, P. 2010. Motor uncoordination and neuropathology in a transgenic mouse model of Machado-Joseph disease lacking intranuclear inclusions and ataxin-3 cleavage products. *Neurobiol Dis.* 40, 163-176.

## **Supplementary material**

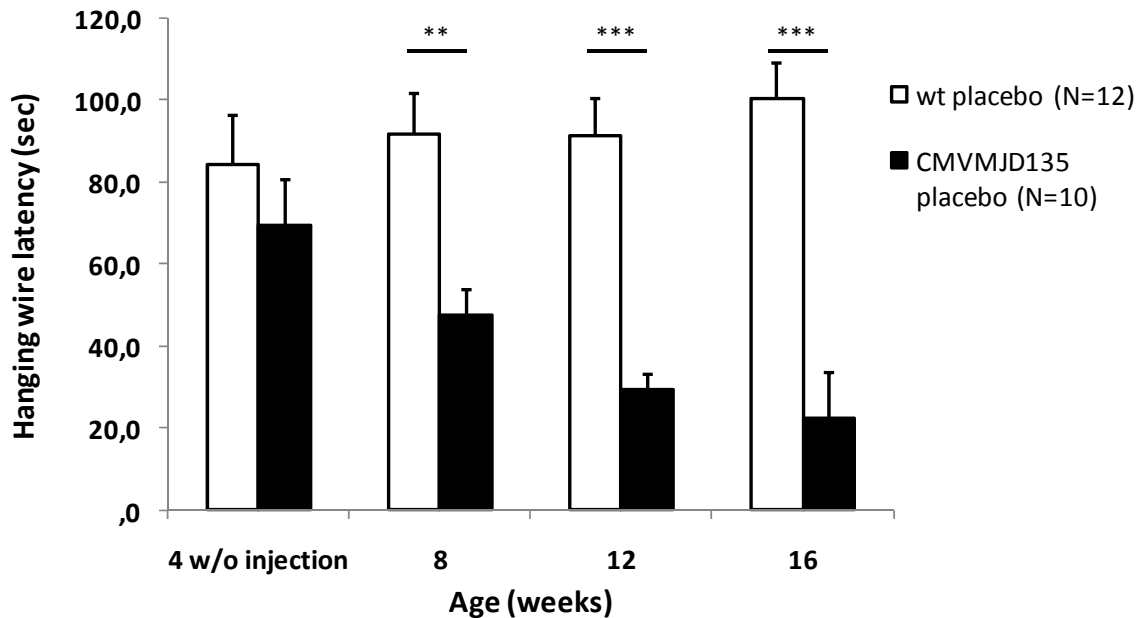
---



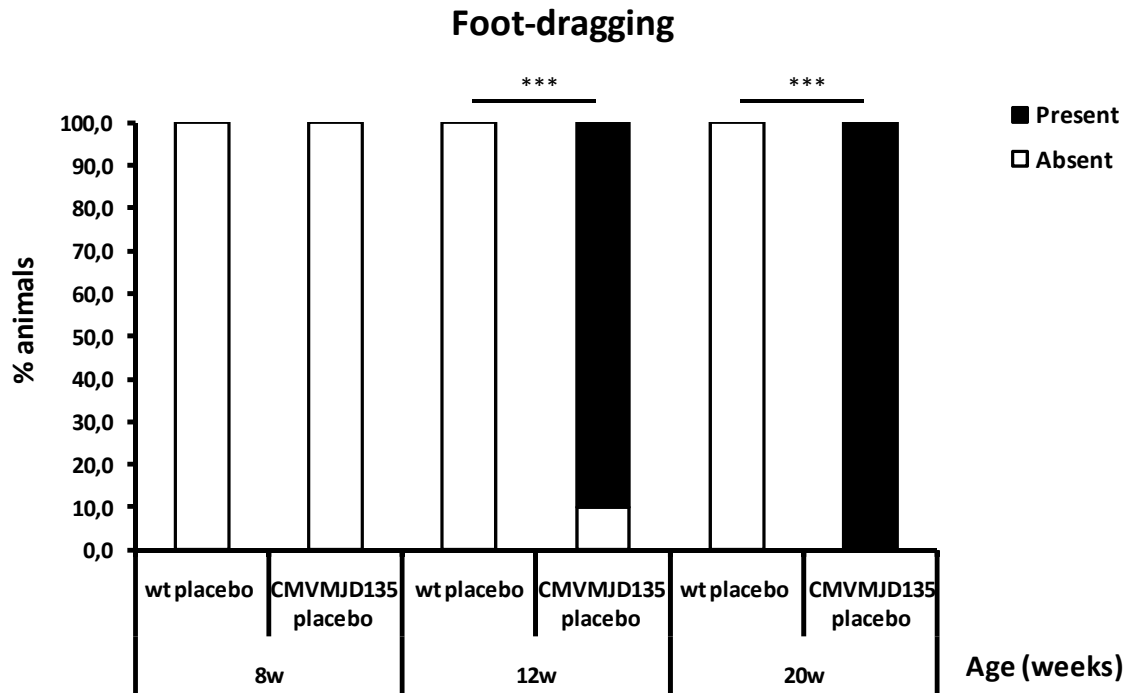




**Supplementary Figure 1.** Body weight (grams) between 4 to 20 weeks of age was depicted for wt and CMVMJD135 mice treated with vehicle. Asterisks indicate significant differences between wild-type control and CMVMJD135 transgenic mice (\* $p < 0.05$ , \*\* $p < 0.01$ , \*\*\* $p < 0.001$ ).



**Supplementary Figure 2.** Motor limb strength evaluation in the hanging wire grip test. CMVMJD135 (♂  $n = 10$ ) and wild-type animals (♂  $n = 12$ ) were tested at 4 weeks of age before the beginning of placebo i.p injections. Asterisks indicate significant differences between wild-type control and CMVMJD135 transgenic mice (\* $p < 0.05$ , \*\* $p < 0.01$ , \*\*\* $p < 0.001$ ).



**Supplementary Figure 3.** Percentage of animals displaying foot-dragging in the footprinting pattern depicted for wt (n=12) and CMVMJD135 (n=10) mice treated with vehicle. Asterisks indicate significant differences between wild-type control and CMVMJD135 transgenic mice (\*p<0.05, \*\*p<0.01, \*\*\*p<0,001).



**Supplementary Figure 4.** Representative walking footprint pattern of CMVMJD135 transgenic mice at 7 months of age showing foot dragging, base width enlargement and shortened step in comparison with wild-type.

# **Chapter 4**

---

Autophagy activation as a therapeutic target strategy for MJD: assessment  
in the CMVMJD135 mouse model



**Autophagy activation as a therapeutic target strategy for MJD: assessment in the CMVMJD135 mouse model**

Silva-Fernandes A<sup>1</sup>, Duarte-Silva S<sup>1</sup>, Teixeira-Castro A<sup>1</sup>, Carvalho A<sup>1</sup>, Maciel P<sup>1</sup>

<sup>1</sup>Life and Health Sciences Research Institute (ICVS), School of Health Sciences, University of Minho, Campus Gualtar, 4710-057 Braga, Portugal; <sup>2</sup>Department of Neurology, Hospital Prof. Fernando Fonseca, E.P.E., Amadora, Portugal.

Corresponding author: Patrícia Maciel. Life and Health Sciences Research Institute (ICVS), School of Health Sciences, University of Minho, Campus Gualtar, 4710-057 Braga, Portugal.

Telephone: 351-253-604824, Fax: 351-253-604820. E-mail: [pmaciel@ecsaude.uminho.pt](mailto:pmaciel@ecsaude.uminho.pt)

### Abstract

A major pathological hallmark in several human neurodegenerative disorders, like Alzheimer's disease, Parkinson's disease (PD) and polyglutamine (polyQ) disorders, including Machado-Joseph disease (MJD), is the formation of intra-neuronal mutant protein aggregates. MJD is an inherited neurodegenerative disease, caused by a CAG repeat expansion in the *ATXN3* gene, resulting in an abnormal protein, ataxin-3. This protein, when mutated, is prone to misfold and form cytoplasmic and nuclear aggregates within neurons inducing a cell-stress response. The diameter pore of the proteasome is thought to abolish the entry of polyQ protein oligomers and larger structures, autophagy being the major pathway for their clearance. Treatment of proteinopathies with drugs that up-regulate autophagy, like rapamycin, has shown promising results in cell, *Drosophila* and mouse models of polyQ diseases.

Temsirolimus (Cell Cycle inhibitor-779) is an analogue of rapamycin that inhibits the mammalian target of rapamycin (m-TOR) and hence up-regulates autophagy. In this study we used two different strategies to up-regulate autophagy, as a therapeutic approach: the administration of lithium, which induces autophagy independently of m-TOR, by reducing the levels of inositol 1,4,5-triphosphate, and of the conjugation of temsirolimus and lithium in the CMVMJD135 transgenic mouse model of MJD. Gain of body weight was slightly higher in the CMVMJD135 lithium-treated group in comparison with the placebo group. However, the majority of the motor deficits observed in the CMVMJD135 mice, namely loss of limb strength, balance deficit, limb claspings and foot-dragging, were not improved in transgenic animals treated with lithium. Interestingly, we observed an apparent improvement in the Rotarod performance of CMVMJD135 lithium-treated mice, however several animals from all the groups have failed to learn this paradigm thus statistical significance was not reached due to low numbers of valid trials. On the other hand, the treatment with the combination of temsirolimus and lithium was deleterious to both wild-type and transgenic animals.

**Introduction**

Machado-Joseph disease (MJD), also known as Spinocerebellar Ataxia type 3 (SCA3), is the most common autosomal dominant ataxia worldwide and is caused by a CAG repeat expansion within the coding region of the ATXN3 gene (Kawaguchi et al., 1994). The clinical variability of the phenotype as well as the age of onset depend on the length of the expanded repeat (Maciel et al., 1995; Paulson, 1999; Gusella and MacDonald, 2000). MJD is a late-onset progressive disease characterized by motor uncoordination and weakness in the arms and legs, spasticity, gait ataxia, difficulty with speech and swallowing, altered eye movements, double vision, and frequent urination (Coutinho and Sequeiros, 1981; Sequeiros and Coutinho, 1993).

MJD shares many features with the other polyQ diseases, such as the formation of cytoplasmic and nuclear inclusions within neurons by the mutant protein (Becher et al., 1998; Wolozin and Behl, 2000). It is assumed that the common toxic gain-of-function mechanisms for the polyQ-containing proteins depend on aggregation and deposition of misfolded proteins leading to neuronal dysfunction and eventually cell death (Winklhofer et al., 2008). Despite the fact that the majority of the proteins associated with spinocerebellar neurodegenerative diseases are widely expressed, the resulting cytotoxicity is in most cases restricted to a few neuronal subtypes of the Central Nervous System (CNS) (Orr and Zoghbi, 2007). Selective cellular conditions and specific protein–protein interactions might confer sensibility to protein misfolding and local insolubility conditions, leading to oligomerization and fibrillization in vulnerable neurons.

Despite well-described clinical and pathological phenotypes, the molecular and cellular events that underlie neurodegeneration in these disorders are still poorly understood. Compelling evidence points to major aetiological roles for interference with transcriptional regulation, protein aggregation and clearance, the ubiquitin-proteasome system and alterations of calcium homeostasis in the neuronal loss observed during the neurodegenerative process. But novel molecular pathways that might be disrupted during disease progression are starting to be identified. These pathways could act independently or, more likely, interact and enhance each other, triggering the accumulation of cellular damage that eventually leads to dysfunction and, ultimately, the demise of neurons through a series of multiple events (Duenas et al., 2006). This suggests that simultaneous targeting of several pathways might be therapeutically necessary to prevent neurodegeneration and preserve neuronal function. The increased (albeit incomplete) understanding of how dysregulation of these pathways mediate disease progression is leading to the first attempts of testing therapeutic



#### **Chapter 4.** Autophagy activation

strategies *in vivo*, which may prove beneficial in the treatment of polyQ diseases. One of such pathways is autophagy, a process resulting by lysosomal degradation of cytoplasmic material, such as defective organelles and unfolded/aggregating proteins.

Rapamycin, an inducer of autophagy, reduces the aggregation of expanded polyQ in transfected cells (Ravikumar et al., 2002), protects against neurodegeneration in a fly model of Huntington disease and improves performance on behavioural tests and decreases aggregate formation in a mouse model of Huntington disease (Ravikumar et al., 2004). Temsirolimus (cell cycle inhibitor-779), a less toxic rapamycin analogue, has been shown to reduce mutant ataxin-3 levels and toxicity and described to ameliorate the disease symptoms in a transgenic mouse model of MJD (Menzies et al., 2010). However, the mouse model used in this study did not display an evident phenotype that could be clearly observed to be altered by drug treatment and thus the need for further validation of the findings was advanced by the authors.

Lithium, an mTOR- independent autophagy inducer was shown to improve motor performance and depression in a mouse model of HD (Wood and Morton, 2003) and to improve neurological function and hippocampal dendritic arborization in a SCA1 mouse model (Watase et al., 2007). Very recently, Rilmenidine, an anti-hypertensive drug, has also been shown to induce autophagy and attenuate the symptoms in a mouse model of HD, by improving the signs of the disease and reducing the amount of the mutant huntingtin fragment (Rose et al., 2010). Based on these findings, induction of autophagy may be an effective therapeutic strategy for this group of disorders, caused by misfolded proteins that are prone to aggregate. In this work, we treated MJD transgenic animals (Chapter 3) chronically with lithium alone (m-TOR-independent pathway) and with temsirolimus plus lithium (m-TOR-dependent and independent pathways, respectively).

**Material and methods****Animals**

Male mice were used in the study since they were expected to show less variability than females in behavioral tests, due to the hormonal female status. Transgenic and non-transgenic drug- and placebo- treated animals were housed at weaning in groups of 5 animals per cage. The progeny produced by mating MJD transgenic with wild-type animals were genotyped at weaning by PCR, as we previously described (Silva-Fernandes et al., 2010). The experiment started at 4 weeks and ended at 24 weeks of age.

All animals were maintained under standard laboratory conditions: an artificial 12 h light/dark cycle (lights on from 8:00 to 20:00 h), with an ambient temperature of  $21 \pm 1$  °C and a relative humidity of 50–60%; the mice were given a standard diet (4RF25 during the gestation and postnatal periods, and 4RF21 after weaning, Mucedola SRL, Settimo Milanese, Italy) and water ad libitum. Health monitoring was performed according to FELASA guidelines (Nicklas et al., 2002), confirming the Specified Pathogen Free health status of sentinel animals maintained in the same animal room. All procedures were conducted in accordance with European regulations (European Union Directive 86/609/EEC). Animal facilities and the people directly involved in animal experiments (SS, ASF, ANC) were certified by the Portuguese regulatory entity – Direcção Geral de Veterinária. All of the protocols performed were approved by the joint Animal Ethics Committee of the Life and Health Sciences Research Institute, University of Minho and IBMC, University of Porto.

**Drug treatment**

The experiment was organized in two arms in which autophagy was induced through two different pathways. For that, we used two different FDA approved compounds, Lithium (Merck) and the conjugation of Lithium and CCI-779 (LC Laboratories). Mice were randomly allocated to LiCl-, placebo-, LiCl+CCI779-treated groups. The final numbers of animals in each group were as follows: LiCl-treated CMVMJD135, n = 10; placebo-treated CMVMJD135, n = 12; LiCl+CCI779-treated CMVMJD135, n=7; LiCl-treated wt, n = 10; placebo-treated wt, n = 12; LiCl+CCI779-treated wt, n=15. The average age at which treatment began was 10 weeks 3 days  $\pm$  5 days (standard deviation).

## **Chapter 4.** Authophagy activation

We used a total of 60 animals, which were housed according to the drug administered, since the experiment was carried out by two experimenters who were blind only to the genetic status of the animals. The treatment started at the asymptomatic age of 5 weeks (see Chapter 3).

Animals were intraperitoneally injected three times a week, except in the week of behavioral tests. Transgenic and non-transgenic animals were treated with 10,4 mg/kg of Lithium as previously described (Wood and Morton, 2003); the same number of transgenic and non-transgenic animals were treated with a solution containing 10,4 mg/kg of Lithium and 20 mg/kg of Temeirolimus (previously described by (Ravikumar et al., 2004)). Lithium stock solutions were prepared at a concentration of 25mg/kg in 0.15 M NaCl, 5% Tween-20 and 5% PEG 400 and Temeirolimus at 50mg/kg in absolute ethanol. Control animals were given a placebo of injection buffer (0.15 M NaCl, 5% Tween-20 and 5% PEG 400) with the same frequency.

### **Weight**

All mice were weighed a week before the start of the drug treatment (4 weeks) and then at 5, 6, 8, 9, 10, 12, 13, 14, 16 weeks of age. Data were converted to percentage change in body weight compared to baseline, this being assessed at the last week before the onset of drug treatment.

### **Behavioral tests**

At 4 weeks of age we tested the motor performance and screened the overall status of the animals by using the Rotarod apparatus and the SHIRPA protocol, respectively, before starting the treatment with the different compounds. The animals were evaluated at 4, 8, 12 and 16 weeks of the in the Rotarod and at 20 and 24 weeks of age in the Beam balance test. The SHIRPA protocol was performed at all ages tested as previously described (Silva-Fernandes et al., 2010).

### **RotaRod analysis**

Mice were tested in a rotarod apparatus (TSE systems, Bad Homburg, Germany) to evaluate their motor performance. The protocol consisted of 3 days of training at a constant speed (15 rpm) for a maximum of 60 s in four trials, with a 10 min interval between each trial. On the fourth day, animals were tested for each of 5 different speeds (8 rpm, 15 rpm, 20 rpm, 24 rpm and 31 rpm) for a maximum of 60 s in two trials, with a 10-min-long interval between each trial. After a one-hour rest period, the animals were subjected to four trials on an acceleration rod (4–40 rpm, 5 min) with a 10–15-long interval between each trial.

### **SHIRPA protocol**

We established a protocol for phenotypic assessment based on the primary screen of the SHIRPA protocol, which mimics the diagnostic process of general neurological and psychiatric examination in humans (Rogers et al., 1997). Each mouse was placed in a viewing jar (15 cm diameter) for 5 min, transferred to a 15-labeled-squares arena (55×33×18 cm), and then a series of anatomical and neurological measures were determined. The full details of the SHIRPA protocol are available at the site: [http://www.mgu.har.mrc.ac.uk/facilities/mutagenesis/mutabase/shirpa\\_summary.html](http://www.mgu.har.mrc.ac.uk/facilities/mutagenesis/mutabase/shirpa_summary.html). In addition, we included the footprint pattern test (Carter et al., 1999), the hanging wire grip test, the vertical pole test, and the counting of rears over 5 min in the viewing jar as a measure of spontaneous exploratory activity. The protocol was adjusted in order to minimize animal handling and to generate uniformity in waiting times between the tests (Rafael et al., 2000).

### **Footprint pattern**

The footprint test was used to evaluate the gait of the animals. To obtain footprints, the hind- and forepaws of the mice were coated with black and red non-toxic paints, respectively. A clean sheet of paper was placed on the floor of the runway for each run. The animals were then allowed to walk along a 100-cm-long×4.2 cm width×10 cm height corridor in the direction of an enclosed black box. Each animal was allowed to achieve one valid trial per age. The footprint patterns were analyzed for four step parameters (all measured in cm): the front- and hind-base width, the foot step uniformity and the length of the step. For each step parameter, values were measured for three consecutive steps, with the exclusion of the first four steps to allow training.

### **Statistical analysis**

Behavioral data were subjected to the non-parametric Mann-Whitney U-test when variables were non-continuous or when a continuous variable did not present a normal distribution (Kolmogorov-Smirnov test  $p < 0.05$ ). Continuous variables with normal distributions (K-S test  $p > 0.05$ ) were analyzed with the Student's t test or Repeated-Measures ANOVA. All statistical analyses were performed using SPSS 16.0 (SPSS Inc., Chicago, IL). A critical value for significance of  $p < 0.05$  was used throughout the study.

Results

Transgenic mice overexpressing full-length human ataxin-3 with an expanded polyQ repeat of 135 glutamines have previously been shown to develop a neuropathological phenotype (Silva-Fernandes et al., in preparation). CMVMJD135 mice manifest MJD-like motor symptoms beginning at two months, when they present a loss of limb strength, given by a significant decrease in the time in the hanging-wire-grip and in the vertical pole test. At 3 months of age animals developed a balance deficit in the beam test and at 4-5 months of age they displayed motor uncoordination in the Rotarod, in addition to tremors, foot dragging and limb claspings and grasping. Locomotor and exploratory activity was decreased in transgenic mice at this stage.

We treated CMVMJD135 transgenic mice with lithium, or lithium + temsirolimus at dosages previously described to activate autophagy (Wood and Morton, 2003; Ravikumar et al., 2004). Before the beginning of injections, at 4 weeks of age, mice were evaluated by the SHIRPA protocol and Rotarod test, and no differences were observed between wild-type and transgenic animals or between placebo and treatment groups.

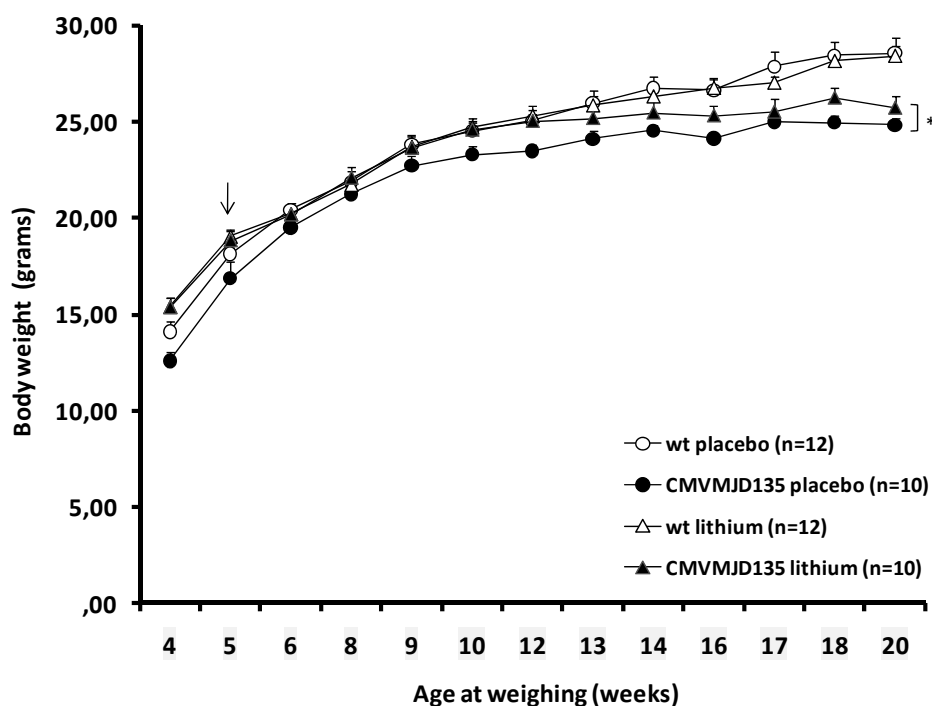


**Figure 1.** Lithium treatment effect on body weight of CMVMJD135 mice and wt animals. The body weight in grams between 4 to 20 weeks of age was depicted for wt and CMVMJD135 mice treated with LiCl or vehicle. Symbols represent mean ± SEM of the different groups. The arrow indicates the beginning of drug administration.

**Lithium treatment****Weight**

Administration of LiCl to WT mice had no effect on body weight compared to vehicle-treatment in control mice. Since 12 weeks of age, vehicle-treated CMVMJD135 mice showed a significant decrease in body weight in comparison with wild-type animals ( $p=0,009$ ). In contrast, CMVMJD135 mice treated with lithium displayed a slightly higher body weight when compared to the vehicle-treated transgenic group ( $p=0,041$ ) (Figure 1). However, since the placebo and lithium-treated transgenic groups already showed differences at 4 weeks (before treatment) ( $p=0,001$ ), we compared the percentual gain of weight; no differences were observed between vehicle- and lithium-treated transgenic animals.

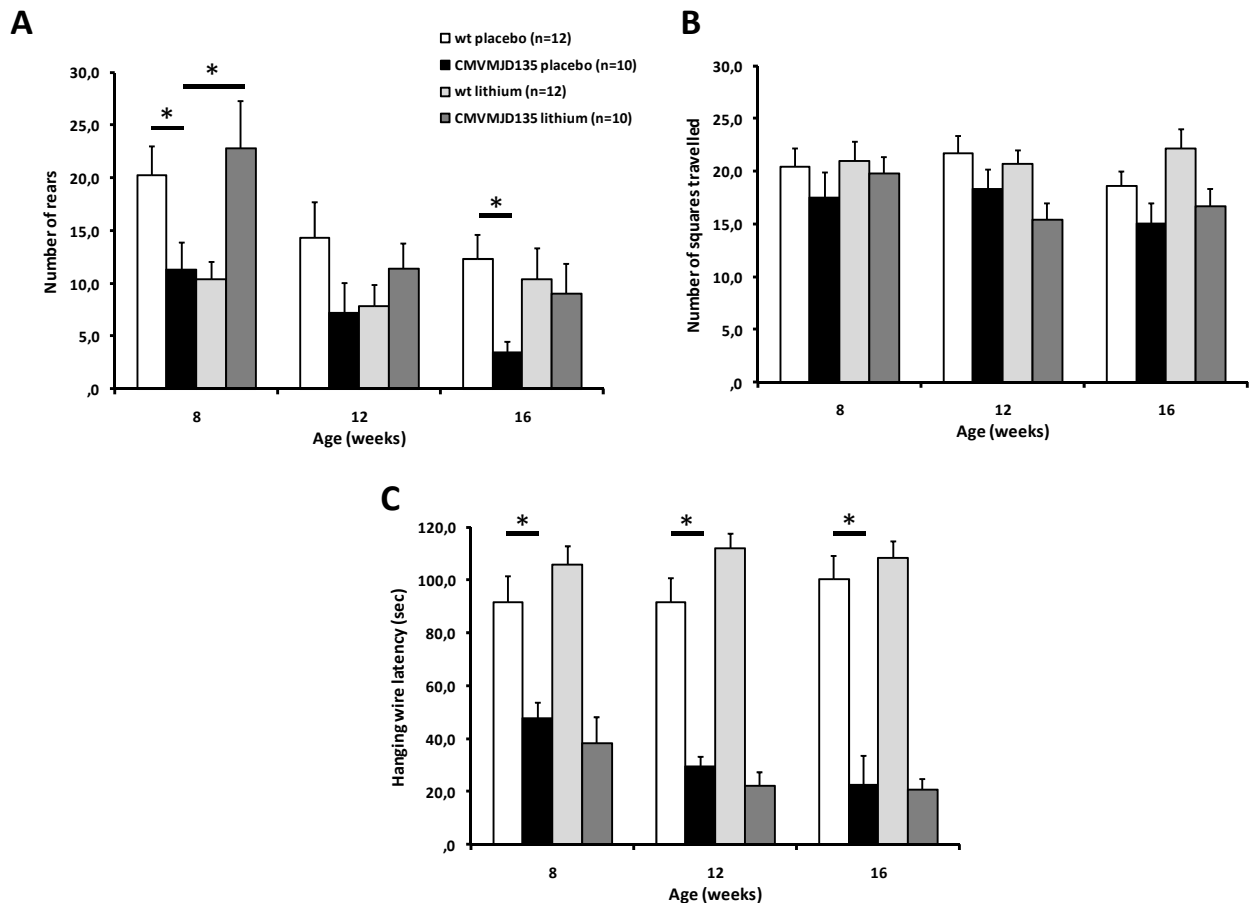


**Figure 2.** Lithium treatment effect in the phenotype of CMVMJD135 mice evaluated by SHIRPA protocol. Asterisks indicate significant differences between wild-type control and CMVMJD135 transgenic mice. Vertical bars represent mean  $\pm$  SEM of the different groups on each test, ( $*p<0.05$ ).

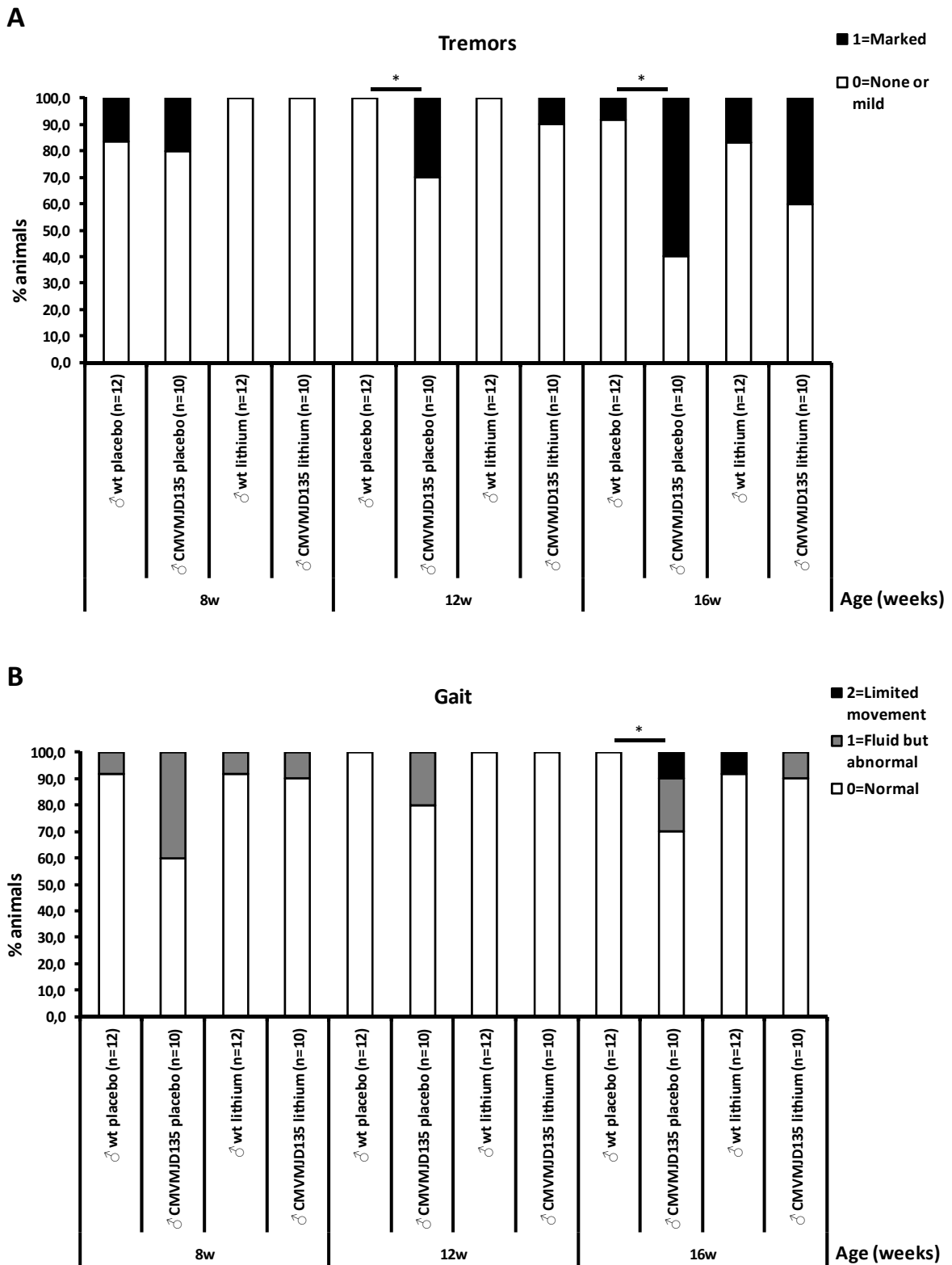


**Figure 3.** Lithium treatment did not affect the effect in the phenotype of CMVMJD135 mice evaluated by SHIRPA protocol, namely the tremors (A) and gait (B). Asterisks indicate significant differences between the animal groups (\* $p < 0.05$ ).

**SHIRPA protocol**

At 8 weeks of age, CMVMJD135 animals treated with lithium showed an increased exploratory activity when compared to placebo-treated transgenics, given by the significant increase in number of rears in the viewing jar ( $p=0,039$ ), reaching the same performance as the wt placebo group (Figure 2A). Intriguingly, wild-type animals treated with lithium showed a significant decrease in the number of rears when compared with wild-type animals treated with placebo at 8 weeks of age ( $p=0,005$ ). At 12 and 16 weeks of age, although CMVMJD135 mice treated with lithium showed a trend towards an increase in the number of rears when compared to the CMVMJD135 placebo group, there was no statistical significance to this difference (Figure 2A). Locomotor activity, given by the counting of the numbers of squares travelled in the arena used in the SHIRPA protocol, did not differ significantly between wt and transgenic animals treated with placebo, although there was a tendency for this activity to be diminished. CMVMJD135 mice treated with lithium displayed no differences in the locomotor activity when compared with CMVMJD135 mice treated with placebo (Figure 2B). As previously described, since the age of 8 weeks CMVMJD135 mice displayed a significant deficit in the hanging wire test. Lithium treatment had no effect in the performance of wild-type animals and transgenic groups in this test (Figure 2C). In the same manner, the treatment of CMVMJD135 mice with lithium did not ameliorate the tremors nor the abnormal gait observed in transgenic mice (Figure 3 A,B)

**Rotarod test**

In the Rotarod test, although the lithium transgenic group appeared to have a better performance than the placebo group, several animals from the wild-type and transgenic groups have failed to learn this paradigm, falling (or letting themselves fall) very quickly. This reduced the number of valid trials and impeached statistical validation (data not shown).

**Footprinting test**

Gait abnormalities were assessed by analyzing the footprint pattern of mice while they walked along a ramp corridor. As described previously, CMVMJD135 mice demonstrated a clear foot dragging, but regarding the measurement of the stride length, hindbase width, frontbase width, and front footprint/hind footprint overlap we did not find any strong differences until 19 weeks of age. We did not observe differences in these four parameters (Figure 4A-D) nor in the percentage of animals displaying foot-dragging between transgenic animals treated with placebo versus lithium (Figure 4E).



**Chapter 4.** Autophagy activation

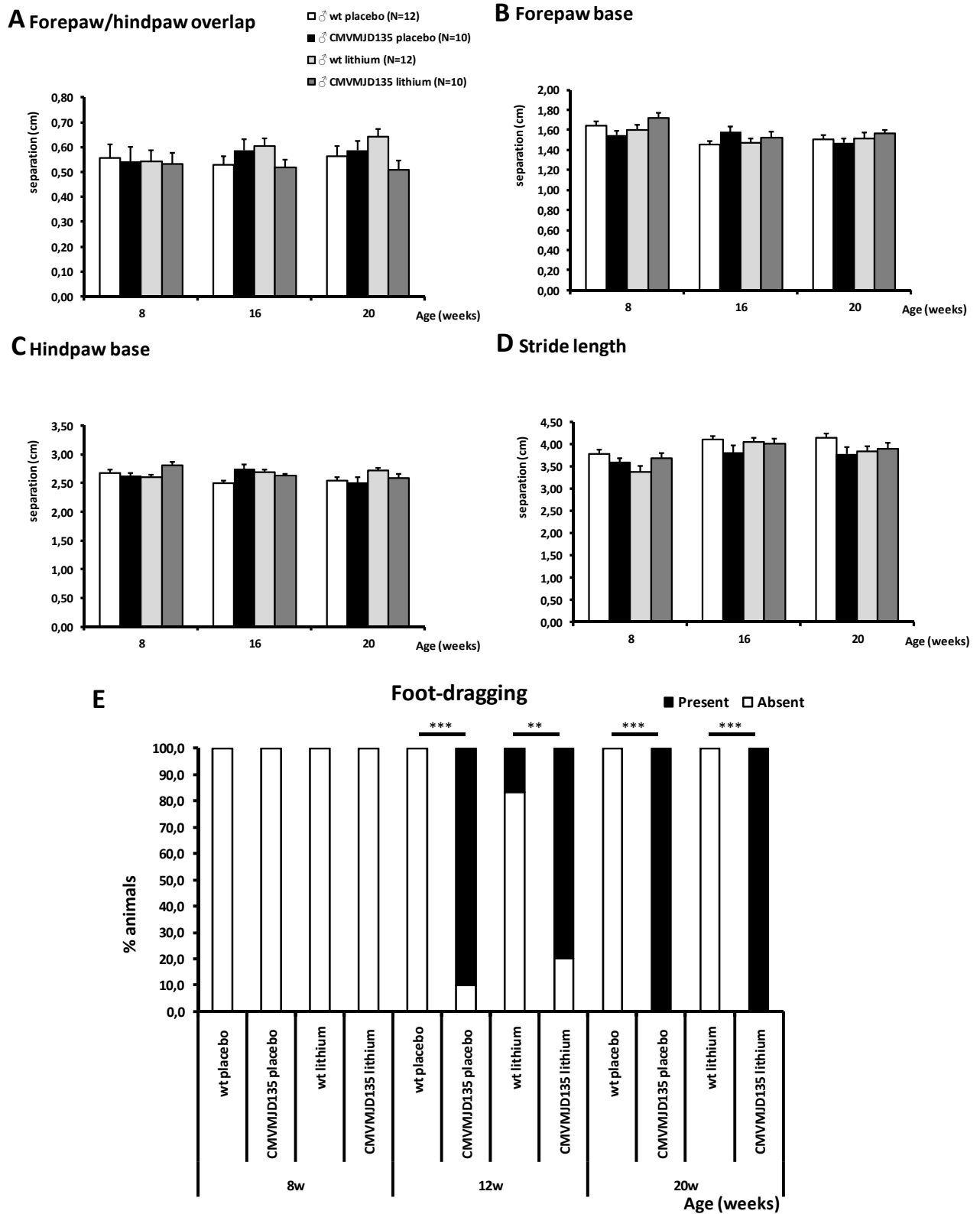


**Figure 4.** Quantitative analysis of the walking footprint patterns produced by wild-type and transgenic mice treated with lithium, based on measurements of stride length (D), hindbase width (C), frontbase width (B), and distance between front and hind footprint placement or overlap (A). Vertical bars represent mean  $\pm$  SEM of the different groups on each test. Percentage of animals displaying foot-dragging (E).

**Lithium+CCI-779 treatment****Weight**

Administration of LiCl+CCI779 to wt mice caused a significant decrease in body weight in comparison to the placebo group ( $p=0,002$ ). This drug combination treatment also diminished significantly the body weight of CMVMJD135 mice when compared to the transgenic vehicle group ( $p=0,001$ ) (Figure 5).

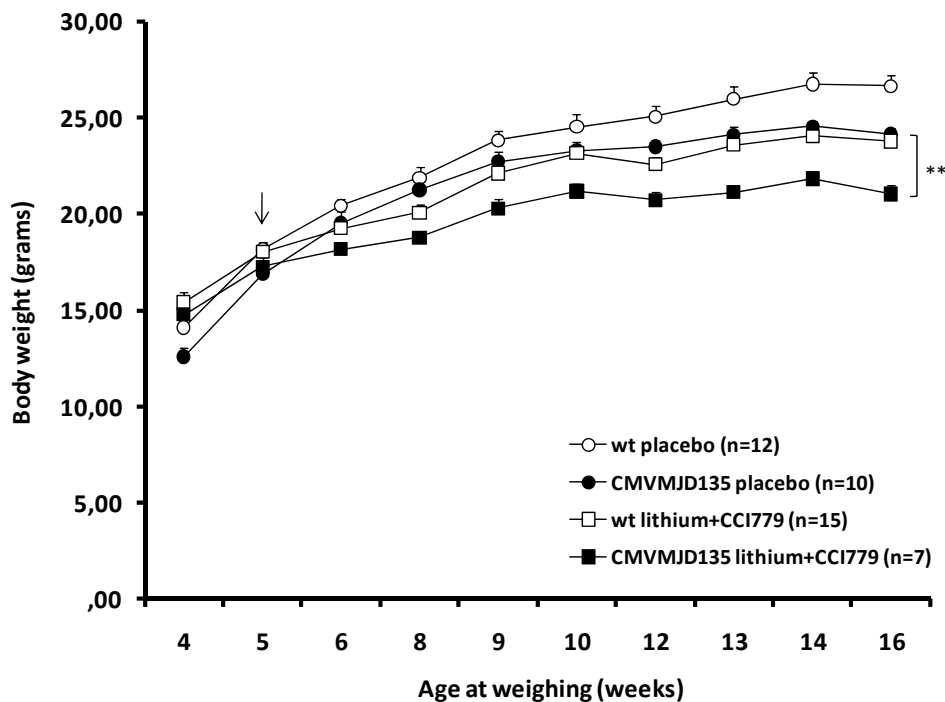


**Figure 5.** Effect of treatment with Lithium+CCI779 in body weight of CMVMJD135 mice and wt animals. The body weight in grams between 4 to 20 weeks of age was depicted for wt and CMVMJD135 mice treated with LiCl+CCI-779 or vehicle. Individual symbols represent mean  $\pm$  SEM of the different groups. The arrow indicates the beginning of drug administration.

**SHIRPA protocol**

At 8 and 16 weeks of age, when CMVMJD135 animals treated with placebo showed a significant decrease in the exploratory activity, transgenic animals treated with lithium+CCI-779 showed an increased exploratory activity, given by the significant increase in the number of rears in the viewing jar ( $p=2,38 \times 10^{-4}$  and  $p=0,008$ , respectively), reaching the same performance as the wt placebo group (Figure 6A). CMVMJD135 mice treated with lithium+CCI-779 also demonstrated a significant increase in the locomotor activity when compared to CMVMJD135 mice treated with placebo at 8

## Chapter 4. Autophagy activation

and 12 weeks of age ( $p=0,018$  and  $p=0,020$ , respectively). However, (i) at 8 weeks wild-type animals treated with lithium+CCI-779 also displayed an increased activity and (ii) at these ages, there were no significant differences between wild-type and transgenic placebo groups in the number of squares travelled in the arena, which means that the observed increase in activity could be related with a general effect of the drug in the animal (Figure 6B). No positive effect of the treatment was observed in the hanging wire test (Figure 6C), gait and tremors (Figure 7).

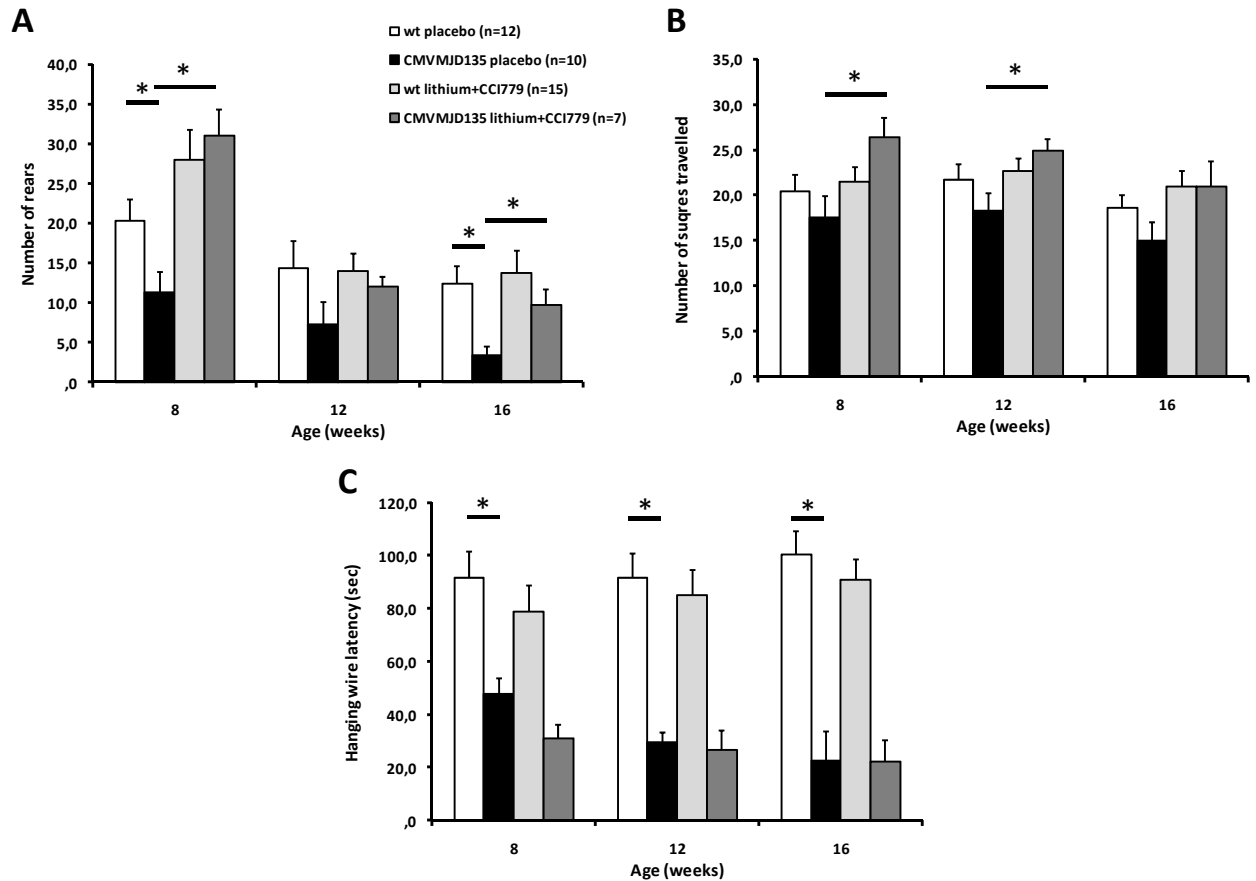


**Figure 6.** Lithium+CCI-779 treatment effect in the phenotype of CMVMJD135 mice as assessed by the SHIRPA protocol. Asterisks indicate significant differences between wild-type control and CMVMJD135 transgenic mice. Vertical bars represent mean  $\pm$  SEM of the different groups on each test, ( $*p<0.05$ ).

### Footprinting test

Footprint patterns of wild-type and CMVMJD135 transgenic mice treated with placebo or lithium+CCI-779 were analyzed for the four parameters described above, as well as concerning the presence of foot-dragging. We did not observe differences in these four parameters evaluated between transgenic animals treated with placebo or with lithium+ CCI-779 (Figure 8A-D). If anything,

there seemed to be a trend for this treatment to cause/worsen foot-dragging in both genotypes, suggesting that the treatment may have neurotoxic effects (Figure 8E).

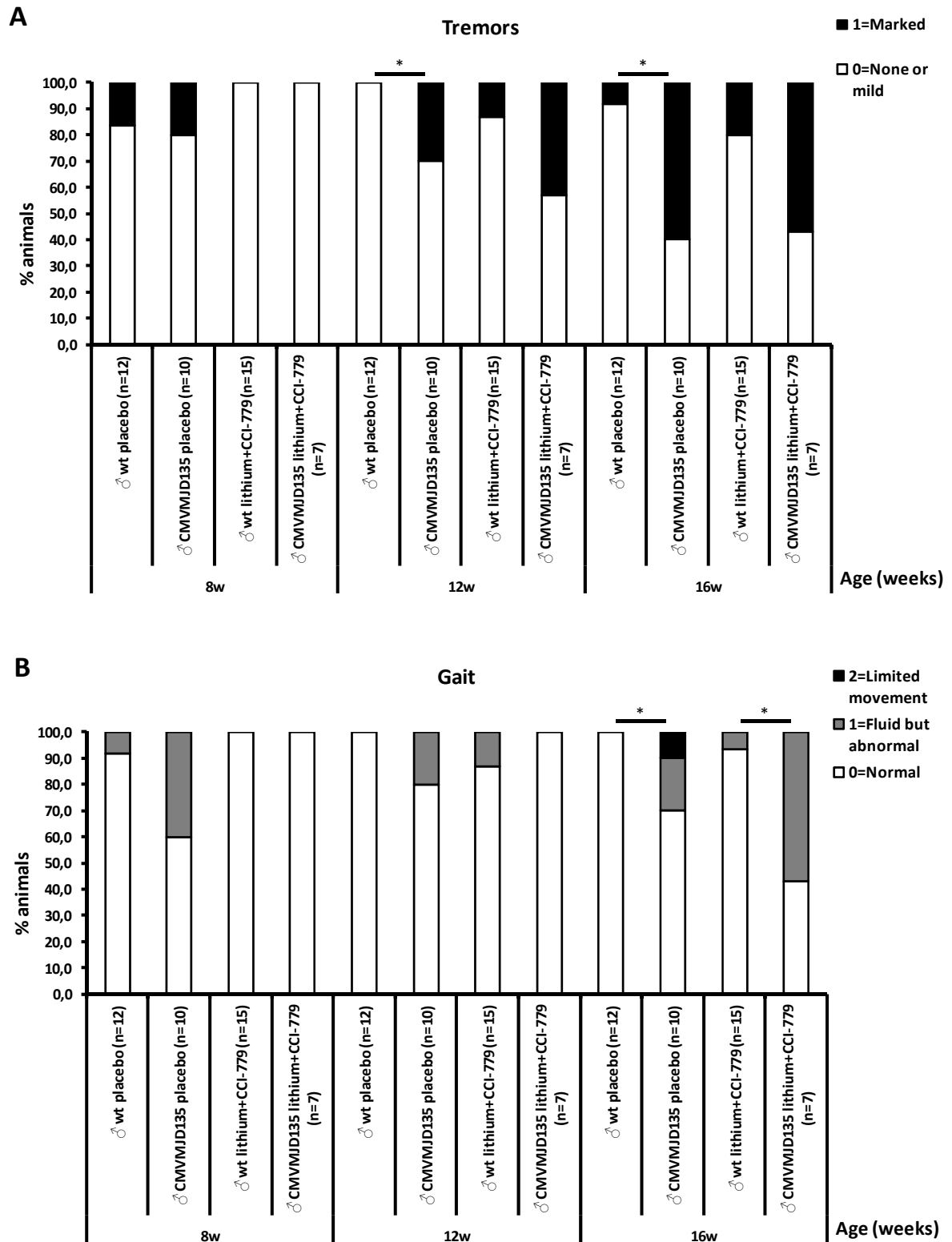


**Figure 7.** Lithium and CCI-779 combined treatment did not improve the phenotype of CMVMJD135 mice evaluated by SHIRPA protocol namely the tremors (A) and gait (B). Asterisks designate significant differences between the animal groups (\*p<0.05).

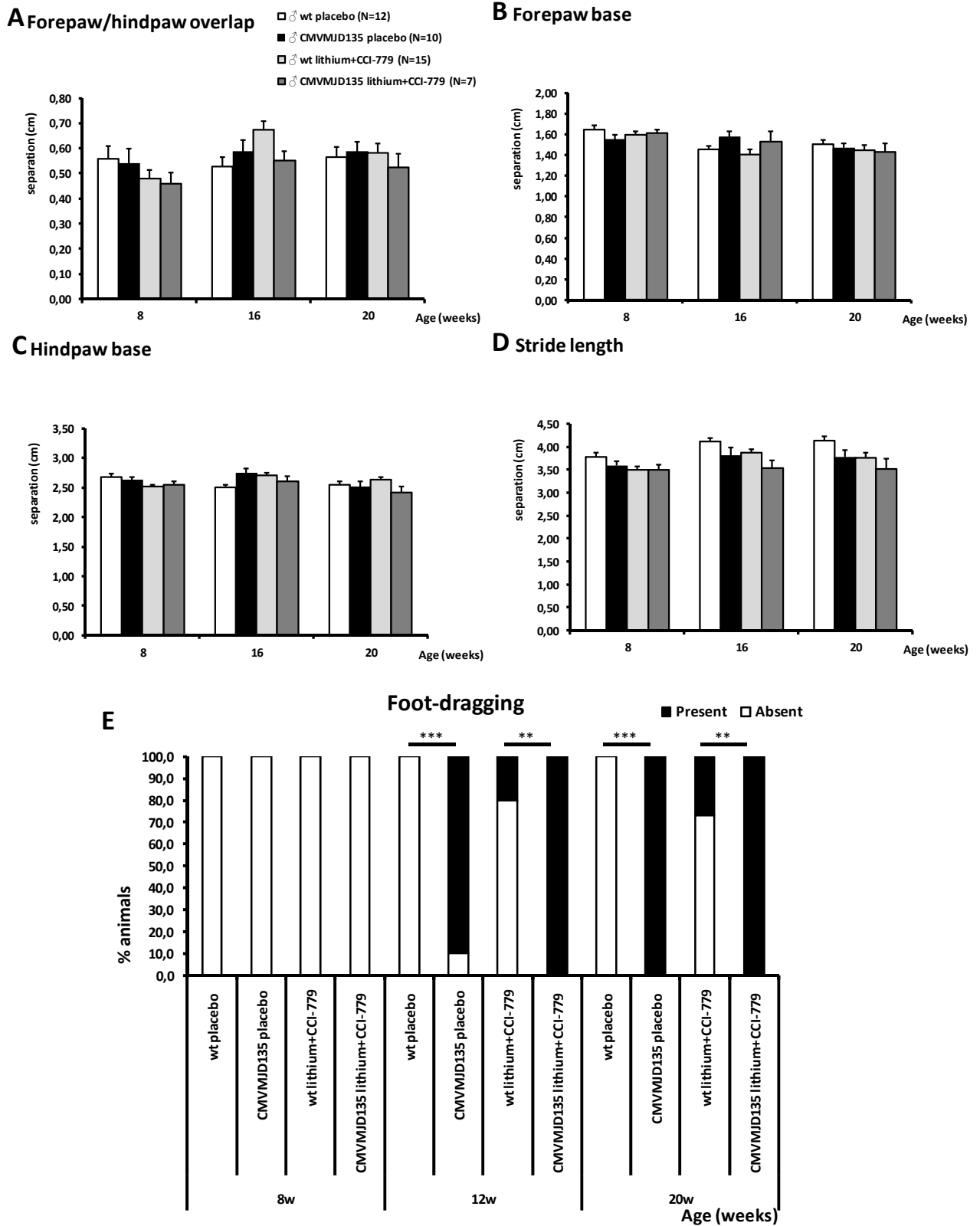


**Figure 8.** Quantitative analysis of the walking footprint patterns produced by wild-type and transgenic mice treated with lithium+CCI-779, based on measurements of stride length (D), hindbase width (C), frontbase width (B), and distance between front and hind footprint placement or overlap (A). Vertical bars represent mean  $\pm$  SEM of the different groups on each test. Percentage of animals displaying foot-dragging (E).

**Discussion**

One promising therapeutic strategy in diseases associated with misfolded protein accumulation is the stimulation of cellular degradation pathways such as macroautophagy. Here we have tested the effect of autophagy activation by lithium and by the combination of lithium and temsirolimus in a MJD mouse model beginning at a pre-symptomatic age. It has been demonstrated in another mouse model of MJD that temsirolimus treatment resulted in an improvement in motor coordination as measured by rotarod performance (Menzies et al., 2010). However, the mouse model used in this study has a very mild phenotype observable only in the Rotarod. Our MJD mouse model could be helpful to test and validate this therapeutic strategy further, due to its more severe phenotype including a broad range of disease features including motor uncoordination/ataxia, loss of limb strength and a locomotor and exploratory activity deficit.

We have observed that wild-type and transgenic animals treated with lithium+ temsirolimus, had a significant decrease in body weight during the treatment period. This body weight loss in both groups could be due to an exacerbated activation of autophagy by the combination of these two drugs. The doses used in this work for autophagy activation had already been tested in the mouse, but separately (Wood and Morton, 2003; Ravikumar et al., 2004). Probably, the combination of these two doses has led to an exacerbated activation of autophagy with deleterious effects for the mice. Interestingly, we observed that CMVMJD135 mice treated with lithium displayed a slightly higher body weight, but a similar percentual gain of weight, when compared to vehicle-treated CMVMJD135 mice. Whereas wild-type animals treated with lithium showed no differences in body weight when compared to vehicle-treated wild-type animals, it has been reported previously that treatment with LiCl pre-symptomatically caused loss of body weight in a HD mouse model and a gain of body weight when LiCl treatment was performed in post-symptomatic animals (Wood and Morton, 2003). Although the eventual gain weight seen in CMVMJD135 mice with lithium treatment might be interpreted as a sign of improved health, several of the marked neurological manifestations seen in CMVMJD135 mice, namely the loss of balance and limb strength as well as the presence of foot-dragging and tremors were not reverted by the treatment with lithium or lithium+CCI-779.

At 8 weeks of age, CMVMJD135 mice demonstrated a deficit in the exploratory behavior given by their reduced number of rears. Lithium treatment rescued this deficit at this age, however at 12 and 16 weeks of age the amelioration in exploratory activity did not reach statistical significance. The effect was most pronounced in young mice possibly because exploratory activity of animals declined

#### **Chapter 4.** Autophagy activation

with age or because animals were reincident in this task and became less curious to explore. The combined treatment of lithium and CCI-779 also led to a significant increase in the number of rears of transgenic mice at 8 and 16 weeks of age. Locomotor activity was also improved in CMVMJD135 mice treated with lithium+CCI-779 when compared to vehicle transgenic mice. The positive effect of drug treatment in the exploratory and locomotor activity of transgenic mice could however, also be related to an effect of the drug in the level of activity of the animal, being independent of the putative MJD phenotype amelioration.

In summary, our results do not validate the use of lithium or lithium+CCI-779, in the dosages here used, as therapeutic strategies for MJD. Although we did not observe a remarkable amelioration of the phenotype of CMVMJD135 mice it could also be important to evaluate if the number of ataxin-3 inclusions in the brains has decreased.

## References

- Becher, M. W., Kotzuk, J. A., Sharp, A. H., Davies, S. W., Bates, G. P., Price, D. L. and Ross, C. A. 1998. Intranuclear neuronal inclusions in Huntington's disease and dentatorubral and pallidolusian atrophy: correlation between the density of inclusions and IT15 CAG triplet repeat length. *Neurobiol Dis.* 4, 387-397.
- Carter, R. J., Lione, L. A., Humby, T., Mangiarini, L., Mahal, A., Bates, G. P., Dunnett, S. B. and Morton, A. J. 1999. Characterization of progressive motor deficits in mice transgenic for the human Huntington's disease mutation. *J Neurosci.* 19, 3248-3257.
- Coutinho, P. and Sequeiros, J. 1981. [Clinical, genetic and pathological aspects of Machado-Joseph disease]. *J Genet Hum.* 29, 203-209.
- Duenas, A. M., Goold, R. and Giunti, P. 2006. Molecular pathogenesis of spinocerebellar ataxias. *Brain.* 129, 1357-1370.
- Gusella, J. F. and MacDonald, M. E. 2000. Molecular genetics: unmasking polyglutamine triggers in neurodegenerative disease. *Nat Rev Neurosci.* 1, 109-115.
- Kawaguchi, Y., Okamoto, T., Taniwaki, M., Aizawa, M., Inoue, M., Katayama, S., Kawakami, H., Nakamura, S., Nishimura, M., Akiguchi, I. and et al. 1994. CAG expansions in a novel gene for Machado-Joseph disease at chromosome 14q32.1. *Nat Genet.* 8, 221-228.
- Maciel, P., Gaspar, C., DeStefano, A. L., Silveira, I., Coutinho, P., Radvany, J., Dawson, D. M., Sudarsky, L., Guimaraes, J., Loureiro, J. E. and et al. 1995. Correlation between CAG repeat length and clinical features in Machado-Joseph disease. *Am J Hum Genet.* 57, 54-61.
- Menzies, F. M., Huebener, J., Renna, M., Bonin, M., Riess, O. and Rubinsztein, D. C. 2010. Autophagy induction reduces mutant ataxin-3 levels and toxicity in a mouse model of spinocerebellar ataxia type 3. *Brain.* 133, 93-104.
- Nicklas, W., Baneux, P., Boot, R., Decelle, T., Deeny, A. A., Fumanelli, M. and Illgen-Wilcke, B. 2002. Recommendations for the health monitoring of rodent and rabbit colonies in breeding and experimental units. *Lab Anim.* 36, 20-42.
- Orr, H. T. and Zoghbi, H. Y. 2007. Trinucleotide repeat disorders. *Annu Rev Neurosci.* 30, 575-621.
- Paulson, H. L. 1999. Protein fate in neurodegenerative proteinopathies: polyglutamine diseases join the (mis)fold. *Am J Hum Genet.* 64, 339-345.
- Rafael, J. A., Nitta, Y., Peters, J. and Davies, K. E. 2000. Testing of SHIRPA, a mouse phenotypic assessment protocol, on Dmd(mdx) and Dmd(mdx3cv) dystrophin-deficient mice. *Mamm Genome.* 11, 725-728.
- Ravikumar, B., Duden, R. and Rubinsztein, D. C. 2002. Aggregate-prone proteins with polyglutamine and polyalanine expansions are degraded by autophagy. *Hum Mol Genet.* 11, 1107-1117.
- Ravikumar, B., Vacher, C., Berger, Z., Davies, J. E., Luo, S., Oroz, L. G., Scaravilli, F., Easton, D. F., Duden, R., O'Kane, C. J. and Rubinsztein, D. C. 2004. Inhibition of mTOR induces autophagy and reduces toxicity of polyglutamine expansions in fly and mouse models of Huntington disease. *Nat Genet.* 36, 585-595.
- Rogers, D. C., Fisher, E. M., Brown, S. D., Peters, J., Hunter, A. J. and Martin, J. E. 1997. Behavioral and functional analysis of mouse phenotype: SHIRPA, a proposed protocol for comprehensive phenotype assessment. *Mamm Genome.* 8, 711-713.
- Rose, C., Menzies, F. M., Renna, M., Acevedo-Arozena, A., Corrochano, S., Sadiq, O., Brown, S. D. and Rubinsztein, D. C. 2010. Rilmenidine attenuates toxicity of polyglutamine expansions in a mouse model of Huntington's disease. *Hum Mol Genet.* 19, 2144-2153.
- Sequeiros, J. and Coutinho, P. 1993. Epidemiology and clinical aspects of Machado-Joseph disease. *Adv Neurol.* 61, 139-153.
- Silva-Fernandes, A., Costa Mdo, C., Duarte-Silva, S., Oliveira, P., Botelho, C. M., Martins, L., Mariz, J. A., Ferreira, T., Ribeiro, F., Correia-Neves, M., Costa, C. and Maciel, P. 2010. Motor



#### **Chapter 4.** Autophagy activation

uncoordination and neuropathology in a transgenic mouse model of Machado-Joseph disease lacking intranuclear inclusions and ataxin-3 cleavage products. *Neurobiol Dis.* 40, 163-176.

Watase, K., Gatchel, J. R., Sun, Y., Emamian, E., Atkinson, R., Richman, R., Mizusawa, H., Orr, H. T., Shaw, C. and Zoghbi, H. Y. 2007. Lithium therapy improves neurological function and hippocampal dendritic arborization in a spinocerebellar ataxia type 1 mouse model. *PLoS Med.* 4, e182.

Winklhofer, K. F., Tatzelt, J. and Haass, C. 2008. The two faces of protein misfolding: gain- and loss-of-function in neurodegenerative diseases. *Embo J.* 27, 336-349.

Wolozin, B. and Behl, C. 2000. Mechanisms of neurodegenerative disorders: Part 1: protein aggregates. *Arch Neurol.* 57, 793-796.

Wood, N. I. and Morton, A. J. 2003. Chronic lithium chloride treatment has variable effects on motor behaviour and survival of mice transgenic for the Huntington's disease mutation. *Brain Res Bull.* 61, 375-383.

# Chapter 5

---

Discussion and future perspectives



Transgenic technology has promoted the establishment of animal models for human genetic disorders which have been crucial to test hypotheses about the mechanisms underlying the disease and to develop and test treatment strategies. In particular, mouse models have been the experimental model of choice in biomedical research due to the remarkable genetic similarity to humans, their small size and low cost maintenance, as well as their short lifespan and fast reproductive rate, allowing the study of disease progression in many individuals throughout their life cycle. Although mouse models have been a remarkable tool in human disease research, several criteria have to be achieved in order to validate a genetically manipulated mouse as a model of a disease. Three criteria are commonly used to validate an animal model (Chadman et al., 2009):

**Construct validity** comprises a conceptual analogy to the **cause** of the human disease. The mouse model has to carry the same biological dysfunction that causes the human disease, such as a gene mutation or anatomical abnormality.

**Face validity:** comprises a conceptual correspondence to the **symptoms/manifestations** of the human disease. Several disease components or endophenotypes may be modeled in animals, namely behavioral symptoms, neuroanatomical pathology, neurophysiological responses, and neurochemical abnormalities.

**Predictive validity** incorporates analogous **response to treatments** that prevent or reverse symptoms in the human disease. In this manner, a specific class of drugs that ameliorates the human symptoms should reverse the traits in the animal model.

In this work, we have created transgenic mice for Machado-Joseph disease and performed an extensive genetic, behavioral and pathological characterization in order to validate them as models for this human disease. Regarding the construct validity, the knowledge of the causative mutation (Kawaguchi et al., 1994) has allowed the generation of cell and animal models for polyQ disease (Marsh et al., 2009) using different versions of mutant human DNA or cDNA, therefore this aspect of the validation is guaranteed. In the case of MJD, the mutation that causes the disorder is an expansion of CAG repeats in the *ATXN3* gene, that ranges (in patients) between 52-86. Our disease models were created by microinjection of a transgene carrying the human cDNA ATXN3c variant carrying a repeat tract coding for 83 (Chapter 2) or 135 polyQs (Chapter 3), into the pCMV vector. Three mouse lineages were established, CMVMJD83, CMVMJD94 and CMVMJD135, expressing human ataxin-3 carrying 83, 94 and 135 glutamines, respectively. Concerning the face validity, we evaluated in these mice models the behavioral and pathological changes that could

resemble MJD. Although the CMVMJD83 mouse is, from the three models generated, the only carrying a CAG repeat tract length previously observed in MJD patients, it did not develop any symptoms of the disease even at more advanced ages (2 years). CMVMJD94 mice developed a mild motor uncoordination phenotype without marked progression, and brain pathology (cell atrophy and gliosis) in the absence of intranuclear inclusions and without apparent cell death. Taking into account these results, we thought it would be necessary to increase the number of CAG repeats, in order to intensify and accelerate the progression of the MJD pathology in a mouse model. In this manner, we generated transgenic animals expressing the expanded ataxin-3 carrying a 135 polyQ tract that manifested a severe phenotype that progresses overtime including loss of limb strength, tremors, motor uncoordination, a balance deficit and an abnormal gait.

Our results could suggest that the CAG threshold to induce MJD symptoms in the mouse may be higher than in humans. Several issues regarding the strategy used in the creation of these transgenic animals that might not completely match with the conditions of the disease in humans, however, could play a role in this threshold difference, namely: (i) the expression of only one isoform of ataxin-3 and (ii) the levels of expression of the transgene. We have used the ataxin-3c isoform, that contains an additional ubiquitin-interacting motif at its C terminus, which has been shown to be expressed in neuronal and non-neuronal tissues (Goto et al., 1997; Schmidt et al., 1998). It has been demonstrated that the expression of the ataxin-3c isoform in transgenic animals driven by a stronger brain promoter (PrP), carrying CAG repeats within the expanded range observed in humans led to the manifestation of motor symptoms (Bichelmeier et al., 2007; Boy et al., 2009; Boy et al., 2010). A YAC model with the entire ATXN3 gene carrying 67, 72 or 84 CAGs under the regulation of its own promoter was also generated, which displayed a mild phenotype (Cemal et al., 2002). Although it is possible that different ataxin-3 isoforms play different roles in the MJD pathogenesis, it is not probable that the behavioral differences observed in the different animals models could be related with the use of a specific isoform of the protein. Indeed, it has been observed that cDNA transgenic mouse models developed a more consistent MJD-like phenotype when compared with the YAC mice (reviewed in (Riess et al., 2008)). Concerning the levels of expression of the transgenic protein, and in agreement with the heterozygous state of most patients, it has been clearly demonstrated that the protein levels of normal and expanded ataxin-3 in human MJD tissues are very similar (Trottier et al., 1995; Paulson et al., 1997a). In our mouse models the protein levels of murine ataxin-3 are higher than human ataxin-3 which could affect (diminish) the manifestation of the disease. Although this could be an important issue in our model, animal models expressing

similar levels of murine and human expanded ataxin-3 have been created, and they display mild behavioral abnormalities (Cemal et al., 2002). Besides these facts, it is also possible that specific features of the mouse species, like the short lifespan or specificities of the cellular mechanism of response to unfolded proteins, could give more resilience to this animal in comparison with humans. Additionally, genetic background differences may be relevant in phenotype manifestation.

Although we had to “challenge” the system with higher CAG repeats, not observed in humans, in order to generate a phenotype, the characterization of this transgenic mouse models at different levels has revealed several similarities with the human disease:

- I. **Presence of behavioral symptoms in hemizyosity genotypes.** This feature is in accordance with the known autosomal dominant transmission of MJD. Interestingly, homozygous transgenic mice displayed more severe symptoms when compared to hemizygous animals. In agreement, homozygous MJD patients have been shown to display an earlier age-at-onset and more severe symptoms, suggesting that gene dosage is an important determinant of age of onset and clinical symptoms (Lang et al., 1994; Lerer et al., 1996; Sobue et al., 1996); i.e. the dominance is incomplete.
- II. **Mendelian segregation.** Several studies have described a distortion of Mendelian segregation patterns for the expanded CAG allele (with a higher transmission of the mutant allele) in human MJD families (Ikeuchi et al., 1996; Riess et al., 1997; Takiyama et al., 1997; Iughetti et al., 1998). However, these results were not widely accepted in the scientific community, because they could be explained by a bias in the selection of the families for the study (Grewal et al., 1999). Our analysis of the transmission of the CMVMJD94 and CMVMJD83 transgenic lineages excluded a “meiotic drive” effect of the expanded allele in these mice, confirming recent results in human families (Bettencourt et al., 2008).
- III. **Intergenerational instability of the expanded allele in maternal and paternal meioses.** CAG instability is one of the main common features of the polyQ diseases, displaying different patterns of CAG variation between them. For most polyQ disorders, a paternal expansion bias has been described, whereas a bias towards expansion is observed in maternal transmissions in FRAXA and DM1. On the other hand, in patients with SCA8, FRDA and FRAXA, a paternal contraction bias has been found (reviewed in (Pearson et al., 2005)). In comparison with the other triplet repeat diseases, the CAG expanded allele in MJD displays one of the lowest degrees of CAG instability; however, both increase and

decrease in size between parents and progeny occur, with larger variations in male than in female transmissions (Maciel et al., 1995). Animal models for polyQ diseases have become very useful in the study of the mechanisms underlying CAG instability. However, a significant number of cDNA transgenic mouse models do not replicate the somatic and germinal instability behaviour observed in human patients (Burrigh et al., 1995; Ikeda et al., 1996; Yvert et al., 2000; Gray et al., 2008). In other cases, the study of the CAG instability has not been performed (Goti et al., 2004; Bichelmeier et al., 2007; Chou et al., 2008). In the case of MJD, the intergenerational instability of the CAG repeat has been studied in our mouse models (CMVMJD94, CMVMJD135) and in a cDNA transgenic mouse model expressing ataxin-3 under the regulation of the *HD* promoter (Boy et al., 2010; Silva-Fernandes et al., 2010). Both works have shown that the CAG repeat tract in MJD mice suffers a mild variation through generations, as happens in MJD families (Maciel et al., 1995), however a transmission gender effect has been observed in these mouse models (paternal transmissions having a bias towards expansions and maternal transmissions towards contractions) that was not observed in humans. To investigate the influence of genetic background on intergenerational instability of the *ATXN3* CAG repeat, we also analyzed CMVMJD94 paternal and maternal transmissions in two different genetic backgrounds (C57Bl/6 and FVB/N). Interestingly, we found a gender effect in the CAG variation only in the C57Bl/6 background, with contractions being more frequent in female meiosis and expansions in male meiosis, while in the FVB/N genetic background a similar frequency of contractions and expansions was observed in both meioses. This is the first study in an MJD model regarding the effect of genetic background in CAG instability. As it was observed in a knock-in HD mouse model, there was no difference in the CAG variation pattern between FVB/N and C57Bl/6 male transmissions (Lloret et al., 2006). However, we observed that the frequency of contractions, expansions, or stable inheritance in the female meioses was different between the two genetic backgrounds (Silva-Fernandes et al., 2010), something that was not evaluated in the study by Lloret and co-workers. Inbred strain-specific differences in instability could be the result of differences a) in the genomic context of the inserted MJD CAG repeat (Brock et al., 1999; Cleary and Pearson, 2003) or b) in protein factors that mediate or protect against repeat instability, such as members of the mismatch repair pathway (Kovtun and McMurray, 2001; van den Broek et al., 2002; Gomes-Pereira et al., 2004). In future studies it will be important to determine the genetic loci involved in the

MJD CAG repeat instability variation pattern, which may lead to novel insight into the underlying mechanisms. The study of the intergenerational instability in the CMVMJD135 mouse model showed a high frequency of repeat contractions in both genders. Although we did not observe expansions in the transmissions that we evaluated is probable that when a higher number of meioses is studied expansions could appear; however, is clear that in this model expansions occur in a lower frequency in comparison with contractions. This tendency to contract could have a cellular protective role or result from negative selection of germline cells carrying higher repeats.

- IV. **Age- and tissue-specific somatic mosaicism.** One of the hypotheses raised in order to clarify the cell-specific vulnerability in polyQ disorders is related with the putative accumulation of larger expansions in the affected areas of the CNS through aging (Telenius et al., 1994; Ishii et al., 1996; Lopes-Cendes et al., 1996; Tanaka et al., 1996). Mouse models for polyQ diseases bring the unique opportunity to perform longitudinal studies through the lifetime in order to understand the pattern of mosaicism of the CAG repeat in different brain regions. Although we have observed a differential mosaicism pattern between different tissues and during aging we did not find a clear correlation between the degree of somatic instability and selective neuronal vulnerability, which was also observed in previous studies performed in human patients and animal models for Huntington disease, Friedreich's ataxia, SCA1 and SCA3 (Telenius et al., 1994; Ishii et al., 1996; Lopes-Cendes et al., 1996; Tanaka et al., 1996). In order to overcome some technical issues from these studies, recent studies have used more accurate and sensitive techniques to dissect the role of somatic mosaicism in polyQ. Although it was possible to observe dramatic mutation length increases (gains of up to 1000 CAG repeats) in the (affected) striatal cells in a knock-in HD mouse model (Kennedy et al., 2003) there are also studies that did not confirm a clear causal relationship between the degree of somatic instability and selective neuronal vulnerability, particularly in the case of SCA1 (Watase et al., 2003).
- V. **Motor symptoms resembling MJD.** The manifestations of MJD include cerebellar ataxia, spasticity, difficulty with speech and swallowing, weakness in arms and legs, clumsiness, frequent urination and involuntary eye movements. Our CMVMJD94 mice developed a mild phenotype observed in the Rotarod test which evaluates motor performance. However, we did not find any alterations in the gait which means that this animal displays a more subtle motor deficit without evident gait ataxia. Interestingly, in the CMVMJD135 mice several



behavioral abnormalities were observed, appearing at different time points of the lifetime and becoming worse overtime. The first sign of the disease was a deficit in two tests that evaluate limb strength and balance. Although loss of body balance is a very consistent symptom in MJD patients, loss of muscle strength is mostly observed in type III patients (Lima and Coutinho, 1980), the mildest form of the disease, so the meaning of these findings is still unclear to us. Possibly these tests are more influenced by balance and coordination than usually considered.

In addition, at a later age CMVMJD135 mice developed an abnormal gait with an enlargement of the base width which is a sign of cerebellar ataxia that is the most frequent clinical manifestation in MJD patients.

- VI. **Genotype-phenotype correlation.** It has been demonstrated that, at least in the case of diseases caused by expansion of (CAG)<sub>n</sub> repeats, there is an inverse correlation between the size of the expanded alleles and clinical presentation, more specifically the age at onset. This phenomenon leads to genetic anticipation, a hallmark of most repeat disorders. Our CMVMJD94 mice have shown to display a inverse correlation between the number of CAG repeats and the manifestation of the motor phenotype, with a squared linear correlation of  $r^2=0,20$ , that in SCA3 patients was observed to be two times higher ( $r^2=0,458$ ) (Maciel et al., 1995). Nevertheless, our correlation study was performed with a population of animals from the CMVMJD94 lineage carrying a narrow range of CAG repeats (91-99 CAGs) in comparison with the wide CAG spectrum in human patients, and one that is associated with mild forms of the disease, thus possibly explaining the lower correlation, as is seen in human patients with shorter repeats.
- VII. **Neuronal pathology in the CNS.** One important hallmark of polyQ diseases are intranuclear inclusion bodies in neuronal cells, which have been observed at late stages in patients, animal and cellular models (Ikeda et al., 1996; Paulson et al., 1997b; Cemal et al., 2002), although their association with MJD pathogenesis is still unclear. It has been demonstrated that neuronal inclusions are present in obviously degenerated CNS regions as well as in spared CNS regions in SCA3 patients (Sudarsky and Coutinho, 1995; Yamada et al., 2004; Rub et al., 2006) supporting the idea that inclusions are not the major player for the fate of neuronal cells. Indeed, our CMVMJD94 mice developed a mild phenotype in the absence of intranuclear inclusions, while CMVMJD135 mice have shown the presence of inclusions at 24 weeks of age in affected and non-affected regions of the CNS. A longitudinal

study will be performed next in our model to determine the timing of appearance of the inclusions in relation to disease.

It is widely accepted that central nervous neurodegeneration in MJD is restricted to the cerebellar dentate nucleus, pallidum, substantia nigra, subthalamic, red, and pontine nuclei, select cranial nerve nuclei and the anterior horn and Clarke's column of the spinal cord (Coutinho et al., 1982; Kanda et al., 1989; Taniwaki et al., 1997; Onodera et al., 1998). However, more recent studies using unconventional serial thick tissue sections have revealed a more extensive degeneration in terminal SCA3 including subcortical components of the somatosensory system, the vestibular nuclei, all ingestion-related brainstem nuclei among others (Rub et al., 2008). In agreement with the pathology observations in MJD patients, we observed cell atrophy in several brain regions such as the pontine nuclei, substantia nigra and thalamus in CMVMJD94 and CMVMJD135 mice. Moreover, the presence of astrogliosis was observed in both mouse models in the vestibular region and the substantia nigra. Astrogliosis has been observed in MJD post-mortem brains (Coutinho et al., 1982; Kanda et al., 1989; Taniwaki et al., 1997; Onodera et al., 1998) as well as in the YAC model for MJD (Cemal et al., 2002).

Concerning the predictive validity we have performed a first pilot therapeutic trial using the CMVMJD135 mice, in which we evaluated if autophagy activation could have an amelioration effect in the MJD symptoms observed in our model. Although we did not know so far if in our model the autophagy pathway is altered, several studies have shown that autophagy activation could have a positive therapeutic effect by the clearance of the protein aggregates in animal models of polyQ diseases and more specifically in MJD (Sarkar and Rubinsztein, 2008; Menzies et al., 2010; Renna et al., 2010). Our results do not demonstrate an amelioration of the motor symptoms in CMVMJD135 mice treated with lithium or with the combination of lithium and CCI-779. During this therapeutic trial we have faced some problems regarding the experimental design, because this experiment was performed almost in parallel with the behavioral characterization of the CMVMJD135 mice, so we had to select behavioral tests to evaluate the phenotype of the animals from the therapy group without knowing a priori which were the best markers to be analyzed, among those included in the extensive phenotype characterization study. In this manner, we will perform new therapeutic trials using better phenotype markers to assess the putative reversion of MJD-like symptoms, as well as evaluate other dosages for the combination of lithium+CCI-779, since we have

## **Chapter 5.** Discussion and future perspective

found a deleterious effect with the dosages used in this study. Preliminary data in a transgenic model of MJD in *C. elegans* has shown that lithium treatment improved the locomotion phenotype observed in this model (Teixeira-Castro A, personal communication). In addition, other pathways will be targeted with specific drugs in order to clarify their putative effect in MJD therapy, namely, protein misfolding and aggregation, mitochondria function and transcription regulation. Additionally, we will perform a temporal evaluation (at asymptomatic and symptomatic stages) of the transcriptome of CMVMJD135 mice in specific regions of the CNS, in order to clarify the pathogenic mechanisms of disease and provide potential therapeutic targets for MJD.

Our main conclusion of the work presented in this thesis is that we were able to establish new transgenic mouse models of MJD with different disease severities showing genetic, pathologic and phenotypic similarities with the human disease that could be very useful in the study of the pathogenesis mechanism of MJD as well as for therapeutic trials.

## References

- Bettencourt, C., Santos, C., Kay, T., Vasconcelos, J. and Lima, M. 2008. Analysis of segregation patterns in Machado-Joseph disease pedigrees. *J Hum Genet.* 53, 920-923.
- Bichelmeier, U., Schmidt, T., Hubener, J., Boy, J., Ruttiger, L., Habig, K., Poths, S., Bonin, M., Knipper, M., Schmidt, W. J., Wilbertz, J., Wolburg, H., Laccone, F. and Riess, O. 2007. Nuclear localization of ataxin-3 is required for the manifestation of symptoms in SCA3: in vivo evidence. *J Neurosci.* 27, 7418-7428.
- Boy, J., Schmidt, T., Wolburg, H., Mack, A., Nuber, S., Bottcher, M., Schmitt, I., Holzmann, C., Zimmermann, F., Servadio, A. and Riess, O. 2009. Reversibility of symptoms in a conditional mouse model of spinocerebellar ataxia type 3. *Hum Mol Genet.* 18, 4282-4295.
- Boy, J., Schmidt, T., Schumann, U., Grasshoff, U., Unser, S., Holzmann, C., Schmitt, I., Karl, T., Laccone, F., Wolburg, H., Ibrahim, S. and Riess, O. 2010. A transgenic mouse model of spinocerebellar ataxia type 3 resembling late disease onset and gender-specific instability of CAG repeats. *Neurobiol Dis.* 37, 284-293.
- Brock, G. J., Anderson, N. H. and Monckton, D. G. 1999. Cis-acting modifiers of expanded CAG/CTG triplet repeat expandability: associations with flanking GC content and proximity to CpG islands. *Hum Mol Genet.* 8, 1061-1067.
- Burright, E. N., Clark, H. B., Servadio, A., Matilla, T., Feddersen, R. M., Yunis, W. S., Duvick, L. A., Zoghbi, H. Y. and Orr, H. T. 1995. SCA1 transgenic mice: a model for neurodegeneration caused by an expanded CAG trinucleotide repeat. *Cell.* 82, 937-948.
- Cemal, C. K., Carroll, C. J., Lawrence, L., Lowrie, M. B., Ruddle, P., Al-Mahdawi, S., King, R. H., Pook, M. A., Huxley, C. and Chamberlain, S. 2002. YAC transgenic mice carrying pathological alleles of the MJD1 locus exhibit a mild and slowly progressive cerebellar deficit. *Hum Mol Genet.* 11, 1075-1094.
- Chadman, K. K., Yang, M. and Crawley, J. N. 2009. Criteria for validating mouse models of psychiatric diseases. *Am J Med Genet B Neuropsychiatr Genet.* 150B, 1-11.
- Chou, A. H., Yeh, T. H., Ouyang, P., Chen, Y. L., Chen, S. Y. and Wang, H. L. 2008. Polyglutamine-expanded ataxin-3 causes cerebellar dysfunction of SCA3 transgenic mice by inducing transcriptional dysregulation. *Neurobiol Dis.* 31, 89-101.
- Cleary, J. D. and Pearson, C. E. 2003. The contribution of cis-elements to disease-associated repeat instability: clinical and experimental evidence. *Cytogenet Genome Res.* 100, 25-55.
- Coutinho, P., Guimaraes, A. and Scaravilli, F. 1982. The pathology of Machado-Joseph disease. Report of a possible homozygous case. *Acta Neuropathol.* 58, 48-54.
- Gomes-Pereira, M., Fortune, M. T., Ingram, L., McAbney, J. P. and Monckton, D. G. 2004. Pms2 is a genetic enhancer of trinucleotide CAG/CTG repeat somatic mosaicism: implications for the mechanism of triplet repeat expansion. *Hum Mol Genet.* 13, 1815-1825.
- Goti, D., Katzen, S. M., Mez, J., Kurtis, N., Kiluk, J., Ben-Haiem, L., Jenkins, N. A., Copeland, N. G., Kakizuka, A., Sharp, A. H., Ross, C. A., Mouton, P. R. and Colomer, V. 2004. A mutant ataxin-3 putative-cleavage fragment in brains of Machado-Joseph disease patients and transgenic mice is cytotoxic above a critical concentration. *J Neurosci.* 24, 10266-10279.
- Goto, J., Watanabe, M., Ichikawa, Y., Yee, S. B., Ihara, N., Endo, K., Igarashi, S., Takiyama, Y., Gaspar, C., Maciel, P., Tsuji, S., Rouleau, G. A. and Kanazawa, I. 1997. Machado-Joseph disease gene products carrying different carboxyl termini. *Neurosci Res.* 28, 373-377.
- Gray, M., Shirasaki, D. I., Cepeda, C., Andre, V. M., Wilburn, B., Lu, X. H., Tao, J., Yamazaki, I., Li, S. H., Sun, Y. E., Li, X. J., Levine, M. S. and Yang, X. W. 2008. Full-length human mutant huntingtin with a stable polyglutamine repeat can elicit progressive and selective neuropathogenesis in BACHD mice. *J Neurosci.* 28, 6182-6195.

## Chapter 5. Discussion and future perspective

- Grewal, R. P., Cancel, G., Leeflang, E. P., Durr, A., McPeck, M. S., Draghinias, D., Yao, X., Stevanin, G., Alnot, M. O., Brice, A. and Arnheim, N. 1999. French Machado-Joseph disease patients do not exhibit gametic segregation distortion: a sperm typing analysis. *Hum Mol Genet.* 8, 1779-1784.
- Ikeda, H., Yamaguchi, M., Sugai, S., Aze, Y., Narumiya, S. and Kakizuka, A. 1996. Expanded polyglutamine in the Machado-Joseph disease protein induces cell death in vitro and in vivo. *Nat Genet.* 13, 196-202.
- Ikeuchi, T., Igarashi, S., Takiyama, Y., Onodera, O., Oyake, M., Takano, H., Koide, R., Tanaka, H. and Tsuji, S. 1996. Non-Mendelian transmission in dentatorubral-pallidoluysian atrophy and Machado-Joseph disease: the mutant allele is preferentially transmitted in male meiosis. *Am J Hum Genet.* 58, 730-733.
- Ishii, S., Nishio, T., Sunohara, N., Yoshihara, T., Takemura, K., Hikiji, K., Tsujino, S. and Sakuragawa, N. 1996. Small increase in triplet repeat length of cerebellum from patients with myotonic dystrophy. *Hum Genet.* 98, 138-140.
- Iughetti, P., Otto, P. A., Zatz, M., Passos Bueno, M. R. and Marie, S. K. 1998. Different behavior in the paternally vs. maternally inherited mutated allele in Brazilian Machado-Joseph (MJD1) families. *Am J Med Genet.* 77, 246-248.
- Kanda, T., Isozaki, E., Kato, S., Tanabe, H. and Oda, M. 1989. Type III Machado-Joseph disease in a Japanese family: a clinicopathological study with special reference to the peripheral nervous system. *Clin Neuropathol.* 8, 134-141.
- Kawaguchi, Y., Okamoto, T., Taniwaki, M., Aizawa, M., Inoue, M., Katayama, S., Kawakami, H., Nakamura, S., Nishimura, M., Akiguchi, I. and et al. 1994. CAG expansions in a novel gene for Machado-Joseph disease at chromosome 14q32.1. *Nat Genet.* 8, 221-228.
- Kennedy, L., Evans, E., Chen, C. M., Craven, L., Detloff, P. J., Ennis, M. and Shelbourne, P. F. 2003. Dramatic tissue-specific mutation length increases are an early molecular event in Huntington disease pathogenesis. *Hum Mol Genet.* 12, 3359-3367.
- Kovtun, I. V. and McMurray, C. T. 2001. Trinucleotide expansion in haploid germ cells by gap repair. *Nat Genet.* 27, 407-411.
- Lang, A. E., Rogaeva, E. A., Tsuda, T., Hutterer, J. and St George-Hyslop, P. 1994. Homozygous inheritance of the Machado-Joseph disease gene. *Ann Neurol.* 36, 443-447.
- Lerer, I., Merims, D., Abeliovich, D., Zlotogora, J. and Gadoth, N. 1996. Machado-Joseph disease: correlation between the clinical features, the CAG repeat length and homozygosity for the mutation. *Eur J Hum Genet.* 4, 3-7.
- Lima, L. and Coutinho, P. 1980. Clinical criteria for diagnosis of Machado-Joseph disease: report of a non-Azorena Portuguese family. *Neurology.* 30, 319-322.
- Lloret, A., Dragileva, E., Teed, A., Espinola, J., Fossale, E., Gillis, T., Lopez, E., Myers, R. H., MacDonald, M. E. and Wheeler, V. C. 2006. Genetic background modifies nuclear mutant huntingtin accumulation and HD CAG repeat instability in Huntington's disease knock-in mice. *Hum Mol Genet.* 15, 2015-2024.
- Lopes-Cendes, I., Maciel, P., Kish, S., Gaspar, C., Robitaille, Y., Clark, H. B., Koeppen, A. H., Nance, M., Schut, L., Silveira, I., Coutinho, P., Sequeiros, J. and Rouleau, G. A. 1996. Somatic mosaicism in the central nervous system in spinocerebellar ataxia type 1 and Machado-Joseph disease. *Ann Neurol.* 40, 199-206.
- Maciel, P., Gaspar, C., DeStefano, A. L., Silveira, I., Coutinho, P., Radvany, J., Dawson, D. M., Sudarsky, L., Guimaraes, J., Loureiro, J. E. and et al. 1995. Correlation between CAG repeat length and clinical features in Machado-Joseph disease. *Am J Hum Genet.* 57, 54-61.
- Marsh, J. L., Lukacsovich, T. and Thompson, L. M. 2009. Animal models of polyglutamine diseases and therapeutic approaches. *J Biol Chem.* 284, 7431-7435.
- Menzies, F. M., Huebener, J., Renna, M., Bonin, M., Riess, O. and Rubinsztein, D. C. 2010. Autophagy induction reduces mutant ataxin-3 levels and toxicity in a mouse model of spinocerebellar ataxia type 3. *Brain.* 133, 93-104.

- Onodera, O., Idezuka, J., Igarashi, S., Takiyama, Y., Endo, K., Takano, H., Oyake, M., Tanaka, H., Inuzuka, T., Hayashi, T., Yuasa, T., Ito, J., Miyatake, T. and Tsuji, S. 1998. Progressive atrophy of cerebellum and brainstem as a function of age and the size of the expanded CAG repeats in the MJD1 gene in Machado-Joseph disease. *Ann Neurol.* 43, 288-296.
- Paulson, H. L., Das, S. S., Crino, P. B., Perez, M. K., Patel, S. C., Gotsdiner, D., Fischbeck, K. H. and Pittman, R. N. 1997a. Machado-Joseph disease gene product is a cytoplasmic protein widely expressed in brain. *Ann Neurol.* 41, 453-462.
- Paulson, H. L., Perez, M. K., Trottier, Y., Trojanowski, J. Q., Subramony, S. H., Das, S. S., Vig, P., Mandel, J. L., Fischbeck, K. H. and Pittman, R. N. 1997b. Intranuclear inclusions of expanded polyglutamine protein in spinocerebellar ataxia type 3. *Neuron.* 19, 333-344.
- Pearson, C. E., Nichol Edamura, K. and Cleary, J. D. 2005. Repeat instability: mechanisms of dynamic mutations. *Nat Rev Genet.* 6, 729-742.
- Renna, M., Jimenez-Sanchez, M., Sarkar, S. and Rubinsztein, D. C. 2010. Chemical inducers of autophagy that enhance the clearance of mutant proteins in neurodegenerative diseases. *J Biol Chem.* 285, 11061-11067.
- Riess, O., Epplen, J. T., Amoiridis, G., Przuntek, H. and Schols, L. 1997. Transmission distortion of the mutant alleles in spinocerebellar ataxia. *Hum Genet.* 99, 282-284.
- Riess, O., Rub, U., Pastore, A., Bauer, P. and Schols, L. 2008. SCA3: neurological features, pathogenesis and animal models. *Cerebellum.* 7, 125-137.
- Rub, U., de Vos, R. A., Brunt, E. R., Sebesteny, T., Schols, L., Auburger, G., Bohl, J., Ghebremedhin, E., Gierga, K., Seidel, K., den Dunnen, W., Heinsen, H., Paulson, H. and Deller, T. 2006. Spinocerebellar ataxia type 3 (SCA3): thalamic neurodegeneration occurs independently from thalamic ataxin-3 immunopositive neuronal intranuclear inclusions. *Brain Pathol.* 16, 218-227.
- Rub, U., Brunt, E. R. and Deller, T. 2008. New insights into the pathoanatomy of spinocerebellar ataxia type 3 (Machado-Joseph disease). *Curr Opin Neurol.* 21, 111-116.
- Sarkar, S. and Rubinsztein, D. C. 2008. Small molecule enhancers of autophagy for neurodegenerative diseases. *Mol Biosyst.* 4, 895-901.
- Schmidt, T., Landwehrmeyer, G. B., Schmitt, I., Trottier, Y., Auburger, G., Laccone, F., Klockgether, T., Volpel, M., Epplen, J. T., Schols, L. and Riess, O. 1998. An isoform of ataxin-3 accumulates in the nucleus of neuronal cells in affected brain regions of SCA3 patients. *Brain Pathol.* 8, 669-679.
- Silva-Fernandes, A., Costa Mdo, C., Duarte-Silva, S., Oliveira, P., Botelho, C. M., Martins, L., Mariz, J. A., Ferreira, T., Ribeiro, F., Correia-Neves, M., Costa, C. and Maciel, P. 2010. Motor uncoordination and neuropathology in a transgenic mouse model of Machado-Joseph disease lacking intranuclear inclusions and ataxin-3 cleavage products. *Neurobiol Dis.* 40, 163-176.
- Sobue, G., Doyu, M., Nakao, N., Shimada, N., Mitsuma, T., Maruyama, H., Kawakami, S. and Nakamura, S. 1996. Homozygosity for Machado-Joseph disease gene enhances phenotypic severity. *J Neurol Neurosurg Psychiatry.* 60, 354-356.
- Sudarsky, L. and Coutinho, P. 1995. Machado-Joseph disease. *Clin Neurosci.* 3, 17-22.
- Takiyama, Y., Sakoe, K., Soutome, M., Namekawa, M., Ogawa, T., Nakano, I., Igarashi, S., Oyake, M., Tanaka, H., Tsuji, S. and Nishizawa, M. 1997. Single sperm analysis of the CAG repeats in the gene for Machado-Joseph disease (MJD1): evidence for non-Mendelian transmission of the MJD1 gene and for the effect of the intragenic CGG/GGG polymorphism on the intergenerational instability. *Hum Mol Genet.* 6, 1063-1068.
- Tanaka, F., Sobue, G., Doyu, M., Ito, Y., Yamamoto, M., Shimada, N., Yamamoto, K., Riku, S., Hshizume, Y. and Mitsuma, T. 1996. Differential pattern in tissue-specific somatic mosaicism of expanded CAG trinucleotide repeats in dentatorubral-pallidolusian atrophy, Machado-Joseph disease, and X-linked recessive spinal and bulbar muscular atrophy. *J Neurol Sci.* 135, 43-50.

## Chapter 5. Discussion and future perspective

- Taniwaki, T., Sakai, T., Kobayashi, T., Kuwabara, Y., Otsuka, M., Ichiya, Y., Masuda, K. and Goto, I. 1997. Positron emission tomography (PET) in Machado-Joseph disease. *J Neurol Sci.* 145, 63-67.
- Telenius, H., Kremer, B., Goldberg, Y. P., Theilmann, J., Andrew, S. E., Zeisler, J., Adam, S., Greenberg, C., Ives, E. J., Clarke, L. A. and et al. 1994. Somatic and gonadal mosaicism of the Huntington disease gene CAG repeat in brain and sperm. *Nat Genet.* 6, 409-414.
- Trottier, Y., Lutz, Y., Stevanin, G., Imbert, G., Devys, D., Cancel, G., Saudou, F., Weber, C., David, G., Tora, L. and et al. 1995. Polyglutamine expansion as a pathological epitope in Huntington's disease and four dominant cerebellar ataxias. *Nature.* 378, 403-406.
- van den Broek, W. J., Nelen, M. R., Wansink, D. G., Coerwinkel, M. M., te Riele, H., Groenen, P. J. and Wieringa, B. 2002. Somatic expansion behaviour of the (CTG)<sub>n</sub> repeat in myotonic dystrophy knock-in mice is differentially affected by Msh3 and Msh6 mismatch-repair proteins. *Hum Mol Genet.* 11, 191-198.
- Watase, K., Venken, K. J., Sun, Y., Orr, H. T. and Zoghbi, H. Y. 2003. Regional differences of somatic CAG repeat instability do not account for selective neuronal vulnerability in a knock-in mouse model of SCA1. *Hum Mol Genet.* 12, 2789-2795.
- Yamada, M., Tan, C. F., Inenaga, C., Tsuji, S. and Takahashi, H. 2004. Sharing of polyglutamine localization by the neuronal nucleus and cytoplasm in CAG-repeat diseases. *Neuropathol Appl Neurobiol.* 30, 665-675.
- Yvert, G., Lindenberg, K. S., Picaud, S., Landwehrmeyer, G. B., Sahel, J. A. and Mandel, J. L. 2000. Expanded polyglutamines induce neurodegeneration and trans-neuronal alterations in cerebellum and retina of SCA7 transgenic mice. *Hum Mol Genet.* 9, 2491-2506.